Solid State Spectroscopy: Laser Spectroscopy of Praseodymium doped Mixed Alkaline Earth Fluorides

A thesis submitted in partial
fulfilment of the requirements for the
Degree of Doctor of Philosophy in Physics
in the
University of Canterbury

by

Khong Yoon Loong

University of Canterbury
1991

Acknowledgements

I wish to dedicate this thesis to my wife Agnes for her patience, constant support and encouragement, to my son Zhi Jian for the joy he brought into our lives and to my parents who have always put the needs of their children ahead of their own.

A special thanks goes to my two supervisors Dr. G.D. Jones and Dr. R.W.G. Syme for their effort in making a spectroscopist out of me and the many helpful discussions and advice on various matters along the way.

To my office mates Marjorie Mujaji, John Laban and Nick Sheen and the rest of the solid state students Keith Murdoch and Charlotte Walshe, thanks for the many hours of delightful conversations in between times when physics just got a bit much.

It has been the good fortune of the Physics Department to have a very competent and efficient group of technical staff. I would like to acknowledge the tremendous help received from Ross Ritchie and Clive Rowe in electronics and Wayne Smith and Ron Culley in the mechanical workshop.

I am also grateful for the help and advice from previous post-graduate students namely Dr. Nigel Cockroft who assisted in my search for a post-doctoral position, Dr. Thomas Han who computerise most of the equipment in this work, Dr. Roger Reeves whose thesis was a useful starting point for my own project and Dr. Mike Reid who helped with the crystal field fits.

To those tea room regulars, thanks for some very interesting discussions during the many morning and afternoon teas and we sure had some rather lively ones.

Financial support has been provided by a Teaching Assistantship from the Physics Department. Grants from the Canterbury Branch of the Royal Society of New Zealand and the New Zealand Institute of Physics have provided the partial support to attend 15th Annual Australian Institute of Physics Condensed Matter Meeting at Wagga-Wagga and to visit the Australian National University at Canberra. Thanks to Dr. Neil Manson who provided the opportunity and support to visit his laboratory at the ANU. Thanks also to the Physics Department at the National University of Singapore, especially to Dr. S.H. Tang, M.H. Kouk and Siew Ching for being excellent hosts during my visit there.

Abstract

The defect centers formed in the double alkaline earth crystals $Ca_{1-x}Sr_xF_2 : Pr^{3+}$, $Ca_{1-x}Ba_xF_2 : Pr^{3+}$, $Sr_{1-x}Ca_xF_2 : Pr^{3+}$ and $Sr_{1-x}Ba_xF_2 : Pr^{3+}$ for x $< 0.02\%$, together with the deuterated versions of these crystals, were investigated using selective laser excitation. All crystals were doped with 0.01% Pr^{3+}. The mixed crystal centers in these systems are derived from the prominent C_{4v} center in the parent $CaF_2 : Pr^{3+}$ and $SrF_2 : Pr^{3+}$ crystals by the replacement of the host alkaline earth cations in the neighbourhood cation spheres of the Pr^{3+} ion by the dopant alkaline earth.

Three fluorine centers for each of the Sr^{2+} and Ba^{2+} doped $CaF_2 : Pr^{3+}$ crystals and two and one centers for the Ca^{2+} and Ba^{2+} doped $SrF_2 : Pr^{3+}$ crystals respectively were studied in detail. For the deuterated crystals, two centers were studied for each of the mixed crystal systems. From the total of 17 centers investigated, four common polarization characteristics were apparent and these were used to classify the centers as types $A1$, $A2$, $A3$ or $A4$. On the basis of the observed polarised fluorescence, the $A1$ and $A2$ centers are found to be consistent with having a C_s and C_{4v} symmetry respectively and models were proposed for these centers accordingly. Ambiguities in the spectroscopic data prevented a presentation of definite models for the $A3$ and $A4$ centers.

Temporal studies in the form of lifetime measurements were performed on these mixed crystal centers and crystal field trends from these studies are presented. Crystal field fits were attempted for some of the C_{4v} centers. Though the results from the fits are tentative at the moment, problems and possible solutions are identified.

The bleaching characteristics of the lower symmetry hydrogenic centers, known as bleaching centers, were studied. Results from the polarization studies here appear to support models previously assigned to the parent bleaching centers. The satellite centers associated with the parent bleaching centers are characterised and discussions of models for these centers are presented.

Contents

List of Figures

List of Tables

Chapter 1

Introduction

The optical spectroscopy of lanthanide ions has contributed significantly to the understanding of atomic theory and yielded some technological applications, most notable of which is the Nd:YAG laser. The emphasis of the work in this dissertation is on the laser spectroscopy of the mixed alkaline earth fluoride crytals doped with praseodymium ions. This chapter introduces the praseodymium ion in the mixed AE[1] fluorite crystal lattice, the technique of selective laser excitation, a brief review of previous work done on mixed crystal systems and an overview of the work in this thesis.

1.1 The Praseodymium doped fluorite lattice

Praseodymium has an atomic number of 59 and belongs to the lanthanide series in the periodic table of elements. The elements in this series are also known as rare earths, abbreviated to 'RE'. The electronic configurations of the RE elements are characterised by a xenon core with three $5d6s^2$ outer electrons and the progressive

[1] alkaline earth

filling of the $4f^n$ shell, commencing with n = 0 for the element lanthanum and progressively incremented by one till n = 14 for lutetium. Praseodymium has n = 2. RE dopants are found almost invariably to be incorporated as tripositive ions in crystals through the removal of the single 5d and the two 6s electrons. The divalent states are also possible in some cases. RE earth ions in crystals have some very interesting optical properties. The electronic transitions in the visible region are observed to be sharp and have energies very close to those of the free ions. These transitions occur between the states of the $4f$ electrons and the sharpness of the crystal spectra is a result of the lanthanide contraction where the 4f shell is drawn inside the $5s^2 5p^6$ shells. This provides a shielding mechanism whereby the perturbation on the optically active 4f electronic states by external influences of the crystal, like atomic charges and lattice vibrations, are weak. Such properties are attractive in that they can be made use of to probe the crystal environment.

The energy level structure of the various multiplets for the Pr^{3+} ion in LaF_3 are as shown in fig. 1.1 and would be similar for the same ion in all crystal hosts. The thickness of the energy bands represent the energy range of the crystal field levels within a multiplet. Two different labelling conventions are used for the multiplets. One gives the LSJ labels and the other uses a single alphabet for each multiplet; for example the ground state is labelled $^3H_4$ or Z as shown in the fig. Both conventions are used in the thesis.

The host alkaline earth fluoride lattice has a face centred cubic structure (fig. 1.2). The fluorine atoms form a cubic lattice cage with a fluorine positioned at each corner while the alkaline earth ions are placed at the centre of every alternate cage. This crystal structure is thermally and mechanically robust and it is also transparent over a wide spectral range making it an excellent host for doping with other ions like the RE's for performing optical studies on them.

The RE's enter the alkaline earth fluoride lattice readily as a tripositive ion replacing a divalent AE ion. The excess positive charge may be compensated by a single negatively charged fluorine ion in an interstitial of the cubic lattice. A light negatively charged hydride ion can serve the same purpose. The interstitial positions

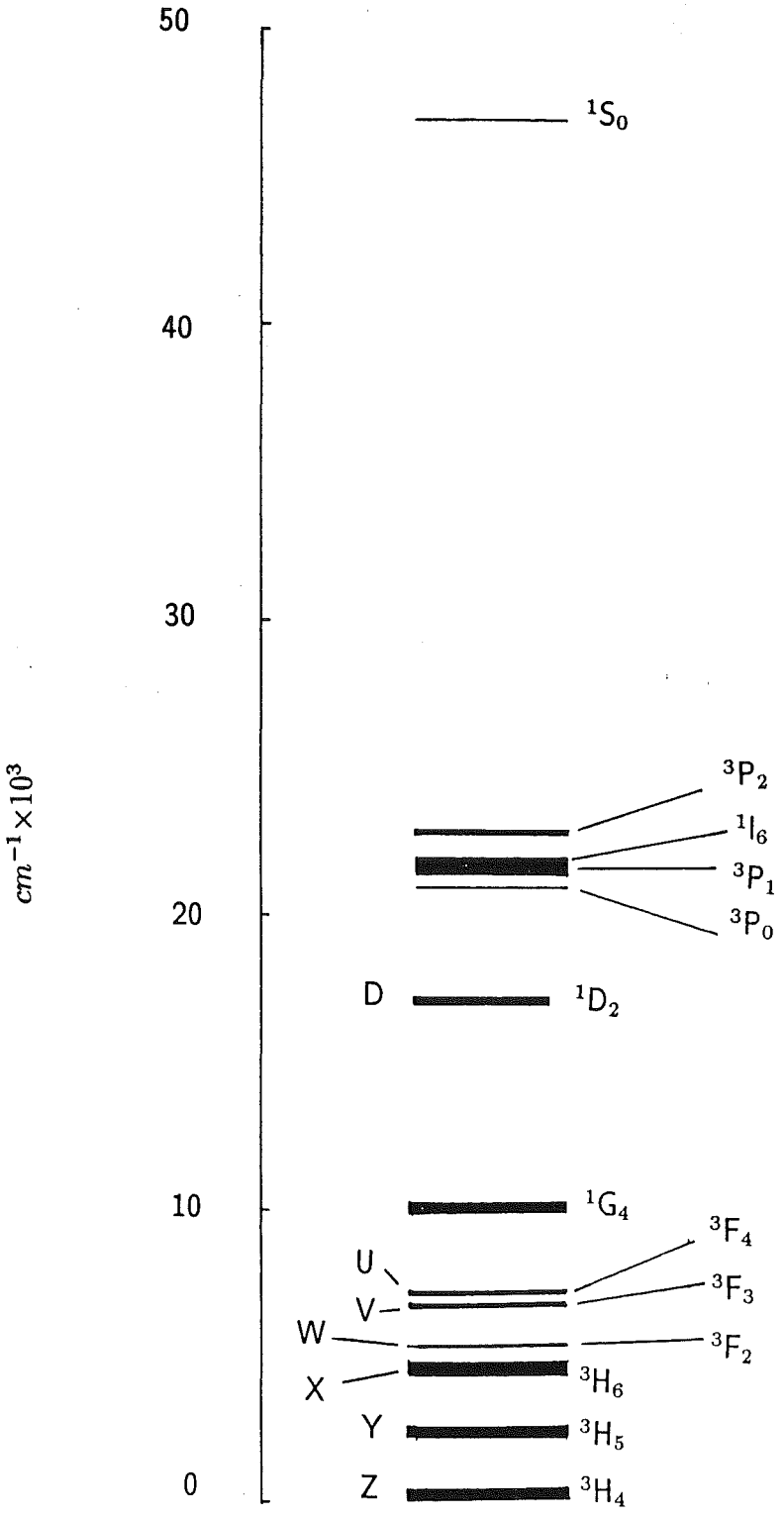

Figure 1.1: Energy level structure of the Pr^{3+} in LaF_3 adpated from Carnall et al [1988].

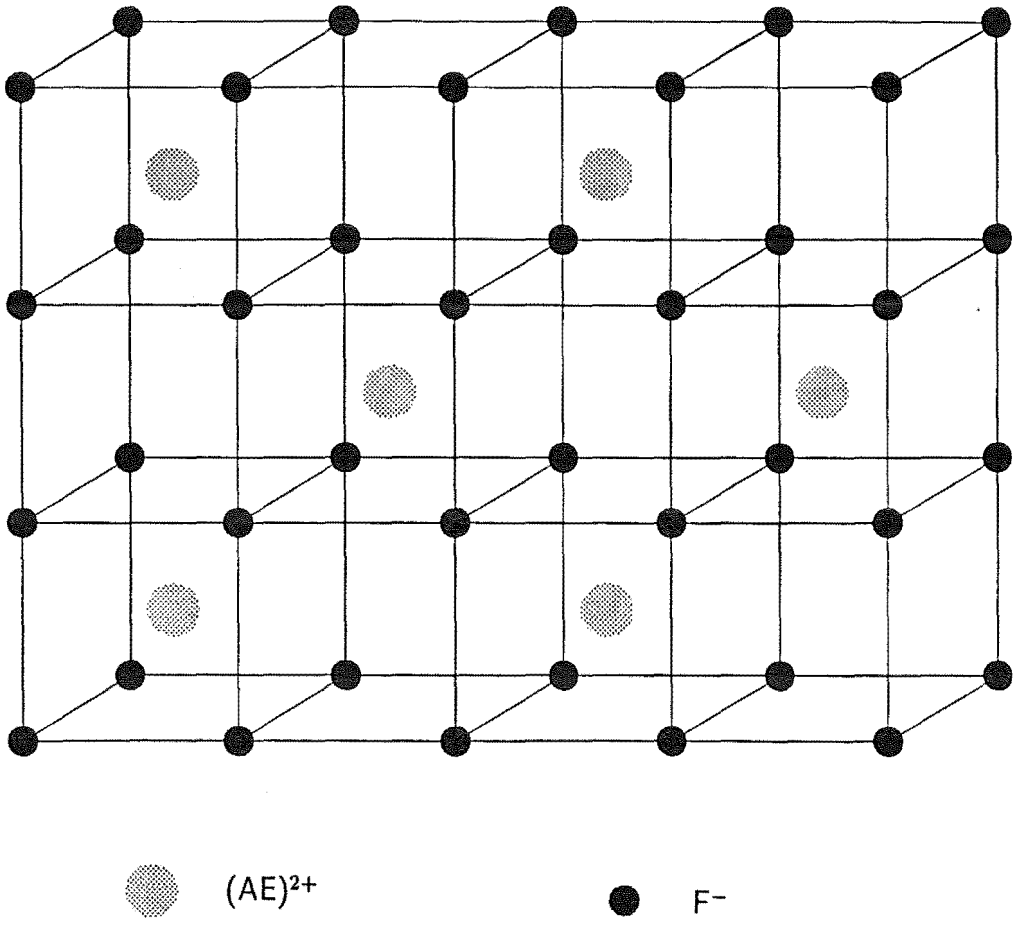

Figure 1.2: The lattice structure of the alkaline earth fluoride crystal.

adopted by these charge compensating ions create what is known as crystallographic symmetry sites or centres. Some examples of crystallographic centres are shown in fig. 1.3. The labels given to these centres are relevant to the symmetry operations that leave the centre unaltered. These operations determine the point group of the centre and there are thirty two possible point groups. In the case of praseodymium in CaF_2 and SrF_2, the predominant symmetry center form is the C_{4v} centre. The different environment experienced by the RE in the crystal in each symmetry lifts the degeneracy of the free ion energy levels, i.e. a degenerate free ion energy level may be split into several different levels in the order of tens to hundreds of cm^{-1} around the original free ion level. This dramatic change is a result of the crystal field acting on the RE. In the first approximation, the crystal field is provided by the point charges of the ligands surrounding the RE. This treatement gives a good agreement with experimental data. The electrostatic field is not necessarily the only contributor to the crystal field. Other effects including covalency or overlap of the ligand orbitals may be significant.

Some of the RE dopant may form cluster centres where two or more RE ions aggregrate within the near neighbourhood of each other. Short range interactions between these ions then become possible and many more transitions can occur as a result. Energy transfers between these close range ions can also give rise to a phenomenon called upconversion where essentially, the emitted frequencies are higher than the pumping frequencies of the laser. Cluster centres in RE doped AE fluorides seem to be an invariable feature of such crystal systems. The latest detailed work on CaF_2:Pr^{3+} indicates that the majority of the twenty two different centres present are cluster centres [Tissue and Wright, 1987]. Only three were found to be single ion centers. The population ratio of the cluster to single ion sites is not well known but the C_{4v} centre has the strongest fluorescence so it is most easily studied. In fact, extensive work has already being done by Reeves [1987] on this particular centre. In this study, a lower concentration of praseodymium doping of 0.01% was chosen in the hope of minimising formation of clusters.

The thrust of the work in this thesis is on the mixed AE fluoride crystal system. By "mixed", we mean the mixture of two different AE in the same crystal doped

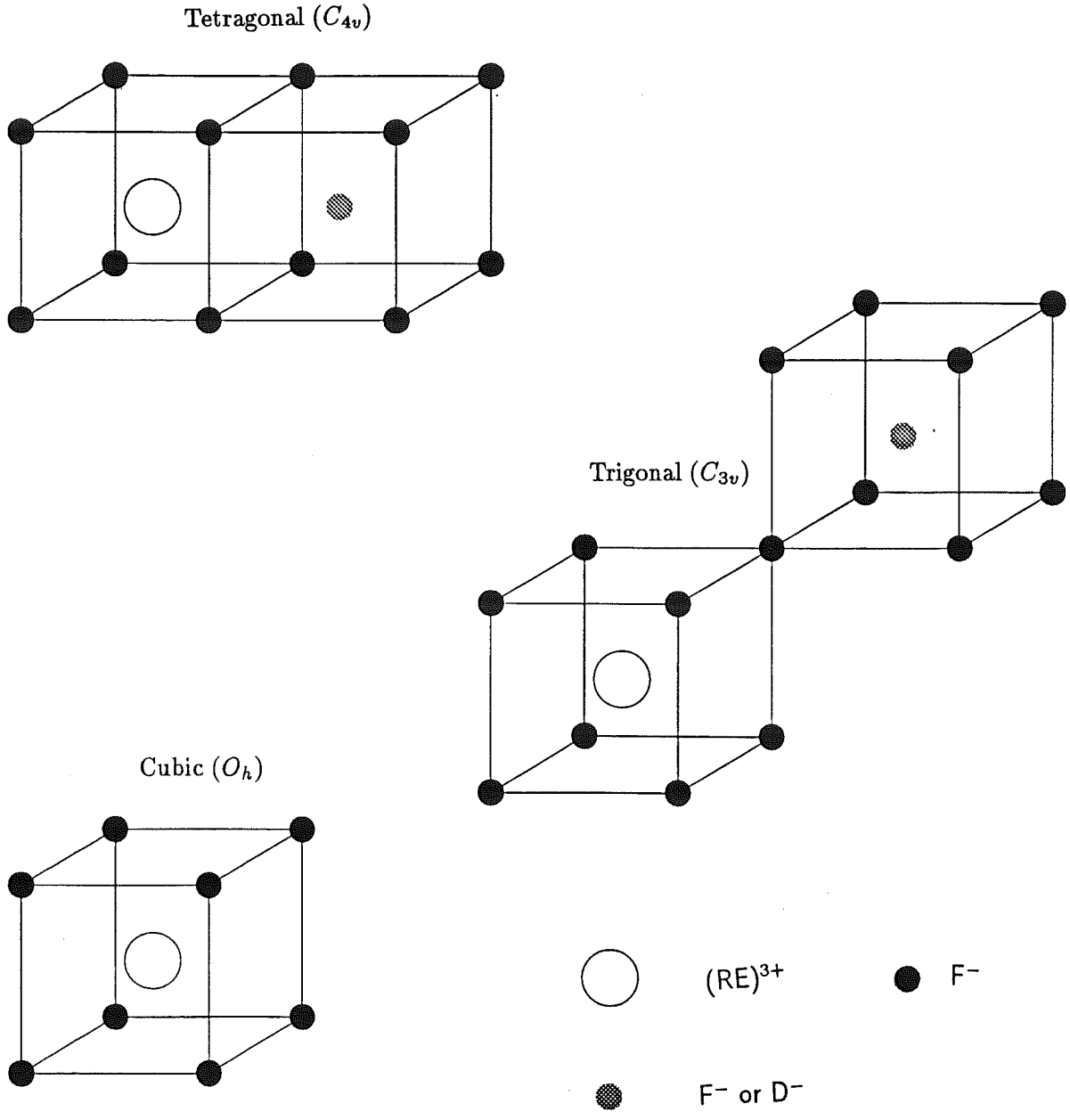

Figure 1.3: Some charge compensation centers formed with the triply charged rare earths.

with Pr^{3+}. There are twelve cations surrounding a single Pr^{3+} ion in the NN [2] and six in the NNN [3] position (fig. 1.4). The NN and NNN cations form the NN and NNN cation spheres. Depending on which host cations the dopant AE cations replace, different crystallographic centres may be created from the original parent C_{4v} centre. As the ionic radius of the guest and host AE cation is different, some spatial distortion to the original arrangement of the ions would occur in the general vicinity of where the substitution has taken place.

The formula for the mixed crystal system is $A_{1-x}B_xF_2 : Pr^{3+}$ where in this study x < 0.02 i.e 2% of the dopant AE cation B is added to host with cation A. The systems studied include A = Ca,Sr and B = Ca,Sr,Ba. The reasons for keeping the alkaline earth dopant low are to ensure that the dominant mixed crystal centers formed are simple and the host lattices are not structurally altered.

1.2 The technique of selective laser excitation

Different centres in the crystal give rise to different sets of energy levels. By sweeping the dye laser over its frequency range, the broadband excitation spectrum observed is a composite of energy transitions from all the sites present. If the laser is tuned to one particular frequency corresponding to the absorption energy of a specific site, the emission spectrum observed arises out of the transitions from the excited state to other states belonging to the same site. This is the basis of selective laser excitation (SLE)[4] first employed by Tallant and Wright [1977] to elucidate the electronic states belonging to various sites in CaF_2:Er^{3+}.

The finite frequency bandwidth of the dye laser used and also in the energy levels that are being excited means that it is not always possible to selectively excite only one site. When the frequencies of two transitions belonging to two

[2]nearest neighbour

[3]next nearest neighbour

[4]or laser selective excitation (LSE)

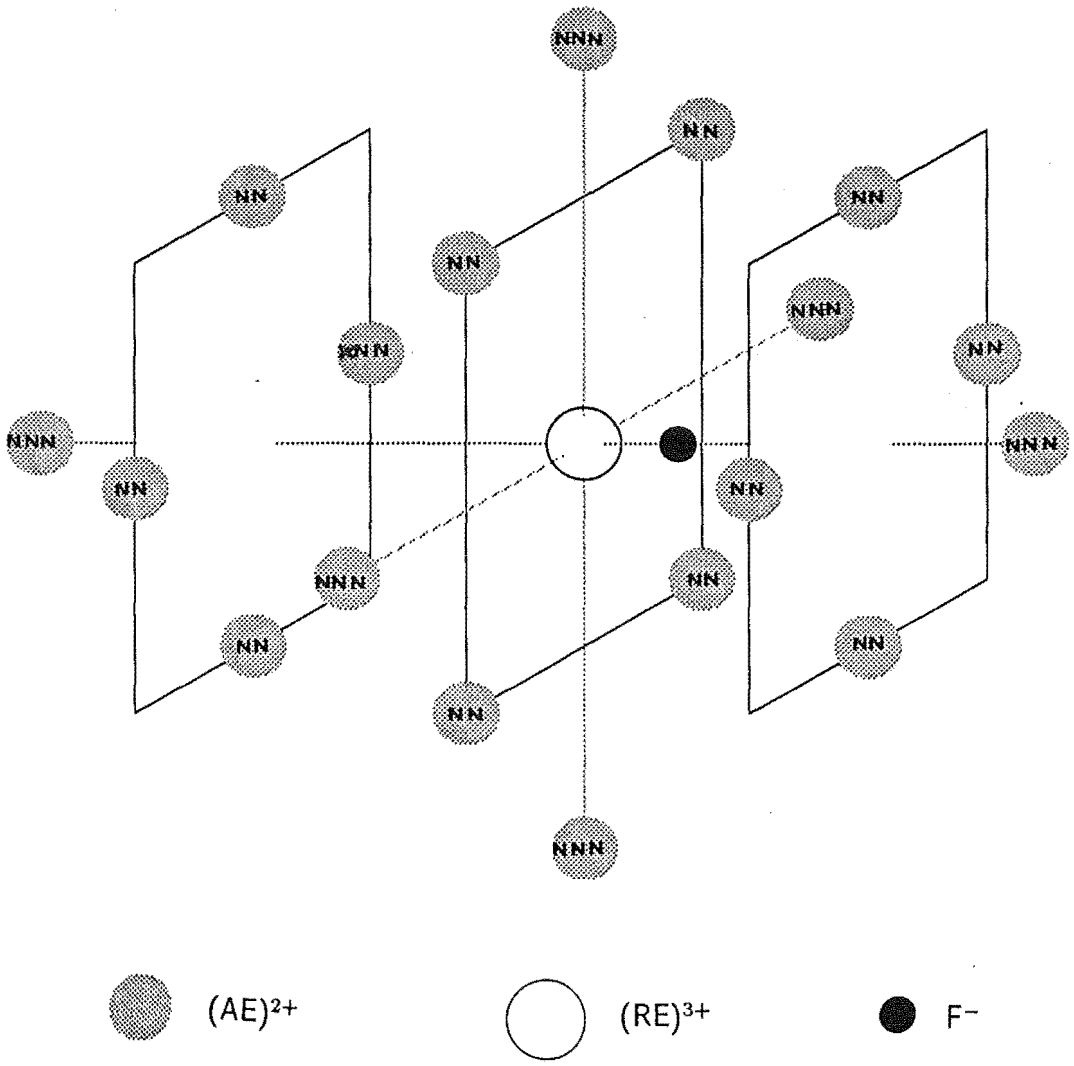

Figure 1.4: The locations of the 12 NN and 6 NNN alkaline earth cations in relation to the rare earth ion which forms a C_{4v} symmetry center

different centers overlap, the bandwidth of the laser may be sufficiently broad to excite both the levels, thus the excitation is no longer selective. Some discrimination may be possible by slightly detuning the laser and observing the relative emission intensities of transitions. Lines belonging to the same site should have the same relative intensities. This is however not satisfactory if too many overlapping bands are simultaneously excited. Such cases are encountered frequently in the mixed crystals since the lines are inhomogeneously broaden creating more opportunities for overlap of the energy levels that are pumped by the laser.

1.3 Some previous work on RE doped mixed crystal systems

Satellite lines to the principal spectra lines are often observed in RE ion spectra in crystals [Hüfner, 1978] and they are characterised by being sharp, possessing well defined polarization consistent with the presence of distinct RE sites differing only slightly from the principal RE sites. Additional impurity ions or distortions of the immediate environment of the RE site can account for such perturbed site configurations. The greater number of satellites observed suggests a variety of these perturbed site configurations in a particular mixed crystal.

A detail investigation of the satellite structures for the case of Nd^{3+} in four RE trichlorides and of Pr^{3+} and Er^{3+} in $NdCl_3$ revealed that the intensity of the satellite lines varied markedly with the host lattice and with any impurity ions present [Prinz and Cohen, 1968]. The perturbed sites responsible for these lines were correlated with crystal dislocations and their tendency to attract impurity ions.

Another comprehensive study of satellite lines in double-doped $LaCl_3$ crystals containing both Pr^{3+} and other (Ce^{3+}, Gd^{3+}, Y^{3+}) RE ions showed that both symmetric (along the crystal c-axis) and asymmetric distortions (perpendicular to the crystal c-axis) occur in the $LaCl_3$ lattice [Fricke, 1979].

The photoluminescence and cathodoluminescence spectra of Er^{3+} in mixed $Ca_{1-x}Sr_xF_2$ crystals have been reported by Aizenberg et al. [1975] and for low Sr^{2+} concentrations, satellite lines were found near lines of the tetragonal Er^{3+} center in CaF_2. At higher concentrations, above 3% of Sr^{2+} doping, strong inhomogenous broadening of the lines and total rearrangement of the spectra were observed. An extension of this work using SLE revealed three distinct mixed crystal centers [Khong, 1985].

1.4 Overview of the project and thesis

The first task of the project was to see if the required mixed crystals could be successfully grown and prepared with the present facilites; most of them could be conveniently grown. Preliminary spectra taken of the Sr^{2+} doped $CaF_2 : Pr^{3+}$ crystal showed considerable promise and subsequently experiments on all four mixed crystal systems yielded some new spectral features distinct from the parent crystals. These then formed the basis of the investigations on the fluorine compensated mixed crystal centers. More information could be obtained from polarised SLE and oriented crystals had to be prepared for this purpose. The discussion of the results from the spectroscopic study of the fluorine mixed crystal centers are presented in chapter 4.

A natural extension was to deuterate the mixed crystals and do a similar study to that already done for the fluorine centers. The deuterated crystals have additional spectral features, chiefly vibronic levels and also some further lower symmetry centers, called bleaching centers. A discourse on the polarised SLE of the deuterated mixed crystals can be found in chapter 5.

Models were proposed for the parent bleaching centers from previous work [Reeves, 1987] and with the experience gained from the polarised studies of the lower symmetry mixed crystal centers, polarised measurements were attempted to shed further light on these models. Additionally, the deuterated mixed crystal centers have weak satellite structures associated with the parent bleaching centers and these were systematically investigated. Chapter 8 deals exclusively with the results from the study

of the bleaching centers.

Temporal studies were carried out on the transitions of the centers investigated using a mechanical chopper and a nitrogen pulsed laser. The chopper was intended for the acquisition of time resolved excitation spectra and its used for discriminating transitions of different lifetimes was demonstrated to be feasible up to a point. Lifetime measurements were recorded for the mixed crystal and parent centers and as the decay rates are related to the square of the crystal field parameters, it was envisaged that some idea of the relative magnitudes of the crystal field values may be gained. The results of this section of work are discussed in chapter 6.

The final part of this work was an attempt to quantify the crystal field of the centers via crystal field fits of the experimental levels obtained. As only a relatively smaller number of experimentally levels were assigned for the lower symmetry mixed crystal centers and a larger number of parameters are needed to specify them, crystal field fits for these centers are not feasible at this stage. Thus, attention was focussed on the C_{4v} parent and mixed crystal centers with the outcome from these efforts presented in chapter 7.

Chapter two of this thesis gives a theoretical outline of the spectroscopic properties of RE ions and chapter three discusses the experimental techniques and instrumentations used in this work. The remaining chapter 9 summarizes the results of the work and concludes the thesis.

Chapter 2

Theoretical Review of Rare Earth Spectra

The spectra of rare earth ions in crystals are complex. A proper analysis of the observed spectroscopic properties involves theoretical consideration, aspects of which are outlined in this chapter. In trivalent RE's, the electrons involved in optical transitions in the visible spectral range are those occupying the partially filled 4f shell. The aim of any theoretical treatment is to account for all possible interactions involving the 4f electrons and to formulate a Hamiltonian to represent these various interactions. An energy matrix can then be constructed using this Hamiltonian and diagonalization of this matrix yields energies which can be compared with the experimental values. The angular dependence of the energy matrix elements may be precisely determined but not the radial integrals. In the semiempirical approach usually employed, the latter are treated as adjustable parameters, fitted to experimental energy values using a least squares iterative process. Estimation of the relative strength of each interaction can be deduced from the values of the various fitted parameters.

Many reviews and books discuss the relevant theory in great detail ([Judd, 1988] , [Hüfner, 1978] ,[Morrison and Leavitt, 1982],[Goldschmidt, 1978],[Wybourne, 1965]

). In this chapter, the interactions which involve the 4f electrons are described in section 2.1. In section 2.2 , a brief discussion on the electron-phonon interaction will be given, followed in section 2.3 by some results on the polarisation behaviour of the Pr^{3+} single ion in the various symmetry sites present in a cubic lattice host like the CaF_2.

2.1 Free Ion and Crystal Field Hamiltonians

Interactions of the 4f electrons both in the free ion and with the crystal potential field may be represented by the following Hamiltonian :

$$H = H_0 + H_{es} + H_{so} + H_{ci} + H_{el-so} + H_{mag} + V_{cf}. \qquad (2.1)$$

The first term is the spherically symmetric central field term and displaces all levels of a given configuration equally without affecting the energy level structure within that configuration. Major features of a configuration are determined by the Coulomb and spin orbit interactions given by the second and third terms respectively. If only these are considered then discrepancies of a few hundred wavenumbers remain between the experimental and theoretical free ion energy values. Additional interactions in the form of configuration interactions (H_{ci}), effective electrostatic - spin orbit interactions (H_{el-so}) and magnetic interactions (H_{mag}) virtually eliminate the discrepancies entirely. References to such calculations for the Pr^{3+} free ion can be found in the review by Goldschmidt[1978] .

When a trivalent RE is placed in a crystalline environment, the spherical symmetry of the free ion is broken and its 2J + 1 degeneracy lifted. This is a consequence of the interaction of the 4f electrons with the crystal field, V_{cf}, provided by the surrounding ligands. Such an interaction is weak for RE^{3+} because the 4f electrons are attracted towards the nucleus and become shielded from external influences by the outer 5s and 5p shells, the so called lanthanide contraction (Wybourne[1965]). The crystal field potential is therefore treated as a perturbation on the free ion energy levels with known eigenvalues and eigenfunctions.

Discussion of each interactions represented by the Hamiltonian of equation 2.1 and expressions for determining their matrix elements follow in this section. Section 2.1.1 examines the interactions for the free ion and section 2.1.2 describes the crystal field interactions and corrections to the standard theory.

2.1.1 Free Ion Hamiltonian

The Hamiltonian of an atom with N electrons and nuclear charge Ze is

$$H' = -\frac{\hbar^2}{2m}\sum_{i=1}^{N}\nabla_i^2 - \sum_{i=1}^{N}\frac{Ze^2}{r_i} + \sum_{i<j}^{N}\frac{e^2}{r_{ij}}, \tag{2.2}$$

where the first and second terms give the total kinetic and potential energy of the electrons in the field of the nucleus and the last term represents the repulsion between pairs of electrons. An initial difficulty with this formulation is that the interelectronic repulsion is too large to be treated as a minor perturbation, hence exact solution to the Schrodinger equation is not possible. This problem is simplified if the central field approximation is used, where a spherically symmetric potential energy function,

$$\sum_i U(r_i) = -\sum_{i=1}^{N}\frac{Ze^2}{r_i} + \left\langle \sum_{i<j}^{N}\frac{e^2}{r_{ij}} \right\rangle, \tag{2.3}$$

is constructed to approximate the sum of the average spherical potential field produced by the other electrons and the nucleus. The last term consist of the spherically averaged electronic repulsions. Each electron is then assumed to move independently in this field. Referring to equation 2.1:

$$H_0 = -\frac{\hbar^2}{2m}\sum_{i=1}^{N}\nabla_i^2 - \sum_{i=1}^{N}\frac{Ze^2}{r_i} + \left\langle \sum_{i<j}^{N}\frac{e^2}{r_{ij}} \right\rangle \tag{2.4}$$

and

$$H_{es} = \sum_{i<j}^{N}\frac{e^2}{r_{ij}} - \left\langle \sum_{i<j}^{N}\frac{e^2}{r_{ij}} \right\rangle. \tag{2.5}$$

The problem is now reduced to solving the Schrodinger equation using the central field Hamiltonian H_0 and treating H_{es} as a perturbation. H_0 describes the main features of the electronic motion and is spherically symmetric. The summation in

H_{es} over the electrons in the filled shells give a constant shift to all the levels within a configuration, while summation over the unfilled shells splits a configuration into L,S *terms.*

The $U(r_i)$ of equation 2.3 is a one electron operator and the eigenfunction of each electron in the central field (eqn. 2.4) is written: as

$$\psi_{nlm_lm_s}(r,\theta,\phi) = \frac{R_{nl}(r)}{r} Y_{lm_l}(\theta,\phi)\chi_{m_s}, \tag{2.6}$$

where the radial wavefunctions R_{nl} depend on U(r), the Y_{lm_l} are the spherical harmonics and χ_{m_s} are the spin functions. To satisfy the Pauli exclusion principle, the Schrodinger equation with a central field Hamiltonian must use the antisymmetrised products (*Slater determinants*) of the above wavefunctions. In so doing, a configuration is defined by the set of quantum numbers $(n_1l_1, n_2l_2, ..., n_Nl_N)$ with each nl^x configuration having a degeneracy $^{2(2l+1)}C_x$. The $4f^2$ configuration of the Pr^{3+} ion is 91 fold degenerate.

To calculate levels due to the electrostatic interaction within a configuration , it is necessary to evaluate the matrix of the non-spherically symmetric part of the electronic repulsion (eqn 2.5) :

$$\left\langle f^n SLJM \left| \sum_{i<j} \frac{e^2}{r_{ij}} \right| f^n S'L'J'M' \right\rangle, \tag{2.7}$$

summing over electrons of incomplete shells. By expanding $\frac{1}{r_{ij}}$ using Legendre polynomials and spherical harmonics, and defining the C_q^k tensor operator by:

$$C_q^k = \left(\frac{4\pi}{2k+1}\right)^{\frac{1}{2}} Y_{kq}, \tag{2.8}$$

where Y_{kq} is a spherical harmonic, the matrix elements in (2.7) can be re-expressed as

$$\sum_k f_k(r) \left\langle f^n SLJM \left| \sum_{i<j} (\mathbf{C_i^k} \cdot \mathbf{C_j^k}) \right| f^n S'L'J'M' \right\rangle. \tag{2.9}$$

For the $4f^2$ equivalent electrons of Pr^{3+} , the matrix elements of (2.9) have the form:

$$\sum_k f_k(r)(-1)^{2l+L} \delta_{LL'} \delta_{M_L M_{L'}} \delta_{SS'} \delta_{M_S M_{S'}} \begin{Bmatrix} l & l & k \\ l & l & L \end{Bmatrix} (l\|C_k\|l)^2 \tag{2.10}$$

where the reduced matrix element is

$$(l\|C_k\|l) = (-1)^l[(2l+1)(2l'+1)]^{1/2}\begin{pmatrix} l & k & l' \\ 0 & 0 & 0 \end{pmatrix} \tag{2.11}$$

and the radial integral is

$$f_k(r) = F^k = e^2\int\int(\frac{r_<^k}{r_>^{k+1}})R_{4f}^2(r_1)R_{4f}^2(r_2)dr_1dr_2. \tag{2.12}$$

The tables of Nielson and Koster[1963] give the values of the electrostatic matrix elements. To use these, new parameters must first be defined with transformation properties of the the groups R_7 and G_2 used in classification of the states. These have the form:

$$E = \sum_{k=0}^{3} e_k E^k. \tag{2.13}$$

Chapter 2 of Wybourne[1965] discuss this point and give the relationships between the parameters E^k and F^k. Tabulations of the *3j* and *6j* symbols used in the expressions can be found in the tables of Rotenberg[1959].

In addition to the electrostatic interactions, various magnetic interactions are also significant. Of these, the spin - orbit interaction gives the major contribution. Evaluation of the spin-orbit matrix elements is also done in the tensor formalism. The spin-orbit coupling Hamiltonian is a product of two rank one tensors acting independently on the spin and orbital part of a wavefunction and can be written as:

$$H_{so} = \sum_i -1^N\zeta(r_i)(\mathbf{s_i}\cdot\mathbf{l_i}), \tag{2.14}$$

with

$$\zeta(r_i) = \frac{\hbar^2}{2m^2c^2r_i}\frac{dU(r_i)}{dr_i}. \tag{2.15}$$

The matrix elements are given by:

$$\left\langle f^nSLJM\left|\sum_{i=1}^{N}\zeta(r_i)(\mathbf{s_i}\cdot\mathbf{l_i})\right|f^nS'L'J'M'\right\rangle =$$

$$\zeta_{4f}(-1)^{J+L+S'}\delta_{JJ'}\delta_{M_JM_J'}\sqrt{84}\begin{Bmatrix} S & S' & 1 \\ L' & L & J \end{Bmatrix}(f^NSL\|\mathbf{V_{11}}\|f^NS'L'). \tag{2.16}$$

Matrix elements of the V_{11} operator are also listed in the tables of Nielson and Koster. The most important effect of the spin-orbit coupling is to mix states of the

same J but different L and S values. In rare earths, the Coulomb and spin-orbit interactions are of comparable magnitude and substantial mixing between different L and S states occurs. It is thus no longer possible to label states using the Russell Saunders or LS coupling scheme but instead the intermediate coupling scheme should be adopted. Diagonalization of the energy matrix with both the electrostatic and spin orbit interactions considered would yield a set of eigenvectors which is a linear combination of L,S terms with the same J values. The dominant $^{2S+1}L_J$ term of these eigenvectors is often used as a label for these intermediate coupling LSJ terms. The intermediate coupling wavefunctions are used in the crystal field calculations as good starting wavefunctions since they do not vary much on inclusion of other interactions.

The deviations of the calculated energy levels when only the electrostatic and spin-orbit interaction are considered can be attributed to mainly to the neglect of the configuration interaction. This is treated by Rajnak and Wybourne[1963] for the case of l^n type configurations using the second order perturbation theory. For a given perturbing configuration, several states $|m_\tau\rangle$ will interact with the states $|\Psi\rangle$ and $|\Psi'\rangle$ belonging to the f^n configuration. Such perturbations may be included by adding to each electrostatic matrix element of the type $\langle f^n\Psi|G|f^n\Psi'\rangle$, a correction factor

$$C(\Psi,\Psi') = -\sum_\tau \frac{\langle f^n\Psi|G|m_\tau\rangle\langle m_\tau|G|f^n\Psi'\rangle}{\Delta E}. \qquad (2.17)$$

G represents the Coulomb repulsion and ΔE is the energy difference between the f^n and perturbing configuration. For the case of rare earths, the contribution from individual configurations is generally small. However, the accumulative effects may be considerable because of the high density of states as the continuum is approached. This correction factor can be represented by :

$$C(\Psi,\Psi') = \sum_k P^k\langle f^n\Psi|\sum_{i>j}^{N}(\mathbf{U}_\mathbf{i}^\mathbf{k}\cdot\mathbf{U}_\mathbf{j}^\mathbf{k})|f^n\Psi'\rangle, \qquad (2.18)$$

where the P^k term contain the radial integrals to be treated as adjustable parameters. The even k part of this correction factor is absorbed in the previous fit when the F^k terms are treated as adjustable parameters, while the odd k terms are not.

The way to deal with these odd k terms is to use the properties of the Casimir

operators to replace the odd k terms by the equivalent expression

$$\delta(\Psi,\Psi')[\alpha L(L+1) + \beta G(G_2) + \gamma G(R_7)]. \tag{2.19}$$

The α, β and γ are parameters of particular linear combinations of P^k with k odd and $G(G_2)$ and $G(R_7)$ are the eigenvalues of Casimir operators for the group G_2 and R_7 used in classifying the states of the f^n configuration.

Better agreement is achieved in the calculation of energy levels if several magnetically correlated corrections are also introduced . The principal two body magnetic correction is that of the electrostatically correlated spin-orbit perturbation. The Hamiltonian for this is represented by:

$$H_{el-so} = \sum_{2,4,6} p_f P^f, \tag{2.20}$$

while that of the spin-spin and spin-other-orbit relativistic corrections is

$$H_{mag} = \sum_{0,2,4} m_h M^h. \tag{2.21}$$

The operators are denoted by p_f and m_h and the adjustable parameters are P^f and the Marvin integral M^h. The addition of these terms in the Hamiltonian does not make a particularly significant energy contribution and will not be discussed further here while the paper by Judd[1968] gives all the relevent details. All the parameters featured in this discussion are used in the crystal field fit in this work but not all of them are varied.

2.1.2 Crystal Field Hamiltonian

It is possible to expand the crystal field potential V_{cf} as a series in the Racah tensor operators that are related to the spherical harmonics (see equation 2.8). The crystal field V_{cf} then takes the form

$$V_{cf} = \sum_{k,q,i} B_q^k (C_q^k)_i, \tag{2.22}$$

where the summation is over the n electrons of of the $4f^n$ configuration. For f electrons the k terms can have values of 0,2,4,6 and since the k=0 term merely provides a constant shift to the levels, it may be ignored. The q values depend on the particular crystal field site symmetry. In the description of the crystal field , one could either use the point group or JM basis. A detailed description of the former can be found in the book by Butler[1981]. Following his methods, under the group reduction chain $0_3 \supset 0_h \supset D_{4h} \supset C_{4v} \supset C_4$, the Hamiltonian for a C_{4v} local symmetry of the RE in the point group basis may be written as :

$$\begin{aligned} V_{C_{4v}} = & X^{2^+2^+0^+00}\sqrt{5}U^{2^+2^+0^+00} + X^{4^+0^+0^+00}\sqrt{9}U^{4^+0^+0^+00} \\ + & X^{4^+2^+0^+00}\sqrt{9}U^{4^+2^+0^+00} + X^{6^+0^+0^+00}\sqrt{13}U^{6^+0^+0^+00} \\ + & X^{6^+2^+0^+00}\sqrt{5}U^{6^+2^+0^+00}. \end{aligned} \tag{2.23}$$

Similarly, the chains $0_3 \supset 0_h \supset D_{4h} \supset C_{4v} \supset C_{2v} \supset C_2$ and $0_3 \supset 0_h \supset D_{4h} \supset C_{4v} \supset C_{2v} \supset C_s$ give the Hamiltonian for C_{2v} and C_s centres as:

$$\begin{aligned} V_{C_{2v}} = & X^{2^+2^+0^+000}\sqrt{5}U^{2^+2^+0^+000} + X^{2^+2^+2^+200}\sqrt{5}U^{2^+2^+2^+200} \\ + & X^{4^+0^+0^+000}\sqrt{9}U^{4^+0^+0^+000} + X^{4^+2^+0^+000}\sqrt{9}U^{4^+2^+0^+000} \\ + & X^{4^+2^+2^+200}\sqrt{9}U^{4^+2^+2^+200} + X^{6^+0^+0^+000}\sqrt{13}U^{6^+0^+0^+000} \\ + & X^{6^+2^+0^+000}\sqrt{13}U^{6^+2^+0^+000} + X^{6^+2^+2^+2^+00}\sqrt{13}U^{6^+2^+2^+2^+00} \\ + & X^{6^+\tilde{0}^+2^+200}\sqrt{5}U^{6^+\tilde{0}^+2^+200} \end{aligned} \tag{2.24}$$

and

$$\begin{aligned} V_{C_s} = & X^{2^+2^+0^+000}\sqrt{5}U^{2^+2^+0^+000} + X^{2^+2^+2^+200}\sqrt{5}U^{2^+2^+2^+200} \\ + & X^{2^+\tilde{1}^+1^+110}\sqrt{5}U^{2^+\tilde{1}^+1^+110} + X^{4^+0^+0^+000}\sqrt{9}U^{4^+0^+0^+000} \\ + & X^{4^+2^+0^+000}\sqrt{9}U^{4^+2^+0^+000} + X^{4^+2^+2^+200}\sqrt{9}U^{4^+2^+2^+200} \\ + & X^{4^+1^+1^+110}\sqrt{9}U^{4^+1^+1^+110} + X^{4^+\tilde{1}^+1^+110}\sqrt{9}U^{4^+\tilde{1}^+1^+110} \\ + & X^{6^+0^+0^+000}\sqrt{13}U^{6^+0^+0^+000} + X^{6^+2^+0^+000}\sqrt{13}U^{6^+2^+0^+000} \\ + & X^{6^+2^+2^+2^+00}\sqrt{13}U^{6^+2^+2^+2^+00} + X^{6^+\tilde{0}^+2^+200}\sqrt{13}U^{6^+\tilde{0}^+2^+200} \\ + & X^{6^+1^+1^+1^+10}\sqrt{13}U^{6^+1^+1^+1^+10} + X^{6^+\tilde{1}^+1^+1^+10}\sqrt{13}U^{6^+\tilde{1}^+1^+1^+10}. \end{aligned} \tag{2.25}$$

The X's and U's are the crystal field parameters and the Racah unit tensor operators respectively, while their superscripts are irrep labels of the site symmetry group.

Calculations are usually done in the JM basis and point group irreps assigned to the eigenvectors. To transform between the JM and point group bases , the tables of Butler[1981] are helpful. Table 2.1 reproduces the entries from Butler's book which can be used to do such the transformations and the transformation between the more commonly used spherical tensors and unit tensors.

The linear combination of tensor operators of a Hamiltonian in the JM basis, as constructed from table 2.1 are orthogonal to each other and have well defined transformation properties under the parent group from which a particular symmetry is derived. The significance of operators orthogonality to ensure that correlations between the parameters are minimized and the fitting equations are well conditioned has been highlighted by Judd[1985] .

Having specified the crystal field Hamiltonian appropriate for the RE^{3+} ion site symmetry, the matrix elements of the crystal field interaction can then be calculated. Following Wybourne[1965] , this is usually done in the JM basis by writing:

$$\langle f^n \alpha SLJJ_z|V_{cf}|f^n \alpha' SL'J'J'_z\rangle = \sum B^k_q \langle f^n \alpha SLJJ_z|\mathbf{U}^k_q|f^n \alpha' SL'J'J'_z\rangle \langle f\|C^{(k)}\|f\rangle, \tag{2.26}$$

where

$$\langle f\|C^{(k)}\|f\rangle = (-1)^3 \cdot 7 \cdot \begin{pmatrix} 3 & k & 3 \\ 0 & 0 & 0 \end{pmatrix}, \tag{2.27}$$

and by successive application of Wigner - Eckart theorem,

$$\langle f^n \alpha SLJJ_z|\mathbf{U}^k_q|f^n \alpha' SL'J'J'_z\rangle = (-1)^{J-J_z} \begin{pmatrix} J & k & J' \\ -J_z & q & J'_z \end{pmatrix} \langle f^n \alpha SLJ\|\mathbf{U}^{(k)}\|f^n \alpha' SL'J'\rangle \tag{2.28}$$

and

$$\langle f^n \alpha SLJ\|\mathbf{U}^{(k)}\|f^n \alpha' SL'J'\rangle = (-1)^{S+L'+J+K}\sqrt{(2J+1)(2J'+1)} \begin{Bmatrix} J & J' & k \\ L' & L & S \end{Bmatrix} \langle f^n \alpha SL\|\mathbf{U}^{(k)}\|f^n \alpha' SL'\rangle. \tag{2.29}$$

The *3j* and *6j* symbols can be found in the tables Rotenberg et al[1959] while Nielson and Koster[1963] tabulates the reduced matrix elements. The crystal field

Transformation from the $O_3 \supset O_h \supset D_{4h} \supset C_{4v} \supset C_4$ to the JM basis:

$$|2^+2^+0^+00\rangle = -|20\rangle$$
$$|4^+0^+0^+00\rangle = +[\sqrt{7}/2\sqrt{3}][|40\rangle + \sqrt{5/14}(|44\rangle + |4-4\rangle)]$$
$$|4^+2^+0^+00\rangle = +[\sqrt{5}/2\sqrt{3}][|40\rangle - \sqrt{7/10}(|44\rangle + |4-4\rangle)]$$
$$|6^+0^+0^+00\rangle = -[1/2\sqrt{2}][|60\rangle - \sqrt{7/2}(|64\rangle + |6-4\rangle)]$$
$$|6^+2^+0^+00\rangle = +[\sqrt{7}/2\sqrt{2}][|60\rangle + \sqrt{1/14}(|64\rangle + |6-4\rangle)]$$

Transformation from the $O_3 \supset O_h \supset D_{4h} \supset C_{4v} \supset C_{2v} \supset C_2$ to the JM basis:

$$|2^+2^+0^+000\rangle = -|20\rangle$$
$$|2^+2^+2^+200\rangle = +1/\sqrt{2}(|22\rangle + |2-2\rangle)$$
$$|4^+0^+0^+000\rangle = +[\sqrt{7}/2\sqrt{3}][|40\rangle + \sqrt{5/14}(|44\rangle + |4-4\rangle)]$$
$$|4^+2^+0^+000\rangle = +[\sqrt{5}/2\sqrt{3}][|40\rangle - \sqrt{7/10}(|44\rangle + |4-4\rangle)]$$
$$|4^+2^+2^+200\rangle = +1/\sqrt{2}(|42\rangle + |4-2\rangle$$
$$|6^+0^+0^+000\rangle = -[1/2\sqrt{2}][|60\rangle - \sqrt{7/2}(|64\rangle + |6-4\rangle)]$$
$$|6^+2^+0^+000\rangle = +[\sqrt{7}/2\sqrt{2}][|60\rangle + \sqrt{1/14}(|64\rangle + |6-4\rangle)]$$
$$|6^+2^+2^+200\rangle = -[1/4\sqrt{2}][\sqrt{11}(|66\rangle + |6-6\rangle) + \sqrt{5}(|62\rangle + |6-2\rangle)]$$
$$|6^+\bar{0}^+2^+200\rangle = -[1/4\sqrt{2}][-\sqrt{5}(|66\rangle + |6-6\rangle) + \sqrt{11}(|62\rangle + |6-2\rangle)]$$

Transformation from the $O_3 \supset O_h \supset D_{4h} \supset C_{4v} \supset C_{2v} \supset C_s$ to the JM basis:

$$|2^+2^+0^+000\rangle = -|20\rangle$$
$$|2^+2^+2^+200\rangle = +1/\sqrt{2}(|22\rangle + |2-2\rangle)$$
$$|2^+\bar{1}^+1^+110\rangle = -\imath/\sqrt{2}(|21\rangle - |2-1\rangle)$$
$$|4^+0^+0^+000\rangle = +[\sqrt{7}/2\sqrt{3}][|40\rangle + \sqrt{5/14}(|44\rangle + |4-4\rangle)]$$
$$|4^+2^+0^+000\rangle = +[\sqrt{5}/2\sqrt{3}][|40\rangle - \sqrt{7/10}(|44\rangle + |4-4\rangle)]$$
$$|4^+2^+2^+200\rangle = +1/\sqrt{2}(|42\rangle + |4-2\rangle$$
$$|4^+1^+1^+110\rangle = -\imath/4[\sqrt{7}(|41\rangle - |4-1\rangle) + (|43\rangle - |4-3\rangle)]$$
$$|4^+\bar{1}^+1^+110\rangle = -\imath/4[(|41\rangle - |4-1\rangle) + \sqrt{7}(|43\rangle - |4-3\rangle)]$$
$$|6^+0^+0^+000\rangle = -[1/2\sqrt{2}][|60\rangle - \sqrt{7/2}(|64\rangle + |6-4\rangle)]$$
$$|6^+2^+0^+000\rangle = +[\sqrt{7}/2\sqrt{2}][|60\rangle + \sqrt{1/14}(|64\rangle + |6-4\rangle)]$$
$$|6^+2^+2^+200\rangle = -[1/4\sqrt{2}][\sqrt{11}(|66\rangle + |6-6\rangle) + \sqrt{5}(|62\rangle + |6-2\rangle)]$$
$$|6^+\bar{0}^+2^+200\rangle = -[1/4\sqrt{2}][-\sqrt{5}(|66\rangle + |6-6\rangle) + \sqrt{11}(|62\rangle + |6-2\rangle)]$$
$$|6^+1^+1^+110\rangle = -\imath/16[\sqrt{11}(|65\rangle - |6-5\rangle) - \sqrt{6}(|61\rangle - |6-1\rangle)5\sqrt{3}(|63\rangle - |6-3\rangle)]$$
$$|6^+\bar{1}^+1^+110\rangle = -\imath 5\sqrt{3}/112[(|65\rangle - |6-5\rangle) + 11\sqrt{14/15}(|61\rangle - |6-1\rangle) + \sqrt{33}/5(|63\rangle - |6-3\rangle)]$$

The B_q^k and $X^{k\lambda}$ parameters can be obtained using the above transformations and the following relationships between the unit and spherical tensors:

$$\mathbf{U}^2 = -(7.2/\sqrt{3.5.7})\mathbf{C}^2$$
$$\mathbf{U}^4 = +(7.\sqrt{2}/\sqrt{7.11})\mathbf{C}^4$$
$$\mathbf{U}^6 = -(7.2.5/\sqrt{3.7.11.13})\mathbf{C}^6$$

Table 2.1: Transformation between the point group and JM basis

operators mix states for which $J_z \neq J_z'$ with the result that J and J_z are no longer good quantum numbers and linear combinations of $|JJ_z\rangle$ states are required to describe the crystal field wavefunctions.

This standard one electron parametrization of the crystal field has been highly successful in that good fits have been obtained for most of the spectra of RE ions in crystalline hosts. However, some anomalies still exist. For example, it has been found that parameters which give a good fit to the other multiplets of Pr^{3+} in $LaCl_3$ and $PrCl_3$ gives a rather large standard deviation for the $^1D_2$ multiplet (Margolis[1961],Yeung and Newman[1987]) . Examples of such deviations in other systems include the $^3K_8$ multiplet of Ho^{3+} in $LaCl_3$[Reid, 1987], $^2H_{\frac{11}{2}}$ of Nd^{3+} in $LaCL_3$ and YAG among others [Li and Reid, 1990] , Eu^{3+} in $LaCl_3$ and Gd^{3+} in $LaCl_3$ [Dieke, 1968] .

One promising approach towards resolving these anamolies is to include electron correlation effects in what is called the *correlation crystal field* (CCF) [Reid, 1987]. A detailed consideration of the CCF formalism is beyond the scope of this work but a subset of the CCF i.e spin correlated crystal field (SCCF) will be discussed since it will be required to resolve the difficulties with fitting the $^1D_2$ multiplet spectral data. Judd[1977] pointed out that 4f electrons with parallel spins lead to a contracted radial wavefunction and therefore smaller crystal field parameters. To include the SCCF, the spherical tensors of the standard crystal field are replaced by :

$$C^k_{q(i)} + b^k(\mathbf{S}\cdot\mathbf{s_i})C^k_{q(i)} \tag{2.30}$$

and as a result, the reduced matrix elements $\langle f^n Sl\|\mathbf{U^k}\|f^n S'L'\rangle$ are modified to

$$\langle f^n Sl\|\mathbf{U^k}\|f^n S'L'\rangle + b^k[S(S+1)/(2s+1)]^{1/2}\langle f^n SL\|\mathbf{V_{1k}}\|f^n S'L'\rangle. \tag{2.31}$$

The introduction of the new parameters, b^k for k = 2,4,6 seemed to improved matters quite considerably in some cases. The SCCF is still by far the most successful improvement and has been used in the analysis of many RE's in crystalline hosts.

2.2 Electron Phonon Interaction

So far no mention has been made of the dynamics of the lattice or the ligands around the RE. In fact, the electronic states of the RE couple with both the lattice phonons and localized modes of any lighter ligands present. The emphasis of this work is on the electronic states of the RE, however, features of the interaction between the RE electrons and the phonon states are apparent in the spectra as additional phonon bands of distinct vibronic levels and in the broadening of the higher levels in a multiplet. A discussion of this interaction therefore seems appropriate. For a more detailed theoretical discussion, the work of Pollack et al [1962] and Newman[1973] can be consulted. This section discuss only the vibronics originating from the modulation of the crystal field by the local mode phonons of hydrogenic ions.

A hydrogenic ion vibrating in a cubic lattice can be treated as a single particle moving in a three dimensional anharmonic potential well of octahehral or tetrahedral symmetry. The general Hamiltonian for such a particle is

$$H_{vib} = \frac{p^2}{2m} + (1/2)\sum A_{ij}Q_iQ_j + \sum B_{ijk}Q_iQ_jQ_k + \sum C_{ijkl}Q_iQ_jQ_kQ_l + \ldots\ldots \quad , \tag{2.32}$$

where the first term is the kinetic energy of the ion and the Q_i's are the normal vibrational coordinates. The first two terms are those of a harmonic oscillator and the rest are the anharmonic terms. The exact form of the Hamiltonian is determined by the point group of the site in which the ion moves. The wavefunctions of a three dimensional harmonic oscillator are $|n_xn_yn_z\rangle$ where the integers n_x, n_y and n_z represent the occupational numbers of the x,y,z oscillators and the associated energies are given by :

$$E_{n_xn_yn_z} = (n_x + 1/2)\hbar\omega_x + (n_y + 1/2)\hbar\omega_y + (n_z + 1/2)\hbar\omega_z. \tag{2.33}$$

The anharmonic terms can be treated as perturbations on the harmonic oscillator and wavefunctions for the anharmonic states are constructed from the linear combinations of the harmonic oscillator wavefunctions which transform as the symmetric representation of the point group.

The electron-phonon interaction Hamiltonian is written as:

$$V_{ev} = \sum_i f_i Q_i + \sum_{i,j} g_{ij} Q_i Q_j + \ldots\ldots\ldots \quad , \tag{2.34}$$

where f_i and g_{ij} are functions of the 4f electronic coordinates and Q_i are the normal vibrational coordinates, which transform according to a particular irreducible representation of point symmetry of the RE centre. For light ions, the normal coordinates are just the ion displacement X,Y,Z and these can be expressed in terms of coordinates, which can be resolved into creation and annihilation operators $\mathbf{a}^\dagger$ and $\mathbf{a}$:

$$Q_i = \sqrt{\hbar/2m_i\omega_i}(\mathbf{a}^\dagger{}_i + \mathbf{a}_i), \tag{2.35}$$

where m_i is the light ion mass, ω_i the angular frequency and

$$\begin{aligned} \mathbf{a}_i|..n_i..\rangle &= \sqrt{n_i}|..n_i - 1..\rangle \\ \mathbf{a}^\dagger{}_i|..n_i..\rangle &= \sqrt{n_i + 1}|..n_i + 1..\rangle \\ \mathbf{a}_i\mathbf{a}^\dagger{}_i|n_i\rangle &= (n_i + 1)|n_i\rangle \\ \mathbf{a}^\dagger{}_i\mathbf{a}_i|n_i\rangle &= n_i|n_i\rangle. \end{aligned} \tag{2.36}$$

The combined Hamiltonian of the electronic and vibrational motion produces vibronic states which are products of the electronic $|\phi\rangle$ and vibrational wavefunctions $|..n_i..\rangle$ of the form

$$\Phi = |\phi\rangle|..n_i..\rangle. \tag{2.37}$$

The energy shift of the vibronic states due to the electron-phonon interaction is :

$$E_{ev} = \langle\Phi|g_{ij}Q_iQ_j|\Phi\rangle + \sum_{i,\psi} \frac{\langle\Phi|f_iQ_i|\Psi\rangle\langle\Psi|f_iQ_i|\Phi\rangle}{E_\Phi - E_\Psi}, \tag{2.38}$$

where the first and second term are the first and second order perturbation energy shifts respectively. To evaluate the first order perturbation shift, equations 2.35 and 2.36 are used to give:

$$\begin{aligned} \langle\Phi|g_{ij}Q_iQ_j|\Phi\rangle &= \langle\phi|g_{ij}|\phi\rangle\langle..n_i..|\mathbf{a}^\dagger{}_i\mathbf{a}_i + \mathbf{a}_i\mathbf{a}^\dagger{}_i|..n_i..\rangle \times \hbar/2m_i\omega_i \\ &= \langle\phi|g_{ij}|\phi\rangle(2n_i + 1)\hbar/2m_i\omega_i. \end{aligned} \tag{2.39}$$

The second order perturbation term involves the intermediate states $|..n_i+1..\rangle$ and $|..n_i-1..\rangle$ and is obtained as follows :

$$\begin{aligned}\sum_i \frac{\langle\Phi|f_iQ_i|\Psi\rangle\langle\Psi|f_iQ_i|\Phi\rangle}{E_\Phi - E_\Psi} &= \sum_{i,\psi}|\langle\phi|f_i|\psi\rangle|^2\left(\frac{|\langle..n_i..|Q_i|..n_i..\rangle|^2}{E_\phi - E_\psi \pm \hbar\omega_i}\right) \\ &= \sum_{i,\psi}\frac{|\langle\phi|f_i|\psi\rangle|^2}{E_\phi - E_\psi}\left(\frac{\hbar}{2m_i\omega_i}\right)(2n_i+1). \qquad (2.40)\end{aligned}$$

An assumption that $E_\phi - E_\psi \gg \hbar\omega_i$ is made in the last step .

2.2.1 Irreps of Vibronic States

The irreps of the various vibronic states can be determined using the group multiplication tables. As an example, consider the coupling of the electronic ground state of the Pr^{3+} ion in a C_{4v} symmetry site, with the local modes of a hydrogenic ion also in a C_{4v} symmetry site. The ground state of the Pr^{3+} is doubly degenerate and has a γ_5 irrep while the z and (x,y) local modes have irreps γ_1 and γ_5 respectively. The following vibronic states arises:

$$\begin{aligned}\gamma_5 \times \gamma_5 &= \gamma_1 + \gamma_2 + \gamma_3 + \gamma_4 \\ \gamma_1 \times \gamma_5 &= \gamma_5 \qquad (2.41)\end{aligned}$$

Coupling with the z local mode retains the two fold degeneracy of the electronic state while coupling with the (x,y) local mode yields four levels. A schematic of the vibronic levels is shown in figure 2.1. The vibronic levels of a C_s center which descended from a C_{4v} center has irreps also shown in figure 2.1.

The electron-phonon interaction can also account for the phenomena of isotope shifts of energies of the electronic transitions of hydrogen centers with different H^- isotopes, for the local mode frequency shifts of vibronics coupled to different electronic levels and, for the splitting of the (x,y) local mode [Reeves, 1987]

2.3 Selection Rules and Polarization in the Mixed Alkaline Earth Crystals

RE ions are usually doped into a regular crystal lattices with well defined site symmetry. In most crystals such as LaF_3 (C_2) and $LaCl_3$ (D_{3h}), the crystal c-axis corresponds to the principal axis for the symmetry of the environment experienced by the RE and well defined polarization effects are expected. For the case of RE ions in the cubic lattice of CaF_2 and SrF_2 , there are a number of equivalent orientations for the principal axis of a chosen symmetry site. It is therefore not immediately obvious if any net polarization effects would be present. Careful analysis of the C_{3v} and C_{4v} symmetries in an overall cubic lattice, with 8 and 6 equivalent orientations respectively, revealed that well defined polarization effects may be observed. These effects are documented elsewhere (Cockroft et al.[1986] and Reeves et al. [1991]) .

This work is concerned principally with the deuterium and fluorine Pr^{3+} C_s and C_{2v} centers in the mixed alkaline earth fluoride crystal systems. The polarization ratios expected for these centers in a cubic lattice are detailed this section. Discussion of particular site symmetries present in Pr^{3+} mixed alkaline earth crystals is first given in section 2.3.1. Section 2.3.2 presents the selection rules and the polarization ratios expected for the C_s and C_{2v} centres. One aspect which has not been dealt with in other work is the geometrical aspects which would lead to the departure of the observed from the expected polarization behaviour. The pattern of polarization degradation for the C_{4v} center will also be discussed in section 2.3.3 .

2.3.1 Symmetries for RE^{3+} ions the Mixed Alkaline Earth Crystals

The basic alkaline earth fluoride cubic lattice and the C_{4v} center environment has been introduced in chapter 1. Just as the C_{4v} centre is due to the cubic symmetry being lowered by the presence of the F^- ion in the nearest interstitial position,

the lowering of the C_{4v} symmetry to C_{2v} or C_s symmetry is brought about by the inclusion of foreign cations close to the RE ion in a tetragonal symmetry crystal field. Surrounding a RE ion in a cubic symmetry site are 12 cations in the nearest neighbour (NN) position and 6 cations in the next nearest neighbour position forming the NN and NNN cation spheres (fig. 1.4). If dopant AE ions replace any of these host cations, the number of resulting arrangements and inequivalent symmetries is dependent on the original symmetry. (Table 2.2) . It is obvious that if too many of the host cations in the NN and NNN sphere are substituted, the number of inequivalent symmetries increases rapidly, making a complete analysis impractical. Idealized diagrams are shown in figure 2.2 for some possible inequivalent symmetries derivable from a parent C_{4v} symmetry centre. Attention is focussed on the centers derived from such a C_{4v} centre because this is the expected dominant species in CaF_2 and SrF_2 crystals with low concentration (< 0.05 percent) of Pr^{3+} doping. There are two possible orientations for both the C_s and C_{2v} centres and these are distinguished by their σ_v reflection planes, i.e. they are at 45^0 to each other. Labels given to differentiate these different geometries are $C_s(a)$, $C_s(b)$, $C_{2v}(a)$ and $C_{2v}(b)$ (fig. 2.2).

The formula of these mixed crystals are of the form $A_{1-x}B_xF_2 : Pr^{3+}$ where A specifies the host cation and B the dopant alkaline earth (AE) cation. In this study, A is Ca^{2+} or Sr^{2+} and B is either Ca^{2+} , Sr^{2+} or Ba^{2+} . The subscript x is the AE dopant concentration with values ranging from 0.005 to 0.03 i.e 0.5 to 3%. In the Raman studies of the $Ca_xSr_{1-x}F_2$ and $Sr_xBa_{1-x}F_2$ mixed crystal systems [Chang et al., 1966], a single Raman-active mode was observed to have a frequency that varies linearly with dopant concentration from $x = 0$ to $x = 1$. In the same study, the x-ray diffraction pattern obtained of the mixed crystals revealed only diffraction lines of a fcc[1] lattice. The x-ray diffraction and Raman data, taken together demonstrates that the mixed crystals are homogeneous and random solid solutions. The statistical relationship

$$P_n = C_n^{18} x^n (1-x)^{(18-n)} \tag{2.42}$$

then provides a quantitative idea of the fraction P_n of all the cation spheres in the

[1]face centered cube

crystal with n foreign cations in both the NN and NNN spheres at x value of doping. A graphical representation of this is shown in figure 2.3. This means that in the concentration regime of less than one percent doping, about 16 % of all the cation spheres are affected by a foreign cation substitution. Of these, at least 94 % would have only one of the cation replaced.

n	Number of possible arrangements	Number of possible inequivalent symmetries from the following parent centers		
		Cubic	Trigonal	Tetragonal
1	12	1	3	3
2	66	4	13	13
3	220	9	44	35

Table 2.2: Number of inequivalent symmetries when ions in the NN cation spheres are substituted by n foreign cations [Aizenberg et al., 1975]

2.3.2 Polarization Behaviour

The three orthogonal components of the electric dipole operator x,y and z transform as a particular irrep under a given point group. In the C_{4v} point group, they may transform either as γ_5 (x,y) or γ_1 (z). For the C_s symmetry, they transform as γ_1 $(x$ *or* $y)$ or γ_2 (z) and for the C_{2v} symmetry, they transform as γ_2 (x) ,γ_4 (y) or γ_1 (z). The requirement for a non vanishing transition probablity between two states $|a\rangle$ and $|b\rangle$ with irreps Γ_a and Γ_b is :

$$\Gamma_a \times \Gamma_{\mathbf{D}_p} \subset \Gamma_b. \tag{2.43}$$

where $\Gamma_{\mathbf{D}_p}$ is the irrep of the dipole operator. As an example, for a C_{4v} center, the emission transition $\gamma_1 \rightarrow \gamma_5$ requires the dipole operator to have an irrep of γ_5 i.e. the radiation emitted is perpendicular to the C_4 axis of the center.

For any polarization effects to be observed at all, it is necessary that the crystals are prepared suitably orientated, usually [100]. The geometry of the laser polarization and crystal fluorescence relative to the crystal [100] face must also be correctly chosen. Figure 2.4 displays the relative positions of all the elements of interest. The E-vector of the laser was arranged to have polarization either in the Z or Y direction, henceforth these two directions are referred to as E_Z or E_Y. Using an analyzer which can be rotated, the emission strength of fluorescence in different directions of polarization can be recorded. The simplest arrangement is to have the analyzer aligned along the two orthogonal X or Y directions. A compact standard convention to specify these orientation geometries is $X(AB)Z$, where X is the direction of propagation of the incident laser beam , Z of the observed fluoresence and A ,B designate the polarisation direction of both the laser and observed fluoresence respectively. The important quantity is the ratio of the observed fluorescence intensity for the analyzer aligned along the X and Y directions and this ratio shall be referred to as the *polarisation ratio*, $(AX):(AY)$, where A is either Y and Z. The labels outside the brackets, X and Z are omitted since they are always the same in this work.

Table 2.3 gives the polarization selection rules for the C_s centre. In the [100] oriented crystal used, the two $C_s(a)$ and $C_s(b)$ geometries give different polarisation

ratios as shown in table 2.4 . Table 2.5 and 2.6 give similar information for the $C_{2v}(a)$ and $C_{2v}(b)$ centres . Appendix A present details on how the ratios are obtained. The π and σ labels indicate the emitted or absorbed polarizaton as being either parallel or perpendicular to z-axis of the centre. The z-axis for the C_s centres is chosen to be perpendicular to the reflection plane while for the C_{2v} centres, it is the C_2 axis.

From the predicted ratios one can deduce the irreps involved in a particular observed transition. For example, if the assumed symmetry is $C_s(b)$ and a *(YX):(YY)* ratio of 0:1 is observed, then the possible transitions are between states with irreps $\gamma_1 \rightarrow \gamma_2$ for the absorption and $\gamma_2 \rightarrow \gamma_1$ for the emission or vice versa. If the excited level has a γ_1 irrep, then the ground level can only be a γ_2 irrep.

In deriving the polarization ratios, the geometry of the participating elements are assumed to be perfect. Some deviation from the ideal ratios is however inevitable. The mixed crystals can be orientated to within about 3 degrees at best. Accuracy of the optical alignment is hard to estimate, as are aberrations of the lenses and they would introduce further deviations. A quantitative idea of the way the polarization ratio is degraded with departure from the ideal geometry may be gained if the incident E-vector is allowed to have zenithal and azimuthal angular variations from the crystallographic axis with respect to which it was suppose to be perfectly aligned. The polarization ratios will now be a function of the two angular variables. These ratios are given in figure 2.5 for the C_{4v} symmetry as contour plots, with θ and ϕ as the zenithal and azimuthal angular deviation respectively. Details of the trigonometric expressions from which these plots are obtained can be found in appendix A.

From plots in figures 2.5 a picture emerges of how each angular parameter affects the polarization ratios. For a C_{4v} center under the $[\sigma, \pi]$ [2] and $[\pi, \sigma]$ cases, the expected ideal *(YX):(YY)* ratio of 1:0 is affected by both θ and ϕ. At θ and ϕ equal to approximately 87 and 3 degrees, the expected ratio of *(YX):(YY)* is only 10:1. For the $[\sigma, \sigma]$ cases the ϕ angle variation on the whole does not change the

[2](σ absorption and π emission)

Table 2.3: Polarization selection rules for the C_s centre

C_s	γ_1	γ_2
γ_1	σ_{xy}	π
γ_2	π	σ_{xy}

Table 2.4: Relative polarization intensities of electric dipole transitions predicted for the C_s centres in a [100] oriented crystal. The propagation direction of the incident laser beam is X and of the observed fluoresence is Z for all cases, hence these labels are excluded.

		$C_s(a)$ centre				$C_s(b)$ centre			
Pump transition	Decay transition	(YY)	(YX)	(ZY)	(ZX)	(YY)	(YX)	(ZY)	(ZX)
$\gamma_1 \rightarrow \gamma_1$	$\gamma_1 \rightarrow \gamma_1$	$0 \leq \frac{(YX)}{(YY)} \leq 1$		1	1	$0 < \frac{(YX)}{(YY)} < \frac{1}{2}$		1	1
	$\gamma_1 \rightarrow \gamma_2$	$\frac{(YX)}{(YY)} \geq \frac{1}{2}$		1	1	0	1	1	1
$\gamma_1 \rightarrow \gamma_2$	$\gamma_2 \rightarrow \gamma_1$	2	1	1	1	1	0	0	0
	$\gamma_2 \rightarrow \gamma_2$	$\frac{(YX)}{(YY)} \geq \frac{1}{2}$		1	1	0	1	1	1
$\gamma_2 \rightarrow \gamma_2$	$\gamma_2 \rightarrow \gamma_1$	$\frac{(YX)}{(YY)} \geq \frac{1}{2}$		1	1	0	1	1	1
	$\gamma_2 \rightarrow \gamma_2$	$0 \leq \frac{(YX)}{(YY)} \leq 1$		1	1	$0 < \frac{(YX)}{(YY)} < \frac{1}{2}$		1	1
$\gamma_2 \rightarrow \gamma_1$	$\gamma_1 \rightarrow \gamma_1$	$\frac{(YX)}{(YY)} \geq \frac{1}{2}$		1	1	0	1	1	1
	$\gamma_1 \rightarrow \gamma_2$	2	1	1	1	1	0	0	0

Table 2.5: Polarization selection rules for the C_{2v} centre

C_{2v}	γ_1	γ_2	γ_3	γ_4
γ_1	π	σ_x	-	σ_y
γ_2	σ_x	π	σ_y	-
γ_3	-	σ_y	π	σ_x
γ_4	σ_y	-	σ_x	π

Table 2.6: Relative polarization intensities for electric dipole transitions predicted for the C_{2v} centres in a [100] oriented crystal for electric dipole transitions. The labels a,b and c correspond to (1,2,3,4) , (2,1,4,3) and (4,3,2,1) respectively. For example, $\gamma_a \rightarrow \gamma_b$ would include the transitions $\gamma_1 \rightarrow \gamma_2$, $\gamma_2 \rightarrow \gamma_1$, $\gamma_3 \rightarrow \gamma_4$ and $\gamma_4 \rightarrow \gamma_3$.

		$C_{2v}(a)$ centre				$C_{2v}(b)$ centre			
Pump transition	Decay transition	(YY)	(YX)	(ZY)	(ZX)	(YY)	(YX)	(ZY)	(ZX)
$\gamma_a \rightarrow \gamma_a$	$\gamma_a \rightarrow \gamma_a$	1	0	0	0	1	0	0	0
	$\gamma_a \rightarrow \gamma_b$	0	1	1	1	0	1	1	1
	$\gamma_a \rightarrow \gamma_c$	0	1	1	1	0	1	1	1
$\gamma_a \rightarrow \gamma_b$	$\gamma_a \rightarrow \gamma_a$	0	1	1	1	0	1	1	1
	$\gamma_a \rightarrow \gamma_b$	2	1	1	1	1	0	1	0
	$\gamma_a \rightarrow \gamma_c$	2	1	1	1	0	1	0	1
$\gamma_a \rightarrow \gamma_c$	$\gamma_a \rightarrow \gamma_a$	0	1	1	1	0	1	1	1

observed ratio as much as the θ angle variation and the overall departure from the ideal *(YY):(YX)* ratio of 2:1 is not as rapid. In the $[\pi, \pi]$ case, the ideal (YY):(YX) of 1:0 is affected only by the angle θ.

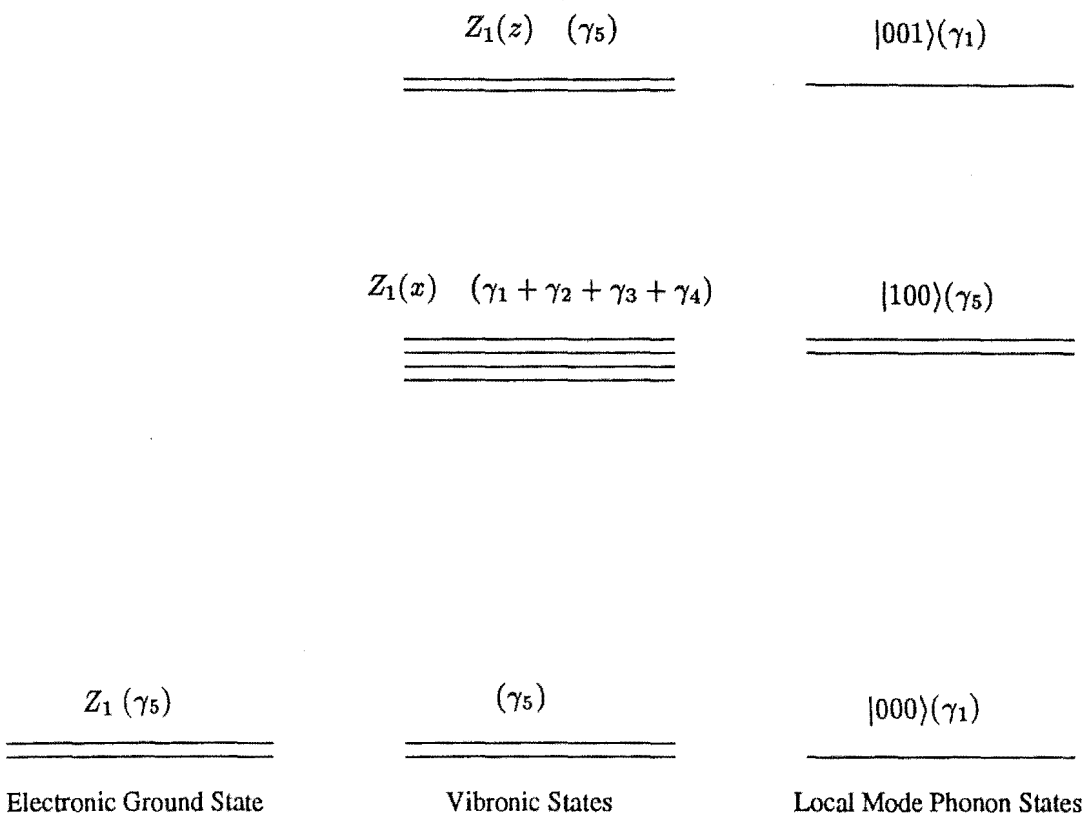

Figure 2.1: Vibronic states from the coupling of the hydrogenic C_{4v} ground state with the local mode phonons

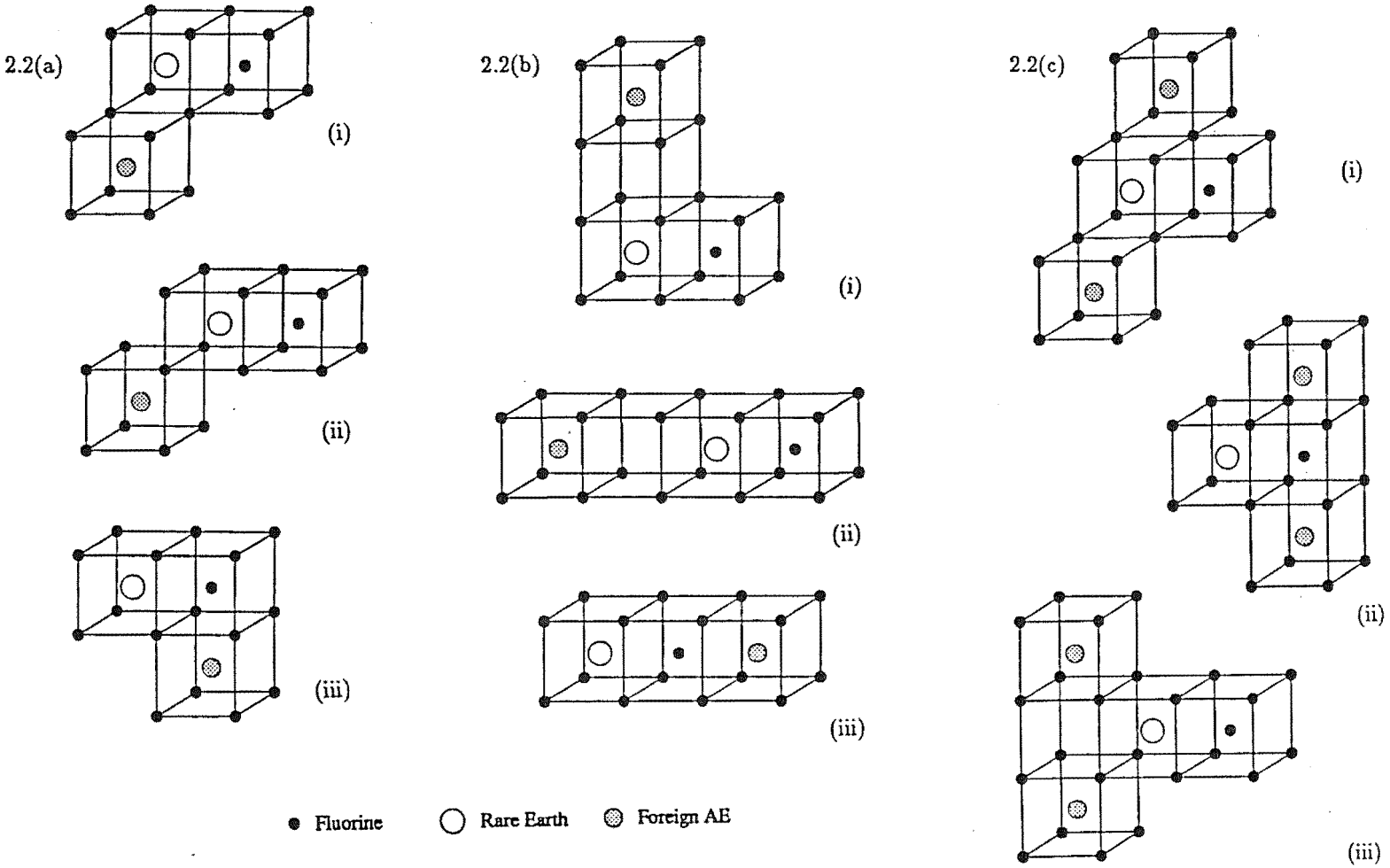

Figure 2.2 Models of some low symmetry sites derived from the parent C_{4v} centre when a foreign alkaline earth cation substitutes that of the host in the NN and NNN position.
(a) NN replacement by one foreign cation; **(i)** $C_s(a)$ centers ; **(ii,iii)** $C_s(b)$ centers
(b) NNN replacement by one foreign cation; **(i)** $C_s(b)$ centre ; **(ii,iii)** C_{4v} centers
(c) NN replacement by two foreign cations; **(i)** $C_{2v}(a)$ centers ; **(ii,iii)** $C_{2v}(b)$ centers
See text for description of labels for centers.

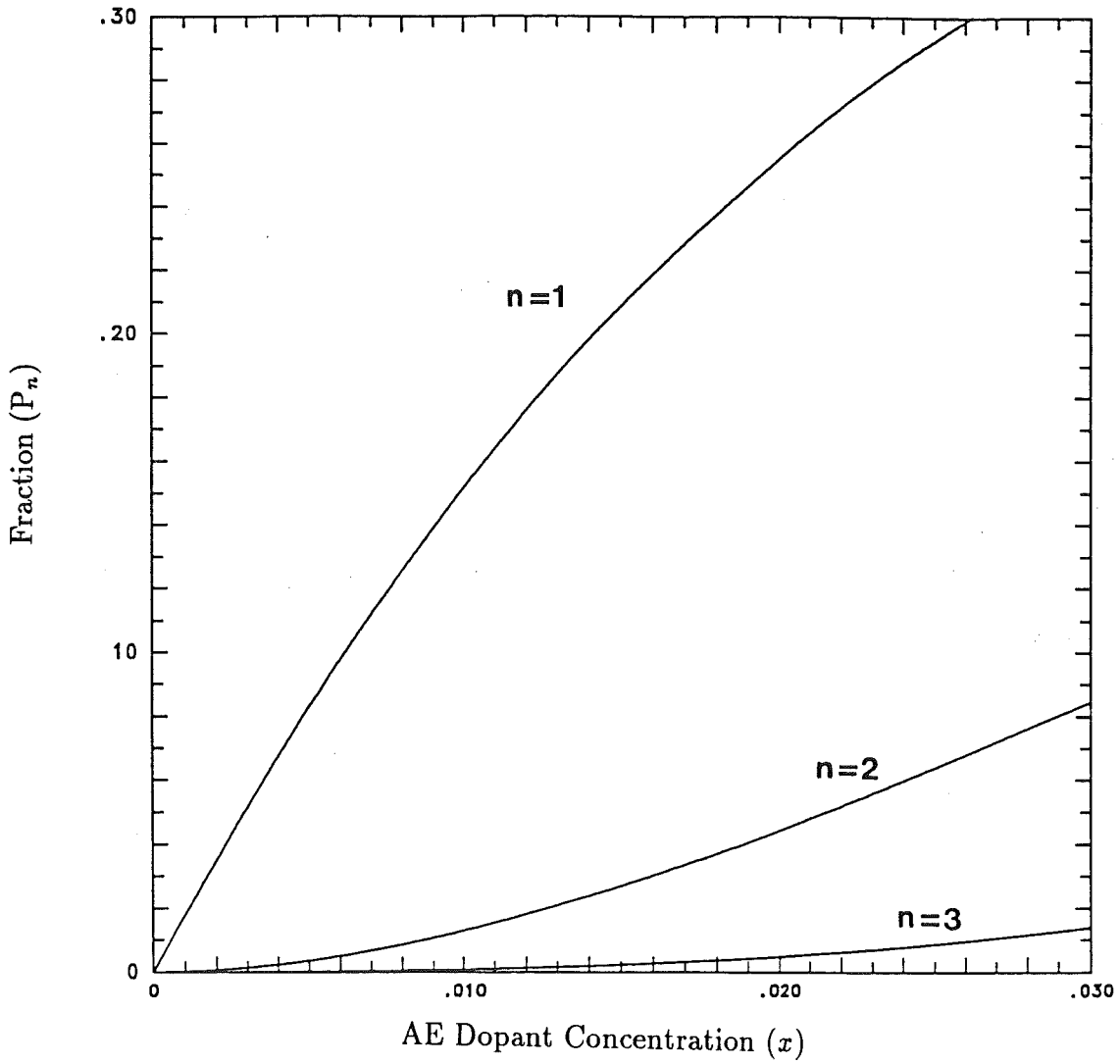

Figure 2.3: Graphical representation of fraction P_n of NN and NNN cation spheres with n number of foreign cations as a function of AE dopant concentration x (See equation 2.42).

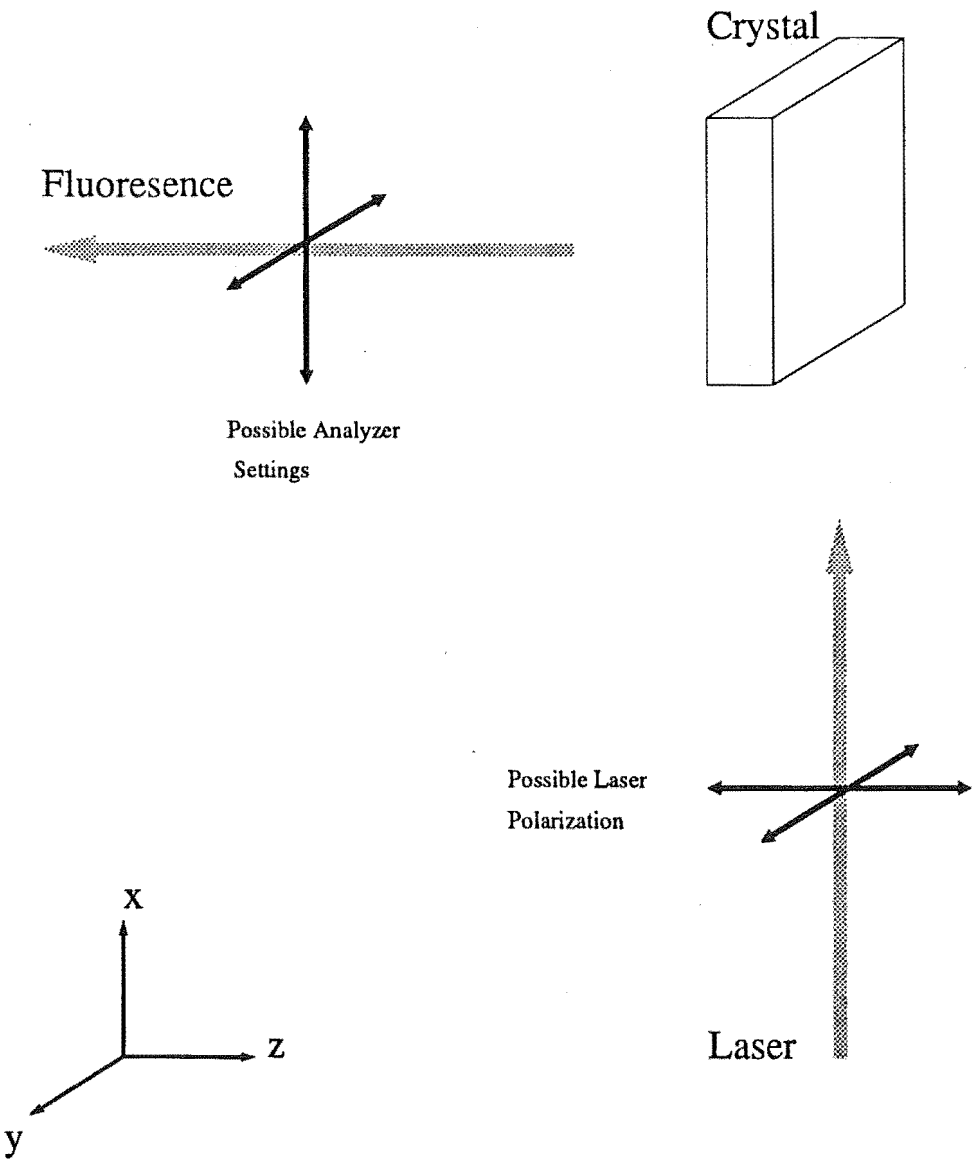

Figure 2.4: Possible orientations of the laser polarization (Z or Y) and analyzer settings (X or Y)

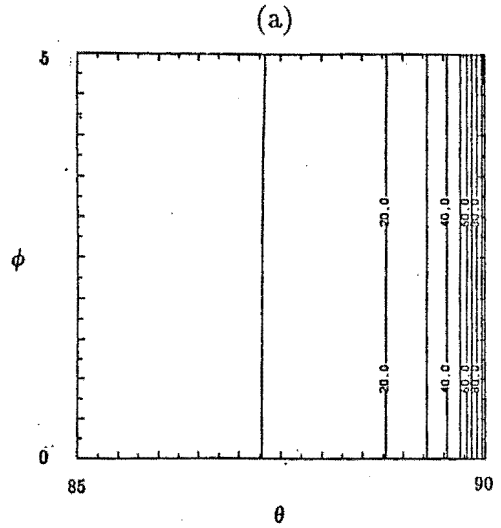

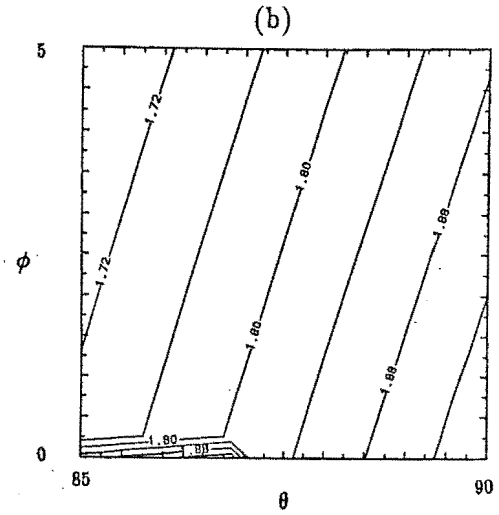

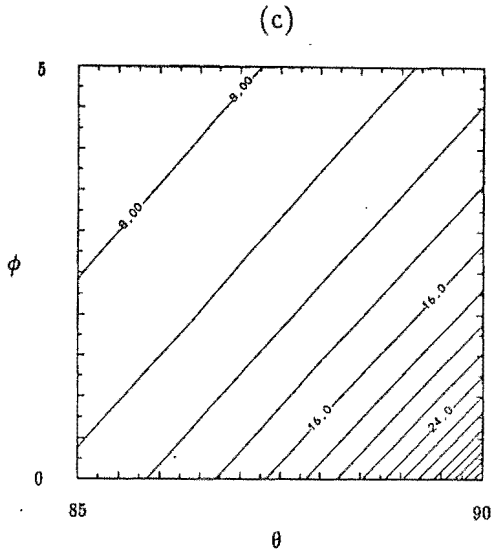

Figure 2.5 : Expected polarisation ratios for the C_{4v} center as the E-vector of the laser radiation deviates by θ and ϕ degrees from the crystallographic (100) axis (see figure A.7) under the following [absorption, emission] conditions:
(a) [π,π] -(YY:YX of 1:0)
(b) [σ,π] - (YX:YY of 1:0)
(c) [σ,π] - (YY:YX of 2:1)

Chapter 3

Experimental Methods and Instrumentation

This chapter comprises four sections discussing in turn the preparation of the crystals (3.1) and the cryosystem (3.2), the C.W. argon ion pumped dye laser system (3.3) and the pulsed dye laser system (3.4).

3.1 Crystal Preparation

All crystals in this work were grown by the author using the Bridgman-Stockbarger technique. Stock material of CaF_2 , SrF_2 and BaF_2 crystal offcuts , purchased from Optovac Inc., was crushed into tiny grains. The charge material consisting of these AE fluoride crystal grains and the dopant in the form of PrF_3 powder was transferred to the bore of a cylindrical graphite crucible of 20cm outer diameter, 10 cm bore and 40cm length. The bottom of the bore consists of a cone approximately 1-2 mm deep. The crucible was slowly lowered through a temperature gradient in an Arthur D. Little RF furnace evacuated to a pressure of less than 10^{-4} torr. For successful crystal growth , the temperature profile should consist of a gradual

descent, a sharp decrease followed by another gradual descent (Landise[1972]). This profile was created on a graphite cylinder (150mm long, 35mm inner diameter) heated inductively by a 12 turn coil with a power setting of approximately 6.5kW. The crucible was lowered through the graphite cylinder at a rate varying from 4 - 8 mm per hour.

A layer of insulation fibre is placed between the coil and this graphite cylinder. Several different fibre blankets were tried. Fibrefrax[1] (96 kg/m^3) gave the best results both in terms of thermal durability and consistency of crystal quality. The Kaowool High Duty Blanket[2](density 96 kg/m^3) worked moderately well but often produced single crystals with polycrystalline formation in the top half. The 128 kg/m^3 version of the same Kaowool proved totally unsatisfactory and appeared to be performing below the manuafacturers specification of 1400^{0}C as the maximum recommended temperature for continuous use.

Single crystal boules were cut into 2 -3 mm slices using a rotary diamond saw and parallel flats were ground on two opposite ends of each slice. All the surfaces of the crystal slices were initially polished using various grades of abrasive paper and then given optically smooth surfaces by polishing with number 800 grit silicon carbide grains on the rough side of a piece photographic paper with water as a lubricant. The (111) cleavage planes (fig. 3.1) of the cubic AE fluoride crystals provided a reference for orienting the crystals for polarisation work. For the parent AE fluoride crystals doped with low concentration of Pr^{3+}, well defined cleavage planes were usually obtained. The mixed AE fluoride crystals are more brittle and less tolerant to mishandling when they were being cleaved or cut. They may yield badly formed planes or shatter when cleaved or may spontaneously cleave when cut. These difficulties were most frequently encountered in crystals doped with Ba^{2+}. When it was not possible to obtain two clean (111) planes for mounting, the plane with the best cleavage was then used as a reference with the less well formed plane grounded and smoothed to fit the mount.

---

[1]Union Carbide, USA

[2]*Morganite Ceramic Fibres Ltd Australia*

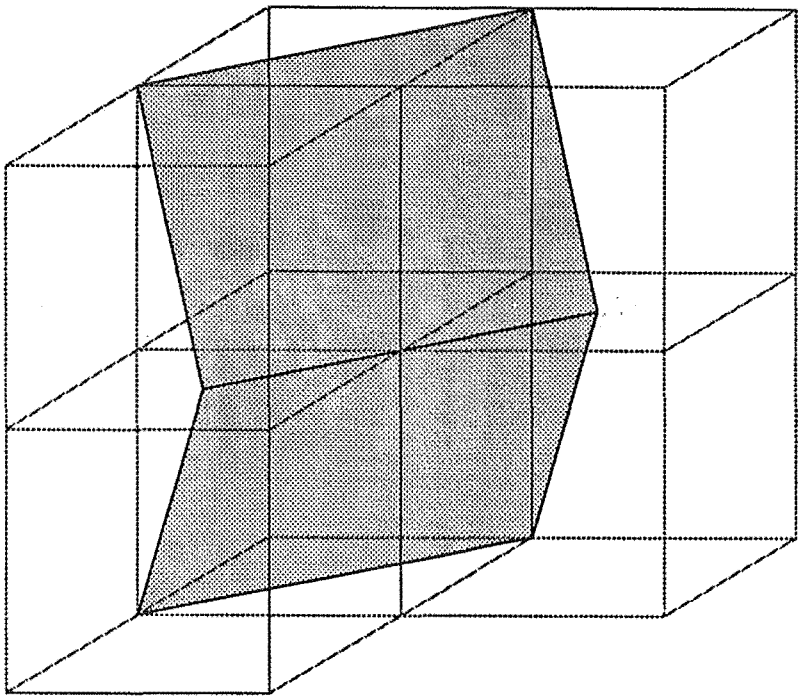

Figure 3.1: The intersecting (111) reference planes (shaded) used for orienting the crystals.

The crystals were deuterated using the process prescribed by Hall and Schumacher [1962]. This process involved heating the crystal in the presence of molten aluminium and up to one atmosphere of deuterium. The crystal and aluminium were thoroughly cleaned with acetone beforehand to remove any residual grease. Two pieces of aluminium coil sandwiched the crystal , which was placed in a alumina crucible and lowered to the bottom of a quartz tube. The tube was attached to a gas filling and evacuation system (fig. 3.2). Normally the system was flushed twice with deuterium, after which a partial deuterium pressure of 20mmHg was introduced. A temperature of $850°C$ was then maintained for 36 - 72 hours in a cylindrical furnace where the length of the quartz tube was inserted. After that time, all the samples were either quenched at room temperature or annealed if they consistently did not survive the quenching process. Mixed crystal samples, especially those doped with Ba^{2+} were more brittle after the hydrogenation process and hence they were mostly annealed.

3.2 Cryosystem

For spectroscopic studies, it was necessary to cool the crystal samples to temperatures as low as 10K, and for this, a CTI-Cryogenics Model 21C two-stage closed-cycle helium refrigerator was used. The crystal holder consisted of a 35mm long copper plate attached to a circular base which mates with the cold head of the refrigerator. There were two 2mm slots on the plate, 15mm apart. Two crystals could be mounted at a time, and lying across each slot. This arrangement allowed observation of the emission in two opposite direction. The emission in one direction could be used to measure the fluoresence spectra while the broadband emission could be measured in the other direction. Indium foil was used to provide improved thermal contact between surfaces. Precise temperature control of the block to 0.1K was possible with a Model 4025 Cryogenic Thermometer/Controller manufactured by Palm Beach Cryophysics Inc. This unit sensed the temperature measured by a silicon diode located at the base plate of the cryosystem second stage and regulated the temperature by adjusting the width or frequency of the current pulses to a heating

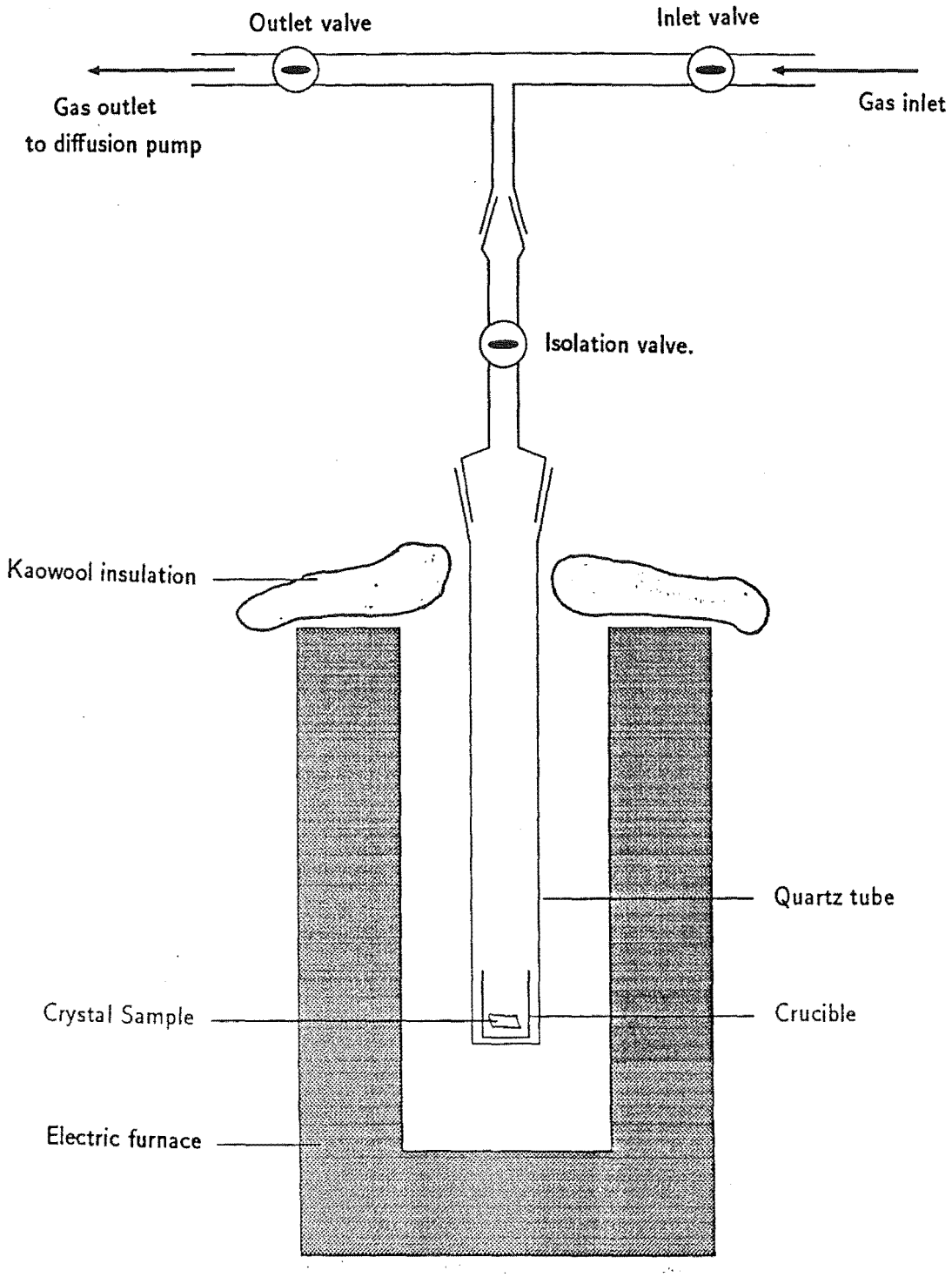

Figure 3.2: Gas filling and evacuation system used for hydrogenation of crystals

element. Most spectral features in this work remain unchanged by temperature increases up to 25K and the majority were recorded at a nominal temperature of 11K as read from the cryogenic controller unit.

3.3 LSE on the CW laser system

A Spectra Physics model 171 , 15W argon ion laser tuned to peak at 514.5 nm, with typical power settings around 2 watts pumped a Spectra Physics model 375 dye laser. The peak output of the dye laser using fresh Rhodamine 590 dye started at approximately 150mW and decreased with dye age. The rate at which the power drops depend on the amount of usage and the dye is usually changed when the peak output falls below 60mW. The measured bandwidth of the dye laser was approximately $0.5cm^{-1}$. The addition of a three plate birefringent filter rotated by a 0.5mm/rev micrometer shaft substantially improved the perfomance of the model 375 unit. The micrometer could be driven manually , electronically[3] or by computer control[4]. A mechanical reproducibility of better than 10^{-3}mm in the micrometer drive was apparent. The frequency output using this scanning system was linear over the whole Rhodamine 590 lasing range and could be reset to within $1cm^{-1}$ between sucessive electronically controlled scans.

To obtain broadband excitation spectra , the crystal fluoresence was collected by a 10cm focal length lens focussed onto a 1/4 metre Bausch and Lomb monochromator with slits set to give a bandpass of approximately 3nm. The grating was adjusted to the 625 - 640 nm range to monitor the fluoresence transitions from the $^1D_2$ multiplet to the broad upper levels of the $^3H_4$ multiplet and to reject the laser pump frequencies. Red Corning filters (CS2-64 and CS2-61) were sometimes used to provide further rejection of the laser frequencies. The signal from a thermoelec-

[3]drive unit and mechanical couplings were designed and built by Ross Ritchie and Wayne Smith respectively.

[4]software added by the author to include routines to drive the stepper motor.

trically cooled (-25°C) Thorn EMI 9558 PMT[5] with an S20 response was recorded by a Keithley Instruments 610B Electrometer which gave an analogue reading corresponding linearly to the fluorescence intensity. The electrometer output was digitised by a voltage to frequency converter , together with a frequency counter with a dynamic range of 0 - 26000 counts, to give an immediate digital display of fluorescence strength. An A/D converter also digitised the electrometer signal for storage and display by an Apple IIe computer. In the studies of the bleaching hydrogenic centres, the electrometer signals were directed to a strip chart recorder.

The emission spectra were measured using a 0.85m focal length SPEX 1403 double monochromator. This spectrometer was equipped with two 1800 grooves/mm gratings blazed at 500nm. The specified dispersion was $10cm^{-1}/mm$ at 514.5nm. To equalize the gratings response to different light polarisation , a Hanle quartz wedge polarisation scrambler was placed over the input slit of the spectrometer. An RCA C31034 PMT themoelectrically cooled to -25°C was used with this spectrometer, in conjuction with a Princeton Applied Research model 1121 discriminator and model 1112 photon counter module. A parallel interface from the module to the Apple IIe provided the means for recording photon counts. Scanning of the Spex1403 was done directly through a Spex industries CD2A driver or indirectly via the Apple IIe controlling the driver.

In the measurement of polarised spectra, the dye laser polarisation was set by a Spectra Physics 310 polarisation rotator. An ordinary polaroid sheet mounted on a rotating frame served as an analyzer in the visible region while an HRB polaroid sheet was used in the infrared region for monitoring the emission polarisation. These were placed between the collimating and focussing lens of the collection optics.

A mechanical chopper with a non-linear response of angular speed vs voltage was used for time resolution laser selective excitations. Figure 3.3 gives the details of this chopper. The adjustable cones together with the variable speed allow some control of the gate width and the gate and sampling period separation. A maximum switching rate of approximately 200Hz gave a minimum gatewidth of $600\mu s$ which

[5]PMT-photomultiplier tube

limit its usefulness to study of transitions with fluoresence lifetimes longer than a few hundred microseconds. Its use for studying the F^- centres was therefore more succesful than those of the more rapidly decaying H^- centres.

3.4 LSE on the pulsed laser system

A Photochemical Research Assn. Inc. model LN1000 nitrogen laser, pumping a model LN107 tunable dye laser, provided the excitation source for pulsed studies. The output of the N_2 laser at 337.1nm provided pulses with an average energy of 1mJ , a FWHM[6] of 600ps and variable repetition rates up to 20Hz. A selection of dyes (Coumarin 460, Coumarin 480 and Rhodamine 640) were used to cover a 400 - 610 nm wavelength range with a output bandwidth of 0.04nm and a maximum average pulse energy of 100uJ. A model DD1790 drive unit is used to scan the dye laser .

For lifetime measurements, the Bausch and Lomb photodetection arrangment as described in section 3.3 was used. The anode of the 9558 PMT was connected to a Stanford Resarch Systems Inc. SR250 Gated Integrator Boxcar with a 50Ω cable and a matching termination. An RCA 931A PMT with a S11 response monitoring the N_2 laser pulses was used to trigger the boxcar. The signals could be amplified or filtered by the boxcar before being directed to a model SR235 Analog Processor. The signal amplified on the analog processor was then collected by an IBM PC via a model SR245 Computer Interface. A TTL synchronizing pulse from the *BUSY* output of the boxcar when it was triggered was first received by channel 1 of the *SYNCH* input at the SR245 which then signaled the PC to begin data acqusition. Gate delays appropriate for a particular transient were automatically varied in a time scan by supplying a voltage ramp at the *EXTERNAL DELAY CONTROL* input of the boxcar. This analogue ramp was generated by the PC through channel 8 of the computer interface. The width of the gate was set between 5 - 15μs to suit the lifetime of the transient.

[6]full width at half maximum intensity

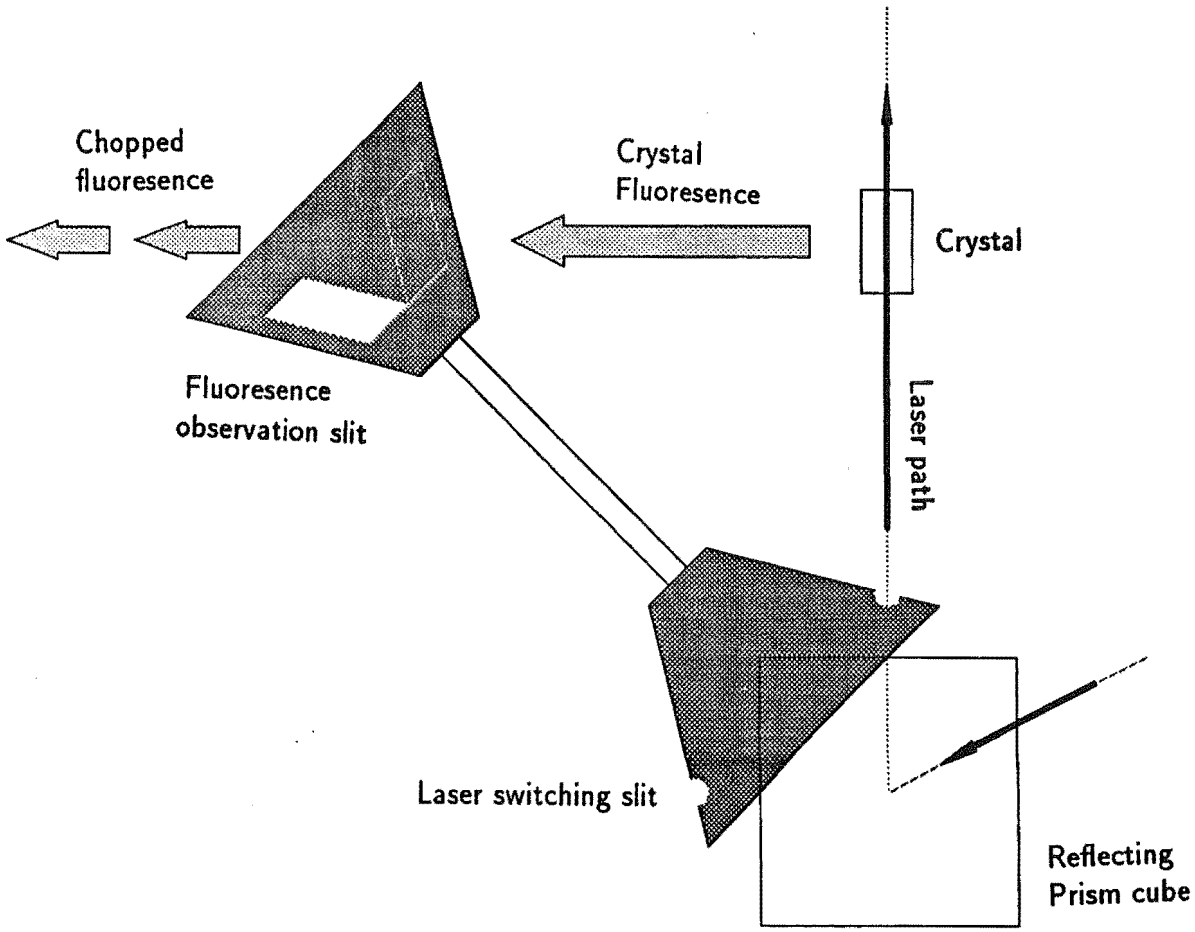

Figure 3.3: Mechanical chopper system for time resolution measurements.

The SR265 software was sufficiently versatile to allow wavelength scans rather than time scans with some modification of the hardware and software. These modifications were carried out here to allow all the experiments which were being run on the CW system to be done on the pulsed system[7]. A new serial line from the second port (COM 2) of the IBM PC was configured to communicate with the DD1790 drive unit. This allowed the IBM to control the driver unit while still having data reception at port COM 1. It would have been possible to disable the *EXTERNAL DELAY CONTROL* by modifying the software, but it was much more straightforward just to unplug channel 8, which effectively put the delay control back on manual control through the boxcar. Each synchronizing pulse then initiated data acquisition and stepping of the grating on the dye laser without moving the preset gate delay. A subroutine was written to provide the control characters which drove the DD1790.

Using this modified system, broadband excitation fluoresence could be performed using the same arrangement as that previously described with the Bausch and Lomb. Selective excitation however was performed with the 0.75m SPEX1700 single monochromator with the same 9558 PMT tube being used. The grating fitted was blazed at 750nm with a dispersion of 1.06nm/mm. A 5 - 10% intensity jitter of the N_2 laser pulses limited the sensitivity of this system for detecting weaker signals. Some improvement was possible by using the *ARGUMENT FILTER* on the the SR235 analogue processor to smooth the signal electronically by rejecting the higher frequency signals. Since only the transition intensities and not lifetimes were required during an excitation scan, it was advantageous to remove the 50Ω termination. This provided a much stronger and smoother signal.

[7]Modifications carried out by the author

Chapter 4

Laser Spectroscopy of the Mixed Crystal Fluorine Centers

When the Pr^{3+} dopant level is low ($< 0.05\%$) in the CaF_2 and SrF_2 hosts, the C_{4v} center with an F^- anion in the NN interstitial, is the most energetically favourable center [Corish et al, 1982] . The predominant features in the excitation spectra of these crystals are those belonging to the C_{4v} center, which has been thoroughly studied by Reeves[1987]. The mixed crystal centers are derived from these parent C_{4v} centers by the additional of further alkaline earth dopants, which lowers the C_{4v} symmetry. These mixed crystal centers were found to have four common spectral characteristics base mainly on the polarisation features they display. The spectroscopic results from studies of the mixed crystal fluorine centers in the four mixed crystal systems $Ca_{1-x}Sr_xF_2 : Pr^{3+}$, $Ca_{1-x}Ba_xF_2 : Pr^{3+}$, $Sr_{1-x}Ca_xF_2 : Pr^{3+}$ and $Sr_{1-x}Ba_xF_2 : Pr^{3+}$, are presented in sections 4.1, 4.2, 4.3 and 4.4, respectively. Discussions of possible models for the mixed crystal centers are also given.

4.1 Mixed Crystal Centers in $Ca_{1-x}Sr_xF_2 : Pr^{3+}$

4.1.1 The Excitation Spectra

Optical absorption is the most straightforward way of determining the relative distributions of different types of centers. However, in the case of Pr^{3+}, the absorption transitions from the $^3H_4$ to $^1D_2$ multiplet are quite weak, being spin forbidden. The excitation spectra reveal the same transitions, which can be recorded at much greater sensitivity for both the C_{4v} center and its modifications because they are effcient emitters. Excitation spectra were therefore preferentially used to determine the absorption lines of the centers present.

Broadband excitation spectra of the $Ca_{1-x}Sr_xF_2 : Pr^{3+}$ crystal system are presented in figure 4.1. The excitation spectra of transitions to the two lowest levels, D_1 and D_2 of the C_{4v} center in the $^1D_2$ multiplet appear as sharp and intense lines in the parent crystal (fig.4.1(c)), with the satellite lines of the mixed crystal centers readily apparent. It is evident that the parent $CaF_2 : Pr^{3+}$ crystal showed traces of the same satellite lines, indicating the presence of the Sr^{2+} dopant alkaline earth cations as inadvertent trace impurities in the crystal growing materials supplied.

At 0.5% concentration of the Sr^{2+} dopant (fig4.1(b)), the line labelled K in fig 4.1(c) present in the parent crystal was absent while the line labelled L had diminished in strength. As the concentration of the alkaline earth dopant increased from 0.5% to 1%, the satellite lines become stronger while the line L grew even weaker. The centers giving rise to the K and L features will be discussed at the end of this section. A general broadening of linewidths was also observed to occur with increasing concentration of the alkaline earth dopant. This inhomogeneous broadening of the lower levels in a multiplet is attributed to the static lattice strain and the variety of centers inherent in all crystals with chemical impurities .

The excitation spectra of each of the Pr^{3+} centers were seperately recorded by

monitoring a single isolated fluorescence line of each center in turn (fig. 4.2). Two spectral pattern types are apparent. The first resembles that of the C_{4v} center with just two excitation lines D_1 and D_2 of the $^1D_2$ multiplet, consistent with an unchanged Pr^{3+} C_{4v} site symmetry (fig. 4.2(b)).

The second spectral pattern consists of four excitation lines to the D_1 and D_2 levels (fig. 4.2(a) and (c)), from the splitting of the ground state γ_5 level of the parent C_{4v} center, which would occur for any Pr^{3+} site symmetry lower than that of the parent C_{4v} center (fig. 4.3). One or more dopant alkaline earth cations, located in either the NN or NNN cation spheres in a position not along the C_4 axis of the C_{4v} center, would lower the symmetry of the parent center to give the four lines observed in the excitation spectra of the lower symmetry centers. The choice of ground state irreps for a lower symmetry center derived from a parent C_{4v} center is restricted to γ_1 or γ_2 for the C_s symmetry configurations and γ_2 or γ_4 for the C_{2v} symmetry configurations.

4.1.2 The Polarised Fluorescence Spectra

For each of the distinct centers found in the excitation spectra monitoring a specific transition, the polarised fluorescence spectra from the D_1 level to the $^3H_4$,$^3H_5$,$^3H_6$ and $^3F_2$ multiplets will be discussed. Since it is useful to compare the polarised fluorescence spectra of these centers, transitions to a particular multiplet for each of these centers will be discussed simultaneously.

The $^3F_2$ multiplet

This multiplet has the simplest spectral features as, with a J value of two, it can have a maximum of five lines. Three distinct polarisation patterns emerged in the fluorescence spectra of the three mixed crystal centers (fig. 4.4). The first clearly shows (YX):(YY) polarisation intensity ratios close to 0:1 or 1:0 (fig. 4.4(a)(i)) in all

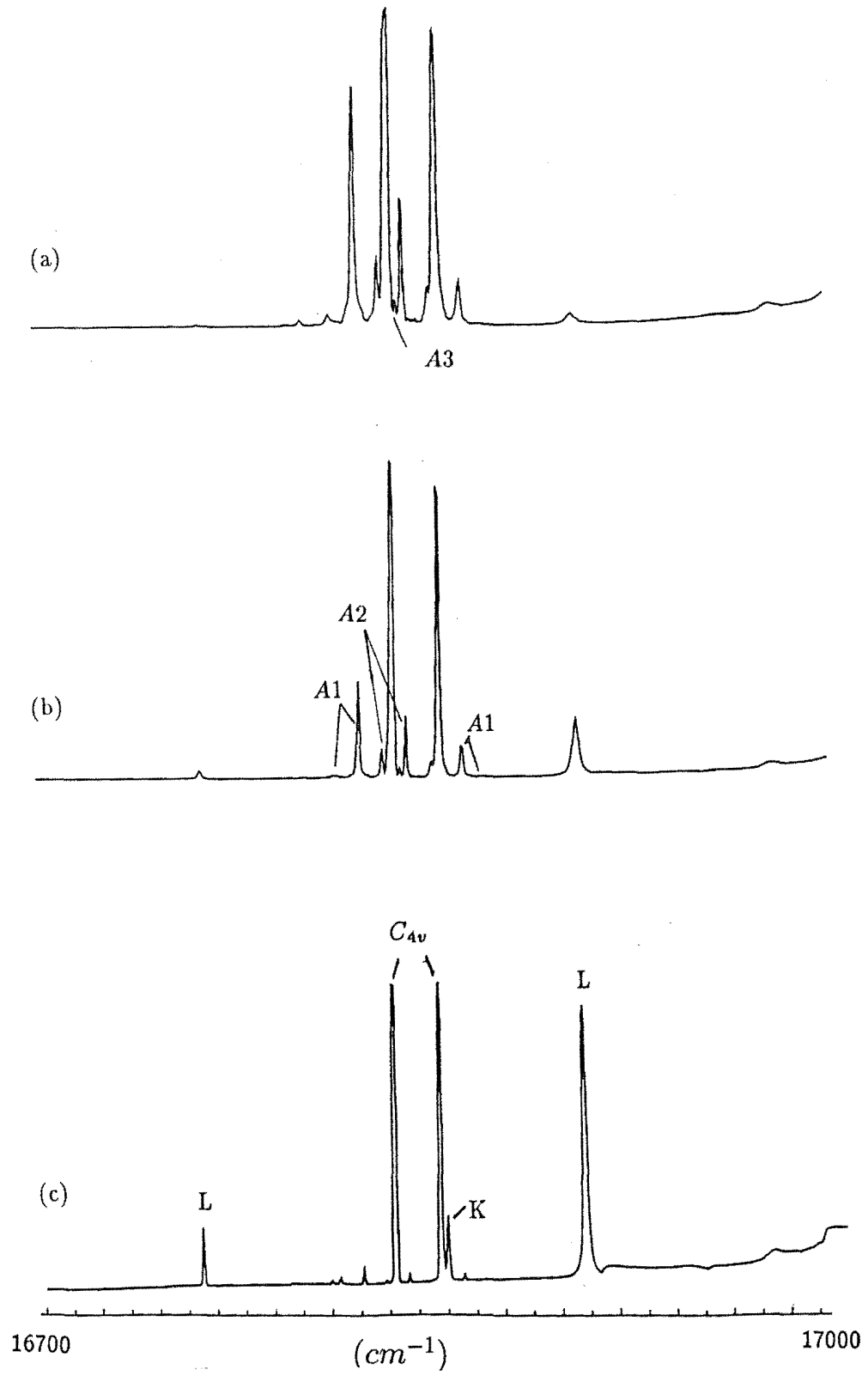

Figure 4.1 Broadband excitation spectra of the $Ca_{1-x}Sr_xF_2 : Pr^{3+}$ crystals, monitoring the $D \rightarrow Z$ transitions at 11K.

(a) 1% Sr^{2+} doping **(b)** 0.5% Sr^{2+} doping **(c)** undoped parent $CaF_2 : Pr^{3+}$ crystal.

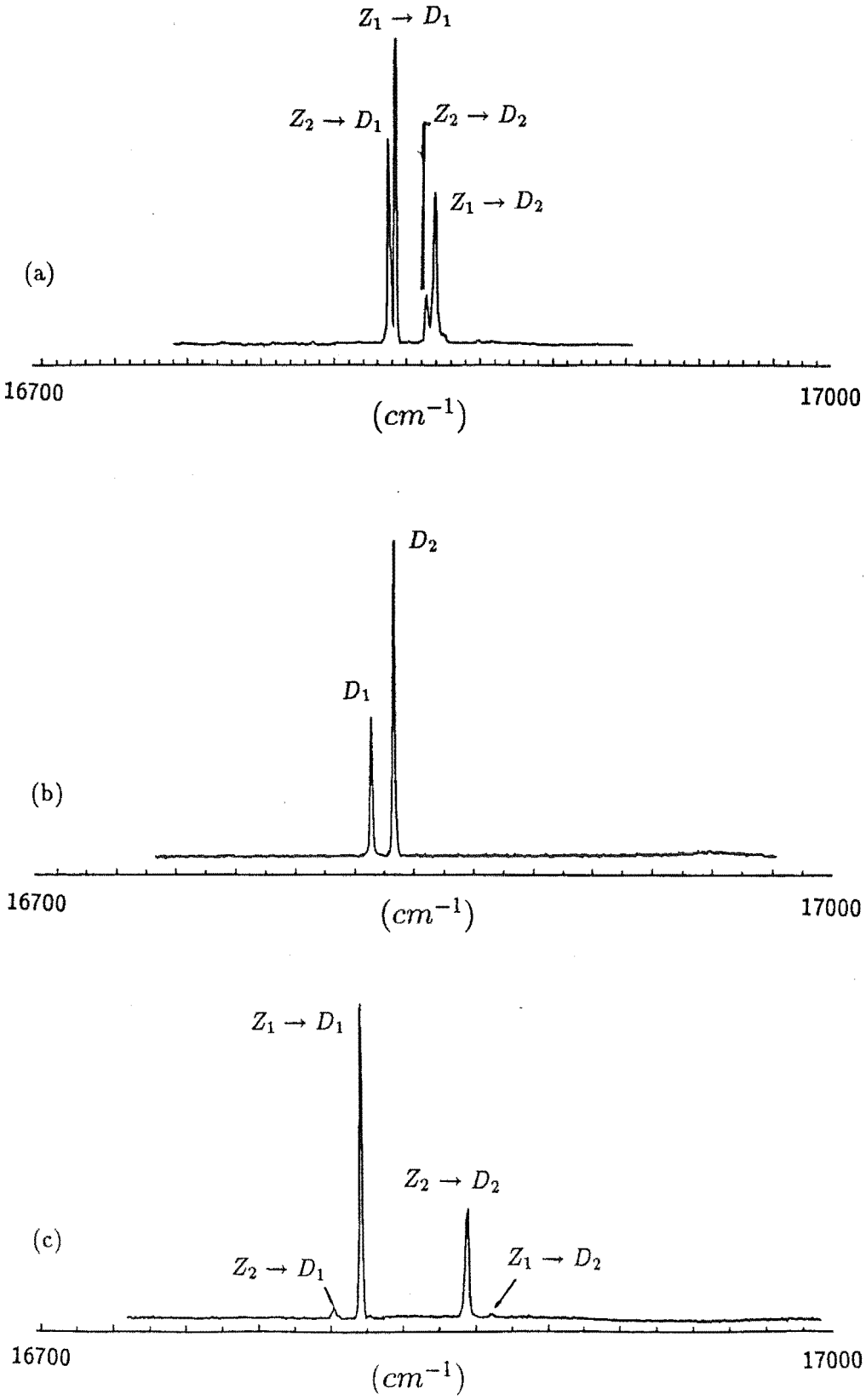

Figure 4.2 Selective excitation spectra of the mixed crystal centers in the 0.5% Sr^{2+} doped CaF_2 cr at 11K obtained by scanning the dye laser and monitoring specific transitions.

(a) the $A3$ center monitoring $14622cm^{-1}$. **(b)** the $A2$ center monitoring $14614cm^{-1}$. **(c)** the $A1$ center monitoring $14605cm^{-1}$.

its transition. Further, the $D_1 \rightarrow W_3$ ($11437cm^{-1}$) and the $D_1 \rightarrow W_5$ ($11422cm^{-1}$) transitions were extinguished in both the X and Y analyzer directions (fig. 4.4(a)(ii)) when the laser polarisation was switched to the Z-direction. Centers exhibiting these polarisation behaviour of transitions are classified as $A1$ type centers.

The second polarisation pattern is similar to that for the C_{4v} parent center with observed (YX):(YY) ratios of approximately 1:0 and 1:2 (fig. 4.4(b)). This center is classified as the $A2$ type center. The third type is classified as the $A3$ type center, which has similar polarisation ratios to the C_{4v} center but clearly has more lines (fig. 4.4(c)), as a result of the single C_{4v} doubly degenerate $W_3(\gamma_5)$ level being split into two distinct levels. With the laser polarised E_Z, both the $A2$ and the $A3$ centers exhibit little intensity difference for their transitions, comparing the X and Y polarisation directions[1].

All mixed crystal system centers display only one of four polarisation patterns and are thus classified accordingly as $A1$,$A2$ or $A3$ centers, with the fourth type, the $A4$ center discussed in section 4.4

Using the selection rules and tables 2.3 to 2.6 together with knowledge of the irreps allowed for the ground state, some idea of the geometry of the three mixed crystal centers can be gained. The $C_s(b)$ configuration with a γ_2 ground state is the only possible configuration, which would explain the observed polarisation behaviour of the $A1$ center. The polarisation behaviour observed for the $A2$ center is consistent with a C_{4v} symmetry Pr^{3+} site in the alkaline earth cubic lattice. For the $A3$ center, the present set of data appears to indicate a model with a $C_{2v}(a)$ site configuration with a γ_2 or γ_4 ground state. Contradictions exist with regards to this assignment and these are discussed in section 4.1.3.

[1]Refer to chapter 2 for the definition of E_Z, X and Y polarisation direction

The $^3H_6$ multiplet

The (YX):(YY) ratios of 1:0 and 0:1 which are characteristic of the $A1$ center are apparent in the transitions to this multiplet (fig. 4.5(a)). The splitting of the C_{4v} center $X_1(\gamma_5)$ level into two levels having γ_1 and γ_2 irrep labels under the C_s symmetry group, is evident at $12611cm^{-1}$ and $12605cm^{-1}$. Similar splittings for the broader X_4 and $X_9, (\gamma_5)$ levels of the C_{4v} center were not observed, most likely because the splittings are small and hence cannot be discriminated within the broadened transition.

For the $A2$ center in this multiplet, the polarisation observed is similar to that of the C_{4v} center, but with the transition from the D_2 level being stronger, as is evident when comparing the $D_2 \rightarrow X_1$ and $D_1 \rightarrow X_1$ transitions at $12618cm^{-1}$ and $12609cm^{-1}$ (fig. 4.5(b)) of the $A2$ center with the corresponding transitions of the parent C_{4v} center. The line at $12413cm^{-1}$ assigned as the $D_2 \rightarrow X_3(\gamma_1)$ transition is more prominent than the equivalent transition in the parent C_{4v} center. Differences in the wavefunctions of the levels for these two C_{4v} symmetry centers would give rise to the dissimilar transition probabilities observed for equivalent transitions in the parent and mixed crystals.

Comparison of the polarised fluorescence of the $A3$ and C_{4v} centers reveals two very similar patterns of fluoresence spectra. In most cases, the levels of the $A3$ center shift by less than $5cm^{-1}$ from the corresponding parent transitions (fig 4.5(c)(i)). To check that the parent C_{4v} center was not being simultaneously excited, the fluorescence spectra of the parent C_{4v} center and the $A3$ spectra were recorded several times and succesive scans of these two centers revealed that the C_{4v}, $D_1 \rightarrow X_1$ transition is $0.3cm^{-1}$ lower in energy than the $D_1 \rightarrow X_2$ transition of the $A3$ center (fig. 4.6(c)(ii)). The degeneracy of the $X_1(\gamma_5)$ level of the parent C_{4v} center is lifted to give two levels, as shown in the spectra at 12628.1 and $12629.6cm^{-1}$, when the symmetry is lowered by the cation subsitutions which gave rise to the $A3$ center.

Given the similarity of the $A3$ and C_{4v} fluorescence spectra and the proximity of the $A3$ satellites to the parent C_{4v} transition observed in the $^1D_2$ level, it is

concluded that the $A3$ center is derived from a small perturbation of the C_{4v} center. This is discussed further in section 4.1.3

The $^3H_5$ multiplet

The characteristic 1:0 and 0:1 polarisation ratios of the $A1$ center manifest themselves again in this multiplet, with the obvious splitting of the C_{4v}, $Y_3(\gamma_5)$ level into two levels , as shown by the two $D \rightarrow Y$ transitions at $14544cm^{-1}$ and $14528cm^{-1}$ (fig 4.6(a)).

As is the case for the $^3H_6$ multiplet, the major difference in the fluorescence spectrum between the parent and the mixed crystal C_{4v} center is the relative transition intensities to levels transforming as the γ_3 irrep, which are stronger in the mixed crystal. Another obvious example of this is the transition to the $Y_4(\gamma_3)$ level of the $A2$ mixed crystal C_{4v} center at $14520cm^{-1}$ (fig 4.6(b)). The $Y_5(\gamma_5)$ level is also less broad compared to transition to the corresponding γ_5 level in the parent C_{4v} center, and the peaks of the transitions from the D_1 and D_2 levels to this level are clearly distinguished at 14461 and $14469cm^{-1}$ for the $A2$ center.

Figure 4.6(c) gives the polarised fluorescence spectra of the $A3$ center, which looks similar to the fluorescence spectra of the parent C_{4v} center. The splitting of the parent C_{4v} center,$Y_3(\gamma_5)$ level is observed at 14563 and $14565cm^{-1}$, labelled Y_4 and Y_3 respectively.

The $^3H_4$ multiplet

The $D \rightarrow Z$ transitions of the $A1$, $A2$ and $A3$ centers are shown in figure 4.7(a),(b) and (c) respectively. Features of the polarisation behaviour previously described for transitions to the other multiplets apply to this multiplet as well. The broad linewidth, approximately $50cm^{-1}$, of the C_{4v}, $Z_6(\gamma_5)$ level precludes any opportunity

of observing splitting into two levels in the spectra for either the $A1$ or $A3$ centers.

The obvious lines at $16704cm^{-1}$ for the $A2$ center and $16632cm^{-1}$ for the $A3$ center are unassigned since it is unclear whether they are of an electronic or vibronic origin. In the case of of the $A2$ center, it is unlikely that the $16704cm^{-1}$ line is of pure electronic origin, as a $D_1(\gamma_1) \rightarrow Z_2(\gamma_2)$ transition is allowed only via a magnetic dipole transition, and the intensity of this transition together with its (YX):(YY) polarisation ratio of 1:2, is not consistent with what might be expected for a magnetic dipole transition which would have given a polarisation ratio of 0:1.

4.1.3 Model Assignments

The summary of the spectroscopic features and discussion of possible models for each of the mixed crystal centers is given below. Table 4.1 lists the energy levels assigned to the $A1$, $A2$ and $A3$ centers for the $Ca_{1-x}Sr_xF_2 : Pr^{3+}$ crystal.

The $A1$ center

The main spectroscopic features of the $A1$ center include:

(i) a ground state splitting of $8cm^{-1}$;
(ii) observed (YX):(YY) polarisation ratios of the type 1:0 and 0:1 when the laser is polarised E_Y;
(iii) extinction of certain transitions with the laser polarised E_Z.

From point (i), it is deduced that the $A1$ center has a symmetry lower than C_{4v}. With laser polarised E_Z, the transitions arising from a $C_s(a)$ type center would not be expected to display any polarisation effect. For a $C_s(b)$ type center, pump and decay transitions between levels with irreps $\gamma_1 \rightarrow \gamma_2$ and $\gamma_2 \rightarrow \gamma_1$ or vice versa,

would give a (YX):(YY) polarisation ratio of 0:0 which distinguishes this center from the $C_s(a)$ center. The $A1$ center exhibits polarisation ratios which are consistent with those expected from a C_s symmetry with a $C_s(b)$ configuration (points (ii) and (iii), refer also to table 2.4).

A single dopant alkaline earth cation substitution in the NNN cation sphere gives a $C_s(b)$ center configuration (fig. 2.2(b)(i)), however, being two lattice spacings away from the Pr^{3+} ion, it is not expected to affect the parent C_{4v} center significantly. In the NN cation sphere, there are two positions where a single cation substitution would give a $C_s(b)$ center (fig 2.2(a)(ii) and (a)(iii)). The ODNMR[2] data of Burum et al(1982) suggest that the lattice environment around the parent C_{4v} center, is more spatially extended in the region between the Pr^{3+} and the interstitial F^-. Therefore, the Sr^{2+} cation with a bigger ionic radius (1.12Å) than the Ca^{2+} cation (0.99Å), is more likely to substitute in this region with the arrangement of figure 2.2(a)(iii). Such a substitution would shift the interstitial F^- from its original position in the parent C_{4v} center. As the Sr^{2+} ion is bigger than the Ca^{2+} cation, it is most likely to open up the lattice even further, which may cause the interstitial F^- to relocate in a position off the original C_4 axis, towards the dopant Sr^{2+} cation. A net effect is a change in crystal field which is manifested in the seperation of the D_1 and D_2 levels, found to be $17cm^{-1}$ and $56cm^{-1}$ for the parent C_{4v} and $A1$ centers respectively.

More direct measurements, like ODNMR which have the potential to probe the actual positions of the F^- anions around the $A1$ center, through the coupling of the Pr^{3+} magnetic moment with the nuclear spin of the surrounding F^- ions could be useful in validating the model assigned.

The $A2$ center

For the $A2$ center, the spectral features of interest are:

[2]Optically Detected Nuclear Magnetic Resonance

(i) no observations of splitting in the ground state Z_1 level;
(ii) (YX):(YY) polarised fluorescence ratios of the type 1:2 and 1:0 when the laser is polarised E_Y;
(iii) equal emission intensities of the transitions observed for the X and Y analyzer directions with the laser polarised E_Z.

It is evident that the $A2$ center has C_{4v} symmetry (points (i) to (iii)). In the mixed crystal this is only possible for cation substitutions in the two NNN arrangements as shown in figure 2.2(b)(ii) & (iii). While both arrangements would give a symmetrical distortion to the lattice fluorines, the NNN substitution of figure 2.2(b)(ii), with the substitutional cation being two lattice cells away from the environment of the parent C_{4v} center is not expected to cause significant perturbation to the center. Hence, the substitution as represented by figure 2.2(b)(iii) seems the more likely configuration for the $A2$ center. Under this model, some axial repositioning of the interstitial F^- anion would occur, most likely towards the dopant Sr^{2+} and away from the Pr^{3+} ion. This is reflected in the differences in the crystal field levels observed for the parent C_{4v} and $A2$ centers.

The $A3$ center

For the $A3$ center, the following were observed:

(i) a ground state splitting of $2.6cm^{-1}$;
(ii) transitions with polarisation ratios of 1:2 and 1:0 similar to the C_{4v} center;
(iii) no polarisation effect for the laser polarised in the E_Z direction;
(iv) the levels in the D multiplet are very close (within $\sim 2cm^{-1}$) to the levels of the parent C_{4v} center;
(v) a fluorescence spectrum pattern very similar to the parent C_{4v} center.

Assignment of a model for the $A3$ center is made difficult by two conflicting pieces of evidence, one supporting and the other opposing the argument for a $C_{2v}(a)$ model

for the $A3$ center.

The $C_{2v}(b)$ and $C_s(b)$ configurations would give (YX):(YY) ratios of only 1:0 and 0:1 and the ratios observed (point(ii)) rule out these models.
While the $C_s(a)$ center could also give the observed polarisation ratios, the polarised spectrum of transitions to the $^3F_2$ multiplet is not consistent with the irreps of the levels expected for a C_s center. The lines at 11447 and $11452cm^{-1}$ originate from the lifting of the two-fold degeneracy of the C_{4v} $W_3(\gamma_5)$ level and if the $A3$ center has a C_s symmetry, one of these lines would have a γ_1 irrep and the other γ_2, both were observed to give (YX):(YY) ratios of 1:2. If the $A3$ center does indeed have a $C_s(a)$ symmetry configuration, then all the transitions observed would only have (YX):(YY) ratios of 1:2 since a C_s center has only two irreps possible for all levels. This is clearly not what was observed. Hence by the process of elimination, the polarisation ratios observed is consistent only with a $C_{2v}(a)$ configuration for the $A3$ center.

A model with a $C_{2v}(a)$ symmetry can only arise with two cation substitutions, however, it is statistically less likely for two substitutions of the host cations (fig 2.2(c)(i)) in the NN sphere at the concentration of the alkaline earth dopant used. The intensity of the emission from the $A3$ center is certainly weak, indicating that the population of the $A3$ centers is low. However, the relative intensities for the $A3$ center have not been found to increase more rapidly than those for the other mixed crystal centers, as the Sr^{2+} doping was increased from 0.5% to 1%. The relative intensity in fact increased linearly with concentration, statistically consistent with a single rather than a double substitution of the host cations around the parent C_{4v} center. The latter situation would give rise to a quadratic dependence in the rate of increase of the relative intensity. This cast some doubts as to whether the $A3$ center does have two cation substitutions

Of these two pieces of evidence, the observed polarisation ratios being consistent with a $C_{2v}(a)$ center appears to be stonger. Whether centers with two cation substitutions can occur without giving a quadratic concentration dependence in the relative transition intensities is debatable. It is possible that the substitutions giving

rise to the a $C_{2v}(a)$ symmetry ascribed to the $A3$ center becomes less favourable, thus accounting for the linear rather than a quadratic rise in relative intensities observed. However, this remains speculative at present.

From the small deviations of the levels observed for the $A3$ center from that of the parent C_{4v} center, it is deduced that the $A3$ center is a slightly modified parent C_{4v} center. Substitutions of Ca^{2+} cations by Sr^{2+} cations in the NN positions would probably produce too large a perturbation to account for the observed spectral features of this center. Hence the $A3$ center is more likely to comprise cation substitutions in the cation spheres beyond the NNN shells.

Based on the discussion of the last two paragraphs, a tentative model with a $C_{2v}(a)$ symmetry that only slightly perturbs the parent C_{4v} center is proposed and shown in figure 4.8

4.1.4 The K and L centers of the parent $CaF_2 : Pr^{3+}$ crystal

Apart from the C_{4v} center, two other centers have prominent lines in the broadband excitation spectra of the $CaF_2 : Pr^{3+}$ crystal, and these are identified as the K and L centers (fig 4.1). The presence of these centers is inhibited by the addition of the Sr^{2+} dopant with transitions of the K center vanishing at 0.5% doping of Sr^{2+}. Figures 4.9(a) and (b) give the excitation spectra in the $^1D_2$ multiplet for the K and L centers respectively.

The K center is noteworthy in having only a few observed transitions. In contrast to the C_{4v} center, there is only one absorption transition, at $16853cm^{-1}$, apparent in its excitation spectrum (fig. 4.9(a)) and its fluorescence spectrum (fig. 4.10) also has fewer transitions. The number of these transitions is consistent with that expected for a Pr^{3+} ion with a C_{3v} site symmetry (Table 4.2). The F^- trigonal center is unexpected for the $CaF_2 : Pr^{3+}$ crystal [Corish et al, 1982] though Kliava et al [1979] reported such a center labelled b′ in their experimental studies. Polarisation

Table 4.1 The energy levels (in cm^{-1}) of mixed crystal centers A1,A2 and A3 in $Ca_{1-x}Sr_xF_2:Pr^{3+}$. Uncertainties are $\pm$ 1 cm^{-1} unless otherwise indicated. The irrep labels for each level are given in brackets except for the *A*3 center where no point group has been assigned.

	A1		A2		A3
D_2	16867.7 $\pm$ 0.5	(γ_1)	16839.2 $\pm$ 0.5	(γ_3)	16851.6 $\pm$ 0.5
D_1	16821.5 $\pm$ 0.5	(γ_1)	16830.3 $\pm$ 0.5	(γ_1)	16837.0 $\pm$ 0.5
W_5	5400	(γ_2)	NA		-
W_4	5394	(γ_1)	-	(γ_4)	5385
W_3	5385	(γ_2)	5387	(γ_5)	5380
W_2	5339	(γ_1)	5332	(γ_1)	5328
W_1	-	(γ_1)	-	(γ_3)	-
X_{13}	-	(γ_1)	NA		-
X_{12}	-	(γ_1)	NA		-
X_{11}	4996	(γ_2)	NA		4969
X_{10}	4945	(γ_1)	-	(γ_3)	4895
X_9	-	(γ_2)	4958	(γ_5)	-
X_8	-	(γ_1)	4873	(γ_1)	-
X_7	-	(γ_2)	-	(γ_4)	-
X_6	4511	(γ_1)	-	(γ_3)	-
X_5	4505	(γ_2)	-	(γ_2)	4508
X_4	4426	(γ_1)	4484	(γ_5)	4474
X_3	4354*	(γ_2)	4418	(γ_1)	-
X_2	4217	(γ_1)	-	(γ_4)	4206
X_1	4211	(γ_2)	4223	(γ_5)	4205

Y_{11}	-	(γ_2)	NA		-
Y_{10}	-	(γ_2)	NA		-
Y_9	-	(γ_1)	NA		-
Y_8	-	(γ_2)	-	(γ_4)	-
Y_7	2405 $\pm$ 10	(γ_2)	2725	(γ_5)	-
Y_6	-	(γ_1)	-	(γ_2)	2398 $\pm$ 10
Y_5	-	(γ_1)	2371	(γ_5)	2317 $\pm$ 5
Y_4	2294	(γ_2)	2320	(γ_3)	2271
Y_3	2278	(γ_1)	2301	(γ_5)	2269
Y_2	2217	(γ_1)	2225	(γ_1)	2212
Y_1	2198	(γ_2)	-	(γ_2)	-
Z_9	-	(γ_1)	NA		-
Z_8	-	(γ_1)	NA		-
Z_7	577	(γ_2)	-	(γ_3)	553
Z_6	530	(γ_1)	532	(γ_5)	535
Z_5	480 $\pm$ 5	(γ_2)	509	(γ_1)	-
Z_4	435 $\pm$ 10	(γ_1)	466*	(γ_2)	437 $\pm$ 10
Z_3	190	(γ_2)	417 $\pm$ 10	(γ_1)	-
Z_2	8	(γ_1)	-	(γ_4)	3
Z_1	0	(γ_2)	0	(γ_5)	0

Levels which could not be unambigously assign are marked with an asterisk.
NA - Excited levels not applicable to the A2 C_{4v} center.

measurements were made for the K center in this work, but no obvious polarisation was apparent. A trigonal symmetry center gives a largely unpolarised spectrum for an excitation by $\gamma_3 \rightarrow \gamma_3$ transitions. Hence, the assignment of this center remains inconclusive at this stage. Table 4.2 lists the tentative energy level assignments made for this center.

Rare earth cluster centers are usually dissociated by heating the crystal to above 950K and this treatment reduced the L center concentration by one half while the K center remained unaffected. Up-conversion is also characteristic of some rare-earth clusters and only the L center showed some rather weak up-conversion. It is therefore concluded that the L center is a cluster center of as yet undetermined symmetry. The emission spectra from the D to the W,X,Y and Z multiplets (fig. 4.11) reveal patterns which are consistent with those expected for a cluster center , i.e. sharp lines appear right through the transitions to each mulitplet, as compared to sharp lines only for transitions to the lower levels of a multiplet for a single Pr^{3+} ion center. Table 4.3 gives the prominent lines as numbered in figure 4.11.

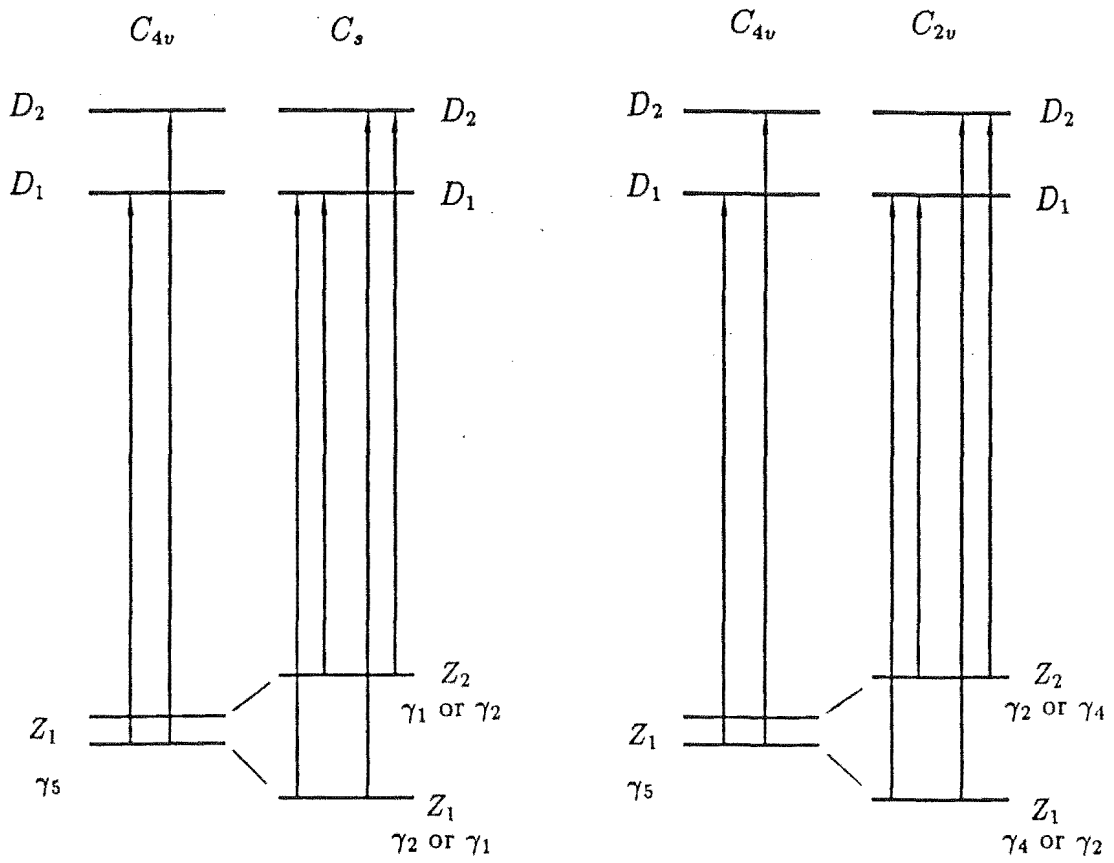

Figure 4.3 The splitting of the C_{4v} center ground state as the symmetry is lowered to C_s or C nd the absorption transitions from the ground states to the D multiplet.

Figure 4.4 $^1D_2 \rightarrow ^3F_2$ Polarised fluoresence spectra of the mixed crystal centers in the 0.5% Sr^{2+} doped CaF_2 crystal at 11K.

(a)(i) the $A1$ center, pumping $16821.5cm^{-1}$. Laser polarised E_Y
(a)(ii) the $A1$ center, pumping $16821.5cm^{-1}$. Laser polarised E_Z
(b) the $A2$ center, pumping $16830.3cm^{-1}$.
(c) the $A3$ center, pumping $16837.0cm^{-1}$.

(a) (i)
(YY)
W_3
W_5
W_2
(YX)
W_4
11360
11420
11480
11540
11600
(cm^{-1})

(a) (ii)
(ZY)
W_2
W_4
(ZX)
W_5
W_3
11360
11420
11480
11540
11600
(cm^{-1})

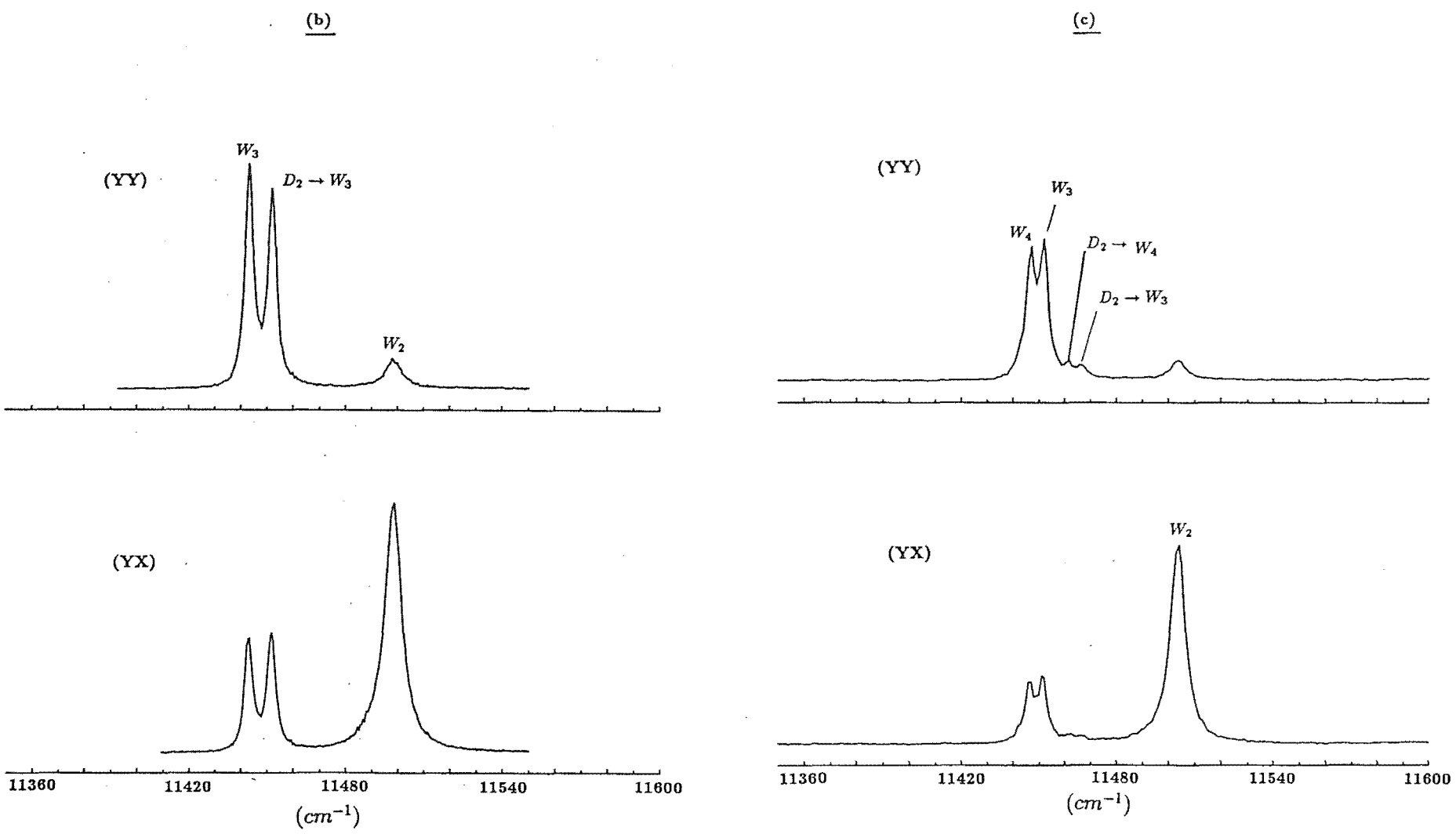
(b)
(YY)
W_3
$D_2 \rightarrow W_3$
W_2
(YX)
11360
11420
11480
11540
11600
(cm^{-1})
(c)
(YY)
W_3
W_4
$D_2 \rightarrow W_4$
$D_2 \rightarrow W_3$
(YX)
W_2
11360
11420
11480
11540
11600
(cm^{-1})

Figure 4.5 $^1D_2 \rightarrow ^3H_6$ Polarised fluoresence spectra of the mixed crystal centers in the 0.5% Sr^{2+} doped CaF_2 crystal at 11K.

(a) the $A1$ center, pumping $16821.5cm^{-1}$.
(b) the $A2$ center, pumping $16830.3cm^{-1}$.
(c)(i) the $A3$ center, pumping $16837.0cm^{-1}$.
(c)(ii) unpolarised fluorescence , pumping $16837.0cm^{-1}$to show the C_{4v},$X_1(\gamma_1)$ level (dotted curve) splitting into two levels in the A3 center.

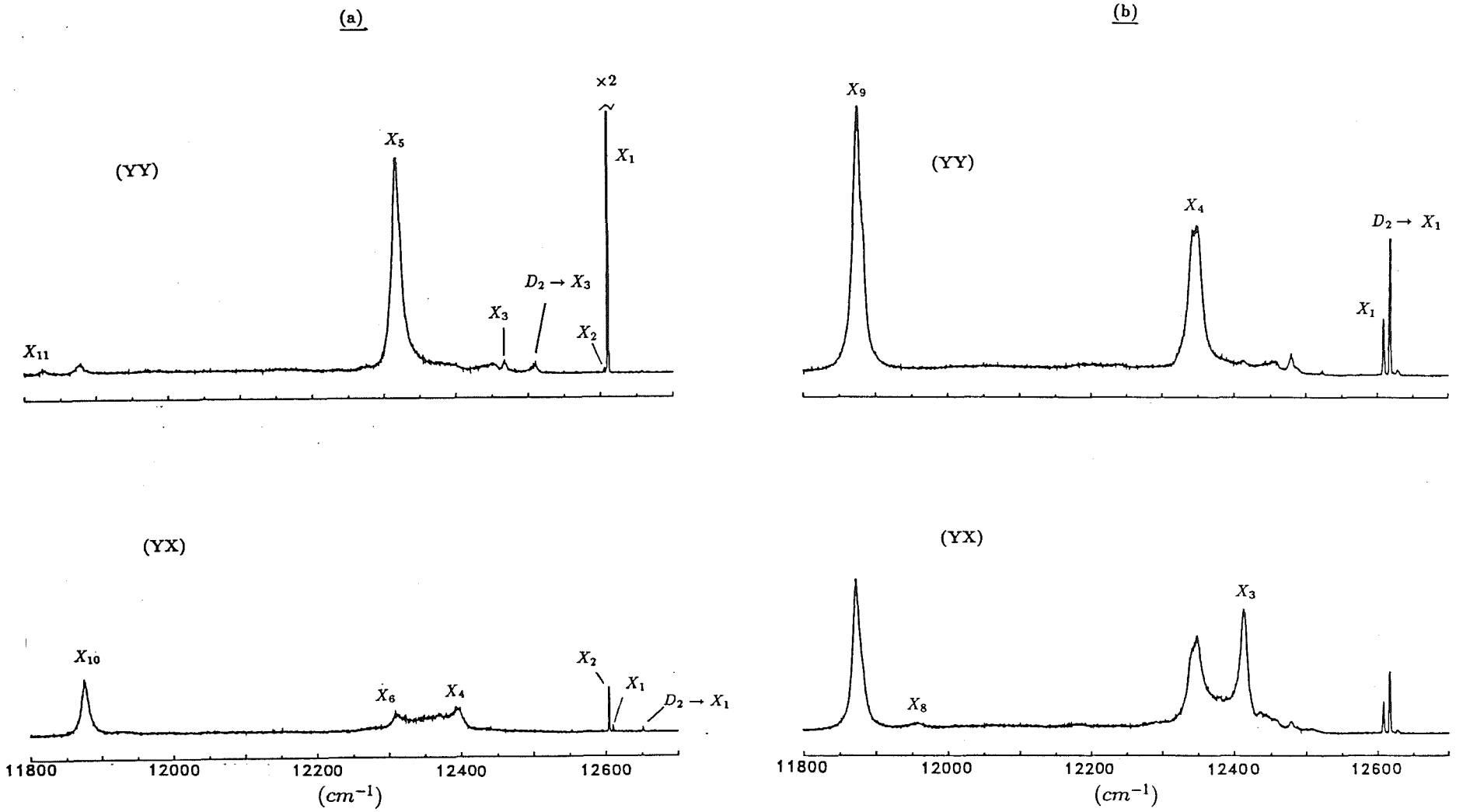
(a)
(YY)
×2
X_5
X_1
$D_2 \rightarrow X_3$
X_3
X_2
X_{11}
(YX)
X_{10}
X_6
X_4
X_2
X_1
$D_2 \rightarrow X_1$
11800
12000
12200
12400
12600
(cm^{-1})
(b)
(YY)
X_9
X_4
$D_2 \rightarrow X_1$
X_1
(YX)
X_8
X_3
11800
12000
12200
12400
12600
(cm^{-1})

(c) (i)
(YY)
X_2
X_1
X_{11}
X_5
$D_2 \rightarrow X_{11}$
(YX)
X_{10}
11800
12000
12200
12400
12600
(cm^{-1})

(c)(ii)
$X_2(A3)$
$X_1(A3)$
$X_1(C_{4v})$
12625
12632
(cm^{-1})

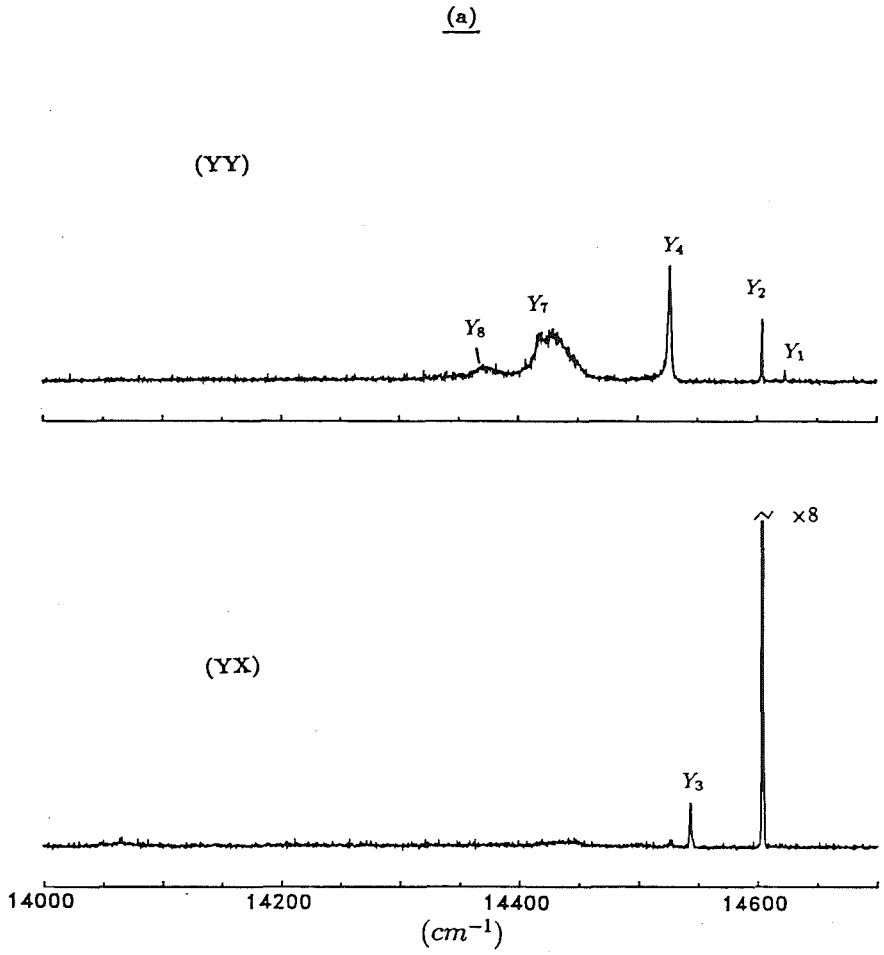

Figure 4.6 $^1D_2 \rightarrow ^3 H_5$ Polarised fluoresence spectra of the mixed crystal centers in the 0.5% Sr^{2+} doped CaF_2 crystal at 11K.

(a) the $A1$ center, pumping 16821.5cm^{-1}.
(b) the $A2$ center, pumping 16830.3cm^{-1}.
(c) the $A3$ center, pumping 16837.0cm^{-1}.

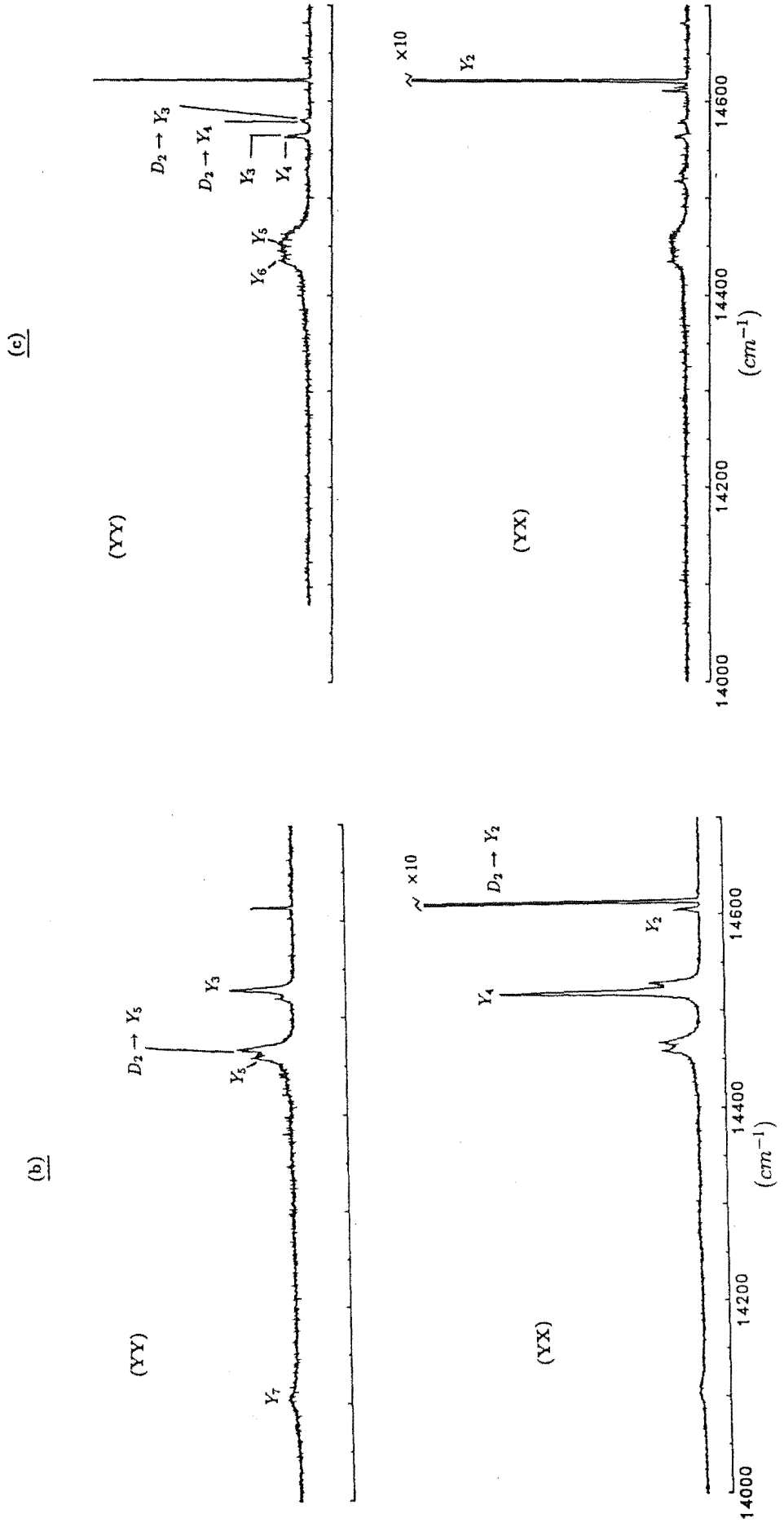
(c)
(YY)
$D_2 \rightarrow Y_3$
$D_2 \rightarrow Y_4$
Y_3
Y_4
Y_5
Y_6
(YX)
×10
Y_2
14000
14200
14400
14600
(cm^{-1})
(b)
(YY)
$D_2 \rightarrow Y_5$
Y_3
Y_5
Y_7
(YX)
×10
$D_2 \rightarrow Y_2$
Y_4
Y_2
14000
14200
14400
14600
(cm^{-1})

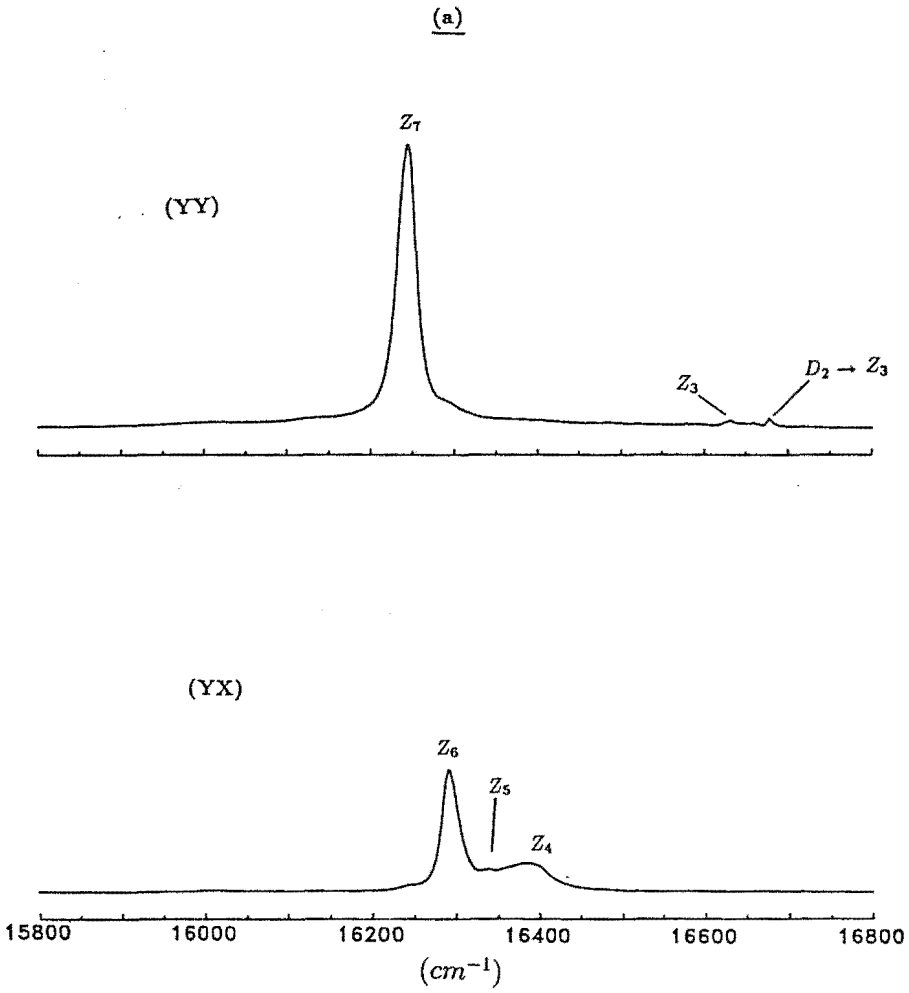

Figure 4.7 $^1D_2 \rightarrow ^3 H_4$ Polarised fluoresence spectra of the mixed crystal centers in the 0.5% Sr^{2+} doped CaF_2 crystal at 11K.

(a) the $A1$ center, pumping $16821.5cm^{-1}$.
(b) the $A2$ center, pumping $16830.3cm^{-1}$.
(c) the $A3$ center, pumping $16837.0cm^{-1}$.

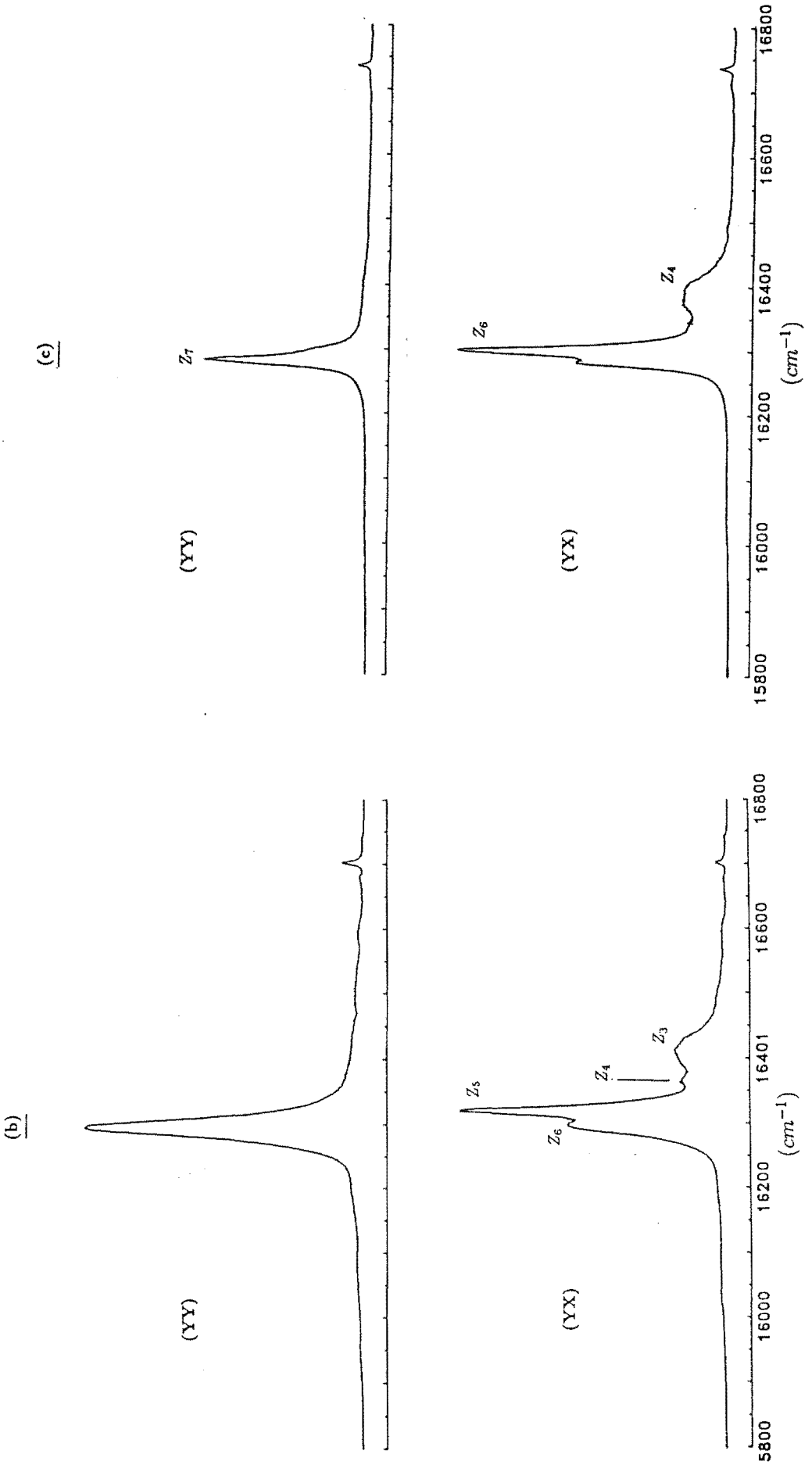
(b)
(YY)
(YX)
Z_5
Z_6
Z_4
Z_3
15800
16000
16200
16401
16600
16800
(cm^{-1})
(c)
(YY)
(YX)
Z_7
Z_6
Z_4
15800
16000
16200
16400
16600
16800
(cm^{-1})

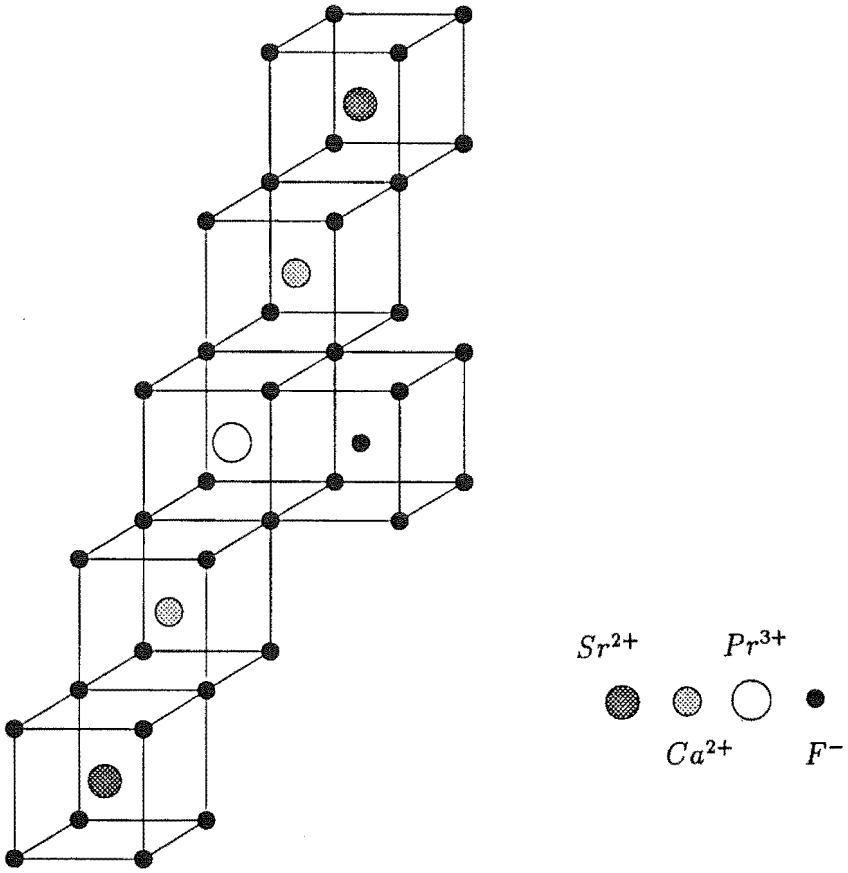

Figure 4.8 A model proposed for the $A3$ center which takes into account the observed polarisation ratios consistent with a $C_{2v}(a)$ center and the small perturbation on the parent C_{4v} center.

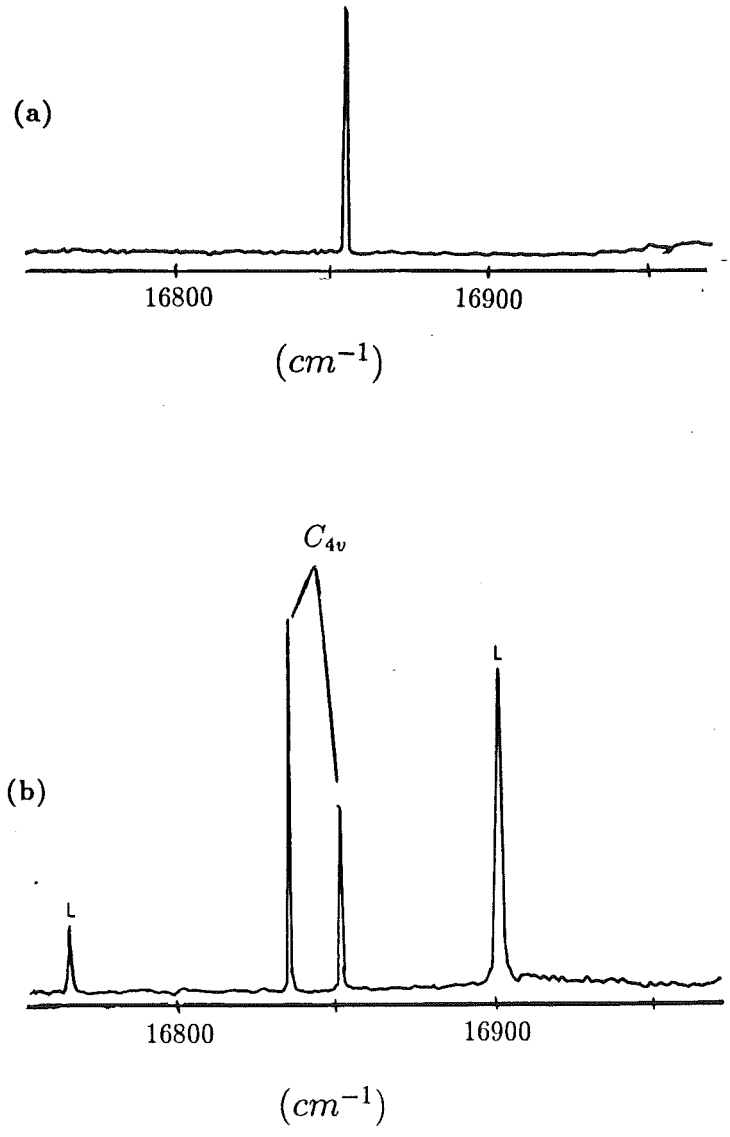

Figure 4.9 Selective excitation spectra of the K and L centers in the $CaF_2 : Pr^{3+}$ crystal at 11K by scanning dye laser and monitoring specific transitions.

(a) the K center, monitoring $14669cm^{-1}$
(b) the L center, monitoring $14337cm^{-1}$

4.2 Mixed Crystal Centers in $Ca_{1-x}Ba_xF_2 : Pr^{3+}$

Three mixed crystal centers were studied in the $Ca_{1-x}Ba_xF_2 : Pr^{3+}$ mixed crystal, each of which can be characterised by their polarised fluorscence. One of these centers is an *on-axis* $A2$ center and the other two are *off-axis* $A1$ centers labelled the $A1(I)$ and $A1(II)$ centers. There are further mixed crystal centers in this crystal system but their transitions were broad and overlapping, hence, LSE on these centers was not fruitful. The spectroscopic results from the three centers studied in detail are given in this section.

4.2.1 The Excitation Spectra

Figure 4.12 shows the broadband excitation spectra of the Ba^{2+} in $CaF_2 : Pr^{3+}$ crystal, with the transitions belonging to the centers $A1(I)$, $A1(II)$ and $A2$ clearly labelled. When the Ba^{2+} doping was increased from 0.6% to 1%, a dramatic change in the broadband excitation spectra was observed with many more new lines appearing. LSE of some of the transitions in the 1% crystal proved difficult with a marked increased in the inhomogeneous broadening of the transitions and the linewidths of several centers were found overlapping within single transition bands . These are indicated by the asterisks in figure 4.12(a). The transition of the parent L center was also observed to have vanished at 0.6% Ba^{2+} doping, while in the Sr^{2+} doped crystal, some residue of lines belonging to this center was apparent even at 1% doping.

The excitation spectra monitoring specific transitions of the mixed three centers are shown in figure 4.13. The $A1(I)$ and $A1(II)$ centers have similar excitation spectra features to the $A1$ center in the $Ca_{1-x}Sr_xF_2 : Pr^{3+}$ mixed crystal. Ground state splittings of $15cm^{-1}$ and $17cm^{-1}$ were measured for the $A1(I)$ and $A1(II)$ centers respectively, each of which is larger than the splitting of $8cm^{-1}$ measured for the $A1$ center in the Sr^{2+} doped crystal. The shift of the D_1 and D_2 energy levels of the $A1(I)$ and $A1(II)$ centers, from the D_1 and D_2 levels of the parent C_{4v}

(a)

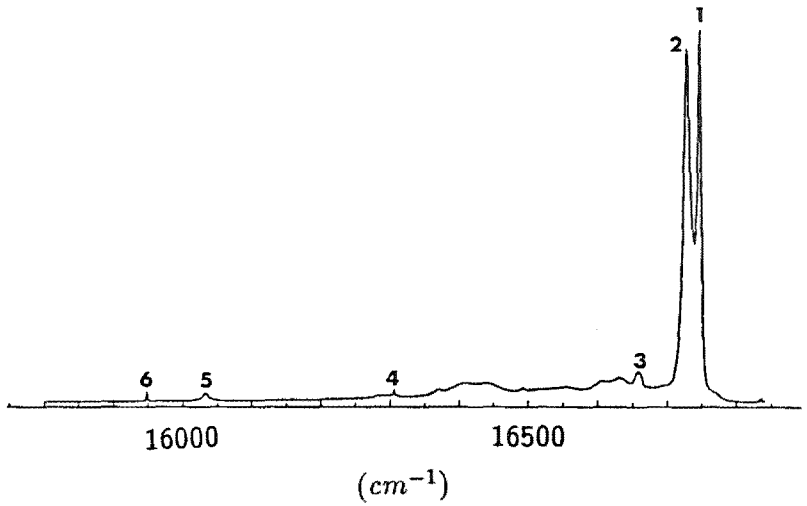

Figure 4.10 Emission spectra of the K center at 11K.

(a) $^1D_2 \rightarrow ^3H_4$ transitions.
(b) $^1D_2 \rightarrow ^3H_5$ transitions.
(c) $^1D_2 \rightarrow ^3H_6$ and $^3F_2$ transitions.

(b)

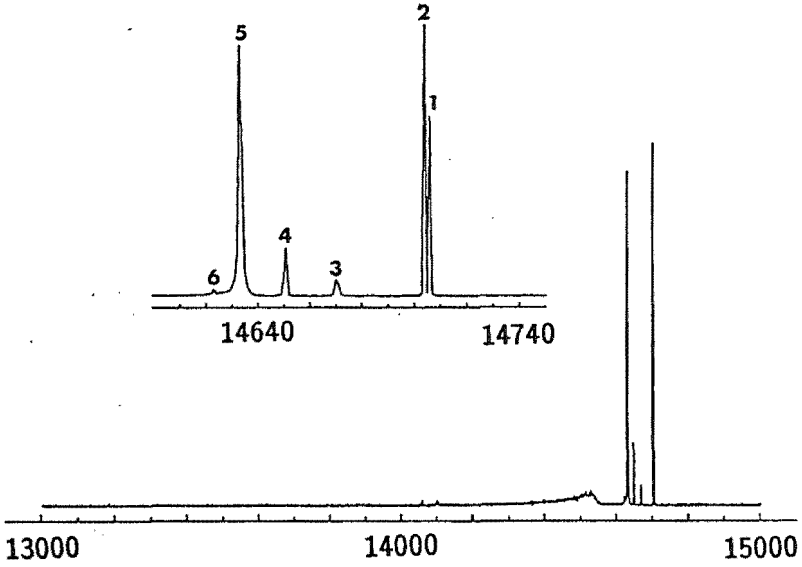

(cm^{-1})

(c)

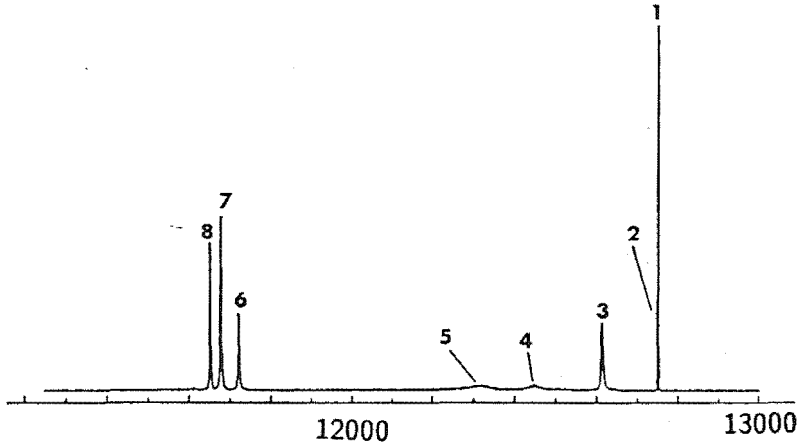

(cm^{-1})

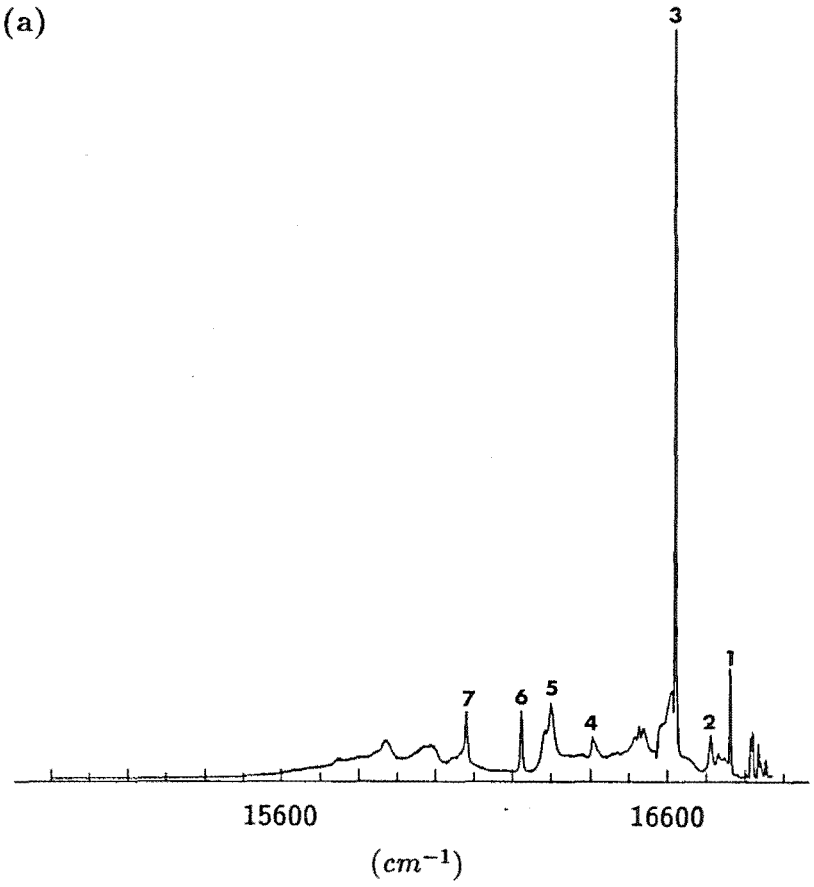

Figure 4.11 Emission spectra of the L center at 11K.

(a) $^1D_2 \rightarrow ^3H_4$ transitions.
(b) $^1D_2 \rightarrow ^3H_5$ transitions.
(c) $^1D_2 \rightarrow ^3H_6$ and $^3F_2$ transitions.

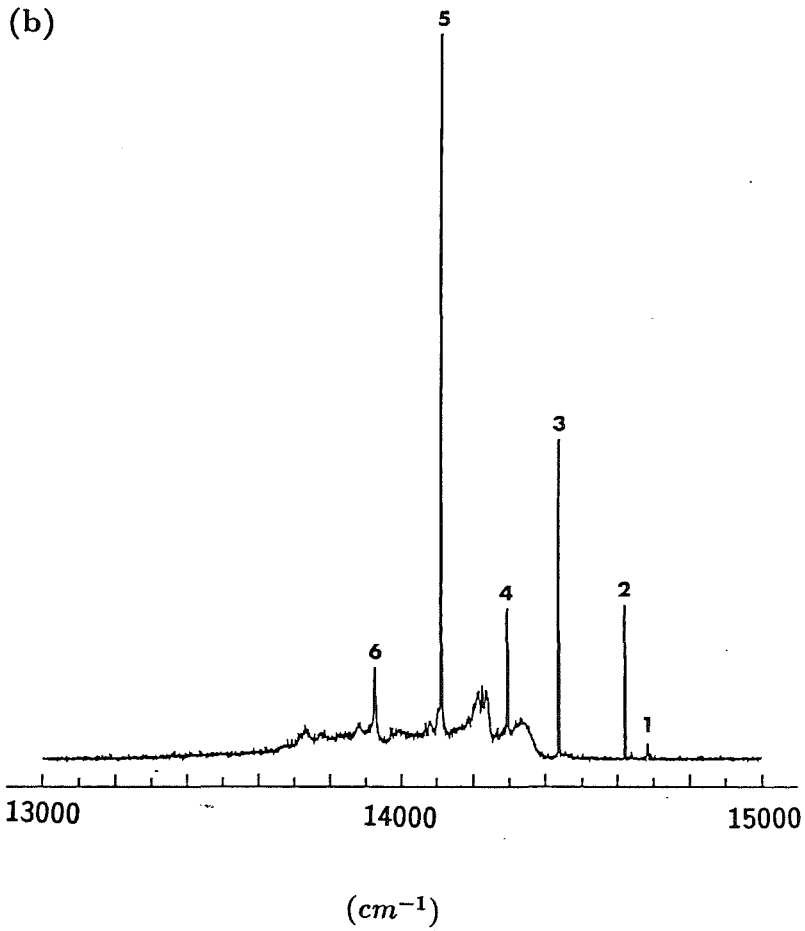
(b)
5
3
4
2
6
1
13000
14000
15000
(cm^{-1})

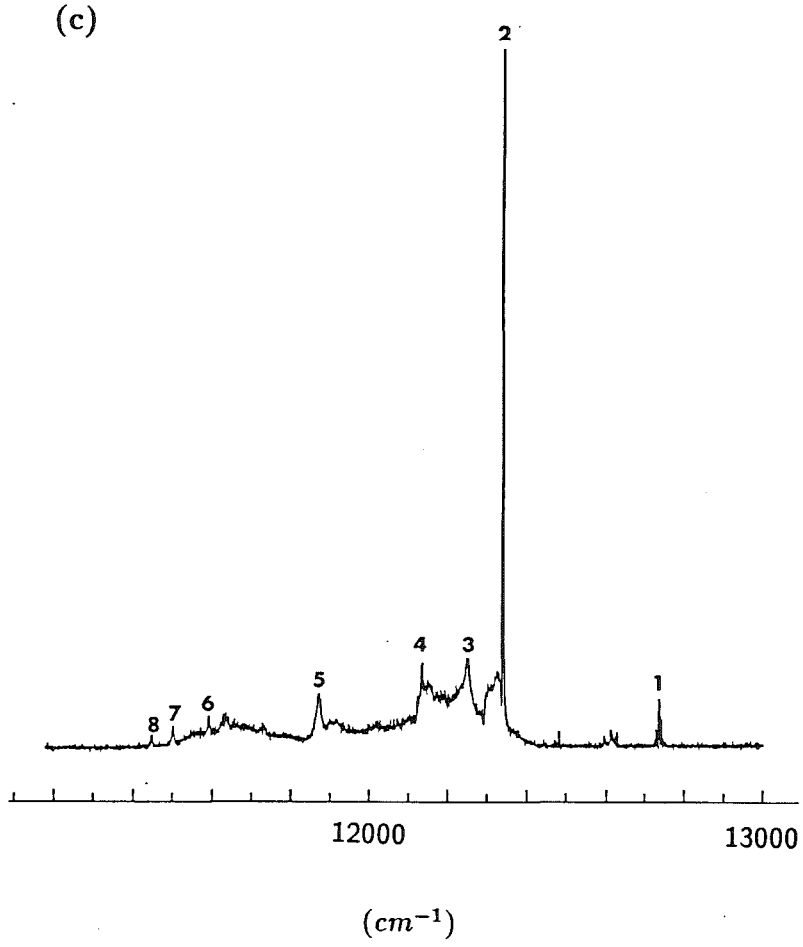
(c)
2
4
3
5
1
8
7
6
12000
13000
(cm^{-1})

Table 4.2 The frequencies of selected transitions observed by pumping 16853.1cm^{-1} level of site K. Uncertainties are $\pm 1 cm^{-1}$. The line number for the transition from the D multiplet to the respective lower multiplets are labelled in the fig 4.9 .

	Line number	Frequencies
$D \rightarrow Z$	1	16748
	2	16729
	3	16659
	4	16306
	5	16032
	6	15498
$D \rightarrow Y$	1	14706
	2	14704
	3	14670
	4	14652
	5	14633
	6	14059
$D \rightarrow X, W$	1	12752
	2	12750
	3	12614
	4	12447
	5	12317
	6	11721
	7	11678
	8	11652

Table 4.3 The frequencies of selected transitions observed by pumping 16903.7cm^{-1} level of site L. Uncertainties are $\pm$ 1 cm^{-1}. The line number for the transition from the D multiplet to the respective lower multiplets are labelled in the fig 4.10.

	Line number	
$D \rightarrow Z$	1	16762
	2	16712
	3	16620
	4	16406
	5	16308
	6	16223
	7	16081
$D \rightarrow Y$	1	14685
	2	14622
	3	14438
	4	14296
	5	14113
	6	13927
$D \rightarrow X, W$	1	12737
	2	12340
	3	12252
	4	12135
	5	11872
	6	11592
	7	11502
	8	11448

center, was also found to be greater in the Ba^{2+} crystal than in the Sr^{2+} doped crystal. For the $A2$ center, an increase of the D_1 and D_2 seperation from $8.9cm^{-1}$ in the Sr^{2+} doped crystal to $29.5cm^{-1}$ in the Ba^{2+} crystal was apparent.

Clearly, the bigger radius Ba^{2+} dopant ion (1.34Å) affects the $CaF_2 : Pr^{3+}$ parent C_{4v} center more than the Sr^{2+} dopant (1.12Å). The larger mismatch in ionic radius between the Ca^{2+} and Ba^{2+} ions would distort the lattice structure further, and these distortions also give rise to more centers than in the Sr^{2+} doped crystal.

4.2.2 The Polarised Fluorescence Spectra

The $^3F_2$ multiplet

As shown in figure 4.14, there are clearly two centers with the characteristic $A1$ center polarised fluorescence in the Ba^{2+} doped $CaF_2 : Pr^{3+}$ crystal. Other than the energy level shifts, the polarised fluorescence patterns of both the $A1(I)$ and $A1(II)$ centers in this multiplet look almost identical when the laser was polarised E_Y. With the laser polarised E_Z, the transitions with a (YX):(YY) ratio of 0:1 when the laser was polarised E_Y, were found to have vanished for the $A1(I)$ center (fig 4.14(a)(ii)) , consistent with a γ_2 absorption and γ_2 emssion for a $C_s(b)$ center. At the time, a similar measurement for the laser polarised E_Z was not made for the $A1(II)$ center but it is expected to have the same behaviour.

The center $A2$ in this crystal shows the characteristic polarisation ratios expected for an on-axis alkaline earth substitution which yields a C_{4v} center (fig. 4.14(b)). The transition to the W_2 level is found to be weaker in intensity when compared with the transition to the W_2 level in the parent C_{4v} center and the Sr^{2+} doped $A2$ center.

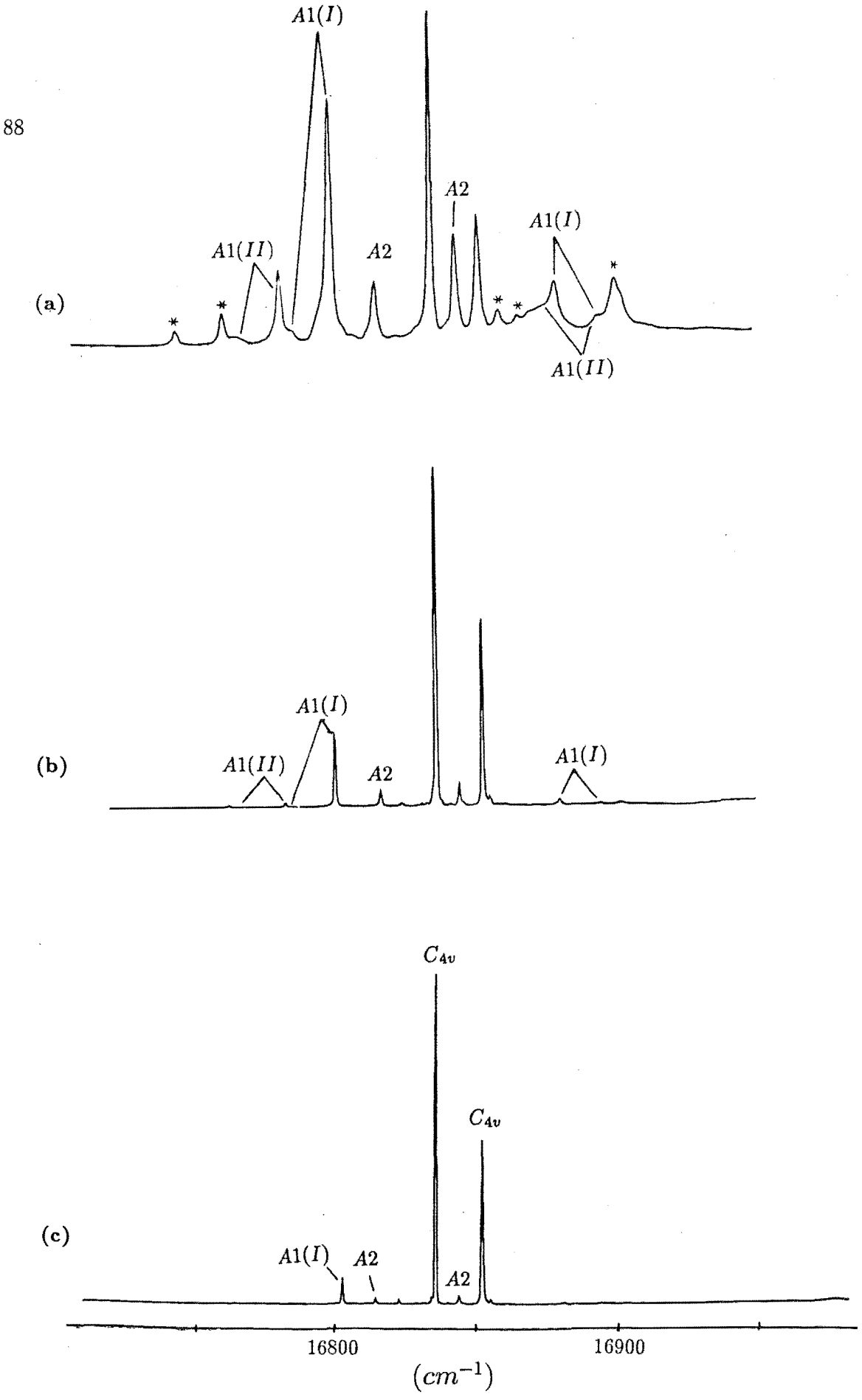

Figure 4.12 Broadband excitation spectra of the $Ca_{1-x}Ba_xF_2 : Pr^{3+}$ crystals, monitoring the $D \rightarrow Z$ transitions at 11K for Ba^{2+} doping of (a) 1% (b) 0.6% (c) 0.3%.
The transitions of several centers make up each line marked with asterisks in (a)

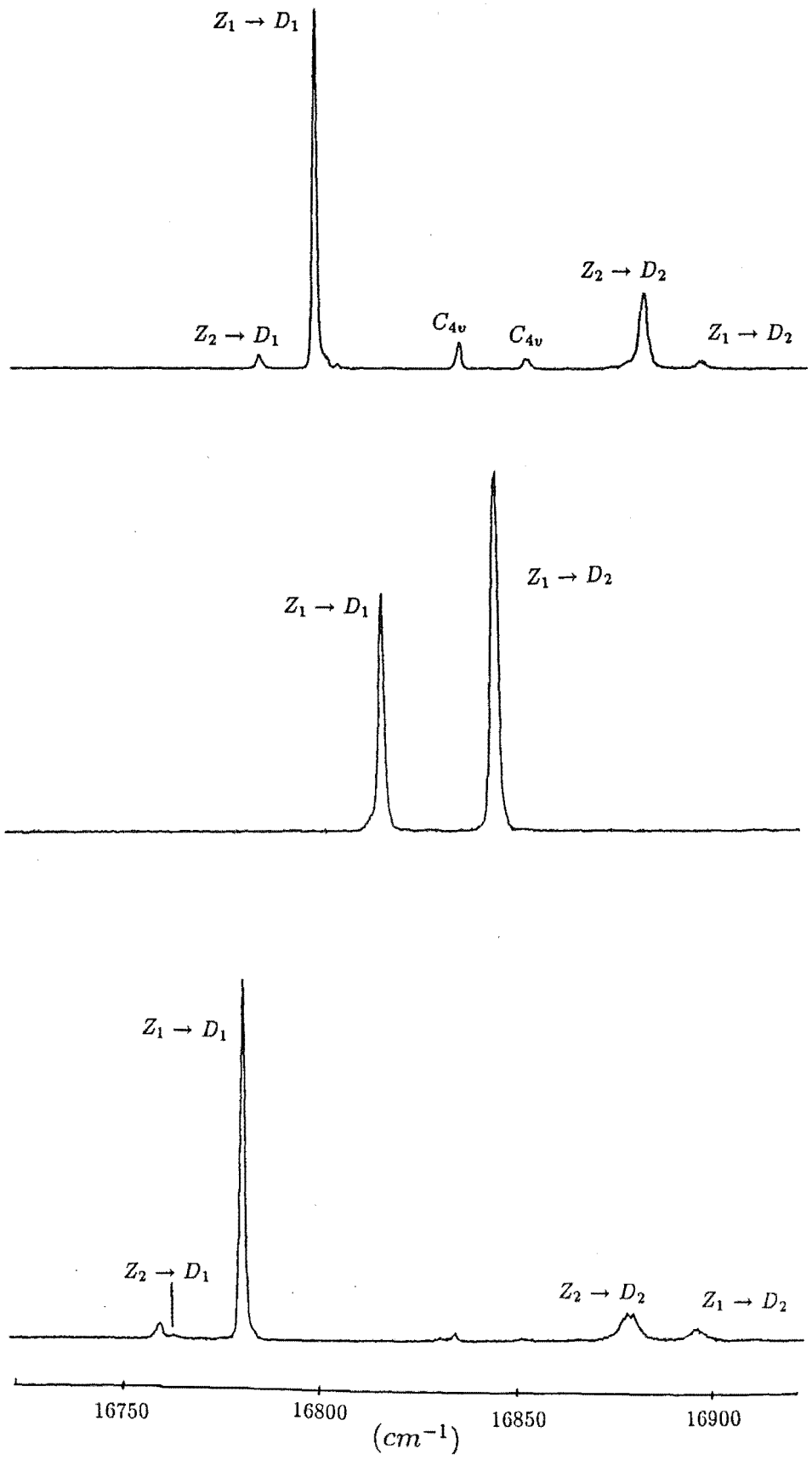

Figure 4.13 Selective excitation spectra of the mixed crystal centers in the 0.6% Ba^{2+} doped CaF_2 crystal at 11K by scanning the dye laser and monitoring specific transitions.

(a) the $A1(I)$ center monitoring $14584cm^{-1}$. (b) the $A2$ center monitoring $14610cm^{-1}$.
(c) the $A1(II)$ center monitoring $14550cm^{-1}$.

The $^3H_6$, $^3H_5$ and $^3H_4$ multiplet

The polarised spectra of transtitions of the three centers to the X, Y and Z multiplets are presented in figures 4.15 , 4.16 and 4.17 respectively , with the polarisation ratios found to be as expected for the respective on and off-axis type centers.

Assignment of the transitions in the $16500cm^{-1}$ to $16700cm^{-1}$ region is not straightforward. While the lines present are possible candidates for transitions, to the Z_2 level for the $A2$ center and Z_3 level for the $A1$ type centers, the coupling of the D_1 and D_2 level with the lattice phonons could give rise to vibronic transitions which also lie in this same spectral region.

The $D_1(\gamma_1) \rightarrow Z_2(\gamma_2)$ transition of the $A2$ center is allowed only as a weak magnetic dipole transition. For the case of the $16689cm^{-1}$ line observed in the $A2$ center, the relatively stronger line intensity suggests that it is more likely to be of a vibronic origin.

The assignment for the $A1$ type centers is even less straightforward in this $16500cm^{-1}$ to $16700cm^{-1}$ spectral region of the $D_1 \rightarrow Z$ transition, since under a $C_s(b)$ symmetry, all electronic transitions are now allowed. The present set of spectral data offers no clear-cut method of isolating the vibronic from the electronic transitions, hence, the present assignment of the transitions to the Z_3 levels is only tentative.

4.2.3 Model Assignments

Table 4.4 summarizes the energy level assignment to the three mixed crystal centers of the Ba^{2+} doped $CaF_2 : Pr^{3+}$ crystal. Discussion of possible models for each of the centers is given below.

Figure 4.14 $^1D_2 \rightarrow ^3F_2$ Polarised fluoresence spectra of the mixed crystal centers in the 0.6% Ba^{2+} doped CaF_2 crystal at 11K.

(a)(i) the $A1(I)$ center, pumping 16796.9 cm^{-1}. Laser polarised E_Y
(a)(ii) the $A1(I)$ center, pumping 16796.9cm^{-1}. Laser polarised E_Z
(b) the $A2$ center, pumping 16813.9cm^{-1}.
(c) the $A1(II)$ center, pumping 16779.3cm^{-1}.

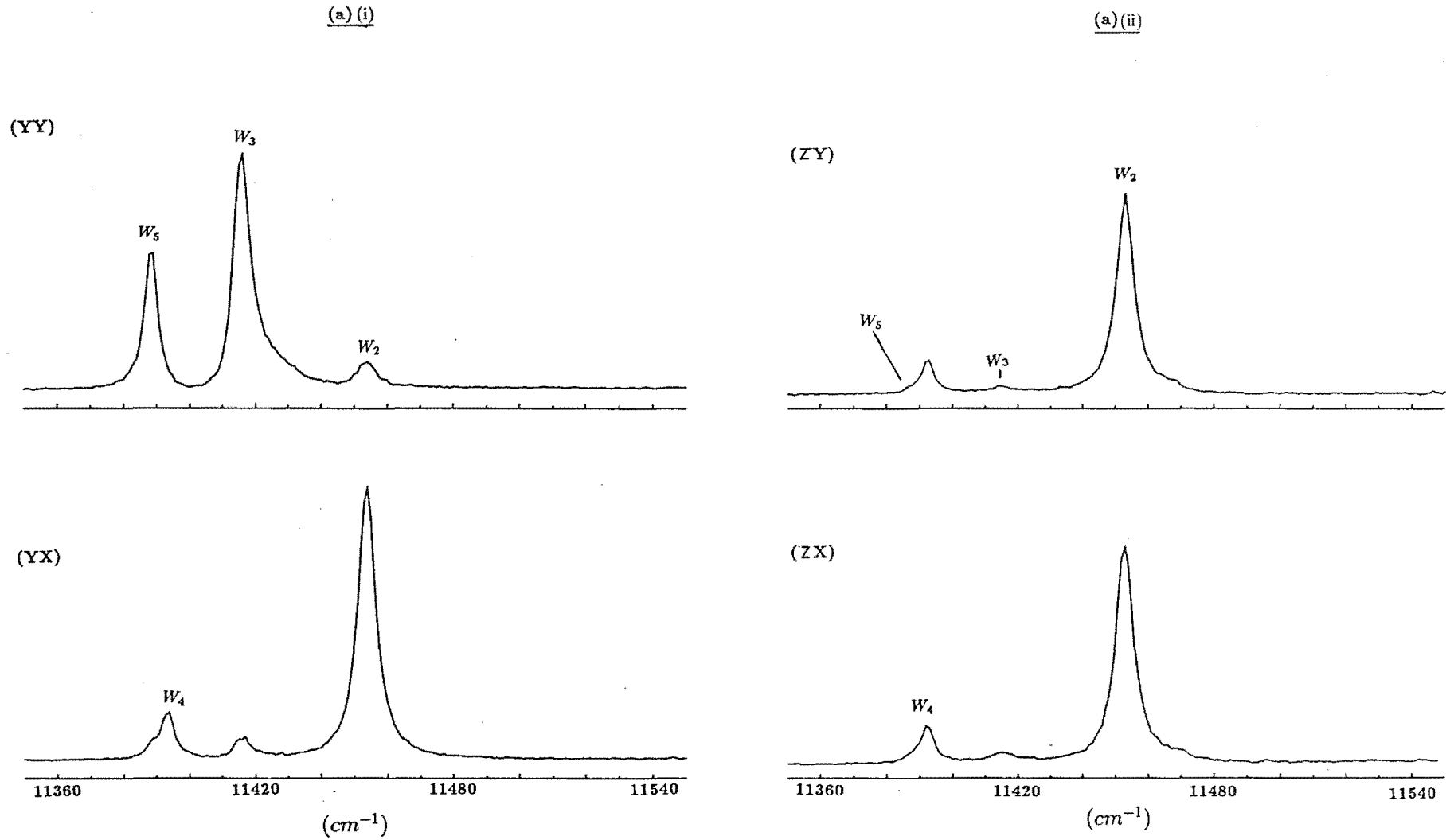
(a) (i)
(YY)
W_5
W_3
W_2
(YX)
W_4
11360
11420
11480
11540
(cm^{-1})
(a) (ii)
(ZY)
W_5
W_3
W_2
(ZX)
W_4
11360
11420
11480
11540
(cm^{-1})

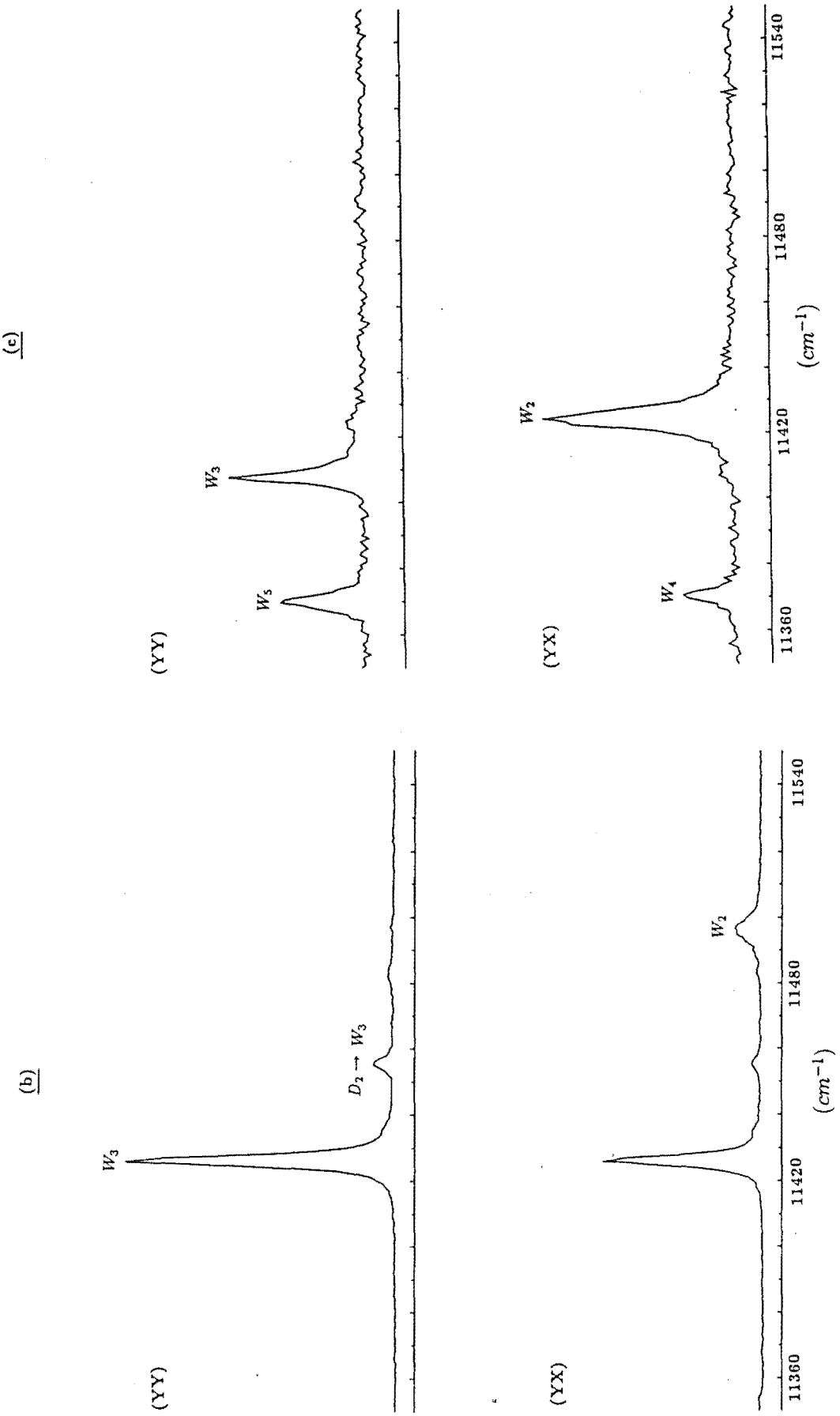
(b)
(YY)
W_3
$D_2 \rightarrow W_3$
(YX)
W_2
11360
11420
11480
11540
(cm^{-1})
(c)
(YY)
W_3
W_5
(YX)
W_2
W_4
11360
11420
11480
11540
(cm^{-1})

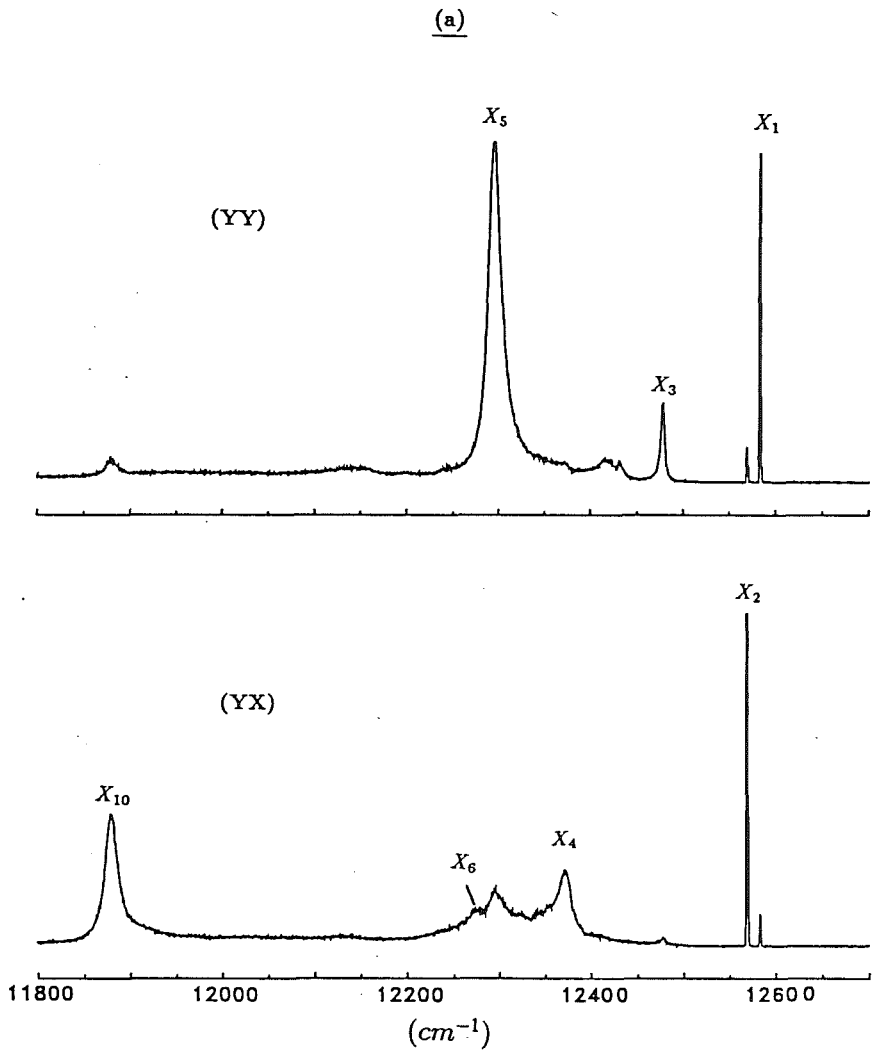

Figure 4.15 $^1D_2 \rightarrow ^3 H_6$ Polarised fluoresence spectra of the mixed crystal centers in the 0.6% Ba^{2+} doped CaF_2 crystal at 11K.
(a) the $A1(I)$ center, pumping 16796.9 cm^{-1}.
(b) the $A2$ center, pumping 16813.9cm^{-1}.

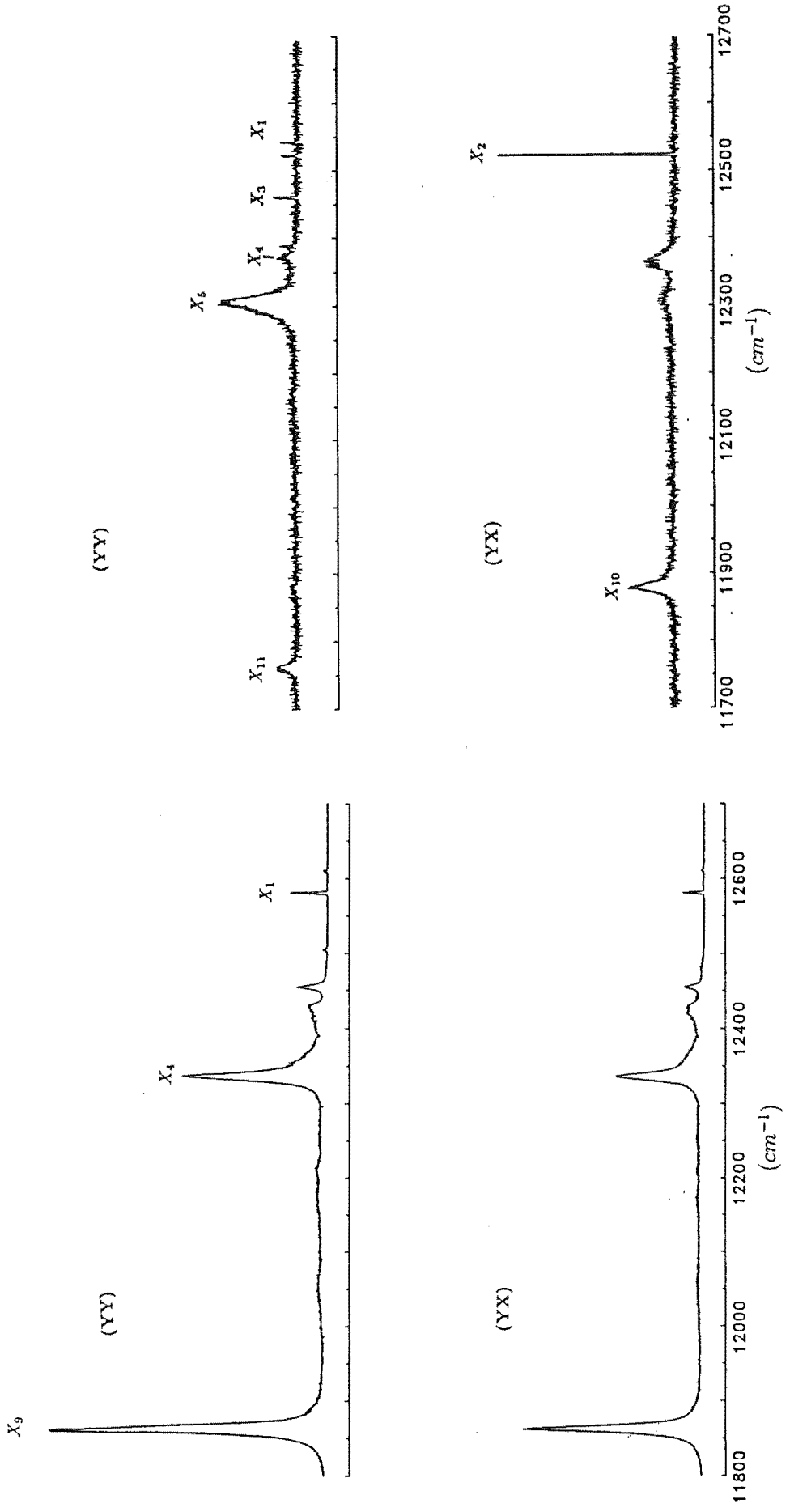
(b)
(YY)
X_9
X_4
X_1
(YX)
11800
12000
12200
12400
12600
(cm^{-1})
(c)
(YY)
X_5
X_4
X_3
X_1
X_{11}
(YX)
X_2
X_{10}
11700
11900
12100
12300
12500
12700
(cm^{-1})

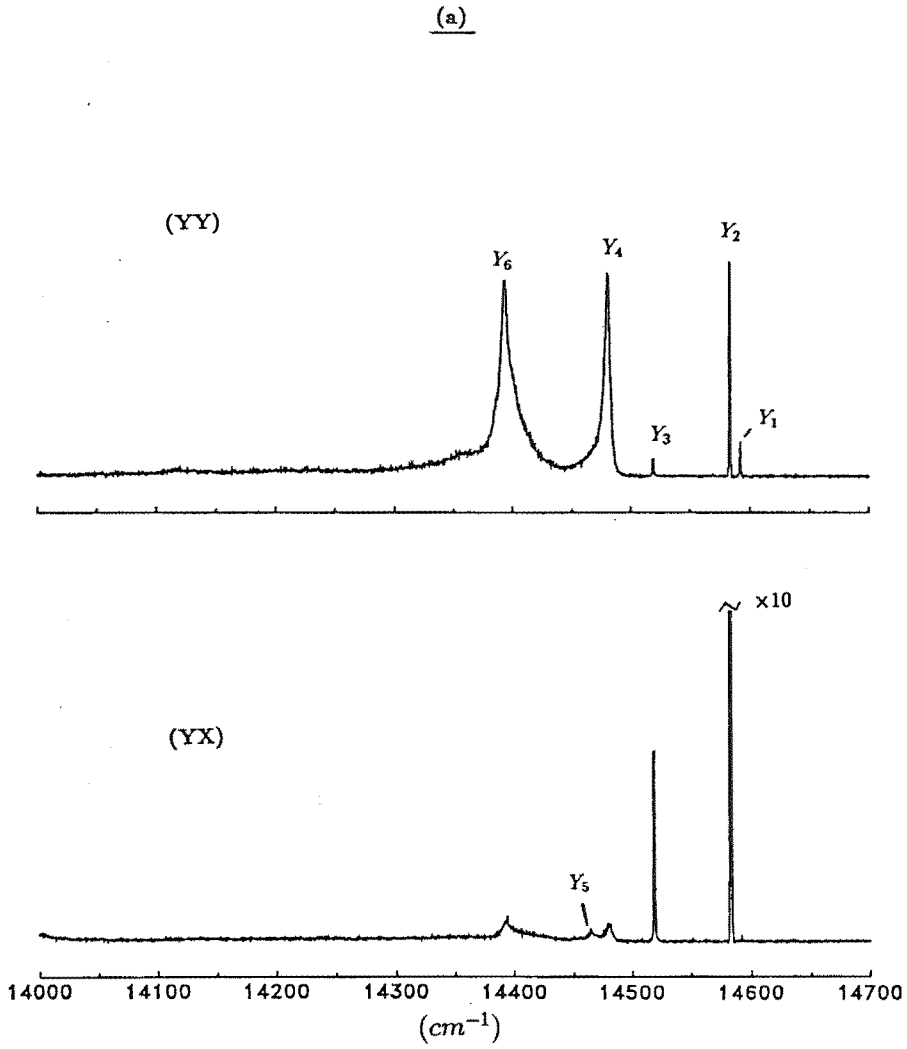

Figure 4.16 $^1D_2 \rightarrow ^3 H_5$ Polarised fluoresence spectra of the mixed crystal centers in the 0.6% Ba^{2+} doped CaF_2 crystal at 11K.

(a) the $A1(I)$ center, pumping 16796.9 cm^{-1}.

(b) the $A2$ center, pumping 16813.9cm^{-1}.

(c) the $A1(II)$ center, pumping 16779.3cm^{-1}.

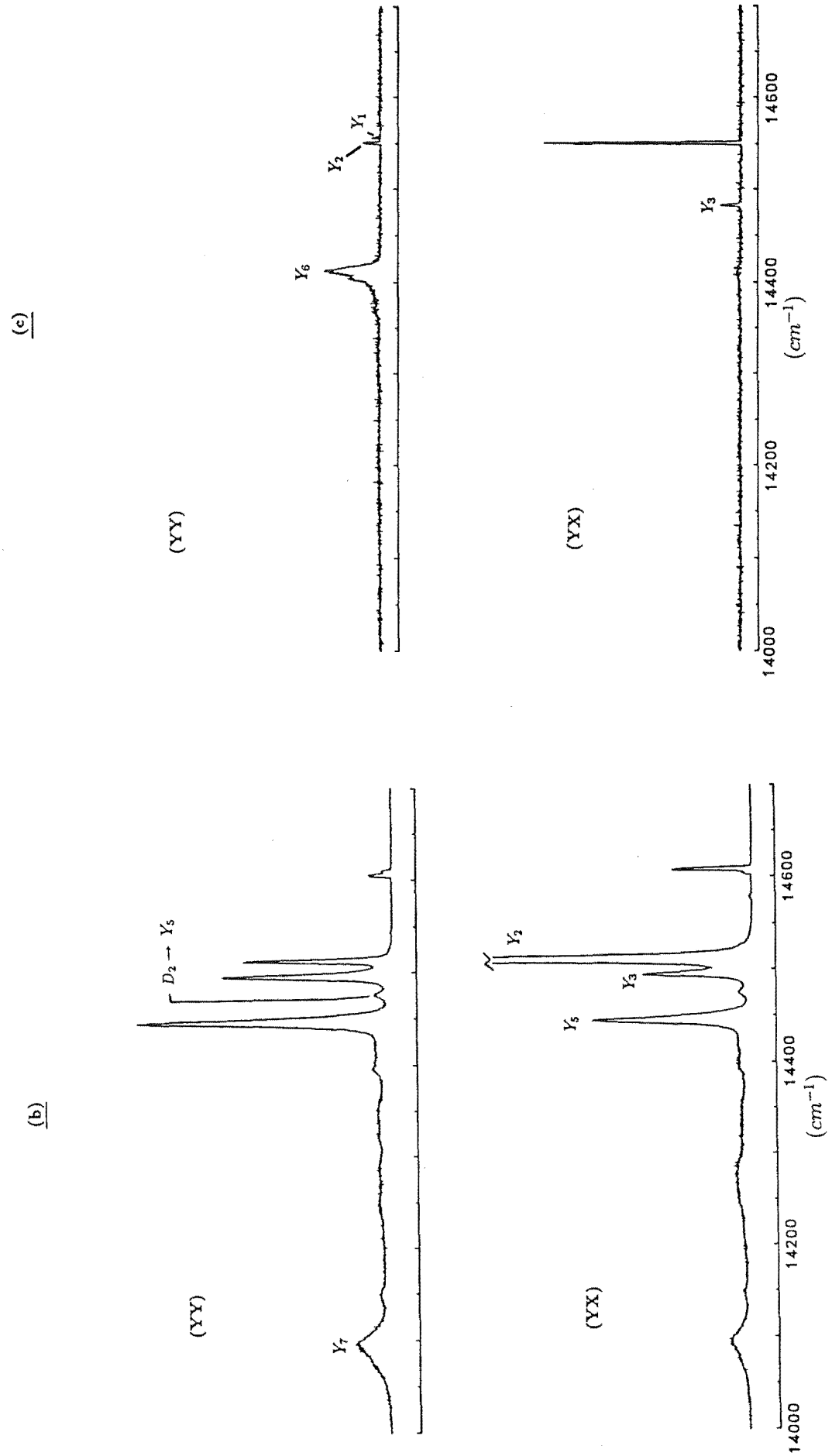
(c)
(YY)
Y_6
Y_2
Y_1
(YX)
Y_3
14000
14200
14400
14600
(cm^{-1})
(b)
(YY)
$D_2 \rightarrow Y_5$
Y_7
(YX)
Y_2
Y_3
Y_5
14000
14200
14400
14600
(cm^{-1})

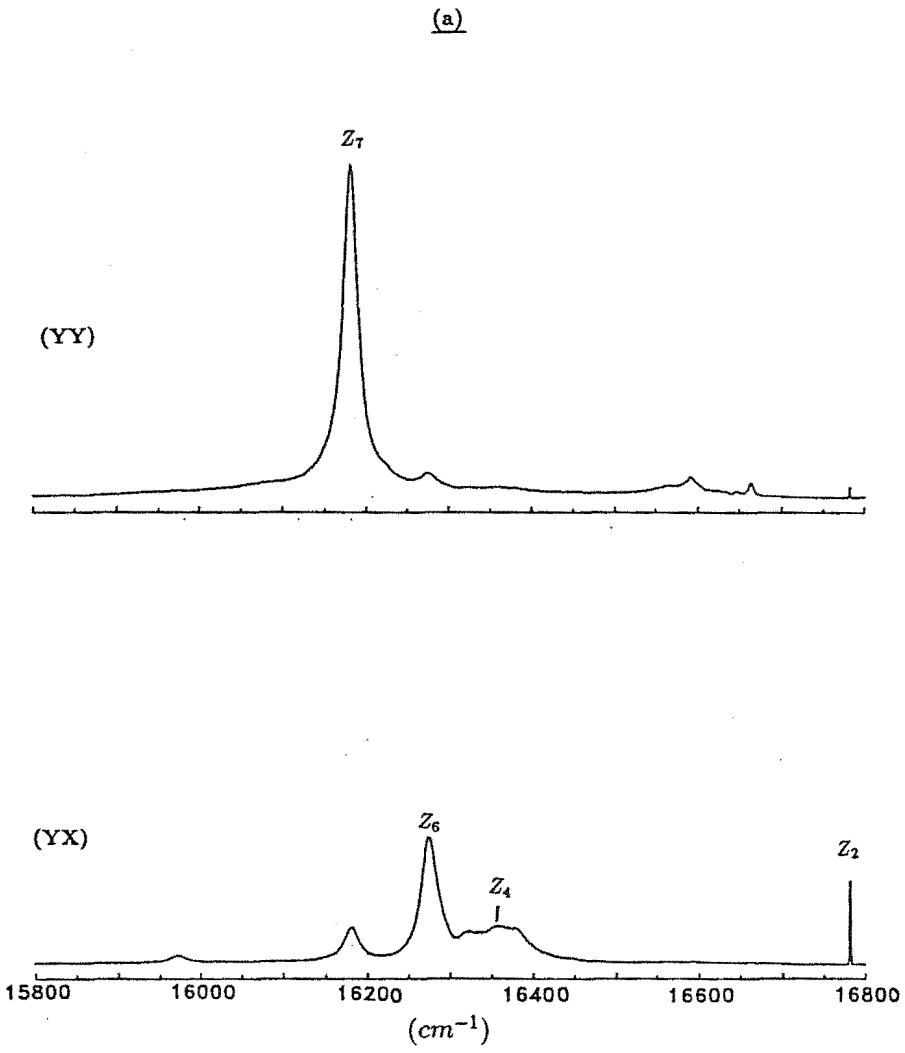

Figure 4.17 $^1D_2 \rightarrow ^3 H_4$ Polarised fluoresence spectra of the mixed crystal centers in the 0.6% Ba^{2+} doped CaF_2 crystal at 11K.

(a) the $A1(I)$ center, pumping 16796.9 cm^{-1}.

(b) the $A2$ center, pumping 16813.9cm^{-1}.

(c) the $A1(II)$ center, pumping 16779.3cm^{-1}.

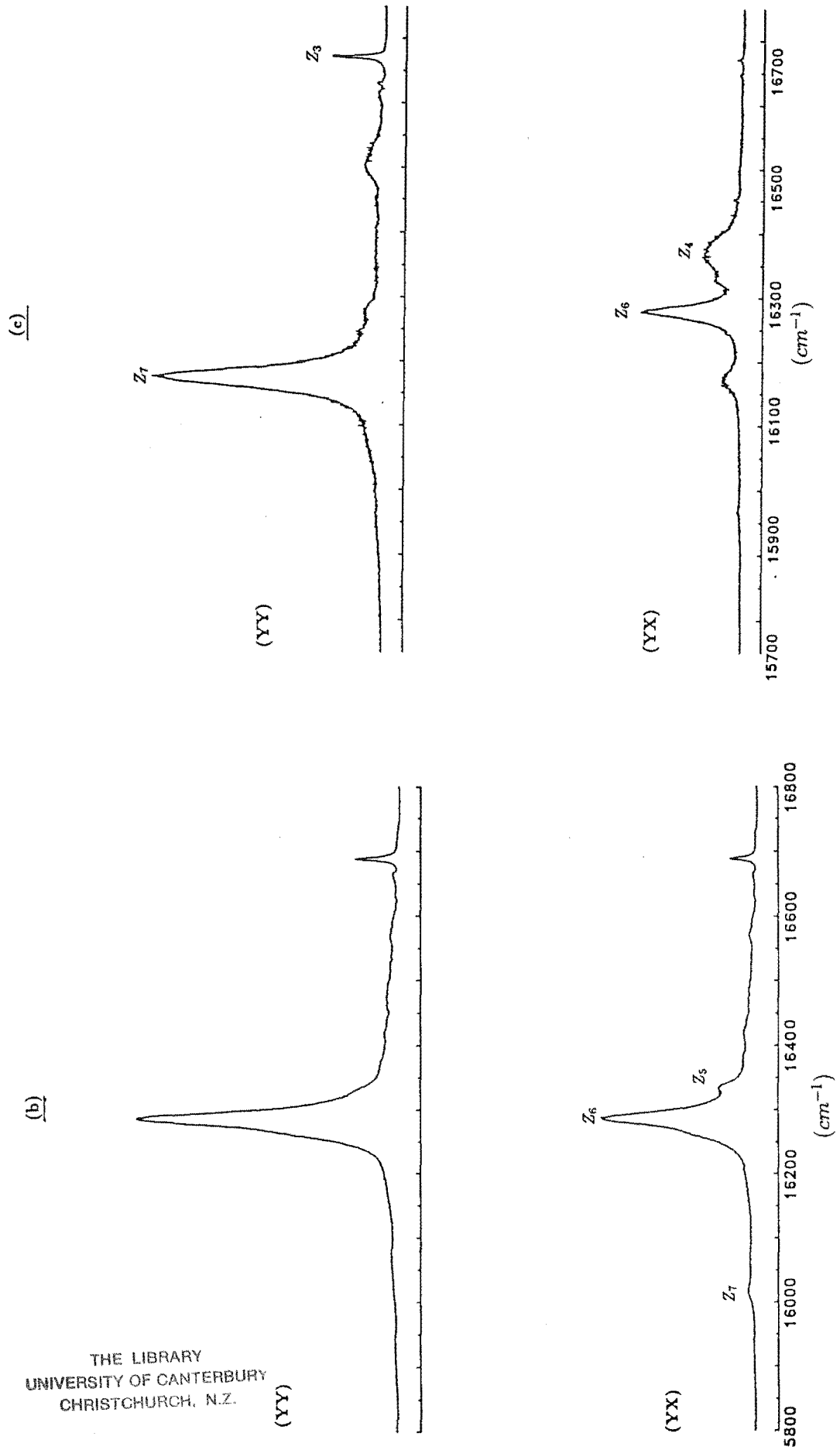

The $A1(I)$ and $A1(II)$ centers

Since both these centers share similar spectral characteristics, it is worthwhile to simultaneously discuss models for both centers. The centers have the following prominent spectral features:

(i) ground state splittings of $15cm^{-1}$ and $17cm^{-1}$ for the $A1(I)$ and $A1(II)$ centers respectively;
(ii) observed (YX):(YY) polarisation ratios of the type 1:0 and 0:1 when the laser was polarised E_Y;
(iii) with the laser polarised E_Z, certain transitions were extinguished. This was recorded for the $A1(I)$ center.

The only model consistent with the polarisation ratios observed is one with a $C_s(b)$ configuration for the $A1(I)$ center. The spectral trends observed in both the $A1(I)$ and $A1(II)$ centers strongly suggest that a $C_s(b)$ center configuration applies to both these centers. Polarisation measurements with the laser in the E_Z direction, with observation of extinction of certain transitions, would directly confirm the $A1(II)$ center as having a $C_s(b)$ type geometry. For the same reasons given for assigning a model to the $A1$ center in the Sr^{2+} doped crystal (sec. 4.1.3), the $A1(I)$ center is most likely to have a single cation substitution with the configuration arrangement as shown in figure 2.2(a)(iii).

Comparing the relative intensities of the transitions of the $A1(I)$ with the $A2$ and $A1(II)$ centers in the broadband excitation spectra (fig 4.12), the relative intensities of the $A1(II)$ center was found to have gained in strength roughly 4 times in relation to the $A1(I)$ and $A2$ centers, when the Ba^{2+} doping was increased from 0.6% to 1%. This is evidence that the model for the $A1(II)$ center requires two foreign Ba^{2+} replacements of the host cations. The energy shift of the $A1(II)$ center from the parent C_{4v} transitions in the D multiplet, was also found to be greater than the $A1(I)$ or $A2$ centers, indicating that the $A1(II)$ center has further distortion of the local environment of the parent C_{4v} center.

Possible models for the $A1(II)$ center would include an additional Ba^{2+} substitution in the C_s reflection plane of the single cation substitution models of figures 2.2(a)(ii) and (iii) or those with the $C_{2v}(b)$ symmetry configuration of 2.2(c)(ii) and (iii). A good starting point for consideration of a model for the $A1(II)$ center would be the single cation substitution model of the $A1(I)$ center, however, the placement of the second substitutional cation cannot be unambigously determined with the present set of data.

The $A2$ center

The main spectroscopic features of this center are the same as those for the $A2$ and the parent C_{4v} centers in the Sr^{2+} doped mixed crystal, hence, this center is assigned as a C_{4v} center with the configuration arrangement as shown in figure 2.2(b)(iii). The D_1 and D_2 splitting in the Sr^{2+} doped $CaF_2 : Pr^{3+}$ crystal is $9cm^{-1}$ and in the Ba^{2+} crystal is $30cm^{-1}$, highlighting the greater change in crystal field brought about by a larger dopant cation in the same position.

Table 4.4 The energy levels (in cm^{-1}) of mixed crystal centers A1(I),A1(II) and A2 in $Ca_{1-x}Ba_xF_2:Pr^{3+}$. Uncertainties are $\pm 1 cm^{-1}$ unless otherwise indicated. The irrep labels for each level is given in brackets.

	A1(I)		A2		A1(II)	
D_2	16895	(γ_1)	16843.4 ± 0.5	(γ_3)	16894	(γ_1)
D_1	16796.9 ± 0.5	(γ_1)	16813.9 ± 0.5	(γ_1)	16779.3 ± 0.5	(γ_1)
W_5	5409	(γ_2)	NA		5410	(γ_2)
W_4	5404	(γ_1)	-	(γ_4)	5408	(γ_1)
W_3	5381	(γ_2)	5389	(γ_5)	5371	(γ_2)
W_2	5344	(γ_1)	5318	(γ_1)	5355	(γ_1)
W_1	-	(γ_1)	-	(γ_3)	-	(γ_1)
X_{13}	-	(γ_1)	NA		-	(γ_1)
X_{12}	-	(γ_1)	NA		-	(γ_1)
X_{11}	-	(γ_2)	NA		5028	(γ_2)
X_{10}	4917	(γ_1)	-	(γ_3)	4936	(γ_1)
X_9	-	(γ_2)	4953	(γ_5)	-	(γ_2)
X_8	-	(γ_1)	-	(γ_1)	-	(γ_1)
X_7	-	(γ_2)	-	(γ_4)	-	(γ_2)
X_6	4518 ± 10	(γ_1)	-	(γ_3)	-	(γ_1)
X_5	4495	(γ_2)	-	(γ_2)	4384	(γ_2)
X_4	4425 ± 5	(γ_1)	4477	(γ_5)	4329*	(γ_1)
X_3	4320	(γ_2)	-	(γ_3)	4257	(γ_2)
X_2	4228	(γ_1)	4340*	(γ_4)	4207	(γ_1)
X_1	4214	(γ_2)	4234	(γ_5)	4191	(γ_2)

Y_{11}	-	(γ_2)	NA		-	(γ_2)
Y_{10}	-	(γ_2)	NA		-	(γ_2)
Y_9	-	(γ_1)	NA		-	(γ_1)
Y_8	-	(γ_2)	-	(γ_4)	-	(γ_2)
Y_7	-	(γ_1)	2718	(γ_5)	-	(γ_1)
Y_6	2405	(γ_2)	-	(γ_2)	2367*	(γ_2)
Y_5	2333	(γ_1)	2368	(γ_5)	-	(γ_1)
Y_4	2317	(γ_2)	-	(γ_3)	-	(γ_2)
Y_3	2279	(γ_1)	2319	(γ_5)	2296	(γ_1)
Y_2	2215	(γ_1)	2302	(γ_1)	2228	(γ_1)
Y_1	2206	(γ_2)	2236	(γ_2)	2223	(γ_2)
Z_9	-	(γ_1)	NA		-	(γ_1)
Z_8	826 ± 5	(γ_1)	NA		-	(γ_1)
Z_7	618	(γ_2)	829*	(γ_3)	606	(γ_2)
Z_6	524	(γ_1)	528	(γ_5)	498	(γ_1)
Z_5	-	(γ_2)	482*	(γ_1)	-	(γ_3)
Z_4	$442^* \pm 10$	(γ_1)	-	(γ_2)	415 ± 10	(γ_1)
Z_3	136	(γ_2)	-	(γ_1)	107*	(γ_2)
Z_2	15	(γ_1)	-	(γ_4)	17	(γ_1)
Z_1	0	(γ_2)	0	(γ_5)	0	(γ_2)

Levels which could not be unambigously assign are marked with an asterisk.
NA - Excited levels not applicable to the A2 C_{4v} center.

4.3 Mixed Crystal Centers in $Sr_{1-x}Ca_xF_2 : Pr^{3+}$

Of the 4 mixed crystal systems studied, this system with Ca^{2+} as a dopant in $SrF_2 : Pr^{3+}$ is unique in being the only system with the ionic radius of the alkaline earth dopant smaller than that of the parent cation. However, the study of this system poses some special difficulties, in that the satellites are located very close to the parent electronic transitions and they also overlap one another. Hence, the study of this system, in particular the assignment of levels, could not be carried out in the same detail as for the Sr^{2+} or Ba^{2+} doped $CaF_2 : Pr^{3+}$ crystal systems.

4.3.1 The Excitation Spectra

Some prominent features of the excitation spectra as displayed in the figures of 4.18 are :

(i) weak satellite line structures;
(ii) a linear dependence in the rate of increase in the relative intensities of the satellite structures with dopant concentration;
(iii) the satellite structures are located not more than $4cm^{-1}$ away from the parent C_{4v} electronic D_1 and D_2 transitions;
(iv) the ground state splittings of the two centers studied were only $2.7cm^{-1}$ and $2.6cm^{-1}$.

Evidently the starting SrF_2 stock material used in the growth of the mixed crystal systems contained traces of both Ca^{2+} and Ba^{2+}, deduced to be at less than 0.1%. This gives rise to the observation of the satellite structures even in the parent crystal. At 0.5% doping, the satellite structures grew more intense but they were still relatively weak compared to the main transitions of the parent C_{4v} center, which suggests that the population of the centers giving rise to the satellite structures are not very large.

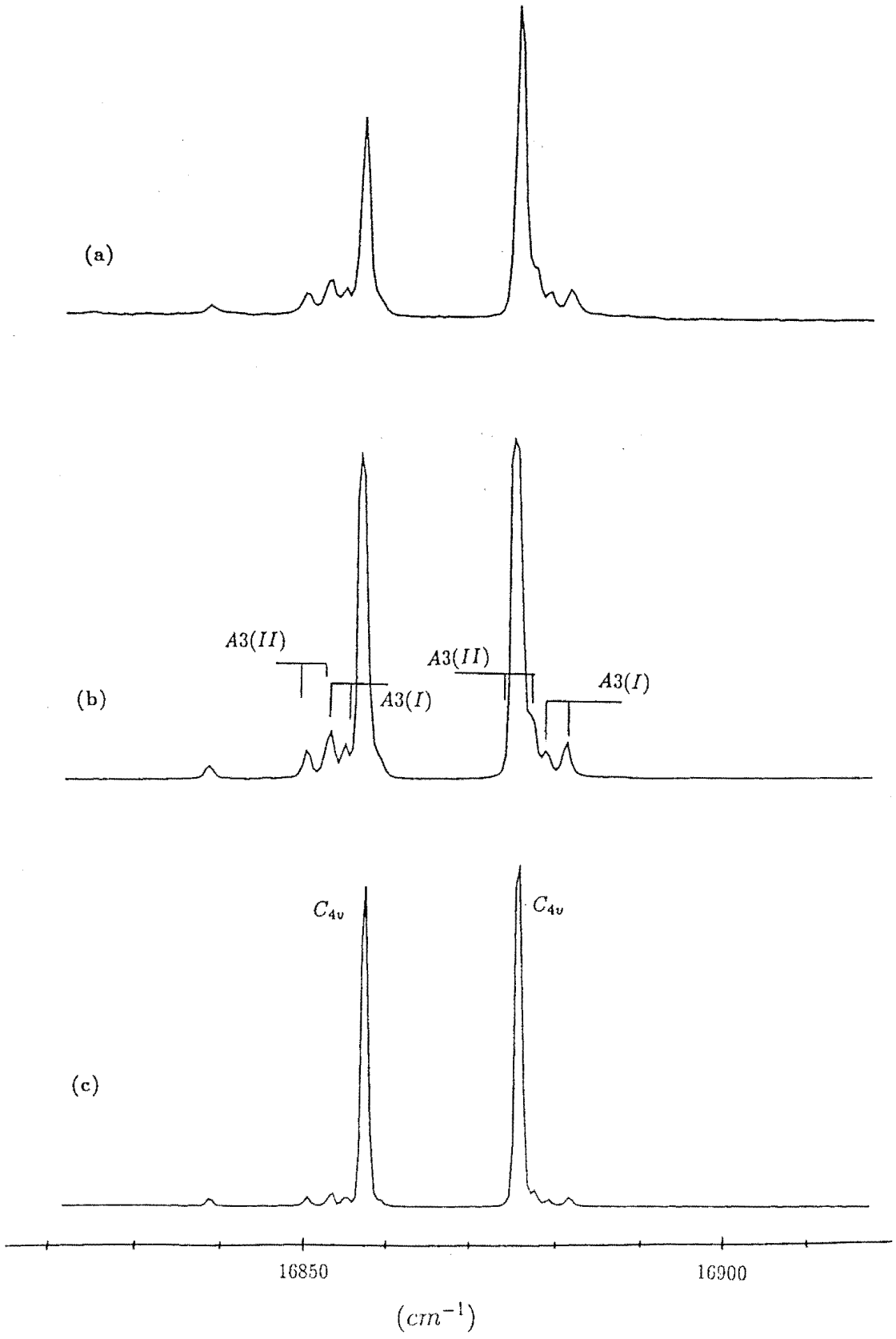

Figure 4.18 Broadband excitation spectra of the $Sr_{1-x}Ca_xF_2 : Pr^{3+}$ crystals, monitoring the $D \rightarrow Z$ transitions at 11K.

(a) 1% Ca^{2+} doping (b) 0.5% Ca^{2+} doping (c) undoped parent $SrF_2 : Pr^{3+}$ crystal.

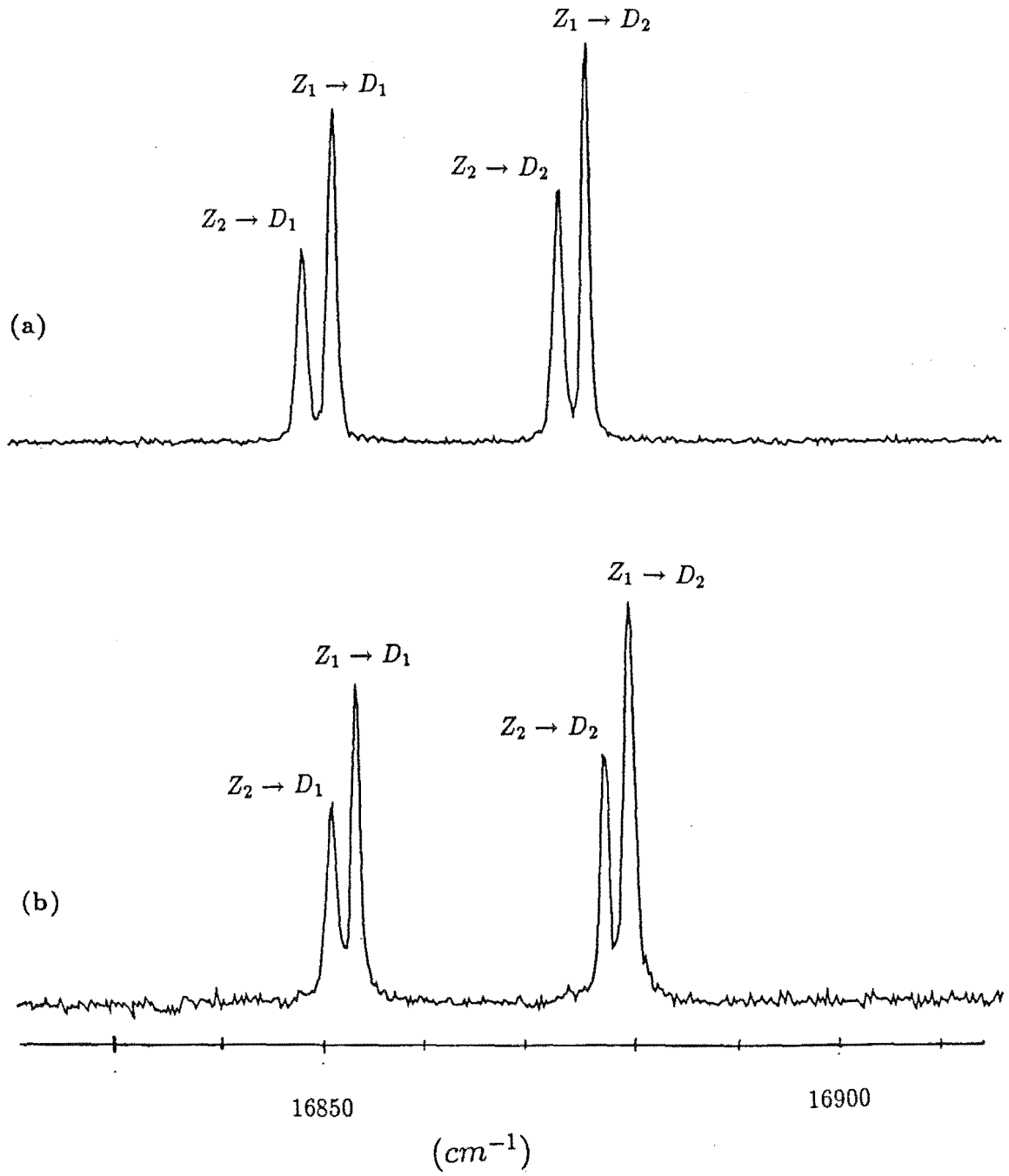

Figure 4.19 Selective excitation spectra of the mixed crystal centers in the 0.5% Ca^{2+} doped SrF_2 crystal at 11K by scanning the dye laser and monitoring specific transitions.

(a) the $A3(II)$ center monitoring $14662cm^{-1}$. (b) the $A3(I)$ center monitoring $14650cm^{-1}$.

Point (ii) indicates the satellites belong to mixed crystal centers with one cation substitution and points (iii) and (iv) suggest that the substitutional Ca^{2+} cations gave only a small perturbation to the parent C_{4v} center to give rise to the mixed crystal center.

Though only two centers were studied, labelled $A3(I)$ and $A3(II)$, both of which displayed the $A3$ type polarisation fluorescence, there is evidence from time resolution studies to be presented in chapter 6 that further centers also contribute to the satellite structures observed in the broadband excitation spectra. Discrimination of these was not possible under the present resolution of the instruments used. The selective excitation monitoring specific transitions clearly reveals the ground splitting of the $A3(I)$ and $A3(II)$ centers (fig 4.19).

4.3.2 The Polarised Fluorescence Spectra

The polarised fluorescence spectra are presented for transitions from the $^1D_2$ to the $^3H_4$, $^3H_5$ and $^3H_6$ multiplets. The best transition to which to tune the laser for selective excitation, in the D multiplet, is the $Z_2 \rightarrow D_1$ transition at $16849.8cm^{-1}$ for the $A3(II)$ center and the $Z_1 \rightarrow D_2$ transition at $16882.7cm^{-1}$ for the $A3(I)$ center. Even so, simultaneous excitation of centers other than those which are of interest was unavoidable.

The $^3F_2$ multiplet

At least two other centers labelled **a** and **b** in figure 4.20 were also excited when the $Z_1 \rightarrow D_2$ transition of the $A3(I)$ center was pumped. An attempt was made to discriminate between these centers by detuning the laser off either side of the $A3(I)$ $Z_1 \rightarrow D_2$ transition peak but met with only partial success. The most probable $D \rightarrow W$ transitions of the $A3(I)$ center are indicated in figure 4.20(a). The polarised fluorescence spectra of the $A3(II)$ center is a little more clear-cut with no obvious

evidence of simultaneous excitation of another center.

The C_{4v}, $W_3(\gamma_5)$ level splitting is not apparent in this multiplet, most probably because the splitting is small and cannot be resolved within the linewidth of the transition. As for the parent C_{4v} center, the laser polarised E_Z gave roughly equal intensities for all the transitions to this multiplet for the $A3(I)$ and $A3(II)$ centers.

Figure 4.20 $^1D_2 \rightarrow ^3F_2$ Polarised fluoresence spectra of the mixed crystal centers in the 0.5% Ca^{2+} doped SrF_2 crystal at 11K.

(a) the $A3(I)$ center, pumping $16882.7cm^{-1}$.

(b) the $A3(II)$ center, pumping $16849.8cm^{-1}$.

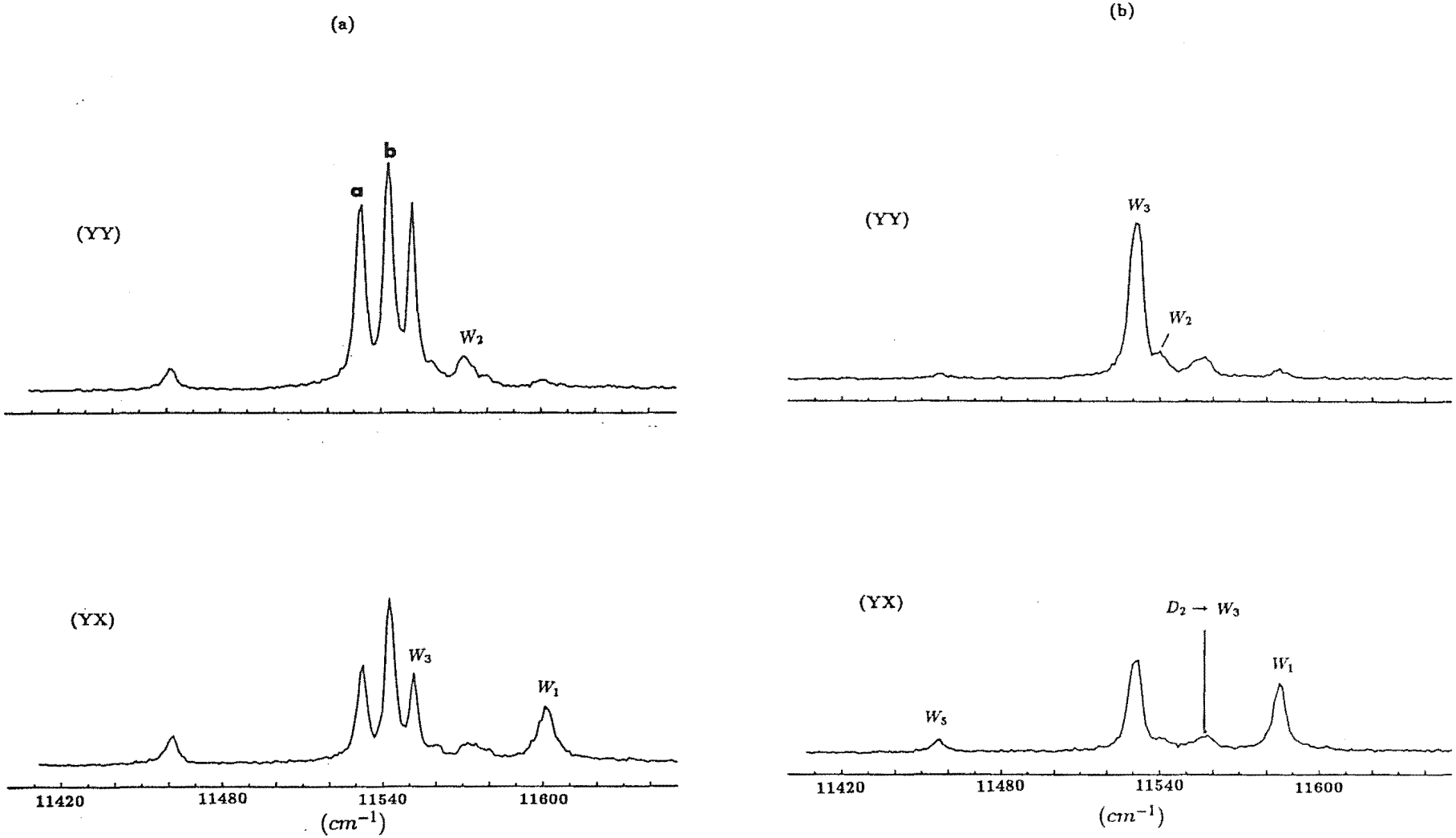
(a)
(YY)
a
b
W_2
(YX)
W_3
W_1
11420
11480
11540
11600
(cm^{-1})
(b)
(YY)
W_3
W_2
(YX)
$D_2 \rightarrow W_3$
W_1
W_5
11420
11480
11540
11600
(cm^{-1})

The $^3H_6$, $^3H_5$ and $^3H_4$ multiplets

The polarised transitions to the rest of the ^3H multiplets are shown to be very similar to the parent C_{4v} center and no obvious splitting of the parent C_{4v}, γ_5 levels is discernible from the transition linewidth where they are expected to occur (figs. 4.21, 4.22, 4.23).

Two features in the fluorescence spectra of the $D \rightarrow X$ transitions were not addressed in the study of the parent C_{4v} center by Reeves(1987). Firstly, the X_1 level with a γ_5 irrep is expected to display a (YX):(YY) polarisation of 1:2, for a $D_1(\gamma_3) \rightarrow X_1(\gamma_5)$ electric dipole transition. A (YX):(YY) ratio of 2:1 was observed instead, which is more consistent with a magnetic dipole transition rather than the electric dipole transition as assigned by Reeves (1987, table IV.2.5). The $D_2(\gamma_1) \rightarrow X_1(\gamma_5)$ transition however, has the expected polarisation ratio for an electric dipole transition.

The second feature concern two lines centered around 12450 and $12461 cm^{-1}$, apparent for $D \rightarrow X$ transitions of the parent C_{4v} center. These two lines have their equivalent in the mixed crystal centers at 12435 and 12446 cm^{-1} for the $A3(II)$ center and 12445 and $12456 cm^{-1}$ for the $A3(I)$ center. In the parent crystal, these two lines appear to be vibronic lines originating from the coupling of the X_1 levels to the lattice phonon states which gave rise to the lines labelled j and k (Reeve 1987 , table IV.2.2). Similarly, the correspoding two lines in the mixed crystal centers $A3(I)$ and $A3(II)$ were also assigned to vibronic transitions.

Figure 4.21 $^1D_2 \rightarrow ^3 H_6$ Polarised fluoresence spectra of the mixed crystal centers in the 0.5% Ca^{2+} doped SrF_2 crystal at 11K.

(a) the $A3(I)$ center, pumping $16882.7cm^{-1}$.

(b) the $A3(II)$ center, pumping $16849.8cm^{-1}$.

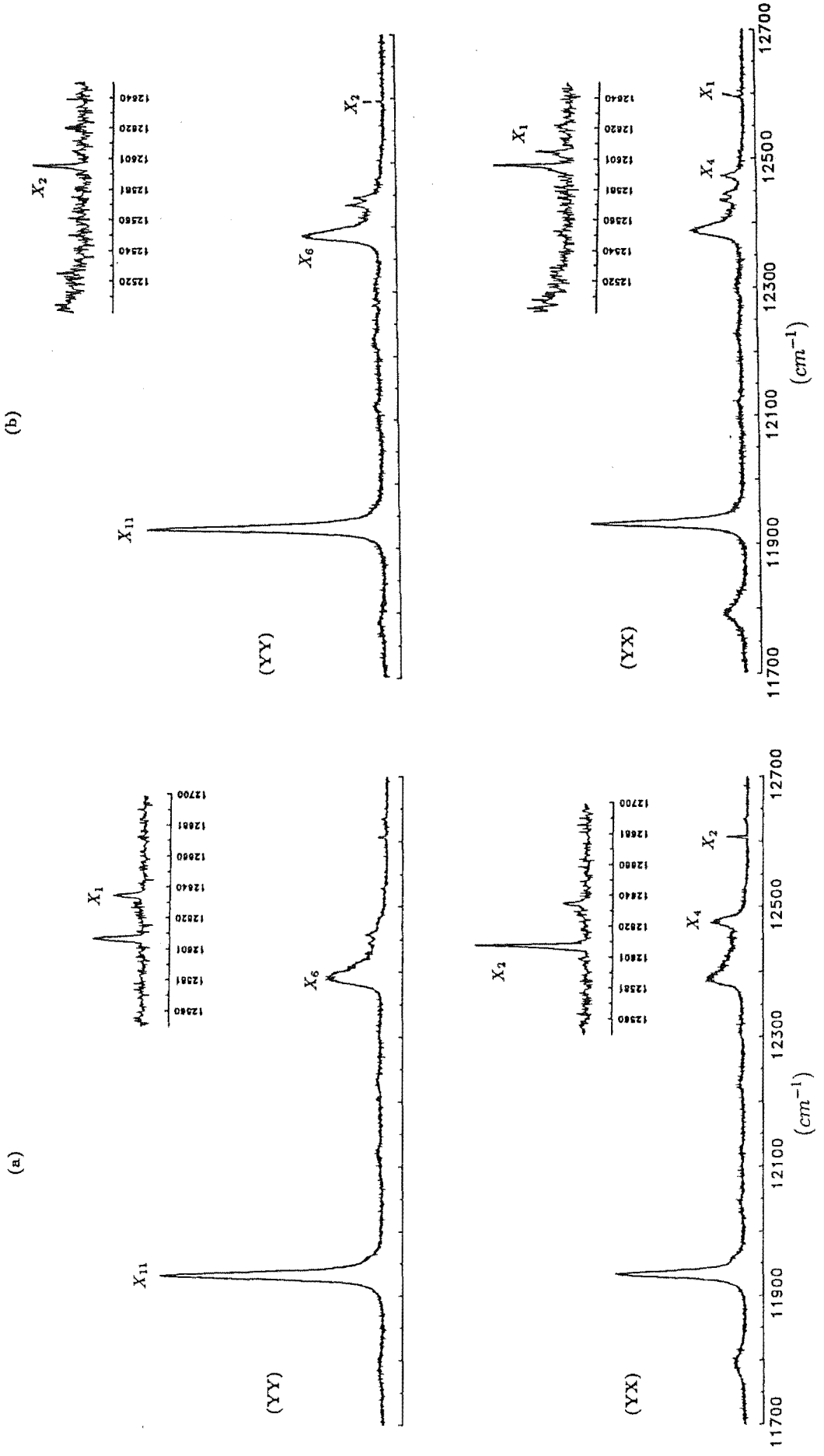
(a)
(b)
(YY)
(YX)
X_{11}
X_6
X_1
X_2
X_4
11700
11900
12100
12300
12500
12700
(cm^{-1})

Figure 4.22 $^1D_2 \rightarrow ^3 H_5$ Polarised fluoresence spectra of the mixed crystal centers in the 0.5% Ca^{2+} doped SrF_2 crystal at 11K.

(a) the $A3(I)$ center, pumping 16882.7cm^{-1}.

(b) the $A3(II)$ center, pumping 16849.8cm^{-1}.

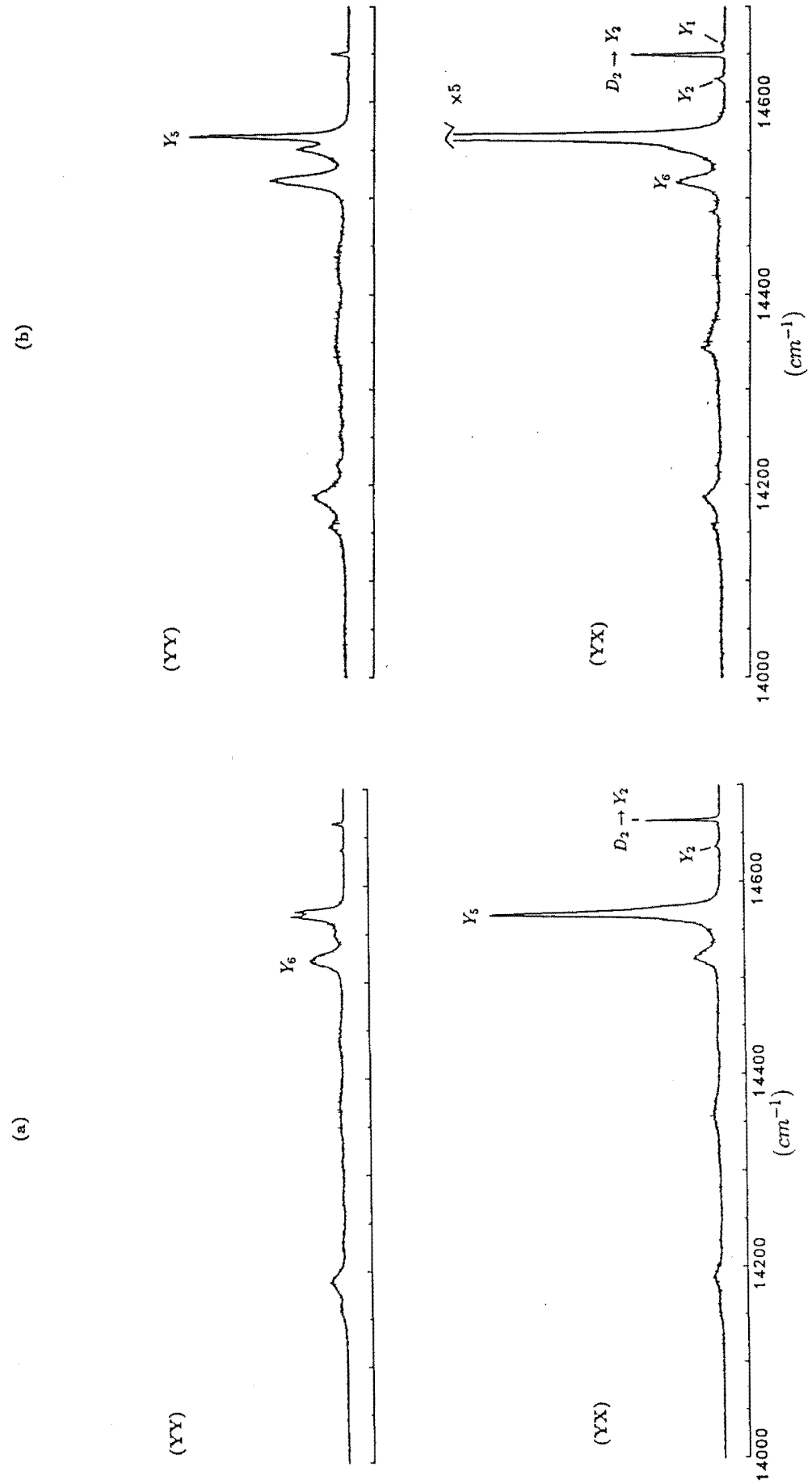
(a)
(YY)
Y_6
(YX)
Y_5
$D_2 \rightarrow Y_2$
Y_2
14000
14200
14400
14600
(cm^{-1})
(b)
(YY)
Y_5
(YX)
×5
$D_2 \rightarrow Y_2$
Y_1
Y_2
Y_6
14000
14200
14400
14600
(cm^{-1})

Figure 4.23 $^1D_2 \rightarrow ^3 H_4$ Polarised fluoresence spectra of the mixed crystal centers in the 0.5% Ca^{2+} doped SrF_2 crystal at 11K.

(a) the $A3(I)$ center, pumping 16882.7cm^{-1}.

(b) the $A3(II)$ center, pumping 16849.8cm^{-1}.

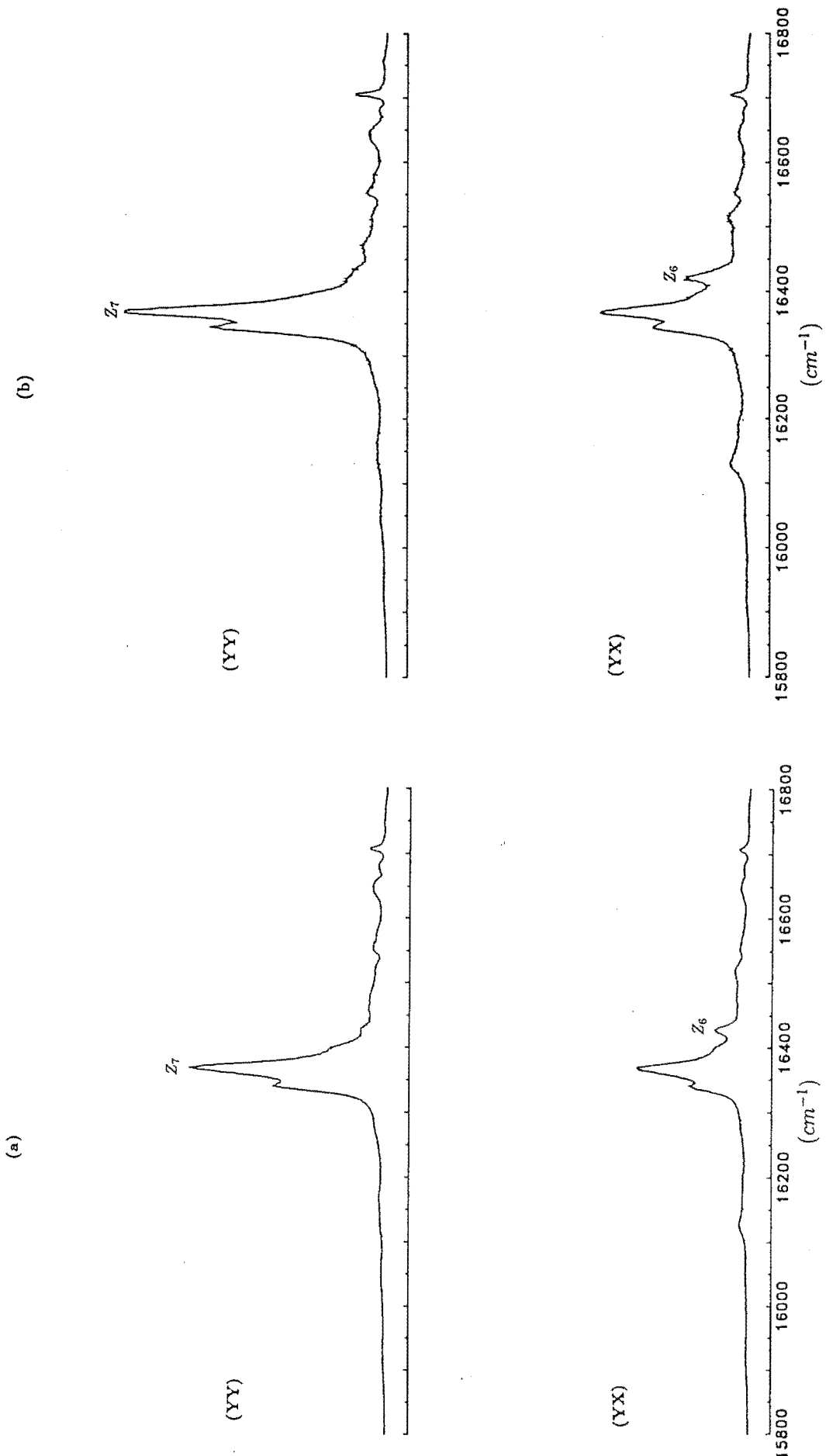
(a)
(b)
(YY)
(YX)
Z_7
Z_6
15800
16000
16200
16400
16600
16800
(cm^{-1})

4.3.3 Discussion

It was discovered from the time resolution studies (chap.6), that the transitions observed in the broadband excitation have contributions from centers which were not studied, because they could not be discriminated in the frequency domain from the myriad of overlapping lines belonging to a host of unstudied centers. Exactly how many of these centers are present is unknown, however, it is clear that some of them lie within the bandwidth of the parent C_{4v}, $Z_1 \rightarrow D_1$ and $Z_1 \rightarrow D_2$ transitions as well as within the satellite structures. Such centers having transitions with energy shift of less than $0.5cm^{-1}$ in the broadband excitation spectra, from the D_1 and D_2 transition band of the parent C_{4v} center, can only arise from a very small perturbation of the parent C_{4v} center.

The intensities in the broadband spectra are a poor guide, to the relative population of the centers since the number of centers which gave rise to the transition bands, is not well determined. Through an incidental contamination of the starting SrF_2 stock material with barium, the line at $16839cm^{-1}$ which belongs to the $A1$ center from a Ba^{2+} substitution (sec. 4.4), could be used as a reference to provide a rough comparison of the relative intensities of the line structures observed in the Ca^{2+} substituted centers. Such a comparison of the relative intensities with the barium $A1$ line at $16839cm^{-1}$ showed no evidence of quadratic rise of the satellite line intensities. Hence, it is very unlikely, that the centers belonging to the lines within the satellite linewidths arose from two cation substitutions.

Like the $A3$ center for the $Ca_{1-x}Sr_xF_2 : Pr^{3+}$ mixed crystal, no firm models could be assigned to the $A3(I)$ and $A3(II)$ centers of this Ca^{2+} doped SrF_2 crystal, based on the present set of spectral data. A tentative assignment of the energy levels are given in table 4.5 for the $A3(I)$ and $A3(II)$ centers. No irrep labels can be given since the symmetry groups of these centers are yet to be determined.

Table 4.5 The energy levels (in cm^{-1}) of mixed crystal centers A4 in $Sr_{1-x}Ba_xF_2:Pr^{3+}$ and A3(I) and A3(II) in $Sr_{1-x}Ca_xF_2:Pr^{3+}$. Uncertainties are $\pm 1 cm^{-1}$. unless otherwise indicated. The irrep labels are not given since no point group has been assign to these centers. brackets.

	A4	A3(I)	A3(II)
D_2	16899.0 ± 0.5	16882.7 ± 0.5	16878.1 ± 0.5
D_1	16838.3 ± 0.5	16854.7 ± 0.5	16852.5 ± 0.5
W_5	5400	5393*	5396
W_4	5320	-	-
W_3	5314	5305*	5321*
W_2	5293	5284*	5313*
W_1	5254	5255	5267
X_{13}	5054*	5061*	5056*
X_{12}	-	-	-
X_{11}	4963	4922*	4915*
X_{10}	4895	-	-
X_9	4456	-	-
X_8	4449	-	-
X_7	4426	-	-
X_6	4417	4466*	4466*
X_5	4407	4447* (γ_2 or $\gamma 4$)	4435 ± 10
X_4	4356	4380*	4380*
X_3	4334	-	-
X_2	4270	-	-
X_1	4265	4421	-

Y_{11}	-	-	-
Y_{10}	-	-	-
Y_9	-	2664*	2670*
Y_8	2338	-	-
Y_7	2316	-	-
Y_6	2297	2334*	2335*
Y_5	2282	2289	2298
Y_4	-	-	-
Y_3	2278	2293*	2301*
Y_2	2226	2219	2203
Y_1	2193*	-	-
Z_9	715 ± 10	734 ± 10	754 ± 10
Z_8	-	490	508
Z_7	531 ± 2	482	486
Z_6	455 ± 2	$428^* \pm 3$	$459^* \pm 5$
Z_5	-	-	-
Z_4	427 ± 5	-	367 ± 5
Z_3	161	-	-
Z_2	10.3 ± 0.5	2.6	2.7
Z_1	0	0	0

Levels which could not be unambigously assign are marked with an asterisk.

4.4 Mixed Crystal Centers in $Sr_{1-x}Ba_xF_2 : Pr^{3+}$

4.4.1 The Excitation Spectra

The broadband excitation spectra of the Ba^{2+} doped $SrF : Pr^{3+}$ revealed one prominent satellite line at $16839cm^{-1}$. This was subsequently found to be a new class of center labelled the $A4$ center (fig. 4.24) based on some differences in polarisation behaviour from the other centers, as will be discussed in section 4.4.2 . Obvious differences between the Ca^{2+} and Ba^{2+} doped SrF_2 crystals, are apparent in the satellite structures at the shoulders of both the D_1 and D_2 lines of the parent C_{4v} center, indicating more Ba^{2+} perturbed sites are present. These were however not studied, since they could not be satisfactorily discriminated against the many transitions present at the shoulders of the main transitions belonging to the parent C_{4v} center.

Selective excitation monitoring $14615.3cm^{-1}$ revealed a spectrum that is similar to that of a $A1$ type center (fig. 4.25). The ground state splitting was found to be $10.3cm^{-1}$.

4.4.2 The Polarised Fluorescence Spectra

Two salient polarisation features exhibited by this center suggests a different classification is required. Firstly, the (YX):(YY) polarisation ratios of the transitions observed are roughly 0:1, 1:2, 4:1 and 1:5 for this center (fig. 4.26(a)(i)). Secondly, with the laser polarised in the E_Z direction, no extinction of emission for any of the transitions was observed in the $D \rightarrow W$ transitions as were the case for the $A1$ type centers, rather, little polarisation effect was observed (fig. 4.26(a)(ii)). Since the combination of these two polarisation features in the $^3F_2$ mulitplet is unique, the center is given a new classification, the $A4$ type center.

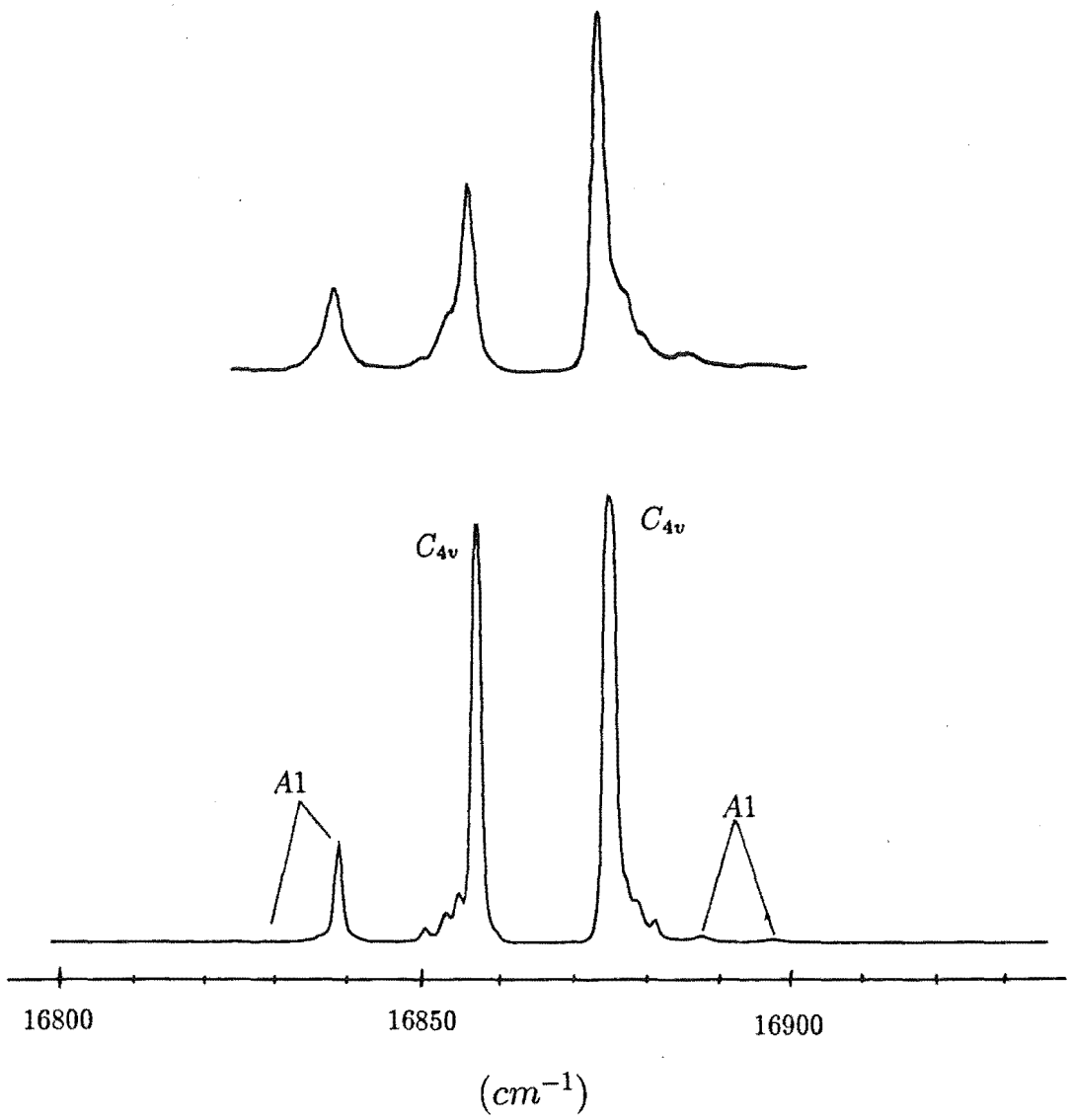

Figure 4.24 Broadband excitation spectra of the $Sr_{1-x}Ba_xF_2 : Pr^{3+}$ crystals, monitoring the $D \rightarrow Z$ transitions at 11K.

(a) 1% Ba^{2+} doping **(b)** 0.5% Ba^{2+} doping

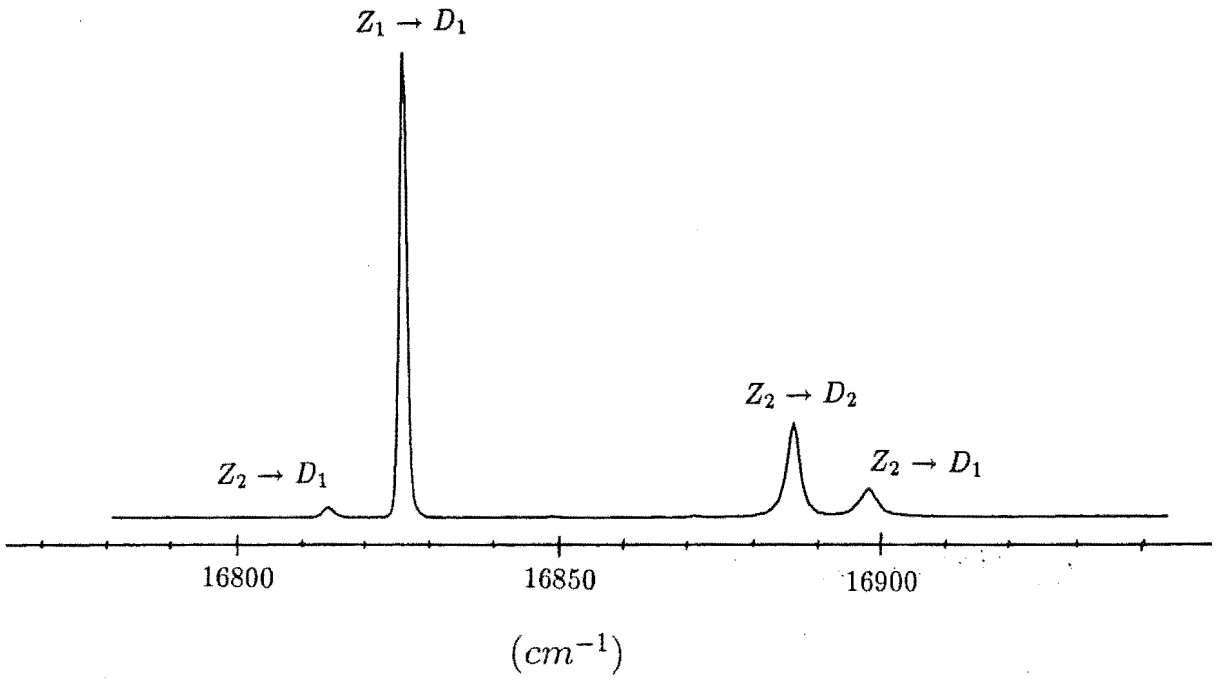

Figure 4.25 Selective excitation spectra of the mixed crystal $A4$ centers in the 0.5% Ba^{2+} doped SrF_2 crystal at 11K by scanning the dye laser and monitoring $14615cm^{-1}$.

Figure 4.26 $^1D_2 \rightarrow ^3F_2$ Polarised fluoresence spectra of the A4 mixed crystal center in the 0.5% Ba^{2+} doped SrF_2 crystal at 11K.

(a)(i) laser polarised E_Y
(a)(ii) laser polarised E_Z

(a) (i)

(YY)
W_4
W_3
W_2
(YX)
W_5
W_1
11420
11480
11540
11600
(cm^{-1})

(a) (ii)

(ZY)
W_2
W_4
W_1
(ZX)
W_5
11420
11440
11461
11480
11500
11520
11540
11561
11581
11600
11620
11640
(cm^{-1})

The $^3H_6$ multiplet displays the full range of polarisation ratios mentioned for this center. At around $12570cm^{-1}$, the splitting of a C_{4v} $X_1(\gamma_5)$ level of $5cm^{-1}$ is apparent (fig. 4.27). The $^3H_5$ multiplet display all the ratios except the (YX):(YY) ratio of 1:2 (fig. 4.28). The $16346cm^{-1}$ line in the $^3H_4$ mulitplet (fig 4.29) also appeared in the $D_1 \rightarrow Z$ emission spectra of the parent C_{4v} center, the origin of this line is still unknown. As in the emission to the $^3H_4$ multiplet of the other centers, the presence of some vibronic lines would introduce some uncertainty in the assignment of levels to this multiplet.

4.4.3 Discussion

A unique feature of the $A4$ center is the great range of polarisation ratios observed. The absorption transitions from both the γ_1 and γ_2 ground state levels to the D multiplet and subsequent emission, of the $C_s(a)$ or $C_s(b)$ symmetry configuration, would only give at most three different types of polarisation ratios. Hence the $C_s(a)$ or $C_s(b)$ centers would not account for all the observed polarisation ratios of the $A4$ center. It appears that the lowest symmetry group C_1 is needed to describe the polarisation ratios observed for the $A4$ center.

The proportional change of broadband transition intensities with Ba^{2+} concentration is more consistent with a single cation subsitition for the $A4$ center. Judging from the energy shift of the $A4$ levels from the parent C_{4v} levels in the D multiplet ($\sim 20cm^{-1}$), indicating a relatively strong perturbation to the parent C_{4v} center, an off-axis barium substitution near to the parent C_{4v} center, in the NN cation sphere, would be a likely model.

To satisfy the criteria for a model with a symmetry lower than the C_s, the substitution must break the reflection plane of the C_s center. The substitutions depicted in figure 2.2(a)(ii) and (iii) would not fit the requirements of the model since the C_s reflection is still preserved.

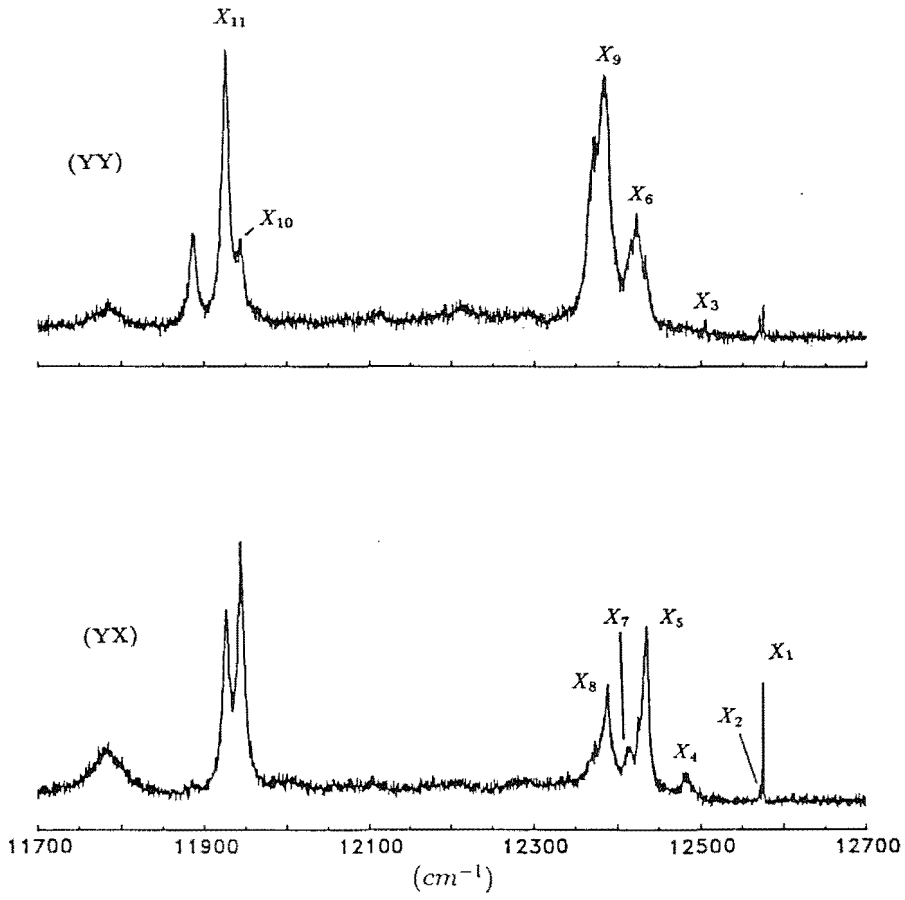

Figure 4.27 $^1D_2 \rightarrow ^3H_6$ Polarised fluoresence spectra of the A4 mixed crystal center in the 0.5% Ba^{2+} doped SrF_2 crystal at 11K.

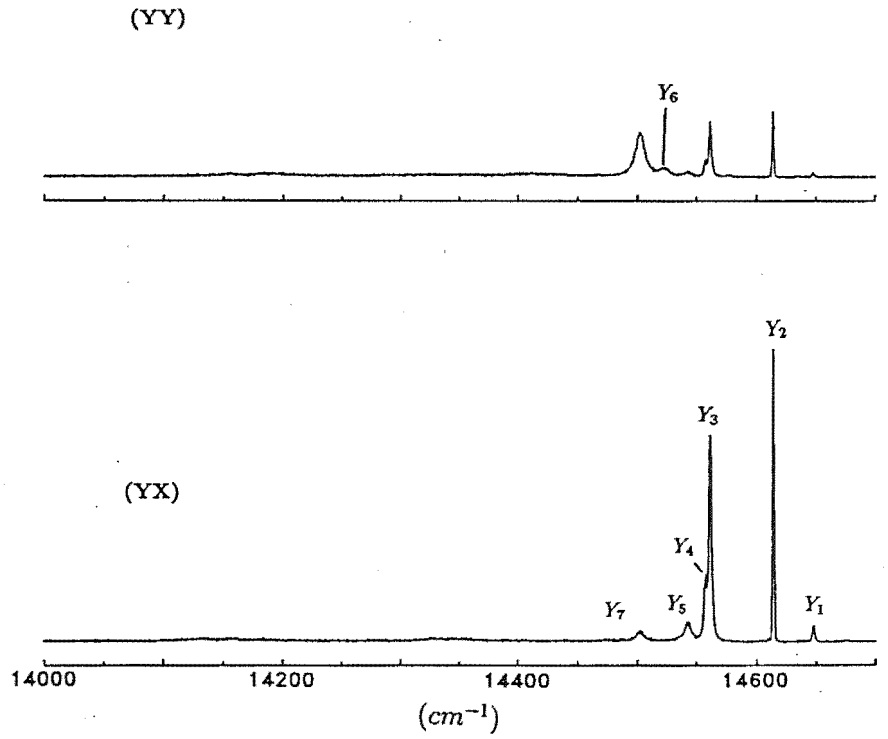

Figure 4.28 $^1D_2 \rightarrow ^3H_5$ Polarised fluoresence spectra of the A4 mixed crystal center in the 0.5% Ba^{2+} doped SrF_2 crystal at 11K.

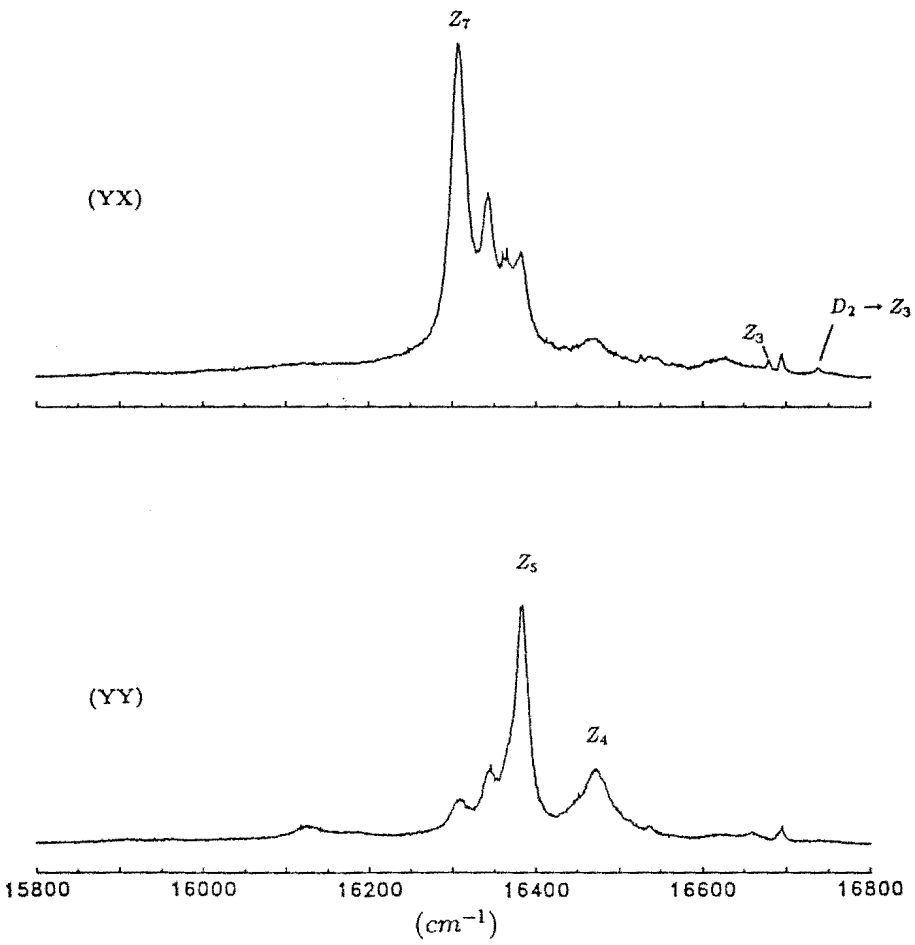

Figure 4.29 $^1D_2 \rightarrow ^3H_4$ Polarised fluoresence spectra of the A4 mixed crystal center in the 0.5% Ba^{2+} doped SrF_2 crystal at 11K.

A model of the distorted lattice fluorine positions in the Pr^{3+} C_{4v} center, was proposed in the ODNMR work by Burum et al[1982]. Figure 9 of their paper, reproduced here in figure 4.30, shows that the lattice fluorines nearest and furthest away from the interstitial F^-, in the NN position from the Pr^{3+} ion, do not have equal distortions. If the off-axis barium is substituted in the position as shown in figure 2.2(a)(i), then it could distort the two F^- ligands between the Pr^{3+} and the Ba^{2+} ion, out of the C_s reflection plane formed by the interstitial F^-, the Pr^{3+} and Ba^{2+} ions. Hence, a possible substitutional arrangement for a likely model would be that of figure 2.2(a)(i) with one or both the lattice fluorines moving out of the C_s reflection plane. This in effect produces a center with the lowest possible symmetry and would give the greater variety of the polarisation ratios observed.

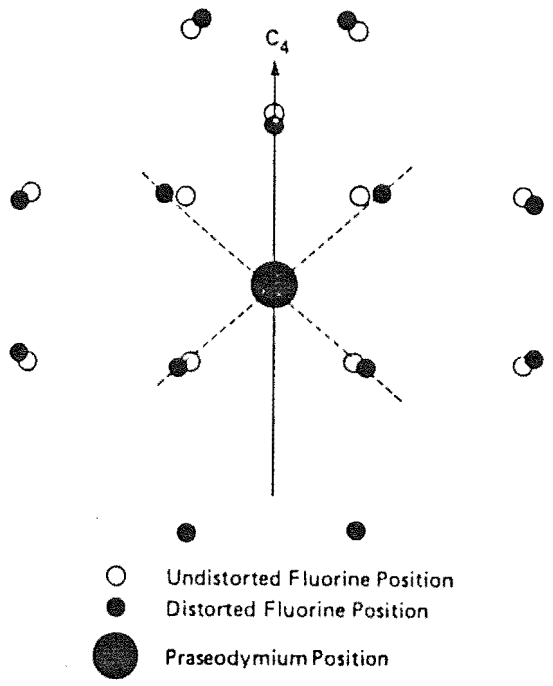

Figure 4.30 Projection of the normal and distorted fluorine and Pr^{3+} positions on a plane containing the C_4 symmetry axis and one of the other [100] axis as determined from the ODNMR studies of Burum et al[1982].

Chapter 5

Laser Spectroscopy of the Deuterated Mixed Crystals

There are basically two reasons for the interest in deuterated crystal systems. Firstly, centers produced from the charge compensation by the D^- ions are analogous to the F^- centers present in these crystals. However, since the deuterium and fluorine ions differ both in size and atomic mass, different crystal field levels will be observed for equivalent charge compensating interstitial positions of these ions. Additionally, the vibrations of the lighter D^- ion will give rise to new spectral features associated with the vibronic levels.

The second reason for studying deuterated crystals is that further centers are present when the D^- ions occupy both the interstitial and lattice positions around the Pr^{3+} ions. This gives rise to lower symmetry centers, which are particularly interesting because of their fluorescence bleaching behaviour. A detail study of the bleaching centers in the deuterated $Ca_{1-x}Sr_xF_2 : Pr^{3+}$ and $Sr_{1-x}Ca_xF_2 : Pr^{3+}$ crystal systems has been performed and will be discussed in chapter 8.

Overall, the selective excitation studies of the D^- mixed crystal centers were not as successful as their F^- counterparts. In most cases, the simultaneous excita-

tion of transitions of several centers was unavoidable. To assign the lines observed to particular D^- mixed crystal centers then required extensive knowledge of the lines originating from the unintentional excitation of other centers. If these are not available, then the assignment would be ambigous. The results from the investigations carried out on the single D^- charge compensation mixed crystal centers in the $Ca_{1-x}Sr_xF_2 : Pr^{3+} : D^-$, $Ca_{1-x}Ba_xF_2 : Pr^{3+} : D^-$, $Sr_{1-x}Ca_xF_2 : Pr^{3+} : D^-$ and $Sr_{1-x}Ba_xF_2 : Pr^{3+} : D^-$ crystals are presented in this chapter in section 5.1, 5.2, 5.3 and 5.4 respectively.

5.1 Mixed Crystal Centers in $Ca_{1-x}Sr_xF_2 : Pr^{3+} : D^-$

5.1.1 The Excitation Spectra

The broadband excitation spectrum of deuterated mixed crystal gave rise to new lines (fig. 5.1(a)) not present in the spectrum of the parent $CaF_2 : D^-$ crystal (fig. 5.1(b)). These deuterated mixed crystal centers are labelled $A1(D^-)$ and $A2(D^-)$ and as will be shown later, display polarised fluorescence that typifies the $A1$ and $A2$ type centers.

Figures 5.2(a) and (b) are the excitation spectra of the D^- $A1$ and $A2$ centers monitoring the $D \rightarrow Y$ transitions at $14564cm^{-1}$ and $14575cm^{-1}$ respectively. The $D_1 \rightarrow Y_3$ transition of the parent C_{4v} center peaking at $14562cm^{-1}$, was sufficiently strong to have the shoulder on the higher energy side of its transition peak, extending to overlap the transition of the the $A1$ center being monitored by the monochromator. Hence some residual excitation lines belonging to the parent F^- C_{4v} center were present. This is not a problem since the C_{4v} levels in the $^1D_2$ mulitplet could be easily identified. The excitation spectrum presents no ambiguity in the assignment of the D_1 and D_2 levels of the D^- $A2$ center in the $^1D_2$ multiplet (fig. 5.2(b)).

An obvious difference in comparing the selective excitation spectra, while mon-

itoring a specific transition of the various C_{4v} centers in the CaF_2 crystal is the relative transition strength of the D_1 and D_2 levels. In order of ascending relative intensity strengths of the D_2 excitation levels are those belonging to the $A2(F^-)$, $C_{4v}(F^-)$, $A2(D^-)$ and $C_{4v}(D^-)$ centers with D_1 and D_2 energy level seperations of 8.9, 16.7, 12.0 and 39.8 cm^{-1} respectively. It seems curious that those centers which have a D_1 and D_2 energy level seperation closer to multiples of $9cm^{-1}$ have stronger D_2 relative intensities. The $A2(D^-)$ center in the Ba^{2+} doped crystal has a D_1 and D_2 seperation of $18.8cm^{-1}$ which seems to go with this trend, in fact, it has the strongest D_2 relative intensity. If the value of $9.4cm^{-1}$ is chosen to establish this trend, then the $A2(F^-)$ center in the Ba^{2+} doped crystal fits in with the overall scheme and with a $D_1 - D_2$ seperation of $29.5cm^{-1}$ it has a D_2 to D_1 intensity ratio between those of the $A2(F^-)$ center in the Sr^{2+} doped crystal and the parent $C_{4v}(F^-)$ center. Table 5.1 summarizes the details of this discussion and shows that the exception to this trend is the $C_{4v}(D^-)$ center.

Since the $D_1 \rightarrow Y_2$ transition was monitored in all cases, the relative transition strengths of the D_1 and D_2 levels in the various C_{4v} centers arise from the combination of the non-radiative $D_2 \rightsquigarrow D_1$ decay efficiencies and the relative absorption strengths of the $Z_1 \rightarrow D_2$ and D_1 transitions. If the former effect is dominant, then these observations could be explained by a lattice phonon mode with an energy of approximately $9.4cm^{-1}$ i.e. closely matching the D_1 and D_2 energy level seperation of the $A2(F^-)$ center.

5.1.2 The Polarised Fluorescence Spectra

The D^- $A1$ and $A2$ centers studied in $Ca_{1-x}Sr_xF_2 : Pr^{3+}$ are classified based on the characteristics of the polarised fluorescence of the transitions observed. This was fully discussed in the chapter 4.1. A discussion of the results from the measurements of the fluorescence spectra for the two mixed crystal D^- centers studied is presented below.

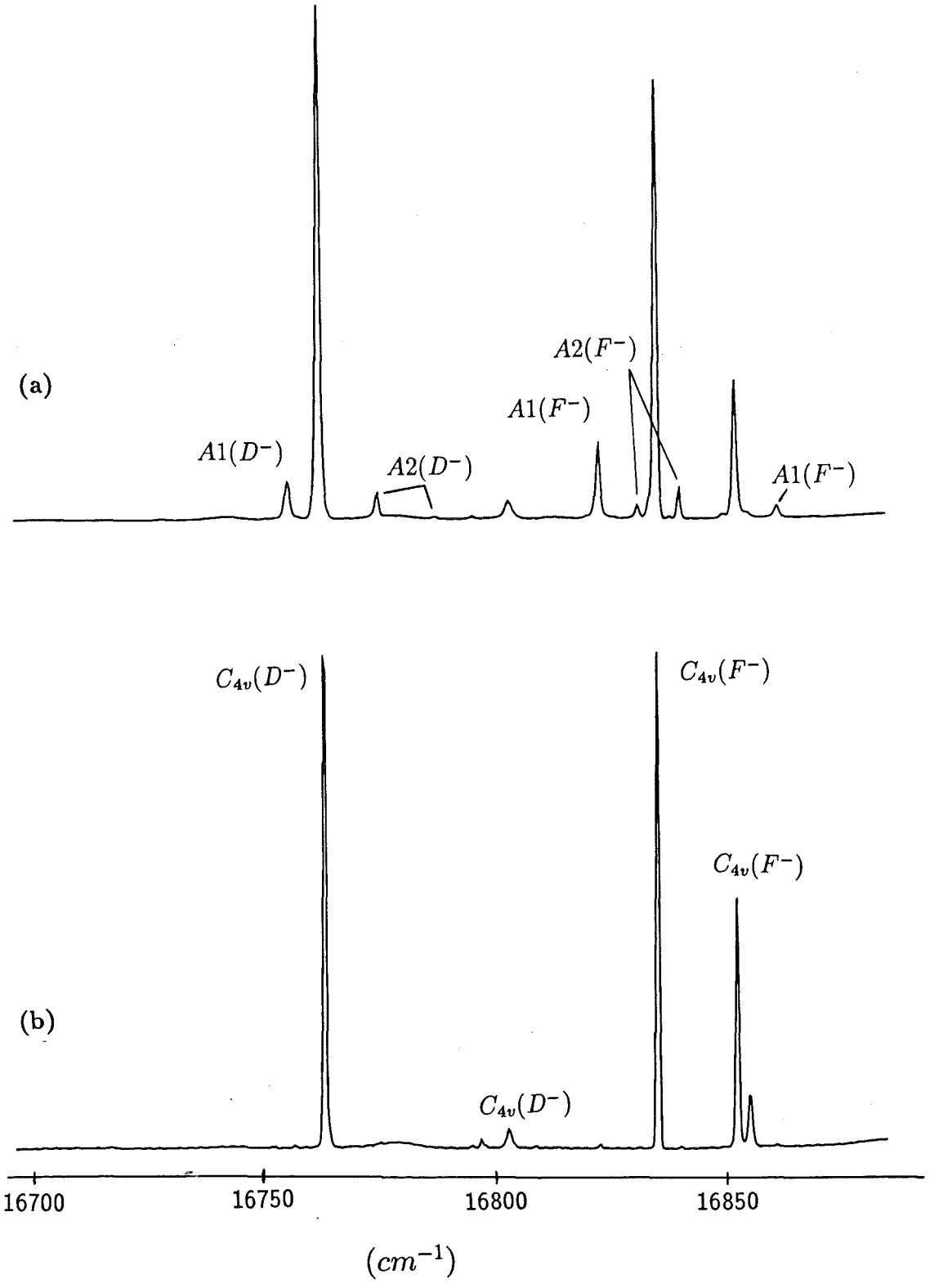

Figure 5.1 Broadband excitation spectra of the deuterated $Ca_{1-x}Sr_xF_2 : Pr^{3+}$ crystals, monitoring the $D \rightarrow Z$ transitions at 11K.

(a) 0.5% Sr^{2+} doping and deuterated for 60 hours.
(b) Parent crystal, deuterated for 60 hours.

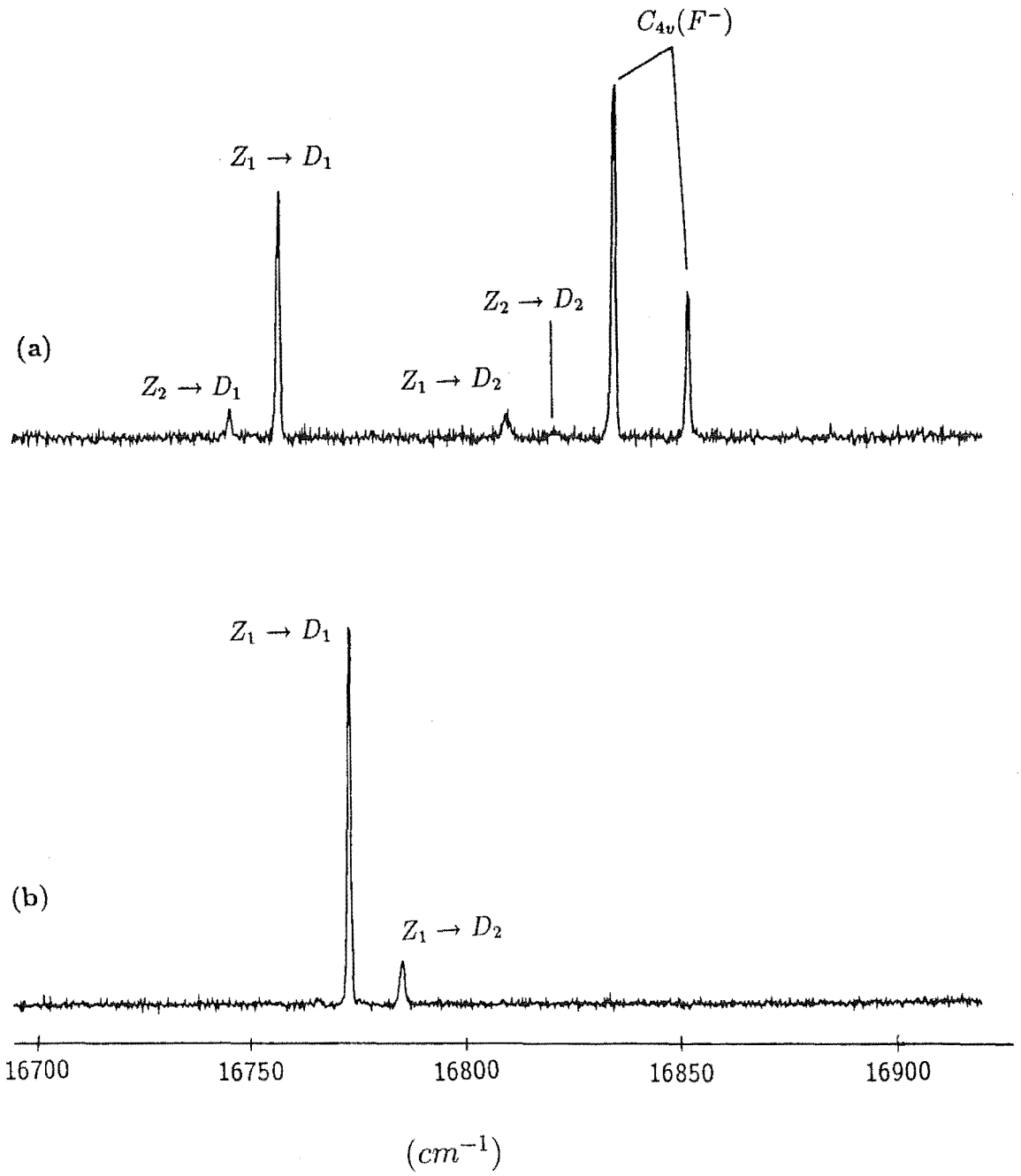

Figure 5.2 Selective excitation spectra of the D^- mixed crystal centers in the 0.5% Sr^{2+} doped CaF_2 crystal at 11K obtained by scanning the dye laser and monitoring specific transitions.

(a) the $A1$ center monitoring $14564cm^{-1}$.
(b) the $A2$ center monitoring $14575cm^{-1}$.

C_{4v} centers	$D_1 - D_2$ seperation $\epsilon\ (cm^{-1})$	Closest multiple of $9.4cm^{-1}$ η	Δ $= \lvert\epsilon - \eta\rvert$ (cm^{-1})	$D_2 : D_1$ Intensity ratios
Ba^{2+} $A2(D^-)$	18.8	18.8	0	5.6
Sr^{2+} $A2(F^-)$	8.9	9.4	0.5	2.3
Ba^{2+} $A2(F^-)$	29.5	28.2	1.3	1.5
$C_{4v}(F^-)$	16.7	18.8	2.1	0.5
Sr^{2+} $A2(D^-)$	12.0	9.4	2.6	0.1
$C_{4v}(D^-)$	39.8	37.6	2.2	0.06

Table 5.1: Correlation between the $D_1 - D_2$ energy level seperation and the relative intensities of the D_2 and D_1 excitation of the C_{4v} centers in the CaF_2 host (see text for details).

As shown in figure 5.3, the $D \rightarrow W$ fluorescence spectra for the D^- $A1$ and $A2$ centers display the appropriate polarised fluorescence signature for the respective types of center, i.e. (YX):(YY) ratios of approximately 1:0 and 0:1 for the $A1$ center (fig. 5.3(a)) and 1:2 and 1:0 for the $A2$ center (fig. 5.3(b)). The characteristic (ZX):(ZY) polarisation ratios of 0:0 and 1:1 were also observed for the $A1$ center . The similiarity in the fluorescence spectra observed for the equivalent class of F^- and D^- mixed crystal centers suggests a close analogy. Therefore, models assigned to the mixed crystal F^- $A1$ and $A2$ centers should apply to the corresponding D^- $A1$ and $A2$ centers as well.

Table 5.2(a) The energy levels (in cm^{-1}) of the D^- mixed crystal centers A1 and A2 in $Ca_{1-x}Sr_xF_2$:Pr^{3+}:D-. Uncertainties are $\pm 1 cm^{-1}$. unless otherwise indicated. The irrep labels for each level are given in brackets.

	A1		A2	
D_2	16805.3 ± 0.5	(γ_1)	16784.8 ± 0.5	(γ_3)
D_1	16754.6 ± 0.5	(γ_1)	16772.8 ± 0.5	(γ_1)
W_5	-	(γ_1)	NA	
W_4	5394	(γ_1)	-	(γ_4)
W_3	5367	(γ_2)	5356	(γ_5)
W_2	5361	(γ_2)	-	(γ_3)
W_1	5304	(γ_1)	5300	(γ_1)
X_{13}	-	(γ_1)	NA	
X_{12}	-	(γ_1)	NA	
X_{11}	5001	(γ_2)	NA	
X_{10}	4942	(γ_1)	-	(γ_3)
X_9	-	(γ_2)	4956	(γ_5)
X_8	4871	(γ_1)	4869	(γ_1)
X_7	-	(γ_2)	-	(γ_4)
X_6	4592	(γ_1)	-	(γ_3)
X_5	4529	(γ_2)	-	(γ_2)
X_4	4482 ±5	(γ_1)	4502	(γ_5)
X_3	-	(γ_2)	4449	(γ_3)
X_2	4179	(γ_1)	-	(γ_4)
X_1	4174	(γ_2)	4185	(γ_5)
Y_{11}	-	(γ_2)	NA	
Y_{10}	-	(γ_2)	NA	
Y_9	-	(γ_1)	NA	
Y_8	-	(γ_2)	-	(γ_4)
Y_7	2420 ± 5	(γ_2)	-	(γ_5)
Y_6	2397	(γ_1)	-	(γ_2)
Y_5	-	(γ_1)	2389 ± 5	(γ_5)
Y_4	2237	(γ_2)	-	(γ_3)
Y_3	2224	(γ_1)	2240	(γ_5)
Y_2	2191	(γ_1)	2198	(γ_1)
Y_1	-	(γ_2)	-	(γ_2)

Z_9	-	(γ_1)	NA	
Z_8	592	(γ_2)	NA	
Z_7	546	(γ_1)	-	(γ_3)
Z_6	529	(γ_1)	547	(γ_5)
Z_5	-	(γ_2)	519†	(γ_1)
Z_4	462 ± 10	(γ_1)	-	(γ_2)
Z_3	196 *	(γ_2)	439 ± 10	(γ_1)
Z_2	10.4	(γ_1)	-	(γ_4)
Z_1	0	(γ_2)	0	(γ_5)

Levels which could not be unambigously assign are marked with an asterisk.
NA - Excited levels not applicable to the A2 C_{4v} center.
† - electronic level inferred from the vibronic transition.

Table 5.2(b) Assignment of the vibronic energy levels (in cm^{-1}) for the D^- mixed crystal centers A1 and A2 in $Ca_{1-x}Sr_xF_2$:Pr^{3+}:D-.

A1		A2	
$Z_1(xa)$	742	$Z_1(x)$	711
$Z_1(za)$	794	$Z_1(z)$	774
$Z_1(zb)$	804	$Z_5(x)$	1229
$Z_4(za)$	1257	$Z_6(z)$	1322
$Z_6(za)$	1316	$X_1(x)$	4906
$Z_8(xa)$	1312	$X_1(z)$	4966
$Z_8(za)$	1377		
$X_1(xa)$	4895		
$X_1(xb)$	4919		

The $D \rightarrow X$ transitions span a region of $1200cm^{-1}$ and the signals are extremely weak. The best approach was to capitalise on the stronger signal from an unpolarised scan to determine regions where there are obvious features of interest. Polarised scans in selected regions of the spectra with a substantially longer integration time of 15 to 30 seconds per data point were then performed. The spectra from these scans are presented in figure 5.4.

Samarium contamination in the PrF_3 powder used in the crystal growth presents annoying problems in the study of deuterated samples. The deuteration process was found to enhance the population of the Sm^{2+} centers in the crystals [Reeves, 1987]. The frequency used in the excitation of the $A1$ and $A2$ centers in the D multiplet coincided with the absorption band of the Sm^{2+} ion, peaking at $16103cm^{-1}$ with a bandwidth of approximately $500cm^{-1}$ and labelled line B in the work of Wood et al [1962]. The strong but decreasing background observed in the $D \rightarrow X$ transition (fig. 5.4(a) and (b)) originates from the transitions of the Sm^{2+} centers which are simultaneously excited. The lines at 12500, 12545 and $12650cm^{-1}$ which appeared for fluorescence spectra of the $A1$ and $A2$ center to the X multiplet, can be attributed to Sm^{2+} transitions (table III, Wood et al, 1962) in the CaF_2 host.

Assigning the levels in the Y mulitplet for the $A1$ center is relatively straightforward, while some additional lines in the same multiplet for the $A2$ center were difficult to account for. By detuning the laser from the excitation frequency, it was found that the intensities of the lines marked with dots in figure 5.5(b) do not correlate with the main transitions belonging to the $A1$ center. The nature of the centers contributing to those extra lines is undertermined in this study.

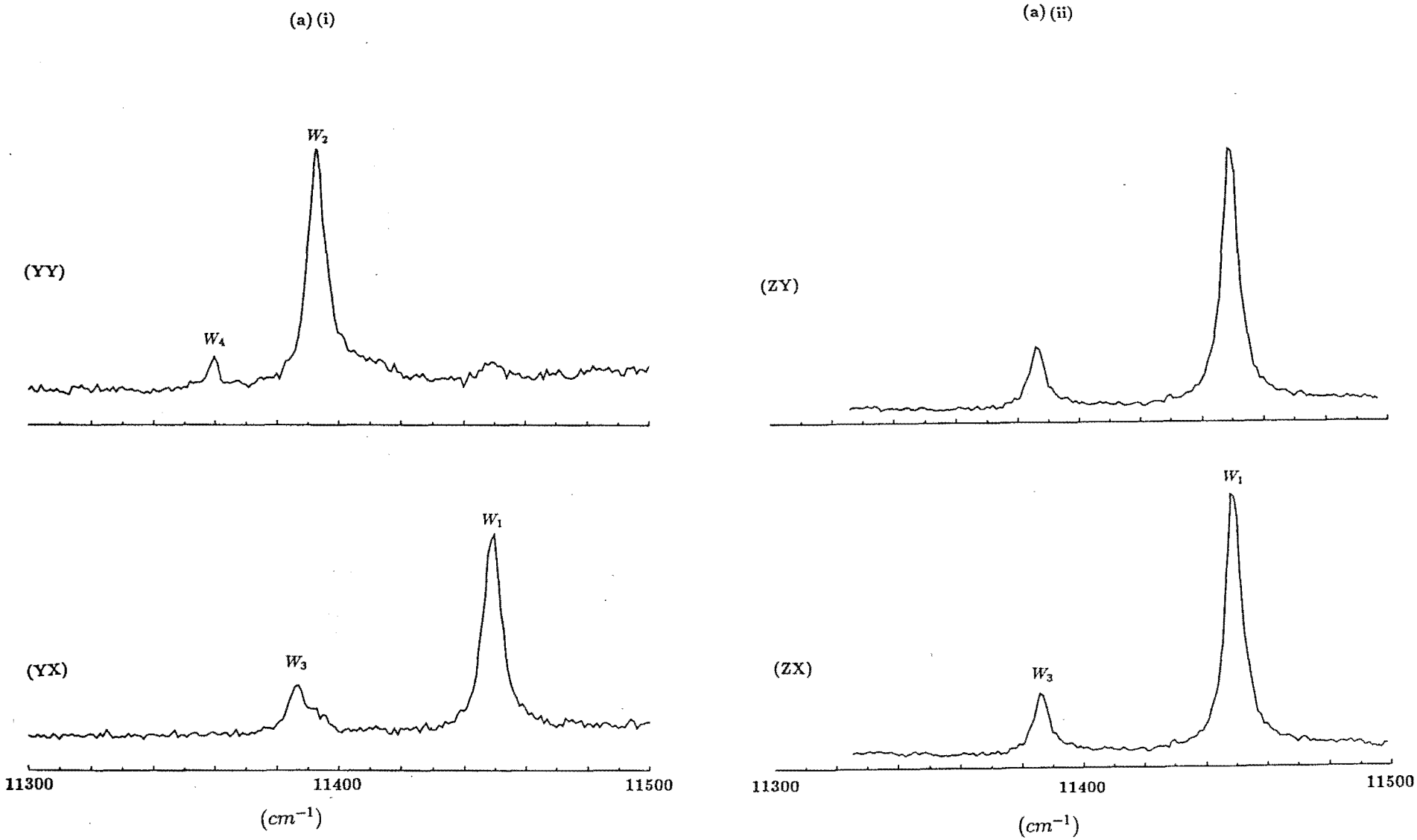
(a) (i)
(a) (ii)
(YY)
(ZY)
(YX)
(ZX)
W_1
W_2
W_3
W_4
11300
11400
11500
(cm^{-1})

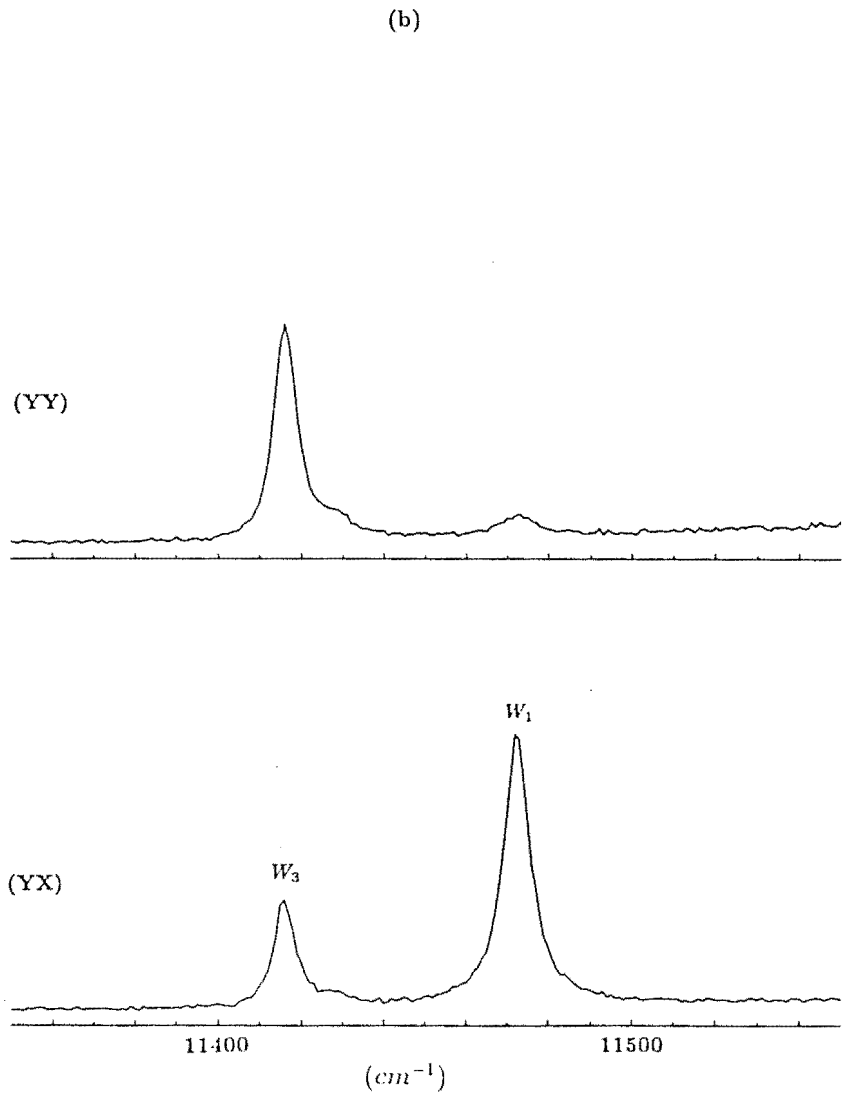

Figure 5.3 $^1D_2 \rightarrow ^3F_2$ Polarised fluoresence spectra of the D^- mixed crystal centers in the 0.5% Sr^{2+} doped CaF_2 crystal at 11K.
(a) the $A1$ center, pumping $16754.6cm^{-1}$.
Laser polarised (i) E_Y and (ii) E_Z.
(b) the $A2$ center, pumping $16772.8cm^{-1}$.

Figure 5.4 $^1D_2 \rightarrow ^3 H_6$ Polarised fluoresence spectra of the D^- mixed crystal centers in the 0.5% Sr^{2+} doped CaF_2 crystal at 11K.

(a) the $A1$ center, pumping $16754.6cm^{-1}$.
(b) the $A2$ center, pumping $16772.8cm^{-1}$.

The bottom trace is the unpolarised spectra.

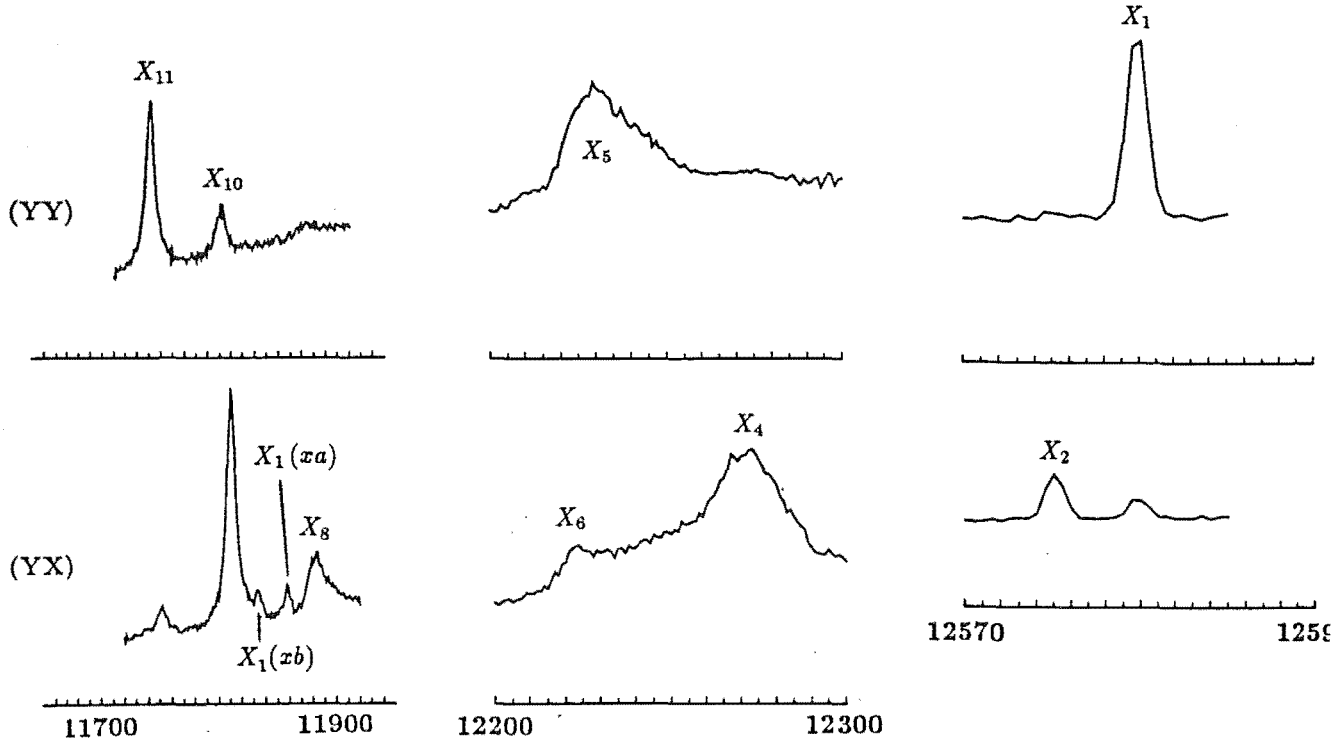
(YY)
X_{11}
X_{10}
X_5
X_1
(YX)
$X_1(xa)$
X_8
$X_1(xb)$
X_6
X_4
X_2
11700
11900
12200
12300
12570

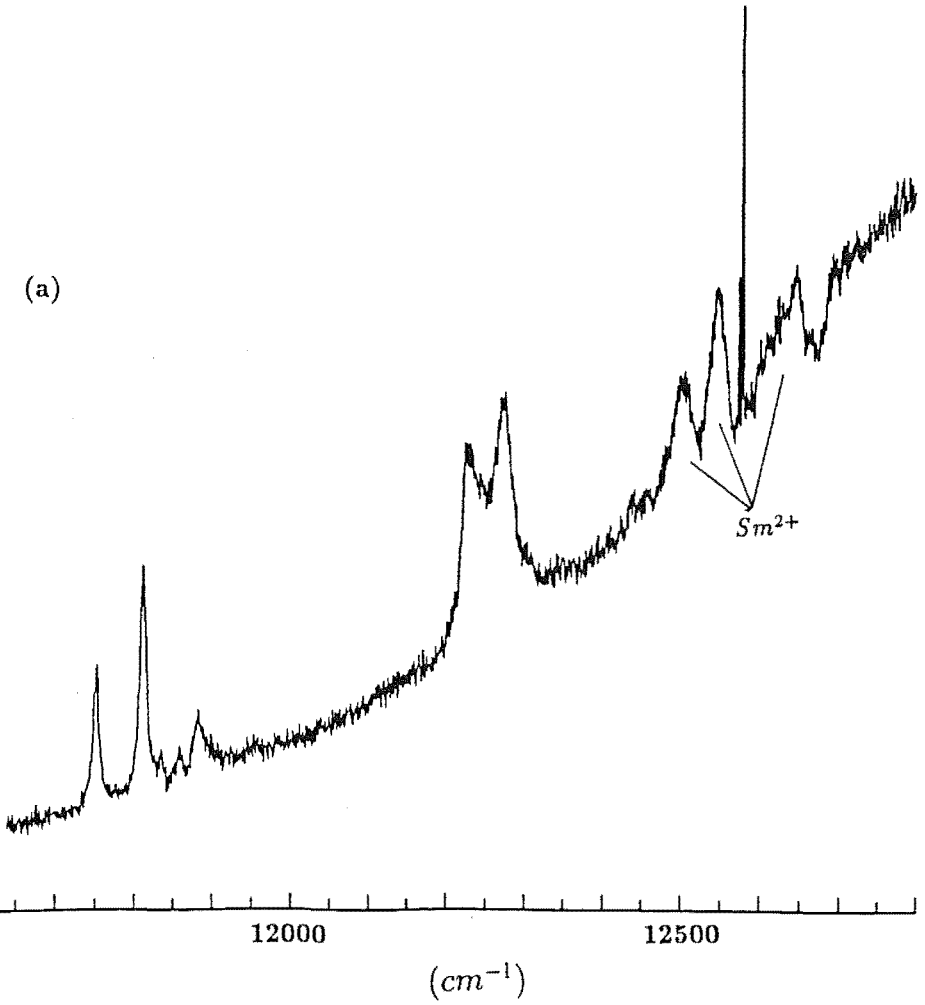
(a)
Sm^{2+}
12000
12500
(cm^{-1})

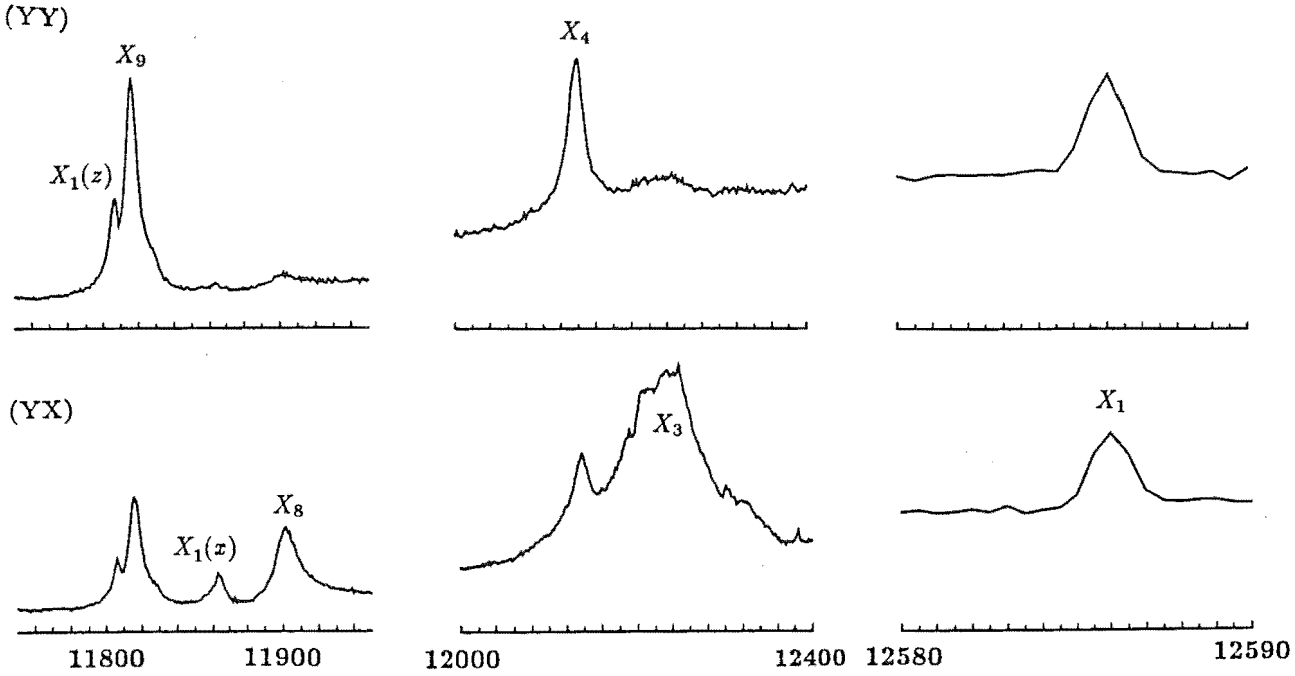
(YY)
X_9
$X_1(z)$
X_4
(YX)
X_8
$X_1(z)$
X_3
X_1
11800
11900
12000
12400
12580
12590

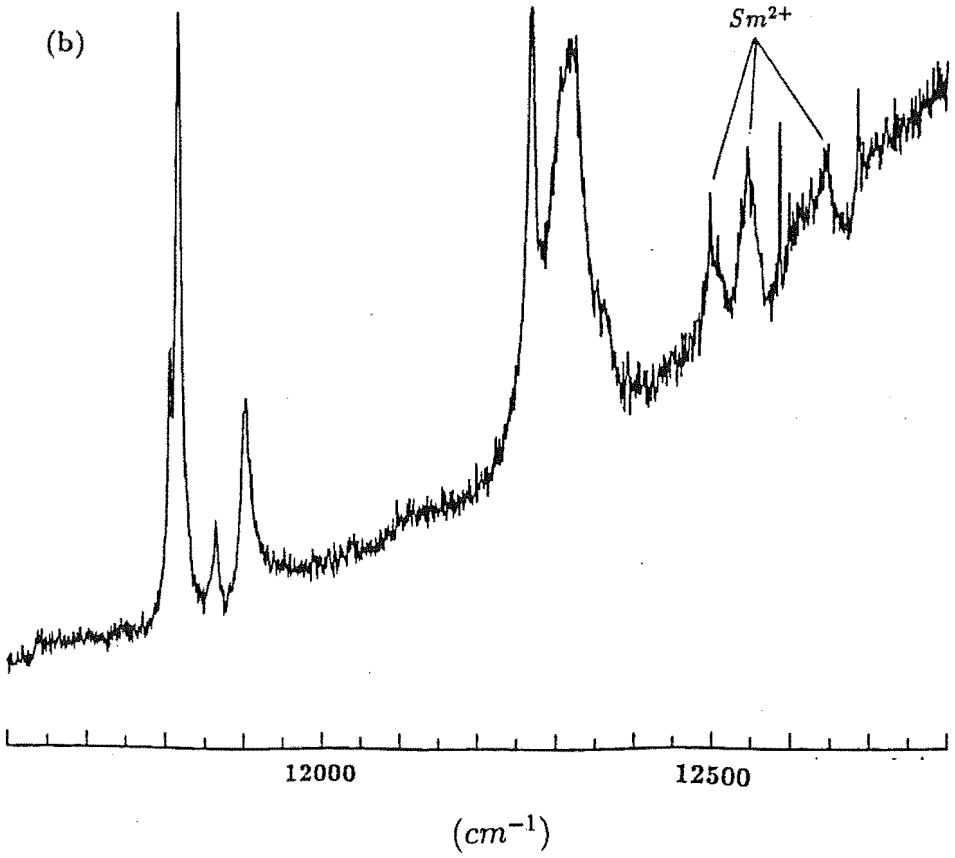
(b)
Sm^{2+}
12000
12500
(cm^{-1})

Figure 5.5 $^1D_2 \rightarrow ^3H_5$ Polarised fluoresence spectra of the D^- mixed crystal centers in the 0.5% Sr^{2+} doped CaF_2 crystal at 11K.

(a) the $A1$ center, pumping $16754.6cm^{-1}$.
(b) the $A2$ center, pumping $16772.8cm^{-1}$.

The lines labelled with dots belong to unrelated centers.

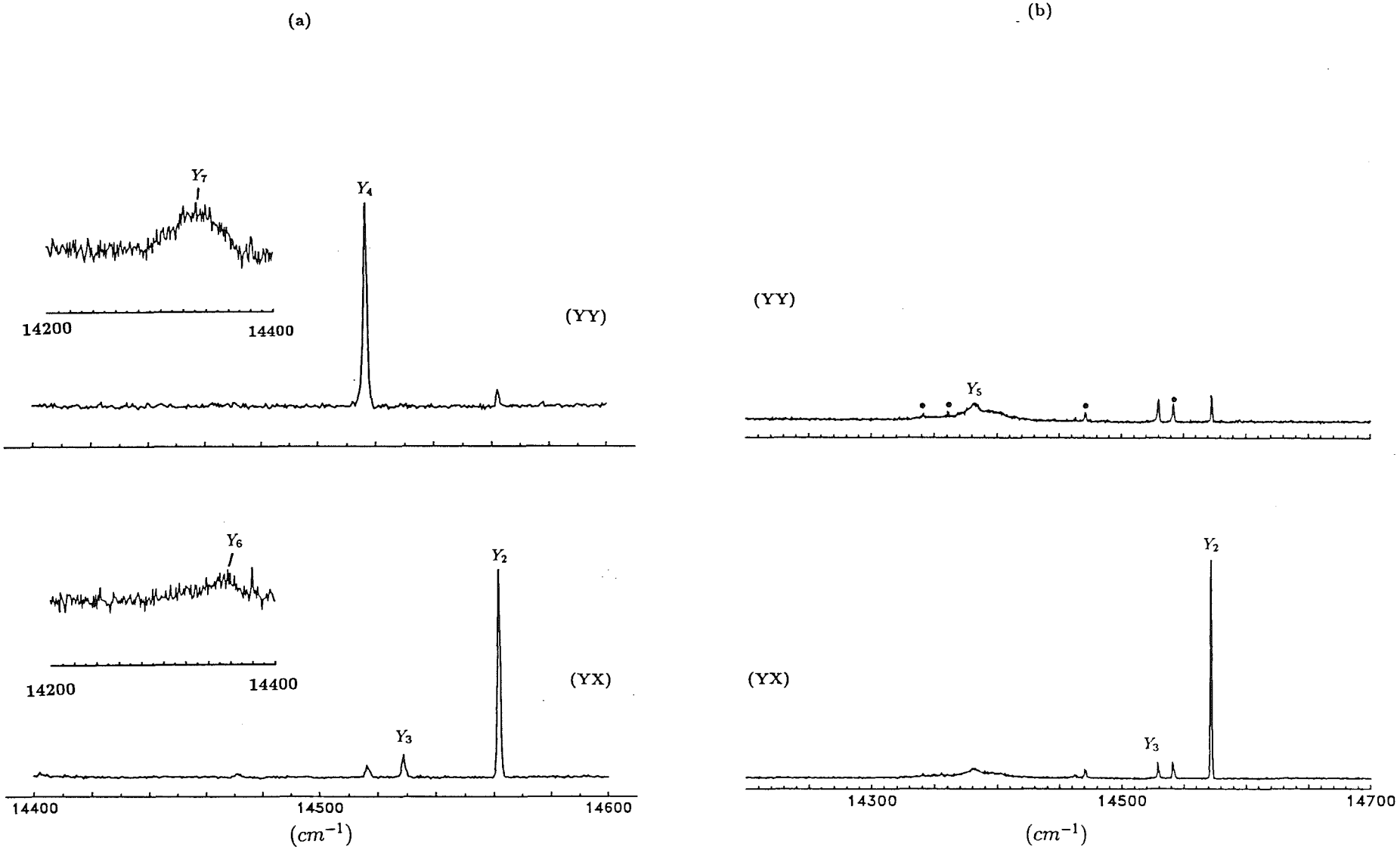
(a)
(b)
Y_7
Y_4
14200
14400
(YY)
Y_5
Y_6
Y_2
Y_3
(YX)
14400
14500
14600
14300
14700
(cm^{-1})

Given the marginal signal to noise ratio of the transitions to the W,X,Y multiplets, the vibronic levels could not be easily observed in transitions to these multiplets, hence no attempt was made to look for them there. The extra vibronic features in the mixed crystal were only studied for the $D \rightarrow Z$ transitions. The $D \rightarrow Z$ transitions of the $A1$ and $A2$ mixed crystal centers are presented in figures 5.6(a)(i) and (b)(i) respectively, with the vibronic transitions distinguised by additional labels in brackets (fig. 5.6(a)(ii) and (b)(ii)). The first label within the bracket, either 'x' or 'z' identifies the C_{4v} center local vibrational mode which gave rise to the vibronic level observed. If the symmetry is lower than C_{4v} as for the case of the $A1$ center, then additional labels 'a' and 'b' will be present within the brackets, to reflect the lifting of the degeneracy of the C_{4v} center vibronic levels. The other labels represent the electronic levels that couple to a particular local vibrational mode to give the observed vibronic levels.

The polarisation ratios expected for the vibronic levels are determined by the irreps of the electronic and vibronic levels involved in the excitation and emission. As an example, for a C_{4v} center, a $Z_1(\gamma_5) \rightarrow D_1(\gamma_1)$ absorption and a $D_1(\gamma_1) \rightarrow Z_1(z)(\gamma_5)$ decay, would require a σ absorption of laser radiation and would give a σ emission of fluorescence, and a (YX):(YY) polarisation ratio of 1:2 is observed [Reeves,1987] as predicted[1]. Similarly, a $D_1(\gamma_1) \rightarrow Z_1(x)(\gamma_1)$ decay gave a (YX):(YY) polarisation ratio of 1:0 as expected for the C_{4v} center.

The transitions to the $Z_1(z)$ and $Z_1(x)$ vibronic levels of the $A2$ center gave the same polarisation ratios as would be expected for a center with a C_{4v} symmetry, thus further confirming the initial model assignment of the $A2$ center as having a C_{4v} symmetry. The other lines (marked with dots) do not belong to the $A2$ center (figure 5.6(b)(ii)).

The $Z_1(z)$ vibronic level of a C_{4v} center, with a γ_5 irrep is doubly degenerate. When the symmetry is lowered to C_s, the lifting of the degeneracy would give two lines, one with an irrep of γ_1 and another of γ_2 of the C_s point group. The fluoresecence spectra of the $A1$ center (fig. 5.6(a)(ii)), assigned a $C_s(b)$ symmetry

[1]refer to chap 2.2

Figure 5.6 $^1D_2 \rightarrow ^3 H_4$ Polarised fluoresence spectra of the D^- mixed crystal centers in the 0.5% Sr^{2+} doped CaF_2 crystal at 11K.

(a) the $A1$ center, pumping $16754.6cm^{-1}$.
(b) the $A2$ center, pumping $16772.8cm^{-1}$.
Unrelated centers are labelled with dots.

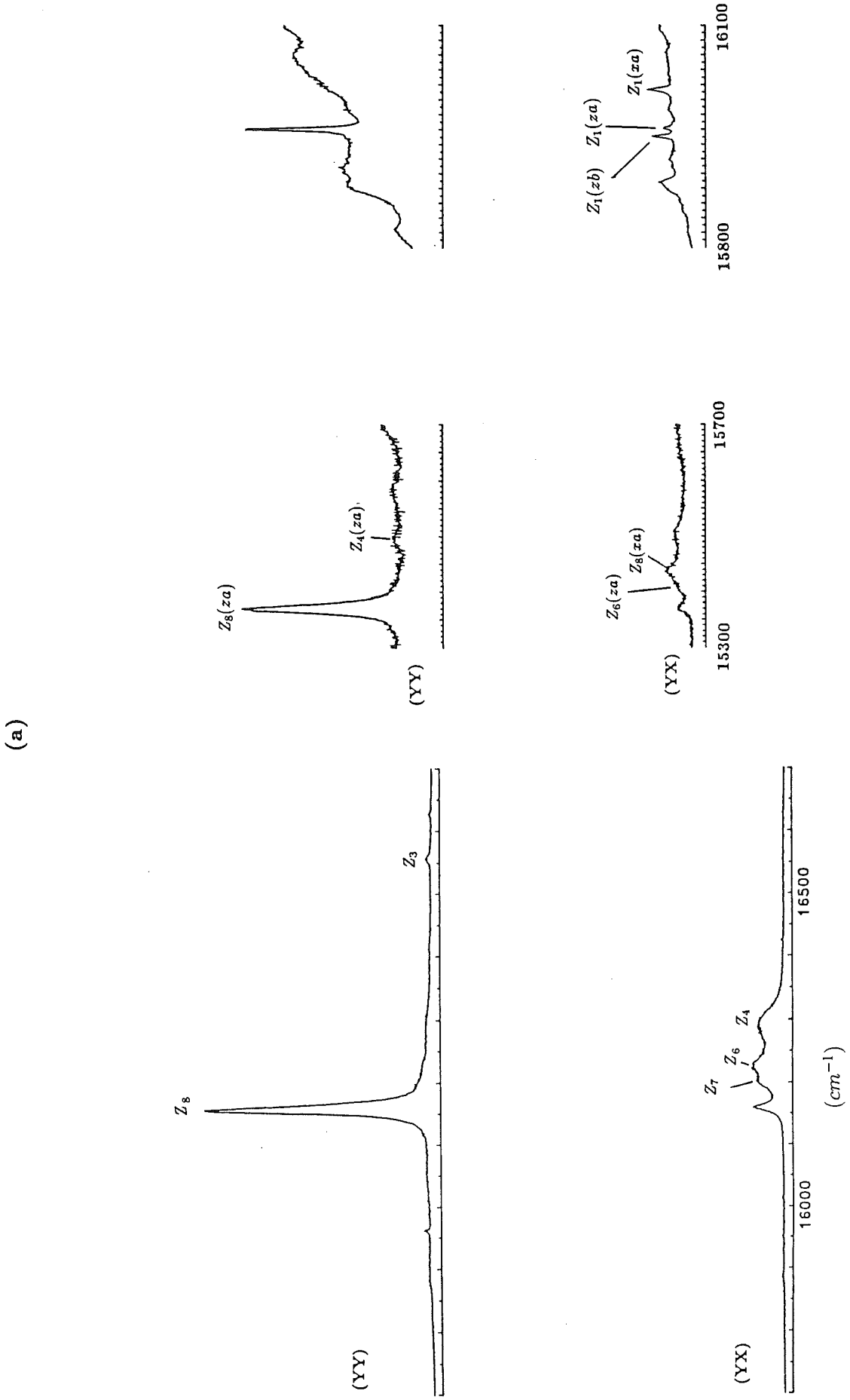
(a)
(YY)
Z_8
Z_3
(YX)
Z_7
Z_6
Z_4
16000
16500
(cm^{-1})
(YY)
$Z_8(za)$
$Z_4(za)$
(YX)
$Z_6(za)$
$Z_8(xa)$
15300
15700
$Z_1(zb)$
$Z_1(za)$
$Z_1(xa)$
15800
16100

(b)

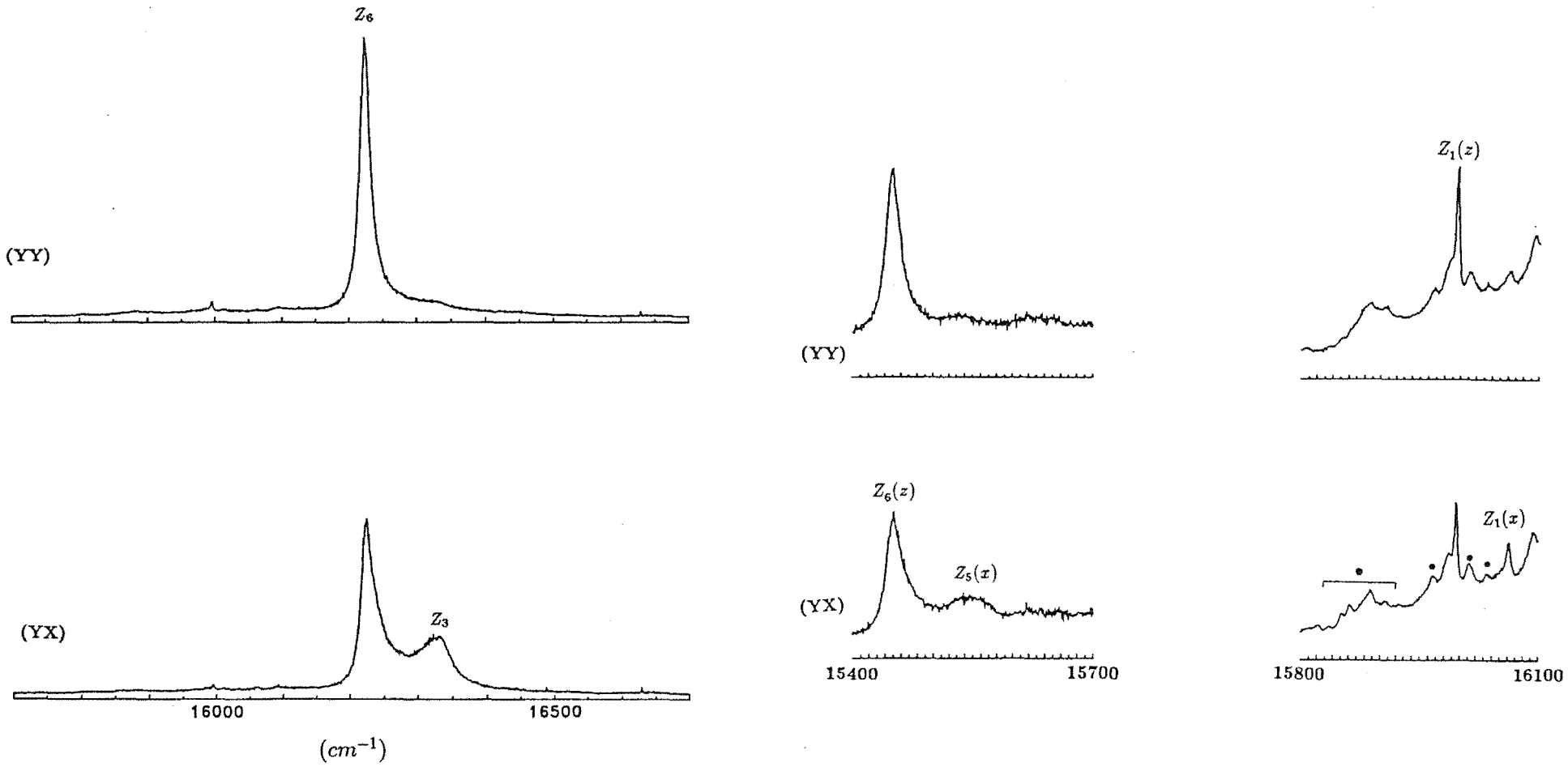
Z_6
(YY)
Z_3
(YX)
16000
16500
(cm^{-1})
$Z_6(z)$
$Z_5(x)$
(YY)
(YX)
15400
15700
$Z_1(z)$
$Z_1(x)$
15800
16100

configuration, demonstrates such a lifting of the degeneracy. Two levels are observed at 15951 and $15961cm^{-1}$, labelled $Z_1(za)$ and $Z_1(zb)$. Further, the polarisation ratios of 1:0 and 0:1 observed are consistent with a $\gamma_2 \rightarrow \gamma_1$ excitation followed by $\gamma_1 \rightarrow \gamma_1$ or $\gamma_1 \rightarrow \gamma_2$ emission transitions of a $C_s(b)$ symmetry center. The C_{4v} $Z_1(x)$, γ_1 or γ_3 level would give rise to a $C_s(b)$ level with a γ_1 irrep in the $A1$ center. The polarisation ratio observed at $16013cm^{-1}$ of 1:0 is in agreement with a terminating level of a γ_1 irrep for a C_s center.

The assignments of the electonic and vibronic levels observed for the $A1$ and $A2$ centers are given in table 5.2.

5.2 Mixed Crystal Centers in $Ca_{1-x}Ba_xF_2 : Pr^{3+} : D^-$

From the study of the undeuterated $CaF_2 : Pr^{3+}$ crystal, it was found that the Ba^{2+} doped crystal gave more mixed crystal centers at a similar concentration of dopant than the Sr^{2+} doped mixed crystal. It was anticipated the concentration of the Ba^{2+} doping should be kept at a minimal level of 0.3%, to keep the increased number of centers after deuteration to a manageable level. Further, as the Ba^{2+} doped crystals did not appear to be able to sustain a prolonged period of deuteration, the crystal used in this study was deuterated only for 24 hours compared to 60 hours of deuteration treatment for the Sr^{2+} doped crystals. This greatly sacrificed the emission output of the D^- centers but improved on the resolution of the lines. As a result, two centers could be satisfactorily studied, but only just. These have the characteristic polarisation of the $A1$ and $A2$ type centers corresponding to the on-off axis and on-axis substitution of the Ba^{2+} cation previously described in chapter 4. The spectroscopic results of these mixed crystal centers are presented below.

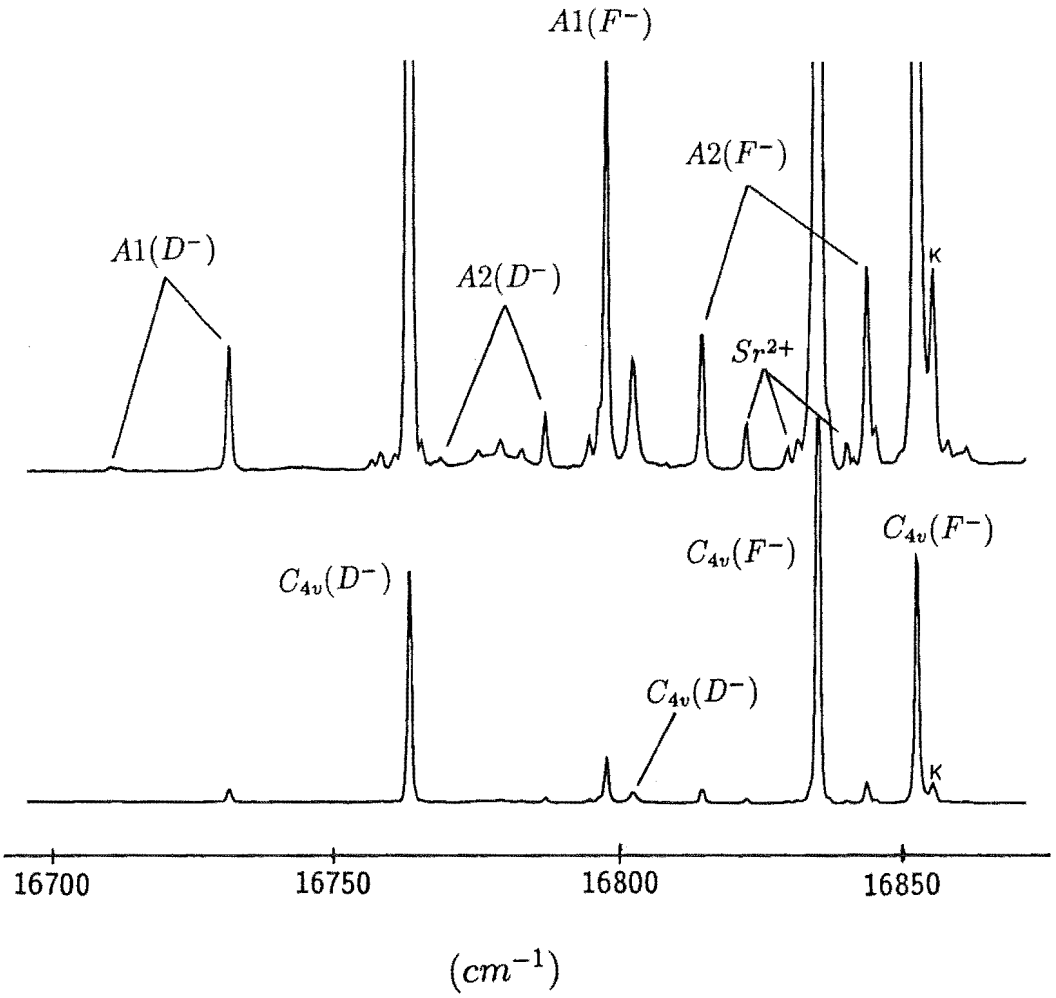

Figure 5.7 Broadband excitation spectra of the deuterated $Ca_{1-x}Ba_xF_2 : Pr^{3+}$ crystals, monitoring the $D \rightarrow Z$ transitions at 11K.

This crystal was doped with 0.3% Ba^{2+} and deuterated for 24 hours. Comparison of this spectrum with the spectrum of the deuterated parent crystal of figure 5.1(b) would reveal the transitions of the Ba^{2+} mixed crystal centers.

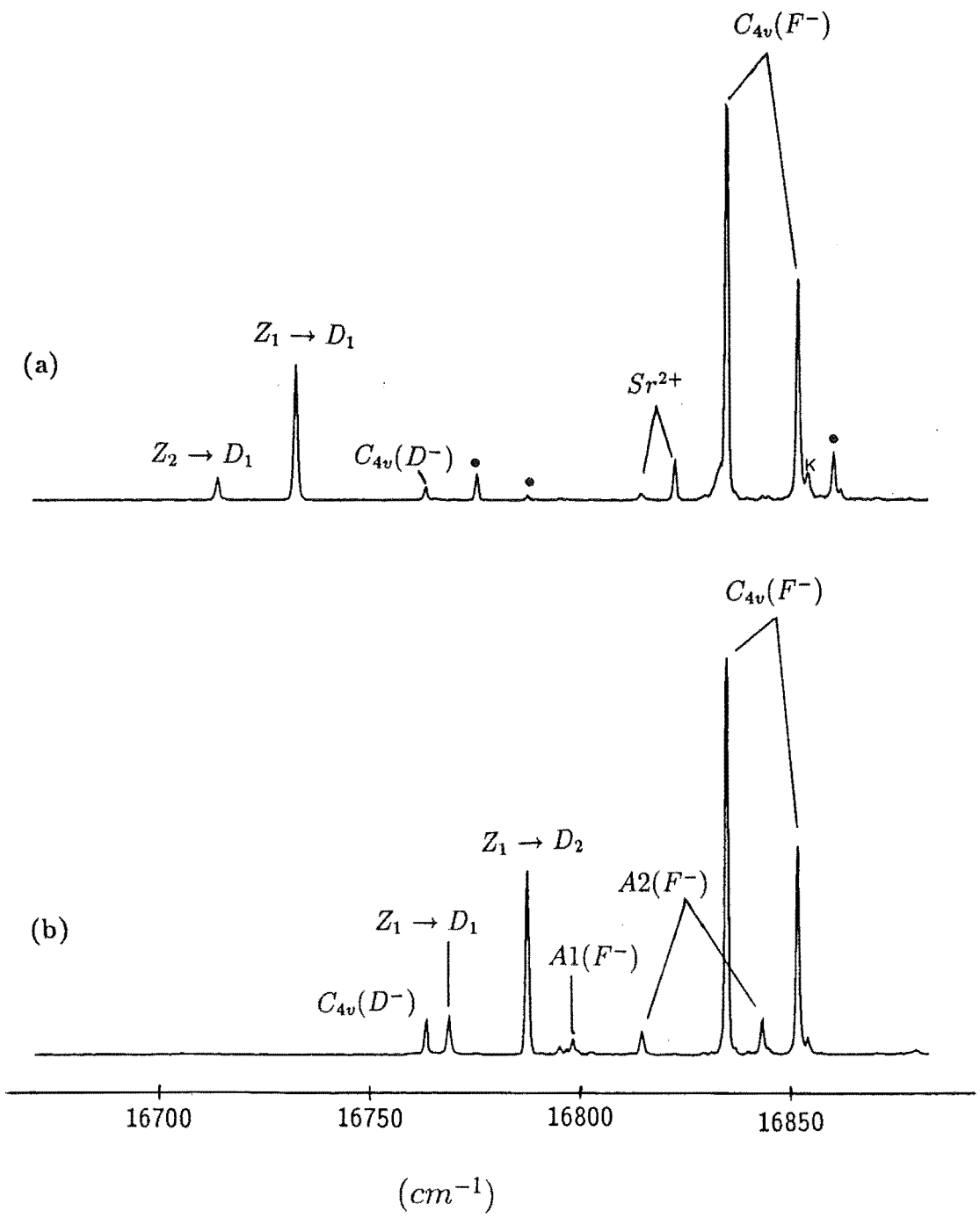

Figure 5.8 Selective excitation spectra of the D^- mixed crystal centers in the 0.3% Ba^{2+} doped CaF_2 crystal at 11K obtained by scanning the dye laser and monitoring specific transitions.

(a) the $A1$ center monitoring $14541cm^{-1}$.
(a) the $A2$ center monitoring $14486cm^{-1}$

Transitions of unrelated centers are marked with dots.

5.2.1 The Excitation Spectra

Not surprisingly, the Ba^{2+} mixed crystal displayed more lines than the Sr^{2+} doped crystal corresponding to the formation of more different type of D^- mixed crystal centers. Two centers, with their most prominent transitions at $16729.9cm^{-1}$ and $16783cm^{-1}$ in the broadband excitation spectra were chosen to be studied (fig. 5.7). There are further weaker transitions belonging to other centers, particularly in the broad transition band centered around $16770cm^{-1}$ and at the shoulders of the parent $C_{4v}(D^-)$ and $A1(F^-)$ D_1 levels. LSE studies of those centers were not feasible. The D^- mixed crystal lines are further away from the parent $C_{4v}(D^-)$ lines compared to those of the D^- mixed crystal centers of the Sr^{2+} doped crystal. This again demonstrates the larger distortion produced by the Ba^{2+} ions on the parent C_{4v} center in this host crystal.

The selective excitation monitoring a specific transition of the $A1$ or $A2$ center and scanning the dye laser through the D multiplet, did not yield spectra that allow convenient identification of the levels that belong to these centers (fig. 5.8). Through prior knowledge of the levels belonging to other centers, it was possible to successfully identify those lines belonging solely to the $A1$ and $A2$ centers. However, the lines labelled with dots in figure 5.8(a) do not belong to either of the mixed crystal centers under discussion nor to any of the centers previously studied.

Attempts to ascertain the D_2 level of the $A1$ center by monitoring different $D \rightarrow Y$ transitions, or by correlating the transition intensities by shifting the monochromator slightly off the transition peaks proved to be unfruitful. The D_2 level remains unidentified at this stage.

As discussed in section 5.1.1, the C_{4v} type centers which have $D_1 - D_2$ energy level seperation values close to mulitiples of $9cm^{-1}$, are expected to have a stronger D_2 transition when the selective excitation is performed by monitoring a transition emitting from the D_1 level. The $D_1 - D_2$ seperation for the $A2(D^-)$ center is $18.8cm^{-1}$ and have the strongest D_2 relative intensities of all the C_{4v} centers studied

Table 5.3(a). The energy levels (in cm^{-1}) of the D^- mixed crystal centers A1 and A2 in $Ca_{1-x}Ba_xF_2$:Pr^{3+}:D-. Uncertainties are $\pm 1 cm^{-1}$. unless otherwise indicated. The irrep labels for each level are given in brackets.

	A1		A2	
D_2		(γ_1)	16784.6 ± 0.5	(γ_3)
D_1	16729.9 ± 0.5	(γ_1)	16765.8 ± 0.5	(γ_1)
W_5	-	(γ_1)	NA	
W_4	5407	(γ_2)	-	(γ_4)
W_3	5381	(γ_2)	5358	(γ_5)
W_2	5359	(γ_2)	-	(γ_3)
W_1	5312	(γ_1)	5291	(γ_1)
X_{13}	-	(γ_1)	NA	
X_{12}	5038 *	(γ_1)	NA	
X_{11}	5024 *	(γ_2)	NA	
X_{10}	4912	(γ_1)	-	(γ_3)
X_9	-	(γ_2)	4947	(γ_5)
X_8	-	(γ_1)	-	(γ_1)
X_7	-	(γ_2)	-	(γ_4)
X_6	-	(γ_1)	-	(γ_3)
X_5	-	(γ_2)	-	(γ_2)
X_4	-	(γ_1)	4482	(γ_5)
X_3	-	(γ_2)	-	(γ_3)
X_2	4189	(γ_1)	-	(γ_4)
X_1	4178	(γ_2)	4209	(γ_5)
Y_{11}	-	(γ_2)	NA	
Y_{10}	-	(γ_2)	NA	
Y_9	-	(γ_1)	NA	
Y_8	-	(γ_2)	-	(γ_4)
Y_7	2434 ± 3	(γ_2)	2345	(γ_5)
Y_6	-	(γ_1)	-	(γ_2)
Y_5	-	(γ_1)	2280 ± 5	(γ_5)
Y_4	2262	(γ_2)	-	(γ_3)
Y_3	2237	(γ_1)	2209	(γ_5)
Y_2	2188	(γ_1)	2198	(γ_1)
Y_1	2185	(γ_2)	-	(γ_2)

Z_9	-	(γ_1)	NA	
Z_8	637	(γ_1)	NA	
Z_7	553 ± 10	(γ_2)	803	(γ_3)
Z_6	495 ± 10	(γ_1)	536	(γ_5)
Z_5	-	(γ_2)	465	(γ_1)
Z_4	450 ± 10	(γ_1)	-	(γ_2)
Z_3	205 *	(γ_2)	403 ± 10	(γ_1)
Z_2	19.1 ± 0.5	(γ_1)	-	(γ_4)
Z_1	0	(γ_2)	0	(γ_5)

Levels which could not be unambigously assign are marked with an asterisk.
NA - Excited levels not applicable to the A2 C_{4v} center.

Table 5.3(b) Assignment of the vibronic energy levels (in cm^{-1}) for the D^- mixed crystal centers A1 and A2 in $Ca_{1-x}Ba_xF_2$:Pr^{3+}:D-.

A1		A2	
$Z_1(xa)$	746	$Z_1(x)$	673
$Z_1(xb)$	761	$Z_1(z)$	745
$Z_1(za)$	781	$Z_6(z)$	1291
$Z_4(zb)$	799		
$Z_8(xa)$	1375		
$Z_8(za)$	1412		

in the CaF_2 host.

5.2.2 The Polarised Fluorescence Spectra

The signals from the fluorescence of the D^- mixed crystals doped with Ba^{2+} are very weak for reasons discussed at the start of this section. Typical integration times of 5 to 15 seconds per data point were required for the fluorescence spectra displayed below.

The $A1$ and $A2$ centers in the $Ca_{1-x}Ba_xF_2 : Pr^{3+} : D^-$ crystal display all the polarisation ratios typifying the respective centers. This is evident for the $D \rightarrow W$ transitions as shown in figures 5.9(a) and (b) for the $A1$ and $A2$ centers respectively.

Using the same method to study the $D \rightarrow X$ transitions as described in section 5.1, the excitation spectra recorded are as shown in figure 5.10. The varying background and lines attributed to Sm^{2+} contamination apparent in the fluorescence spectra of the Sr^{2+} mixed crystal centers are again present. The $A1$ and $A2$ transitions were extremely weak even without the analyzer in placed, hence the discrimination of most transitions of the $A1$ and $A2$ centers was marginal. The region between 12100 and $12300cm^{-1}$ for the $A1$ center was found to be too weak for polarised measurements to be taken.

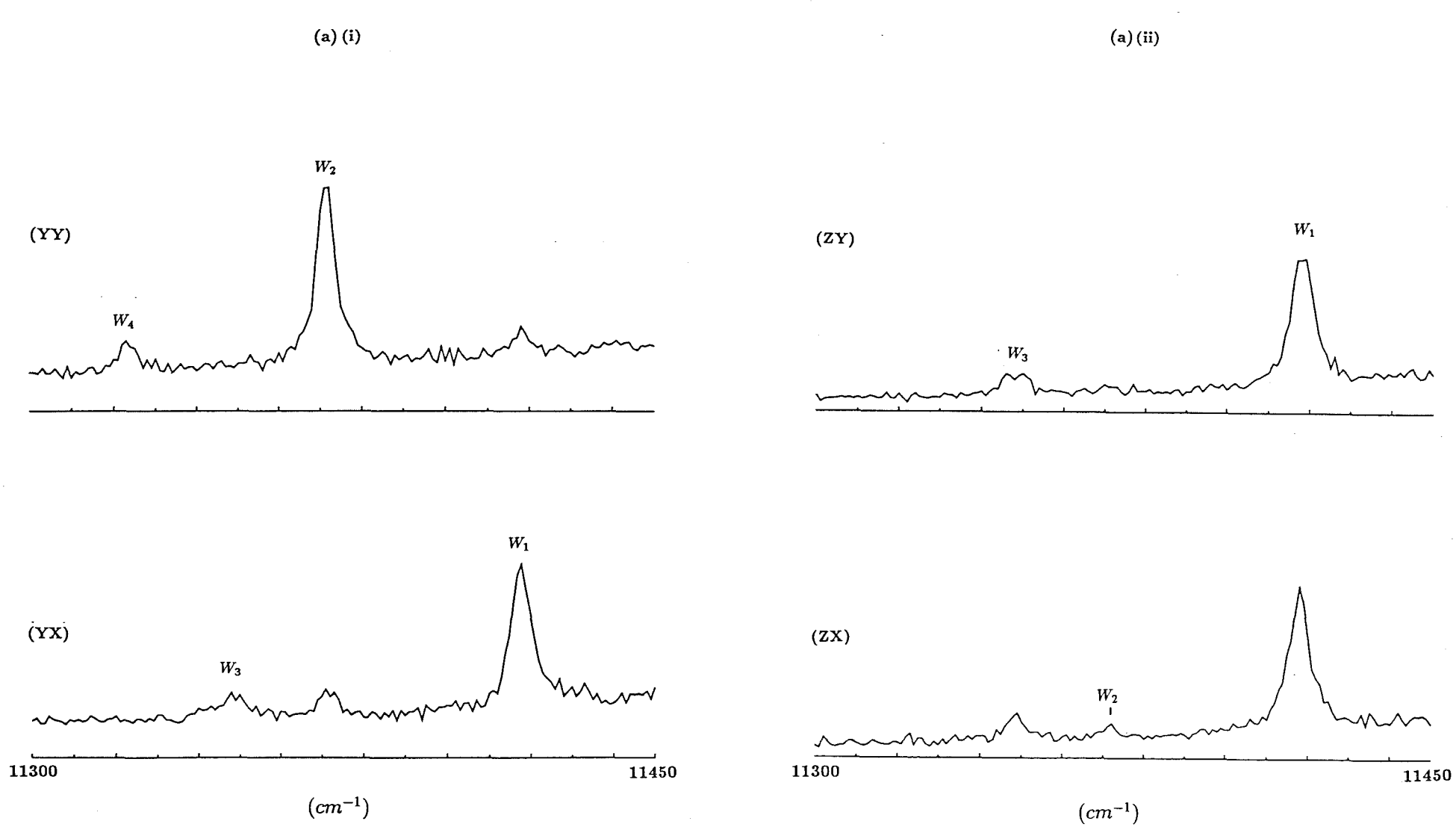
(a) (i)
(a) (ii)
(YY)
W_2
W_4
(ZY)
W_1
W_3
(YX)
W_1
W_3
(ZX)
W_2
11300
11450
(cm^{-1})
11300
11450
(cm^{-1})

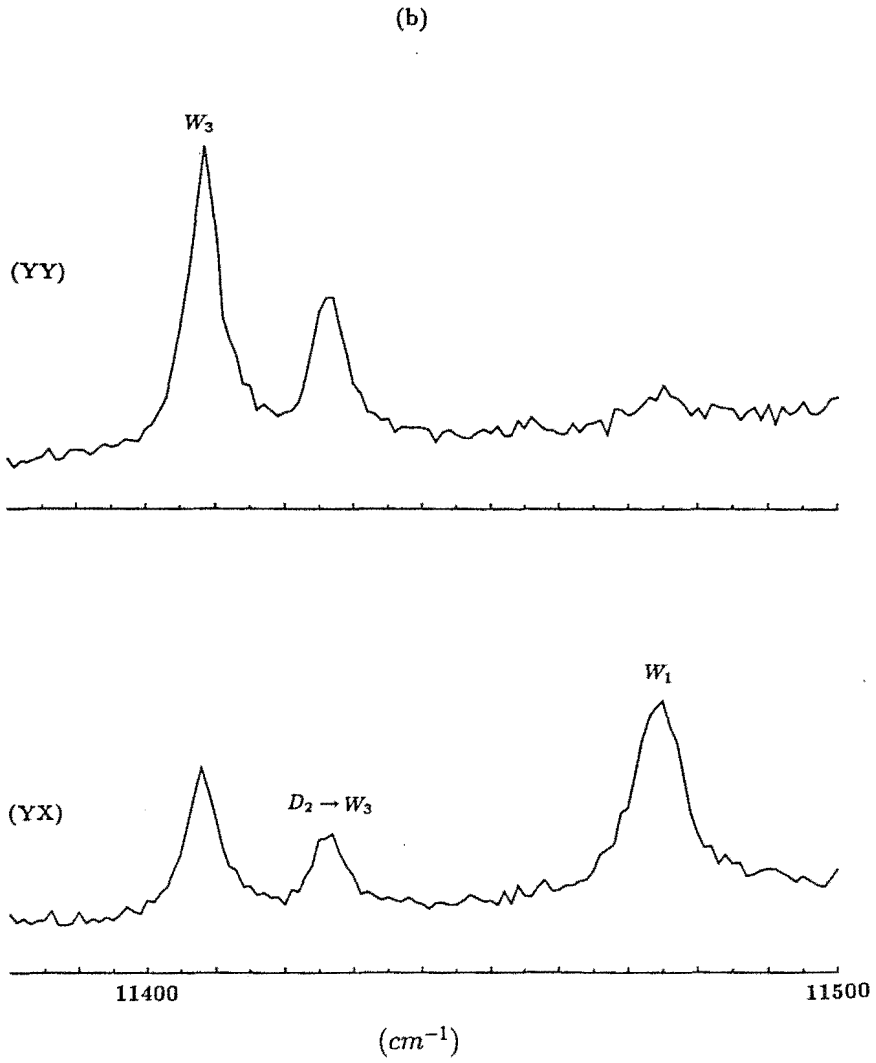

Figure 5.9 $^1D_2 \rightarrow ^3F_2$ Polarised fluoresence spectra of the D^- mixed crystal centers in the 0.3% Ba^{2+} doped CaF_2 crystal at 11K.
(a) the $A1$ center, pumping 16729.9cm^{-1}.
Laser polarised (i) E_Y and (ii) E_Z.
(b) the $A2$ center, pumping 16765.8cm^{-1}.

Figure 5.10 $^1D_2 \rightarrow ^3 H_6$ Polarised fluoresence spectra of the D^- mixed crystal centers in the 0.3% Ba^{2+} doped CaF_2 crystal at 11K.

(a) the $A1$ center, pumping $16729.9cm^{-1}$.
(b) the $A2$ center, pumping $16765.8cm^{-1}$.

The trace at the bottom right hand corner is the unpolarised

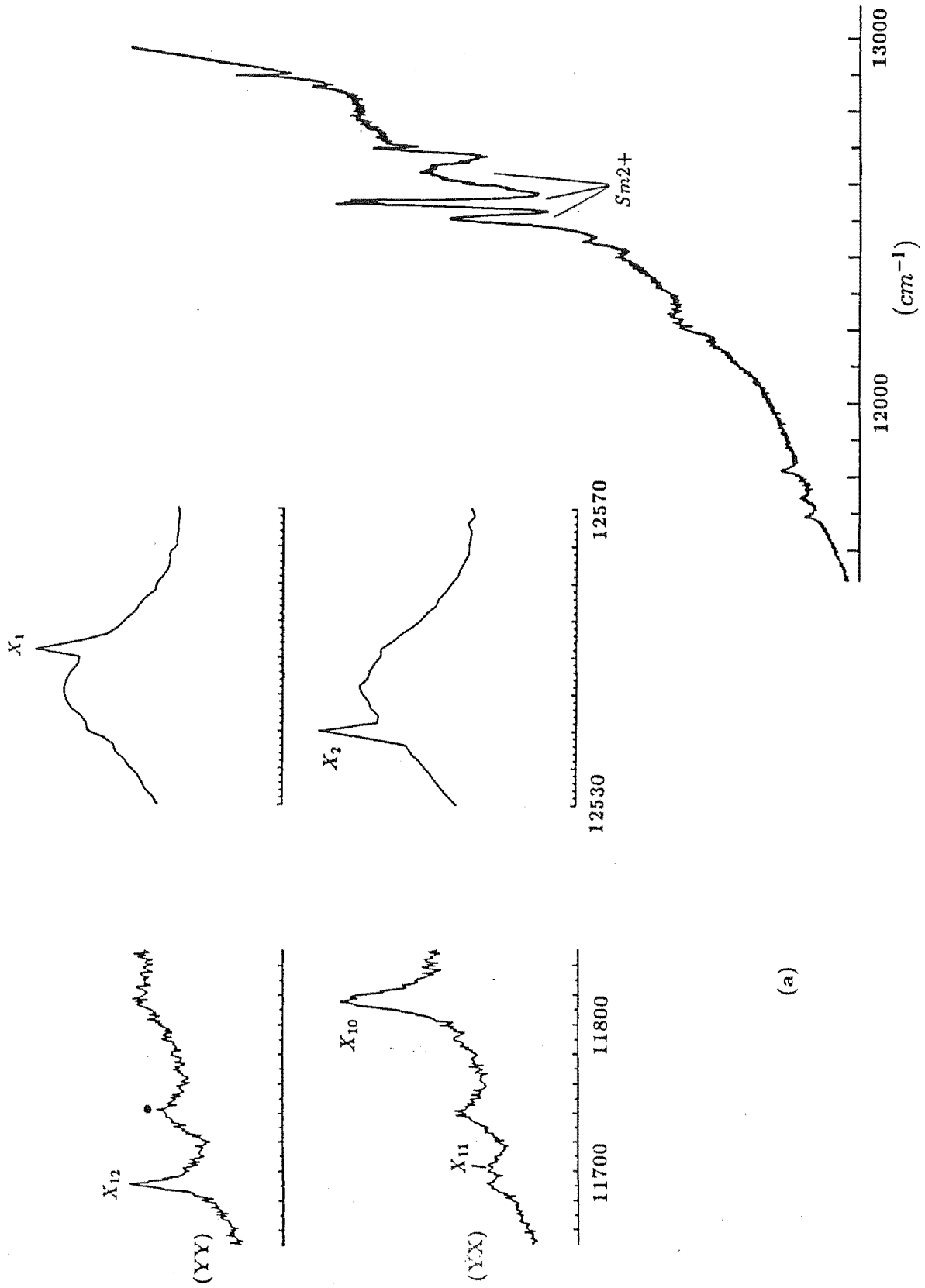
(a)
(YY)
(YX)
X_{12}
X_{11}
X_{10}
X_2
X_1
$Sm2+$
11700
11800
12530
12570
12000
13000
(cm^{-1})

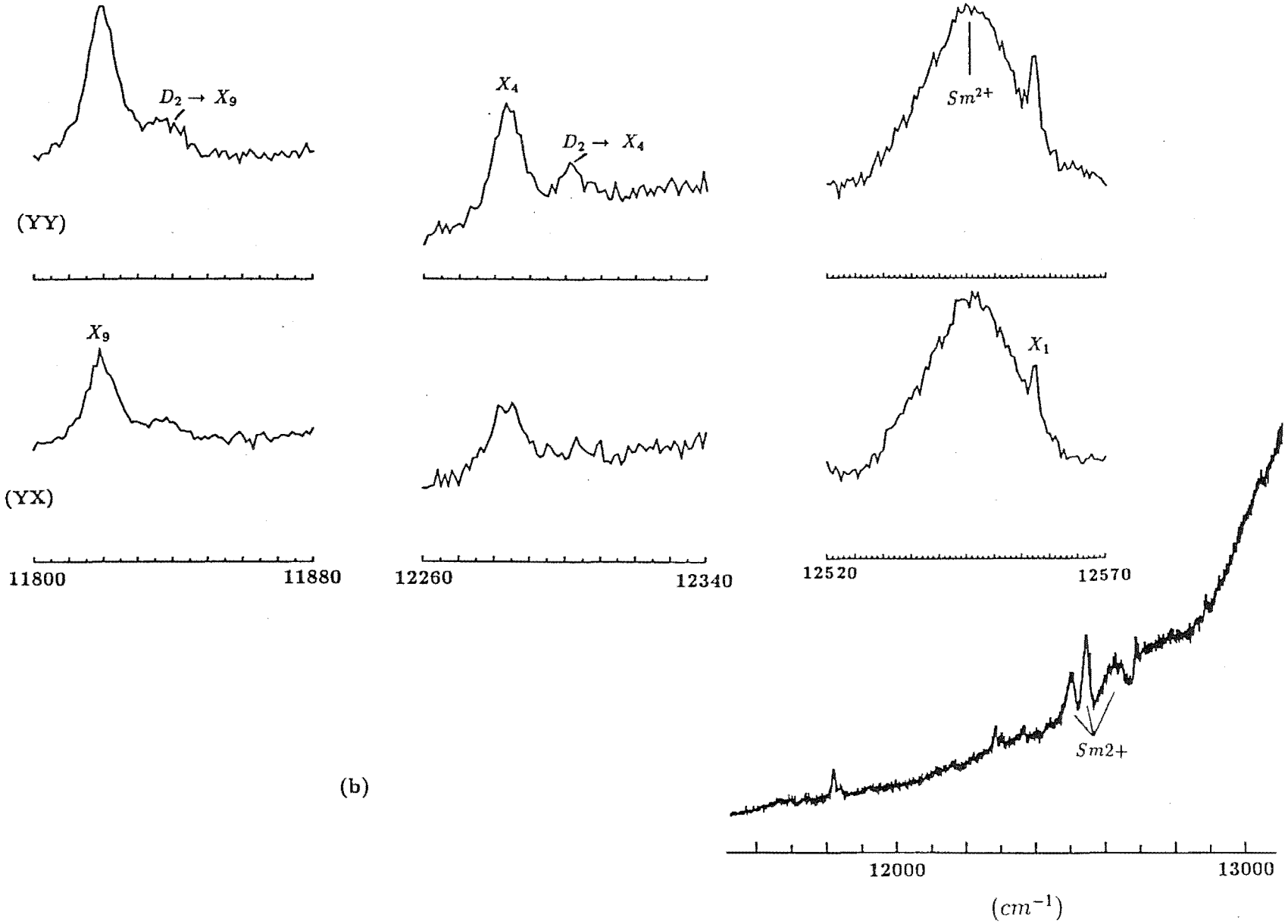
$D_2 \rightarrow X_9$
(YY)
X_9
(YX)
11800
11880
X_4
$D_2 \rightarrow X_4$
12260
12340
Sm^{2+}
X_1
12520
12570
Sm2+
12000
13000
(cm^{-1})

(b)

Figure 5.11 $^1D_2 \rightarrow ^3H_5$ Polarised fluoresence spectra of the D^- mixed crystal centers in the 0.3% Ba^{2+} doped CaF_2 crystal at 11K.

(a) the $A1$ center, pumping $16729.9cm^{-1}$.
(b) the $A2$ center, pumping $16765.8cm^{-1}$.

The transitions of unrelated centers are labelled with dots.

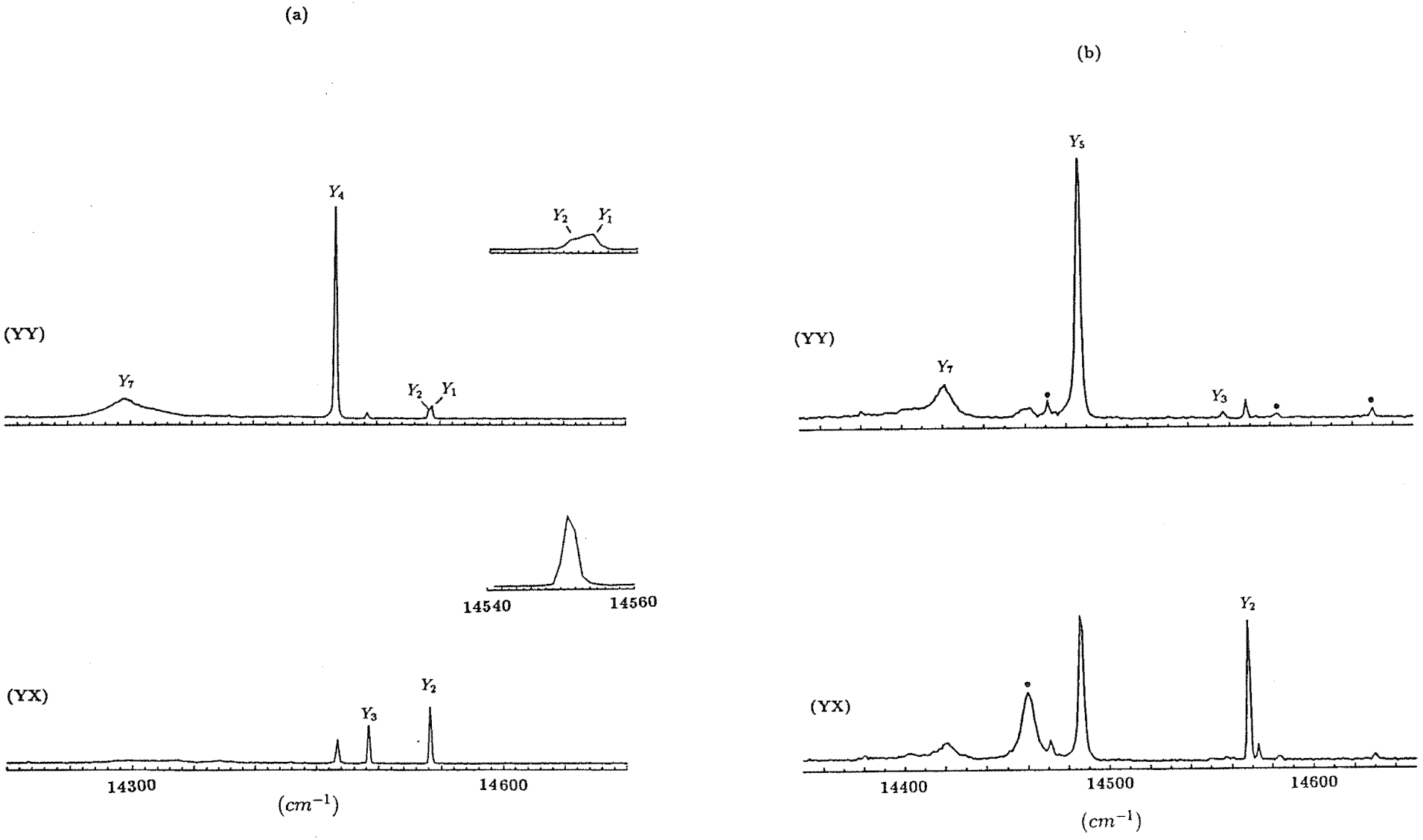
(a)
(YY)
Y_4
Y_2 Y_1
Y_7
Y_2 Y_1
14540
14560
(YX)
Y_2
Y_3
14300
14600
(cm^{-1})
(b)
Y_5
(YY)
Y_7
Y_3
Y_2
(YX)
14400
14500
14600
(cm^{-1})

Fluorescence transitions from the D to Y multiplet for the $A1$ and $A2$ centers are displayed in figure 5.11. There appear to be many more lines than expected, for the $A2$ center to this multiplet. Subsequent investigations revealed these lines, which are labelled with dots in figure 5.11(b), belong to other unrelated centers.

Figures 5.12(a)(i) and (b)(i) give the electronic transitions of the $D \rightarrow Z$ transitions of the $A1$ and $A2$ centers. For the $A2$ center, a few overlapping transitions are apparent between 16600 to $16680cm^{-1}$. The (YX):(YY) polarisation ratios of 1:2 observed would require a γ_5 level to be assigned to these lines for consistency with the $A2$ center having a C_{4v} symmetry. However, a γ_5 level is not expected in this spectral region and hence these lines cannot be due to electronic dipole transitions of the $A2$ center. It is most likely they originate from the vibronics associated with the lattice phonons or from other unknown centers.

The vibronic levels in the Z multiplet of the $A2$ center are identified amidst the noisy background (fig. 5.12(b)(ii)) by correlation of the transition intensities while tuning and detuning the laser excitation frequency around $16785cm^{-1}$. At $15964cm^{-1}$, a line appeared which does not fit into the overall vibronic scheme. However, it has an (YX):(YY) polarisation ratio of 1:0 consistent with the $D_2(\gamma_3) \rightarrow Z_7(\gamma_3)$ transition. Further a much weaker emission is supportive evidence that this transition originates from the D_2 level. Therefore, the $15964cm^{-1}$ line is attributed to the $D_2(\gamma_3) \rightarrow Z_7(\gamma_3)$ transition , hence identifying the Z_7 level of the $A2$ center.

For the $A1$ center, the vibronics are clearly identified in figures 5.12(a)(ii). The lifting of the two-fold degeneracy of the C_{4v} $Z_1(z)(\gamma_5)$ level is evident at 15949 and $15931cm^{-1}$ with polarisation ratios as discussed for the case of the $A1$ D^- center in the Sr^{2+} doped crystal. A prominent extra line with an (YX):(YY) ratio of 0:1 was found at $15969cm^{-1}$. This can be attributed to the splitting of the 4-fold degeneracy of the vibronic level from the coupling of the electronic ground state γ_5 level with the (x, y) local mode vibrations.

Table 5.3 lists the energy level assignment of the $A1$ and $A2$ centers studied.

Figure 5.12 $^1D_2 \rightarrow ^3 H_4$ Polarised fluoresence spectra of the D^- mixed crystal centers in the 0.3% Ba^{2+} doped CaF_2 crystal at 11K.

(a) the $A1$ center, pumping $16729.9cm^{-1}$.
(b) the $A2$ center, pumping $16765.8cm^{-1}$.

The transitions of unrelated centers are labelled with dots.

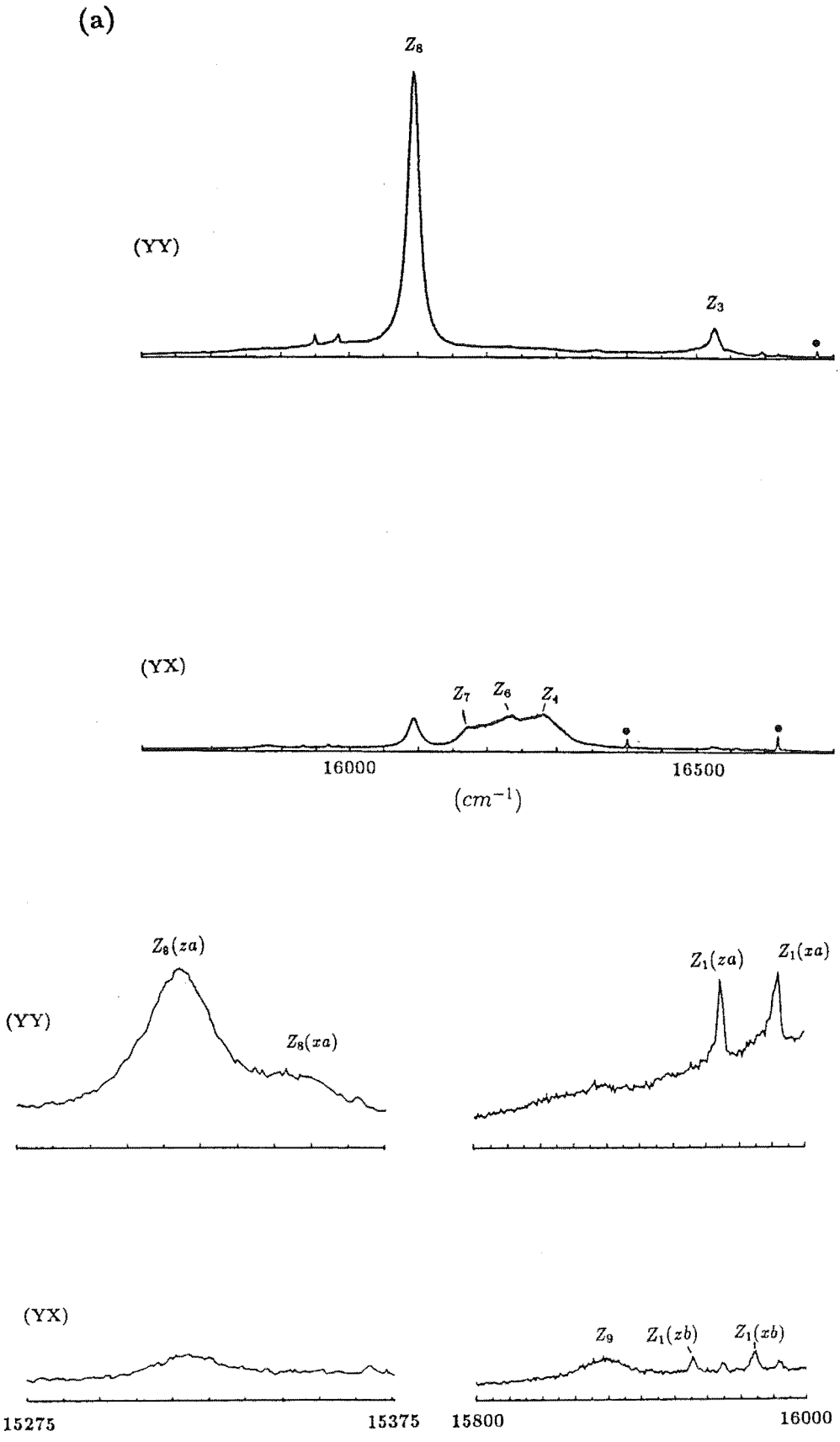
(a)
Z_8
(YY)
Z_3
(YX)
Z_7 Z_6 Z_4
16000
16500
(cm^{-1})
$Z_8(za)$
(YY)
$Z_8(xa)$
$Z_1(za)$
$Z_1(xa)$
(YX)
Z_9 $Z_1(zb)$ $Z_1(xb)$
15275
15375
15800
16000

(b)

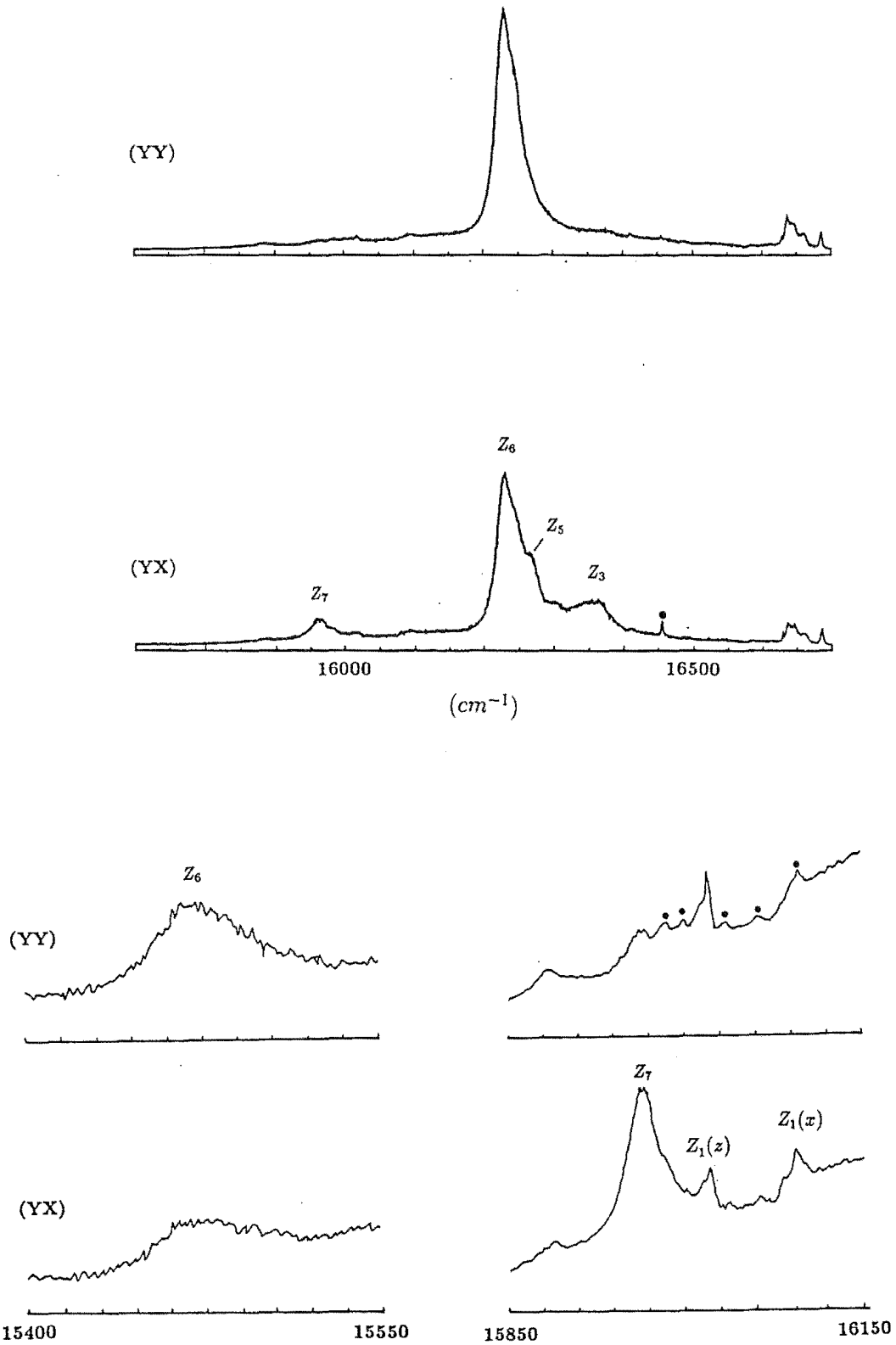
(YY)
(YX)
Z_6
Z_5
Z_3
Z_7
16000
16500
(cm^{-1})
(YY)
Z_6
(YX)
15400
15550
Z_7
$Z_1(z)$
$Z_1(x)$
15850
16150

5.3 Mixed Crystal Centers in $Sr_{1-x}Ca_xF_2 : Pr^{3+} : D^-$

Two centers were studied in this crystal, both displaying the $A3$ type polarisation behaviour and are labelled $A3(I)$ and $A3(II)$ accordingly. A proper study of the D^- mixed crystal centers in this crystal system is hampered by some degree of uncertainty in the number of centers actually being excited since the lines are closely overlapped. Therefore, the levels obtained could not be confidently assigned.

5.3.1 The Excitation Spectra

A cursory examination of the the broadband excitation spectrum (fig. 5.13) reveals several unresolved line structures which are broad and tend to merge together. Some of these broader transition lines probably arise from the D_2 levels of bleaching centers like those found in the excitation spectra of the C_s centers in the CaF_2 host crystal (chap. 8), while others belong to mixed crystal centers. LSE investigations of these broader transitions belonging to the mixed crystal centers could not be satisfactorily performed due to extensive overlapping of these lines.

From the experience gained from the study of the F^- satellite structures, the positions of the D^- satellite structures suggest that they are associated with the D_2 levels of the mixed crystal centers hence it is likely that the D_1 and D_2 levels are very close together, center at $16820.1cm^{-1}$.

A definite assignment of the levels in the D multiplet for the $A3(I)$ and $A3(II)$ centers by selective excitation via monitoring a line and scanning the dye laser was not possible. While the satellite lines found in the broadband spectrum were positively identified to be those of the $A3(I)$ and $A3(II)$ centers (fig. 5.14), it is uncertain whether they should be assigned as absorption to the D_1 or D_2 levels of the mixed crystal centers. However, following the trend found in the study of the F^- satellites, the D^- satellites located on the higher energy shoulder of the C_{4v} D^- line would be the lines resulting from the Z_1 and Z_2 to D_2 transitions of the several

mixed crystal centers.

In the work of Reeves[1987], the D_2 level of the parent C_{4v} D^- center was never found. It was hoped that the location of the satellite structures in the mixed crystal system would eventually lead to an assignment of the D_2 level. If the satellite structures indeed give the D_2 levels of the $A3(I)$ and $A3(II)$ centers, then the D_1 and D_2 levels of the parent C_{4v} center are centered at $16820.1cm^{-1}$ and seperated by less than $0.2cm^{-1}$, below the resolution limit of the SPEX1403 monochromator used.

5.3.2 The Polarised Fluorescence Spectra

To get the polarised spectra, the $Z_2 \rightarrow D$ transitions at 16821.1 and 16822.2 cm^{-1} for the $A3(I)$ and $A3(II)$ centers respectively, would appear to be the best frequencies to be pumped by the dye laser for optimal selectivity in the excitation. Undoubtedly, cross-pumping of several transitions would be unavoidable and possibly, the strong overlap of the centers would also promote cross-relaxation of energy from one center to another. In view of these, the assigment of the levels would be highly ambigous.

Examination of the $D \rightarrow W$ polarised fluorescence spectra for both the $A3(I)$ and $A3(II)$ centers reveals only the (YX):(YY) polarisation ratios 1:2 or 1:0 characteristic of the $A3$ type centers (fig 5.15). The transitions centered at $11525cm^{-1}$ of the $A3(I)$ center appears to show a splitting of the D^- parent C_{4v} $W_3(\gamma_5)$ level, though this splitting is presently not well resolved. The excitation of the line at 16822.2 cm^{-1} of the $A3(II)$ center gave more structure then expected for this multiplet. By the usual techniques, the lines that do not appear to belong to the $A3(II)$ center were identified (fig. 5.15(b), labelled with dots). This leaves the two lines at 11573 and $11526cm^{-1}$ as those of the $D \rightarrow W_1$ and $D \rightarrow W_3$ transition of the $A3(II)$ center.

A positive assignment of the lines in the 12250 to 12700 cm^{-1} region of the

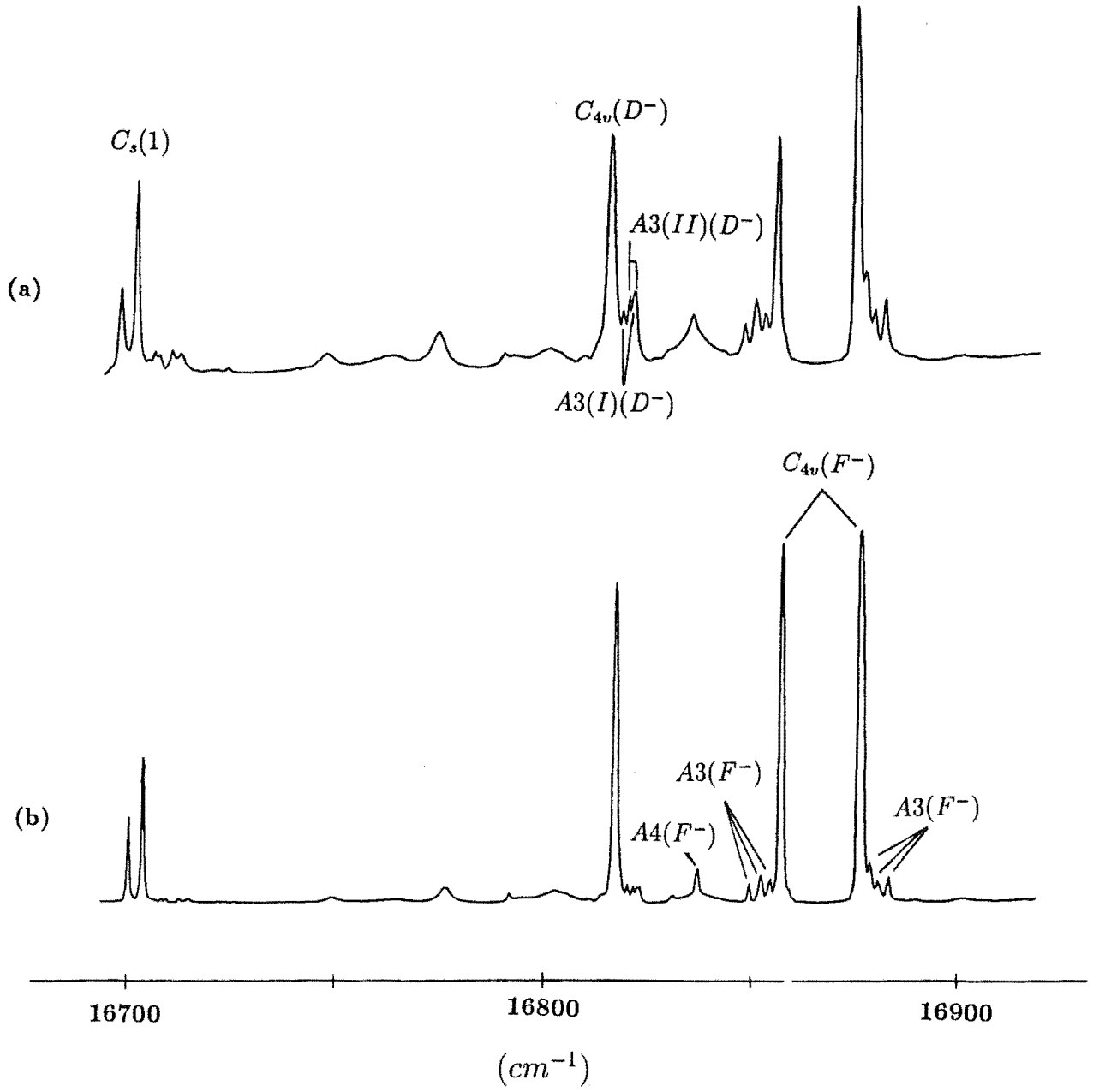

Figure 5.13 Broadband excitation spectra of the $Sr_{1-x}Ca_xF_2 : Pr^{3+}$ crystals, monitoring the $D \rightarrow Z$ transitions at 11K.

(a) 1% Ca^{2+} doping and deuterated for 48 hours.
(b) parent crystal, deuterated for 48 hours.

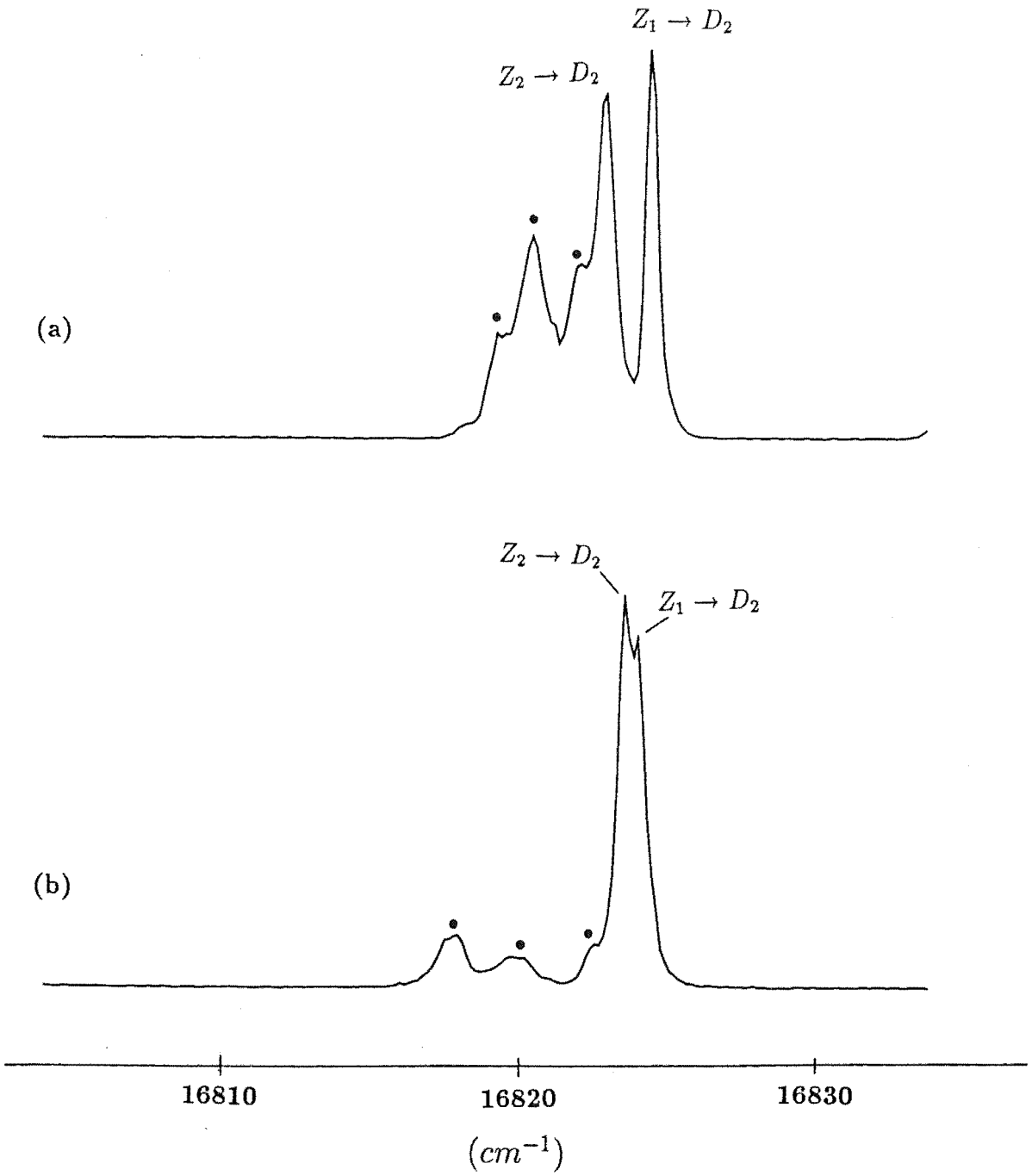

Figure 5.14 Selective excitation spectra of the D^- mixed crystal centers in the 1% Ca^{2+} doped SrF_2 crystal at 11K obtained by scanning the dye laser and monitoring specific transitions.

(a) the $A3(I)$ center monitoring $14618cm^{-1}$.
(a) the $A3(II)$ center monitoring $14624cm^{-1}$.

The transitions of unrelated centers are labelled with dots.

Table 5.4(a) Tentative energy levels (in cm^{-1}) of the D^- mixed crystal centers A3(I) and A3(II) in $Sr_{1-x}Ca_xF_2$:Pr^{3+}:D-. The D_2 level was chosen to be the emitting level. Uncertainties are $\pm 1 cm^{-1}$ unless otherwise indicated. The irrep labels are not given since the actual symmetries of the centers are undetermined at present.

	A3(I)	A3(II)
D_2	16824.8 ± 0.5	16824.6 ± 0.5
D_1	16824.8 ± 0.5	16824.6 ± 0.5
W_5	-	-
W_4	-	-
W_3	5294	-
W_2	5296	5287
W_1	5253	5251
X_{13}	5063± 10	5064± 10
X_{12}	-	4933
X_{11}	4927	4927
X_{10}	4834	4828
X_9	-	-
X_8	-	-
X_7	-	-
X_6	-	-
X_5	-	-
X_4	-	-
X_3	-	-
X_2	-	-
X_1	-	-
Y_{11}	-	-
Y_{10}	-	-
Y_9	-	-
Y_8	-	-
Y_7	-	-
Y_6	2338	2338
Y_5	2306	2310
Y_4	-	-
Y_3	2258	2256
Y_2	2204	2200
Y_1	-	-

Z_9	739 ± 10	749 ± 10
Z_8	-	-
Z_7	500	504
Z_6	$466^* \pm 5$	$470^* \pm 5$
Z_5	-	-
Z_4	386 ± 5	382 ± 5
Z_3	-	-
Z_2	2.6 ± 0.5	1.5 ± 0.5
Z_1	0	0

Levels which could not be unambigously assign are marked with an asterisk.

Table 5.4(b) Tentative assignment of the vibronic energy levels (in cm^{-1}) for the D^- mixed crystal centers A3(I) and A3(II) in $Sr_{1-x}Ca_xF_2$:Pr^{3+}:D-.

A3(I)		A3(II)	
$Z_1(xa)$	663	$Z_1(xa)$	665
$Z_1(xb)$	673	$Z_1(xb)$	685
$Z_1(za)$	678	$Z_1(za)$	698
$Z_7(za)$	1183	$Z_1(zb)$	711
		$Z_7(za)$	1192

$D \rightarrow X$ transitions (fig. 5.16) is not possible at this stage for either $A3(I)$ or $A3(II)$ centers. For the parent C_{4v} D^- center, this region contained more lines than expected from those expected if the lines were all due to electronic transitions. Reeves[1987] assigned all these as vibronic levels from the coupling with the lattice phonons except one with an (YX):(YY) polarisation ratio of 1:2 consistent with a $D_1(\gamma_3) \rightarrow X_4(\gamma_5)$ transition at $12335cm^{-1}$. In the mixed crystal case however, there is insufficient evidence from the polarisation measurements to provide a definite assignment to any of the lines. The transitions to the upper levels of the X multiplet seem to have more clear-cut polarisation ratios and a tentative assignment was therefore possible.

Figure 5.15 $^1D_2 \rightarrow ^3F_2$ Polarised fluoresence spectra of the D^- mixed crystal centers in the 1% Ca^{2+} doped SrF_2 crystal at 11K.

(a) the $A3(I)$ center, pumping $16821.1cm^{-1}$.
(b) the $A3(II)$ center, pumping $16822.2cm^{-1}$.

The transitions of unrelated centers are labelled with dots.

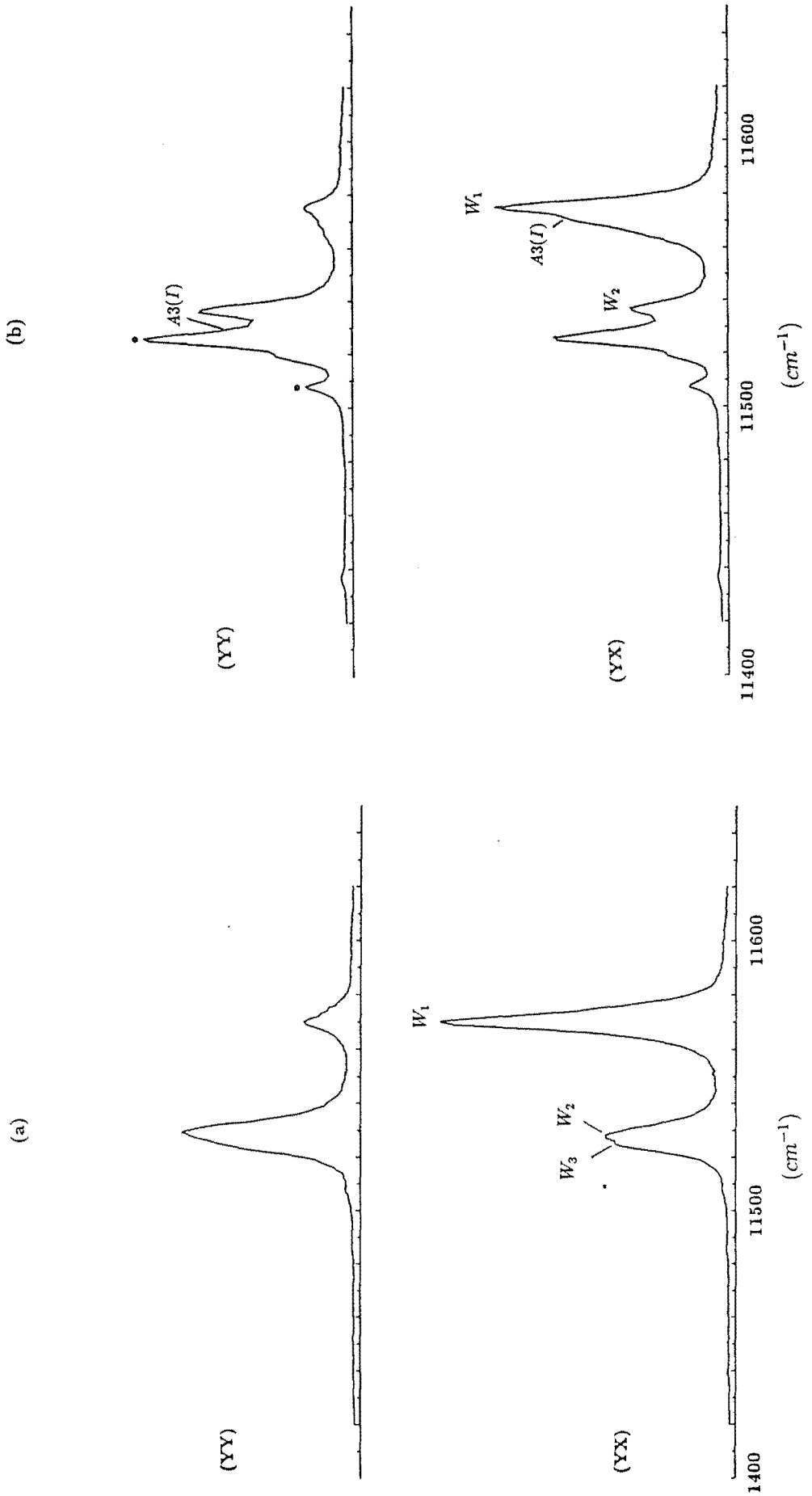
(a)
(YY)
(YX)
W_1
W_2
W_3
11400
11500
11600
(cm^{-1})
(b)
(YY)
(YX)
A3(I)
W_1
W_2
11400
11500
11600
(cm^{-1})

Figure 5.16 $^1D_2 \rightarrow ^3 H_6$ Polarised fluoresence spectra of the D^- mixed crystal centers in the 1% Ca^{2+} doped SrF_2 crystal at 11K.

(a) the $A3(I)$ center, pumping 16821.1cm^{-1}.
(b) the $A3(II)$ center, pumping 16822.2cm^{-1}.

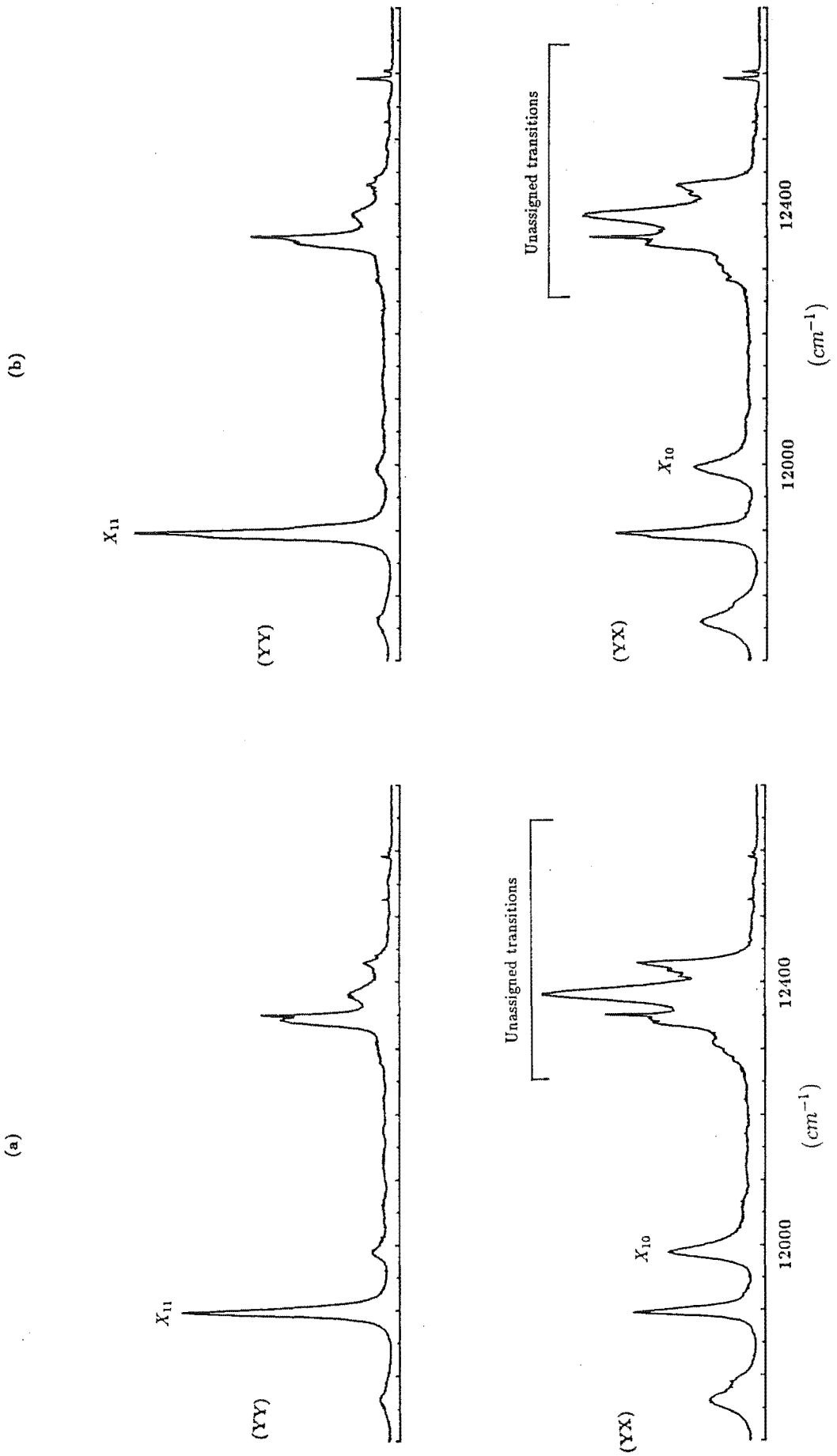
(a)
(YY)
X_{11}
(YX)
X_{10}
Unassigned transitions
12000
12400
(cm^{-1})
(b)
(YY)
X_{11}
(YX)
X_{10}
Unassigned transitions
12000
12400
(cm^{-1})

Figure 5.17 $^1D_2 \rightarrow ^3H_5$ Polarised fluoresence spectra of the D^- mixed crystal centers in the 1% Ca^{2+} doped SrF_2 crystal at 11K.

(a) the $A3(I)$ center, pumping 16821.1cm^{-1}.
(b) the $A3(II)$ center, pumping 16822.2cm^{-1}.

The transitions of unrelated centers are labelled with dots.

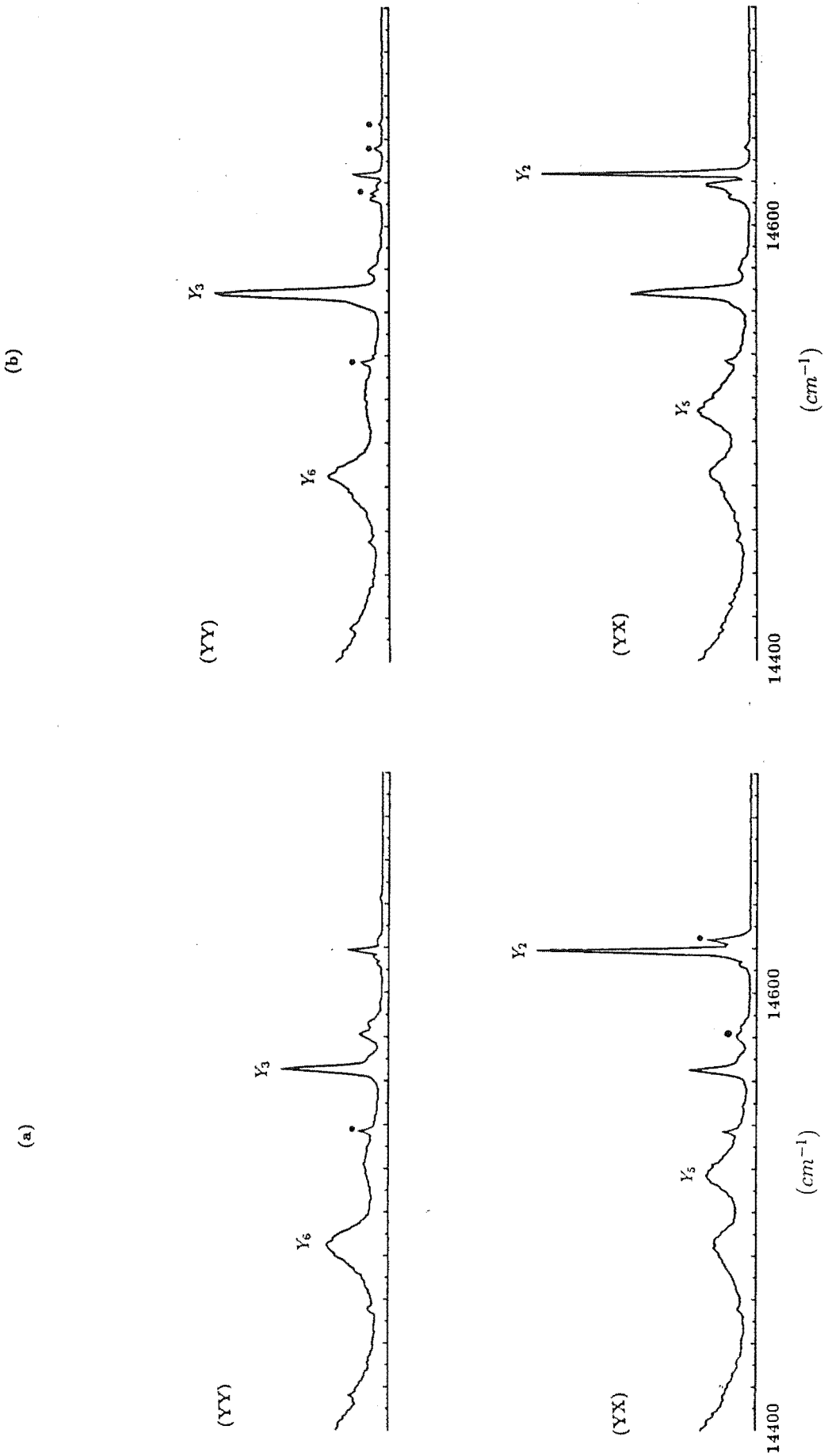
(a)
(YY)
Y_6
Y_3
(YX)
Y_5
Y_2
14400
14600
(cm^{-1})
(b)
(YY)
Y_6
Y_3
(YX)
Y_5
Y_2
14400
14600
(cm^{-1})

Figure 5.17 shows the $D \rightarrow Y$ transitions. One feature of the $A3$ type centers is the similarity of their fluorescence spectra to that of the parent C_{4v} center. This feature is exhibited in transitions to this multiplet. Some other lines not belonging to the $A3(I)$ and $A3(II)$ centers were also present and these most likely originate from the other mixed crystal centers not studied.

The $D \rightarrow Z$ electronic and vibronic transitions are shown in figure 5.18(a) and (b) respectively. Attempts to assign the vibronic levels for the $A3(I)$ and $A3(II)$ centers with the present set of data would be futile since many more lines were observed then expected. This region of the spectra also contain the Sm^{2+} band at $16142cm^{-1}$, further complicating the assignment. In spite of these difficulties, a tentative assignment of the vibronic levels is indicated in figure 5.18(a)(ii) and (b)(ii) and table 5.4 lists the assignments of levels for the two centers studied.

5.4 Mixed Crystal Centers in $Sr_{1-x}Ba_xF_2 : Pr^{3+} : D^-$

Two D^- mixed crystal centers were also studied in the $Sr_{1-x}Ba_xF_2 : Pr^{3+} : D^-$ crystal. One of these has a polarised fluorescence characteristic of the $A4$ center. The other mixed crystal center studied appears to have polarised fluorescence more consistent with a mixed crystal $A2$ center which has a C_{4v} symmetry. Discussion of these two centers follows below.

5.4.1 The Excitation Spectra

Figures 5.19 presents the broadband excitation spectrum in the D multiplet of the $Sr_{1-x}Ba_xF_2 : Pr^{3+} : D^-$ crystal studied. Apart from the position of the satellite structures, the features of this spectrum are not very different from those of the $Sr_{1-x}Ca_xF_2 : Pr^{3+} : D^-$ crystal. The $A4$ center $Z_1 \rightarrow D_1$ line at $16795.2cm^{-1}$ could still by and large, be selectively pumped though this transition seems to

Figure 5.18 $^1D_2 \rightarrow ^3H_4$ Polarised fluoresence spectra of the D^- mixed crystal centers in the 1% Ca^{2+} doped SrF_2 crystal at 11K.

(a) the $A3(I)$ center, pumping 16821.1cm^{-1}.
(b) the $A3(II)$ center, pumping 16822.2cm^{-1}.

(a)

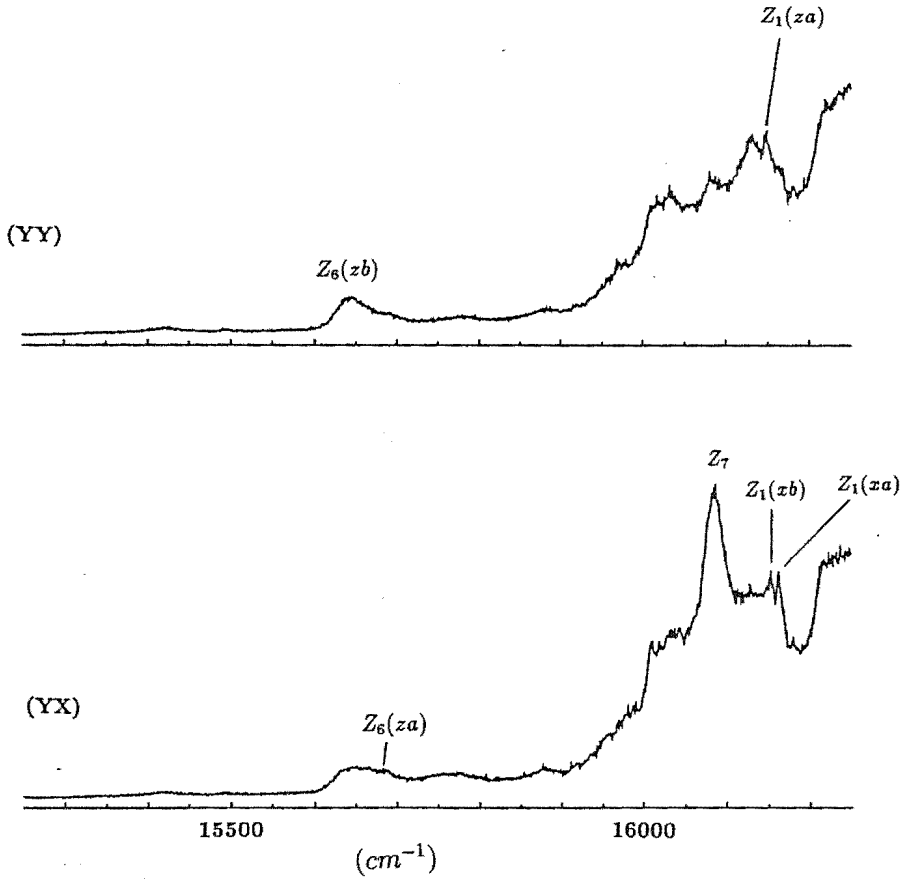
(YY)
$Z_1(za)$
$Z_6(zb)$
(YX)
Z_7
$Z_1(xb)$
$Z_1(xa)$
$Z_6(za)$
15500
16000
(cm^{-1})

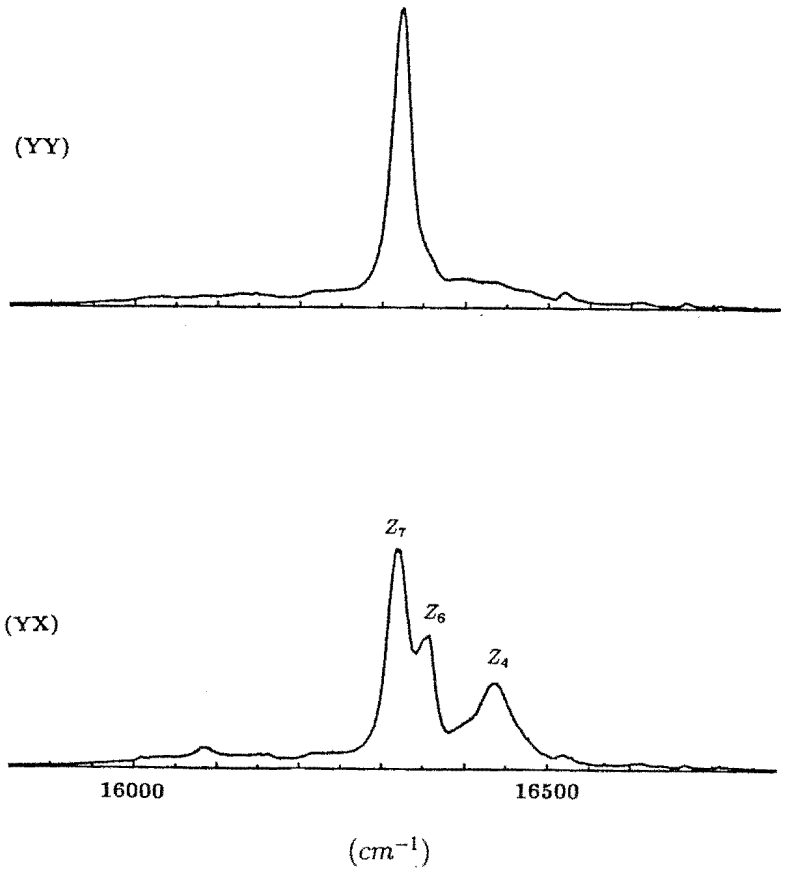
(YY)
(YX)
Z_7
Z_6
Z_4
16000
16500
(cm^{-1})

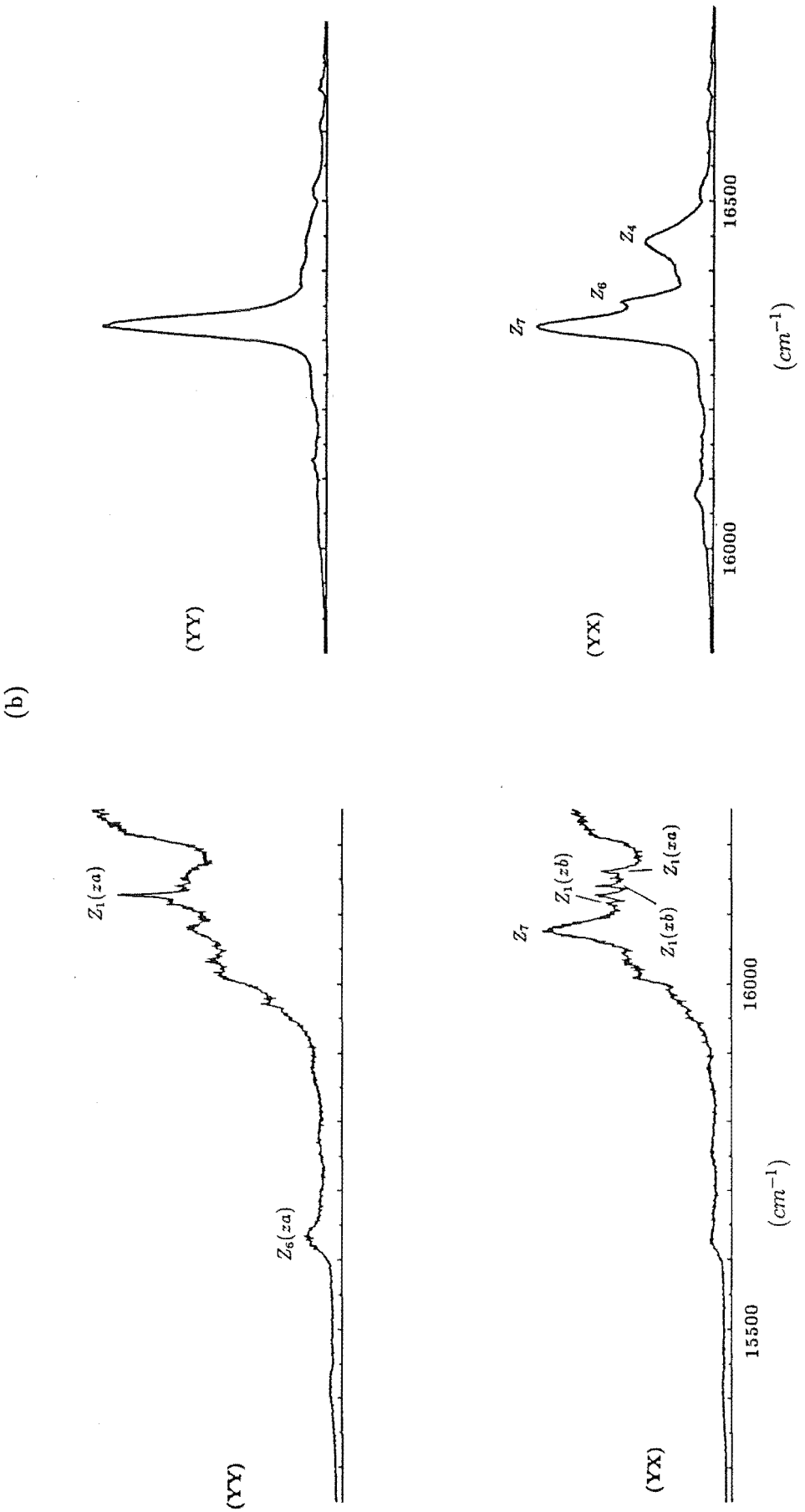
(b)
(YY)
(YX)
Z_7
Z_6
Z_4
16000
16500
(cm^{-1})
(XY)
(YX)
$Z_1(za)$
$Z_6(za)$
Z_7
$Z_1(zb)$
$Z_1(xb)$
$Z_1(xa)$
15500
16000
(cm^{-1})

reside on top of a broader but weaker band. However, the same cannot be said of the $A2$ center. The $Z_1 \rightarrow D_1$ transition at $16805.6cm^{-1}$ of the $A2$ center lies on a relatively stronger transition band and would not be suitable for pumping. The $Z_1 \rightarrow D_2$ transition at $16833.5cm^{-1}$ is more suitable but there is still an overlap of this line with other transitions, the major one being the the $Z_1 \rightarrow D_1$ transition of the $A4(F^-)$ center.

The selective excitation spectra monitoring the transitions of the $A2$ and $A4$ centers at 14520.4 and $14586.4cm^{-1}$ respectively are as shown in figure 5.20. Lines from many more centers contributed to these excitation spectra and they are readily identified from previous work in this thesis. This set of spectra best highlights the difficulties that could be encountered in the LSE of a multisite crystal system and the importance of an accurate set of spectral data of a simpler system with a reduced number of sites, before the study of a more complicated system is attempted.

From the similar properties of their polarised transitions, the $A4(D^-)$ and $A4(F^-)$ centers are deduced to have analogous structures. The presence of an $A2(D^-)$ center suggests that the $A2(F^-)$ center must also be present as well though the transitions of the $A2(F^-)$ center were not observed when the undeuterated Ba^{2+} doped $SrF_2 : Pr^{3+}$ crystal system was studied. A possible reason for this is that the smaller ionic radius mismatch between the Sr^{2+} and Ba^{2+} ions means that an on-axis substitution of a Sr^{2+} ion by the dopant Ba^{2+} ion does not give a sufficiently large change in the crystal field to allow the levels of the $A2(F^-)$ center to be discriminated from the parent C_{4v} transitions.

5.4.2 The Polarised Fluorescence Spectra

The simpler $D \rightarrow W$ transitions best illustrate the polarisation features of the $A2$ and $A4$ type centers as shown in figures 5.21(a) and (b) respectively. Polarisation ratios found for the $A2$ center, together with the lack of a ground state energy level splitting in the excitation spectrum of this center confirms the assignment of a C_{4v}

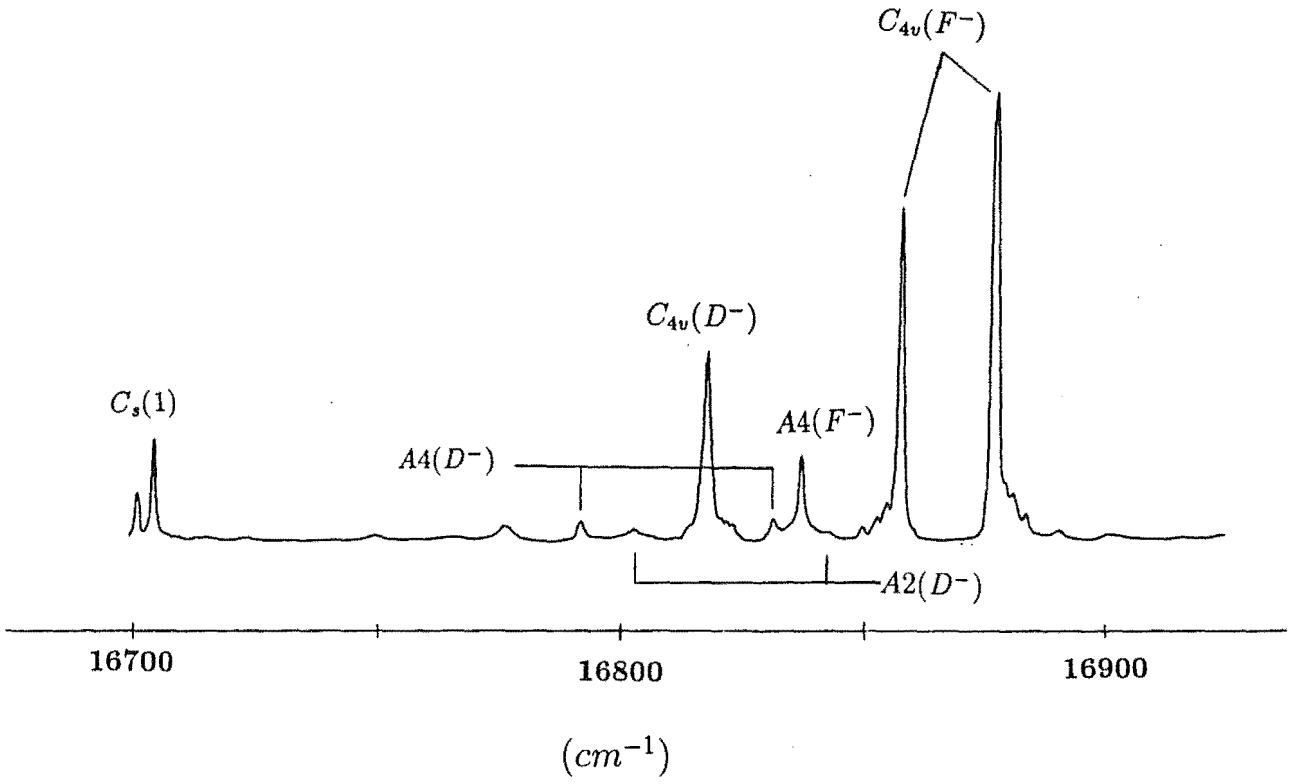

Figure 5.19 Broadband excitation spectra of the $Sr_{1-x}Ba_xF_2 : Pr^{3+}$ crystals, monitoring the $D \rightarrow Z$ transitions at 11K. This crystal was doped with 0.5% Ba^{2+} and deuterated for 32 hours.

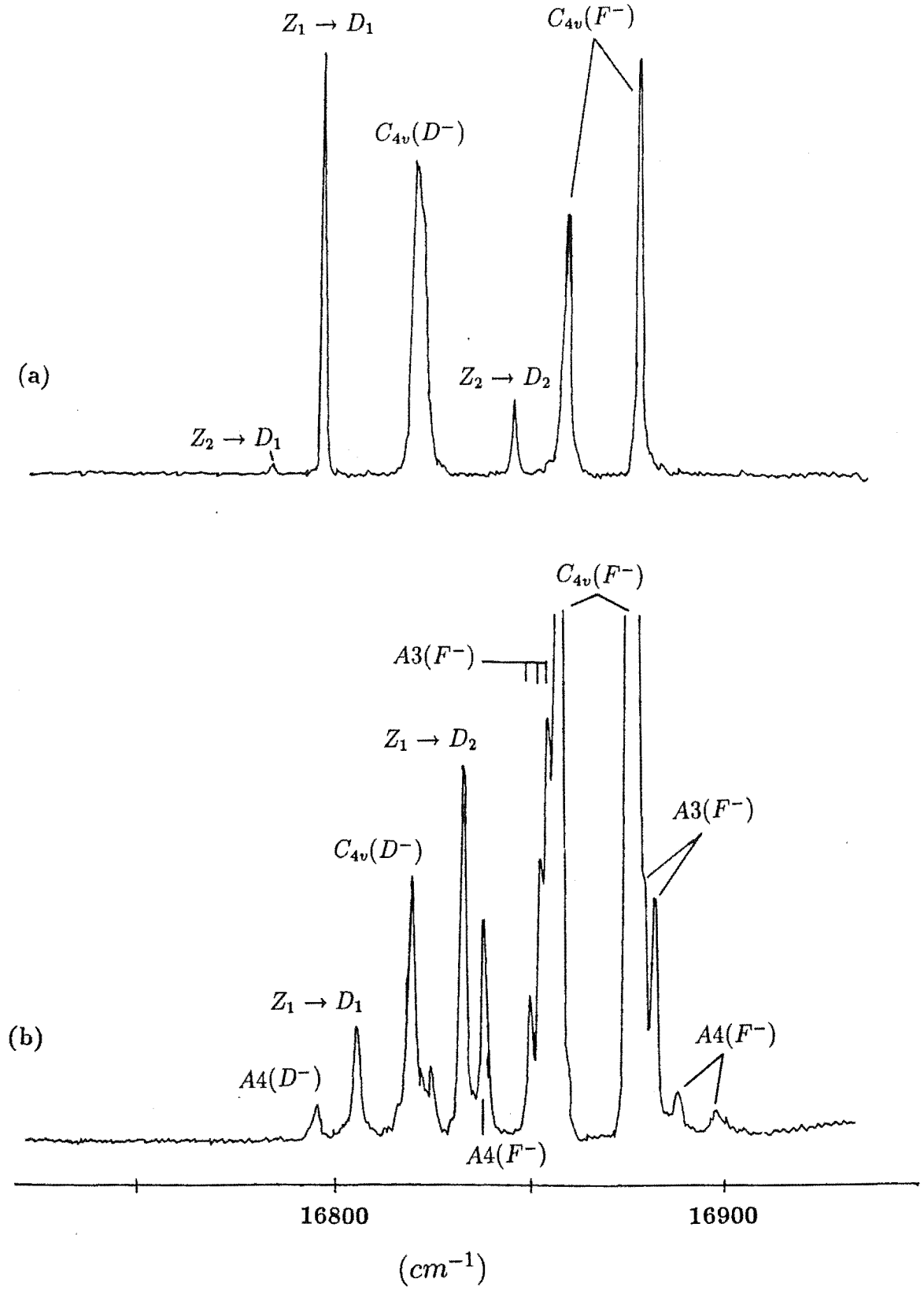

Figure 5.20 Selective excitation spectra of the D^- mixed crystal centers in the 0.5% Ba^{2+} doped SrF_2 crystal at 11K obtained by scanning the dye laser and monitoring specific transitions.

(a) the $A4$ center monitoring $14586cm^{-1}$.
(b) the $A2$ center monitoring $14520cm^{-1}$.

symmetry to this center. The discussion of the F^- $A4$ center in section 4.4 applies to the D^- $A4$ center studied here as well, the hallmark of this type of center being the greater range of polarisation ratios observed, which appears to necessitate a model which has the lowest symmetry group, C_1.

The distingushing polarisation ratios for both these centers are also evident in the transitions to the X,Y,Z multiplets. as shown in figures 5.22, 5.23, 5.24 respectively. The assignment of the levels in the X multiplet is less successful as was the case for the parent C_{4v} center. The major difficulty, as discussed in section 5.3, is associated with the vibronics due to the lattice phonons. Weaker transitions from sites other than those of interests were also present and they could, by and large be discriminated from the transitions of the center being studied. There is an anomaly in the fluorescence spectra of the $A2$ center for the X multiplet. This concerns the transition to the X_{10} level. Given the assignment of a γ_3 irrep to this level, it is expected that the (YX):(YY) polarisation ratio observed should be 1:0. The ratio observed was closer to 3:1. It is likely that other unrelated centers also contributed to this transition band. A similar problem was also encountered in attempts to assign the transition band at $16085cm^{-1}$ in the transitions to the Z multiplet.

The sharpest and strongest line due to the Sm^{2+} impurity in SrF_2 crystals is at $14351cm^{-1}$. It appeared in the fluorescence spectra of the $A2$ and $A4$ centers being studied and makes assignment of the Y_7 and Y_8 levels of the $A2$ center impossible. The richness of the spectra due to the unavoidable simultaneous excitation of a few centers in the $D \rightarrow Z$ transitions for both the centers studied preclude a confident assignment of the levels in this multiplet. Other than the Z_6 and Z_3 levels for the $A2$ center, the remaining weaker lines are due to vibronic transitions and excitation of other centers. Too much doubt remains as to the origin of these lines, hence no assigments were made for them. Table 5.5 present the assignments of the levels for these centers.

Table 5.5(a) The energy levels (in cm^{-1}) of the D^- mixed crystal centers A4 and A2 in $Sr_{1-x}Ba_xF_2$:Pr^{3+}:D-. Uncertainties are $\pm 1 cm^{-1}$ unless otherwise indicated. The irrep labels for the levels of the $A4$ center are not given since the symmetry is not known at present.

	A4	A2	
D_2	16853.7 ± 0.5	16832.7 ± 0.5	(γ_3)
D_1	16794.4 ± 0.5	16804.8 ± 0.5	(γ_1)
W_5	-	NA	
W_4	-	5372	(γ_4)
W_3	5296	5296	(γ_5)
W_2	5399	-	(γ_3)
W_1	5261	5235	(γ_1)
X_{13}	5060 ± 10	NA	
X_{12}	4958	NA	
X_{11}	4891	NA	
X_{10}	4824 ± 10	5050 ± 10	(γ_3)
X_9	-	4912	(γ_5)
X_8	-	4797	(γ_1)
X_7	-	-	(γ_4)
X_6	-	-	(γ_3)
X_5	4473	-	(γ_2)
X_4	-	4460	(γ_5)
X_3	-	-	(γ_3)
X_2	4236	4372	(γ_4)
X_1	4232	-	(γ_5)
Y_{11}	-	NA	
Y_{10}	-	NA	
Y_9	-	NA	
Y_8	-	-	(γ_4)
Y_7	-	-	(γ_5)
Y_6	2339 ± 5	-	(γ_2)
Y_5	2310	2286 ± 5	(γ_5)
Y_4	2271	2268	(γ_3)
Y_3	2254	-	(γ_5)
Y_2	2208	2259	(γ_1)
Y_1	2190	-	(γ_2)

Z_9	-	(γ_1)	NA
Z_8	538	(γ_1)	NA
Z_7	467 * $\pm$ 5	(γ_2)	-
Z_6	457 $\pm$ 5	(γ_1)	485
Z_5	-	(γ_2)	-
Z_4	381 $\pm$ 10	(γ_1)	-
Z_3	162 *	(γ_2)	422 $\pm$ 10
Z_2	12.0 $\pm$ 0.5	(γ_1)	-
Z_1	0	(γ_2)	0

Levels which could not be unambigously assign are marked with an asterisk.
NA - Excited levels not applicable to the A2 C_{4v} center.

Table 5.5(b) Tentative assignment of the vibronic energy levels (in cm^{-1}) for the D^- mixed crystal centers A4 and A2 in $Sr_{1-x}Ba_xF_2$:Pr^{3+}:D-.

A4		A2	
$Z_1(xa)$	579	$Z_1(x)$	645
$Z_1(za)$	666	$Z_1(z)$	653
$Z_6(za)$	1126	$Z_6(z)$	1133
$Z_8(xa)$	1115	$Z_7(z)$	1367
$Z_8(za)$	1202		
$Z_9(za)$	1393		

(a) (i)

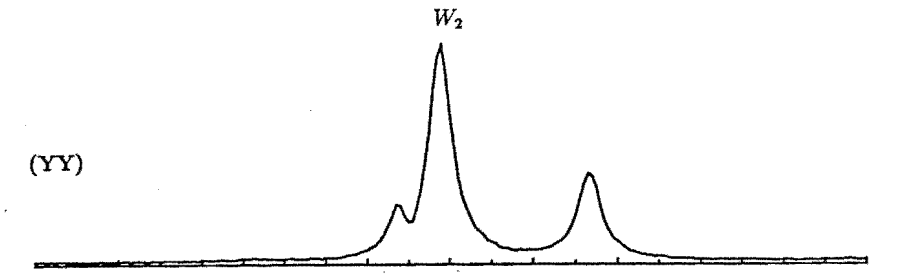
W_2
(YY)

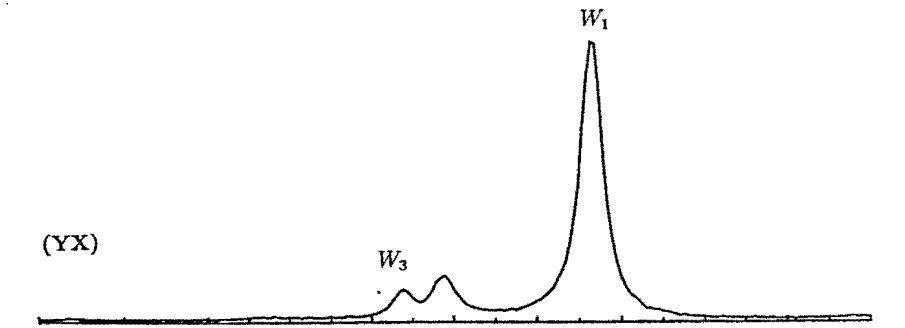
W_1
(YX)
W_3
11400
11500
11600
(cm^{-1})

(a)(ii)

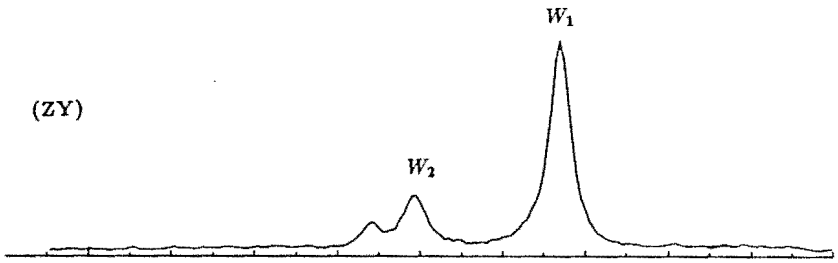
W_1
(ZY)
W_2

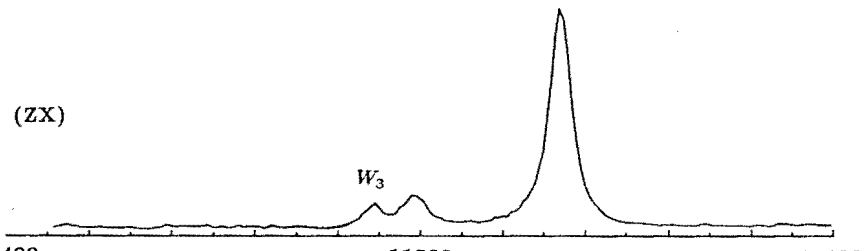
(ZX)
W_3
11400
11500
11600

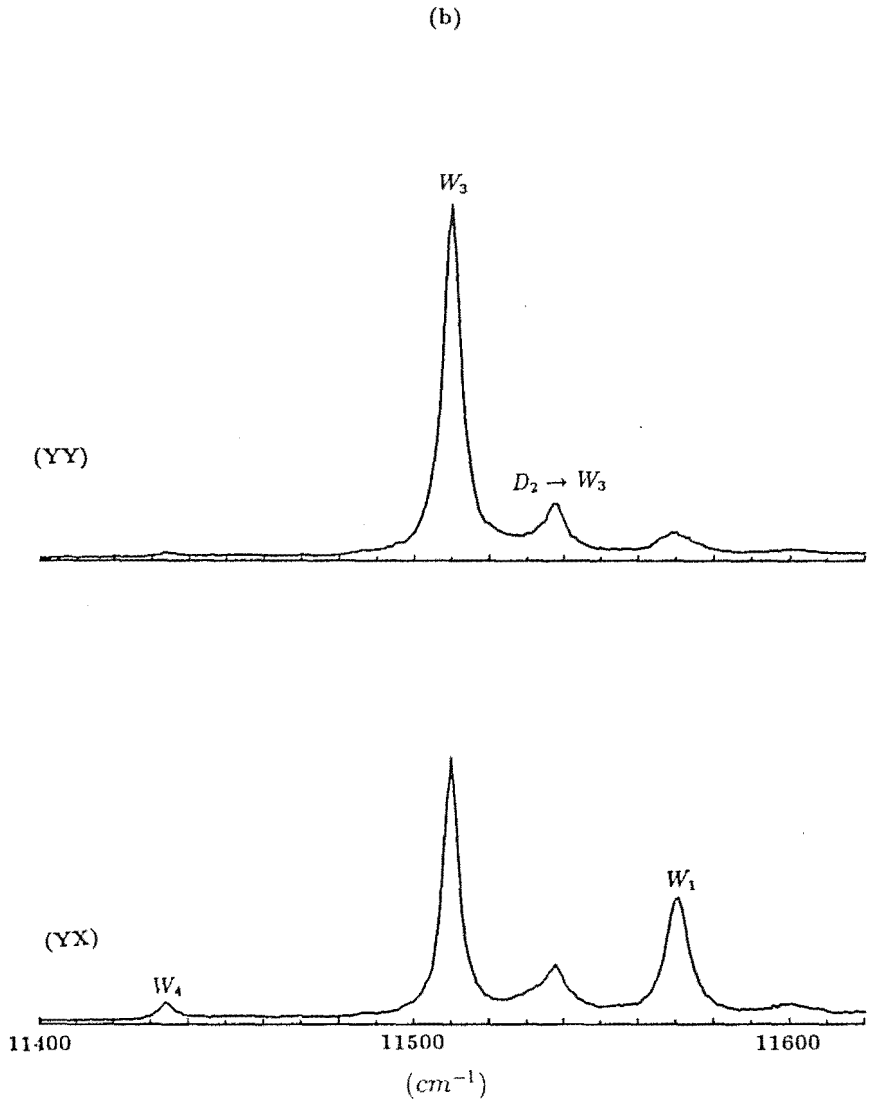

Figure 5.21 $^1D_2 \rightarrow ^3F_2$ Polarised fluoresence spectra of the D^- mixed crystal centers in the 1% Ba^{2+} doped SrF_2 crystal at 11K.

(a) the $A4$ center, pumping 16794.4cm^{-1}.
(b) the $A2$ center, pumping 16804.8cm^{-1}.

Figure 5.22 $^1D_2 \rightarrow ^3H_6$ Polarised fluoresence spectra of the D^- mixed crystal centers in the 1% Ba^{2+} doped SrF_2 crystal at 11K.

(a) the $A4$ center, pumping 16794.4cm^{-1}.
(b) the $A2$ center, pumping 16804.8cm^{-1}.

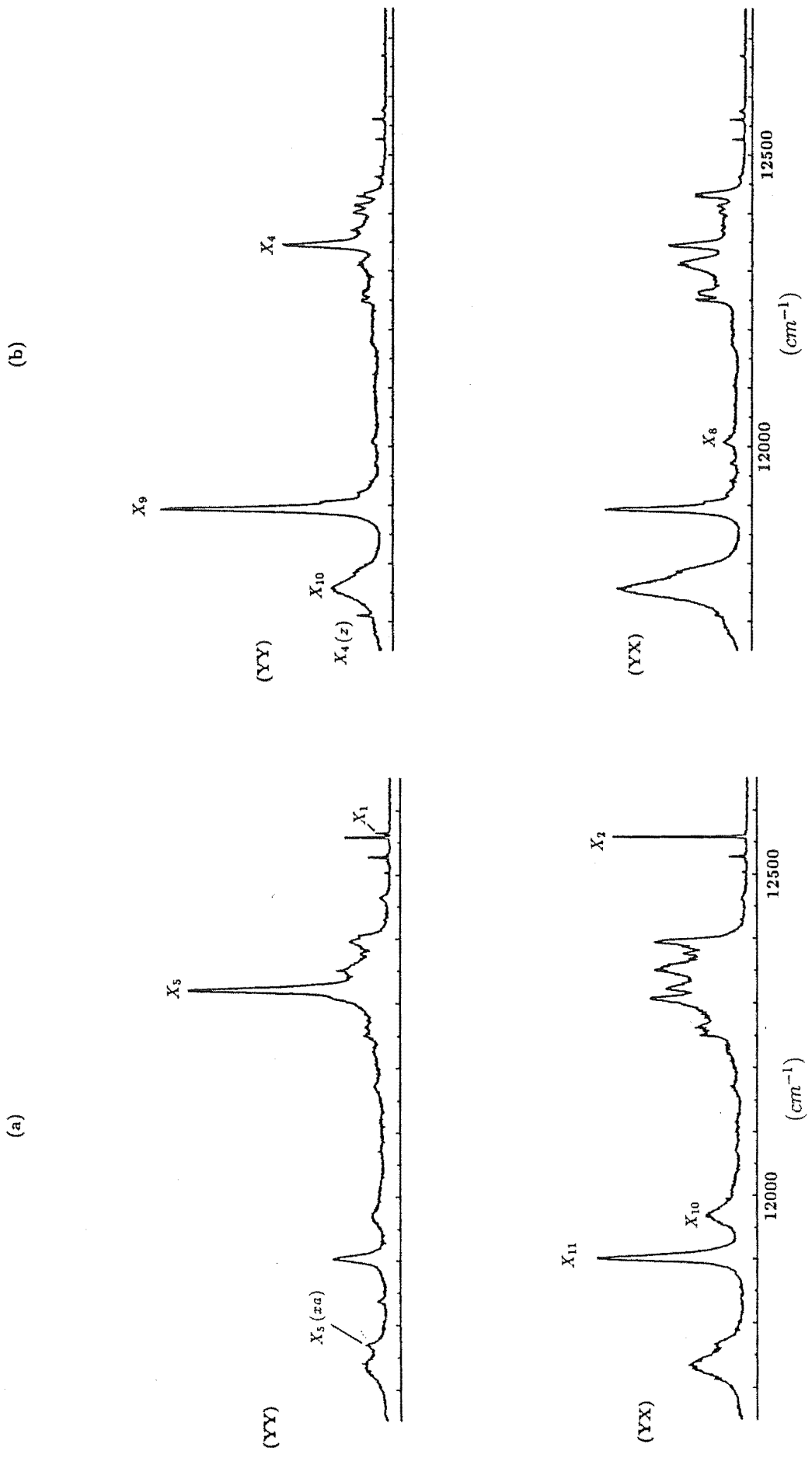
(a)
(YY)
X_5
$X_5(xa)$
X_1
(YX)
X_{11}
X_{10}
X_2
12000
12500
(cm^{-1})
(b)
(YY)
X_9
X_{10}
$X_4(z)$
X_4
(YX)
X_8
12000
12500
(cm^{-1})

Figure 5.23 $^1D_2 \rightarrow ^3H_5$ Polarised fluoresence spectra of the D^- mixed crystal centers in the 1% Ba^{2+} doped SrF_2 crystal at 11K.

(a) the $A4$ center, pumping $16794.4cm^{-1}$.
(b) the $A2$ center, pumping $16804.8cm^{-1}$.
The transitions of unrelated centers are labelled with dots.

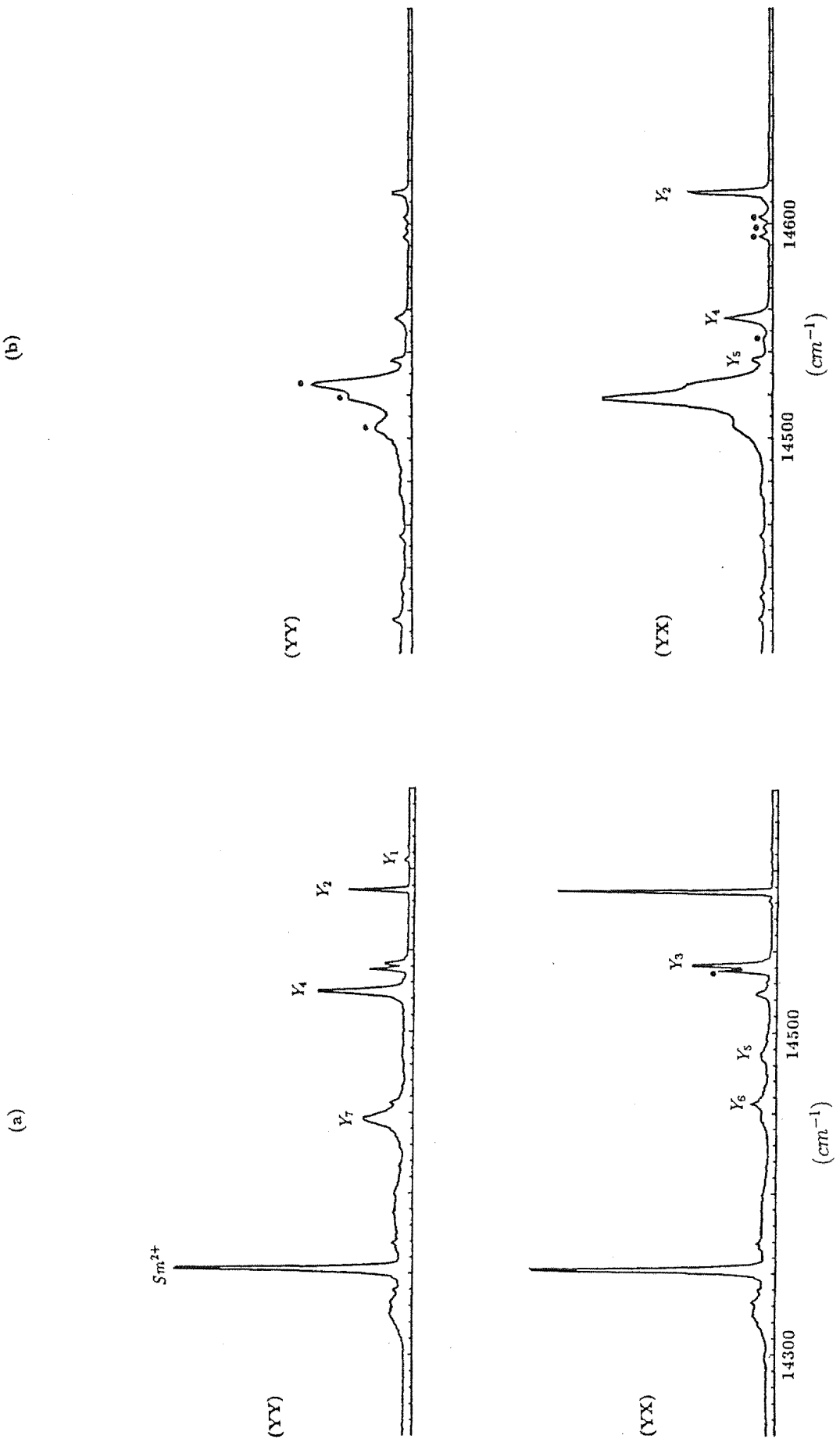
(a)
(YY)
Sm^{2+}
Y_7
Y_4
Y_2
Y_1
(YX)
Y_6
Y_5
Y_3
14300
14500
(cm^{-1})
(b)
(YY)
(YX)
Y_5
Y_4
Y_2
14500
14600
(cm^{-1})

Figure 5.24 $^1D_2 \rightarrow ^3 H_4$ Polarised fluoresence spectra of the D^- mixed crystal centers in the 1% Ba^{2+} doped SrF_2 crystal at 11K.

(a) the $A4$ center, pumping 16794.4cm^{-1}.
(b) the $A2$ center, pumping 16804.8cm^{-1}.

The transitions of unrelated centers are labelled with dots.

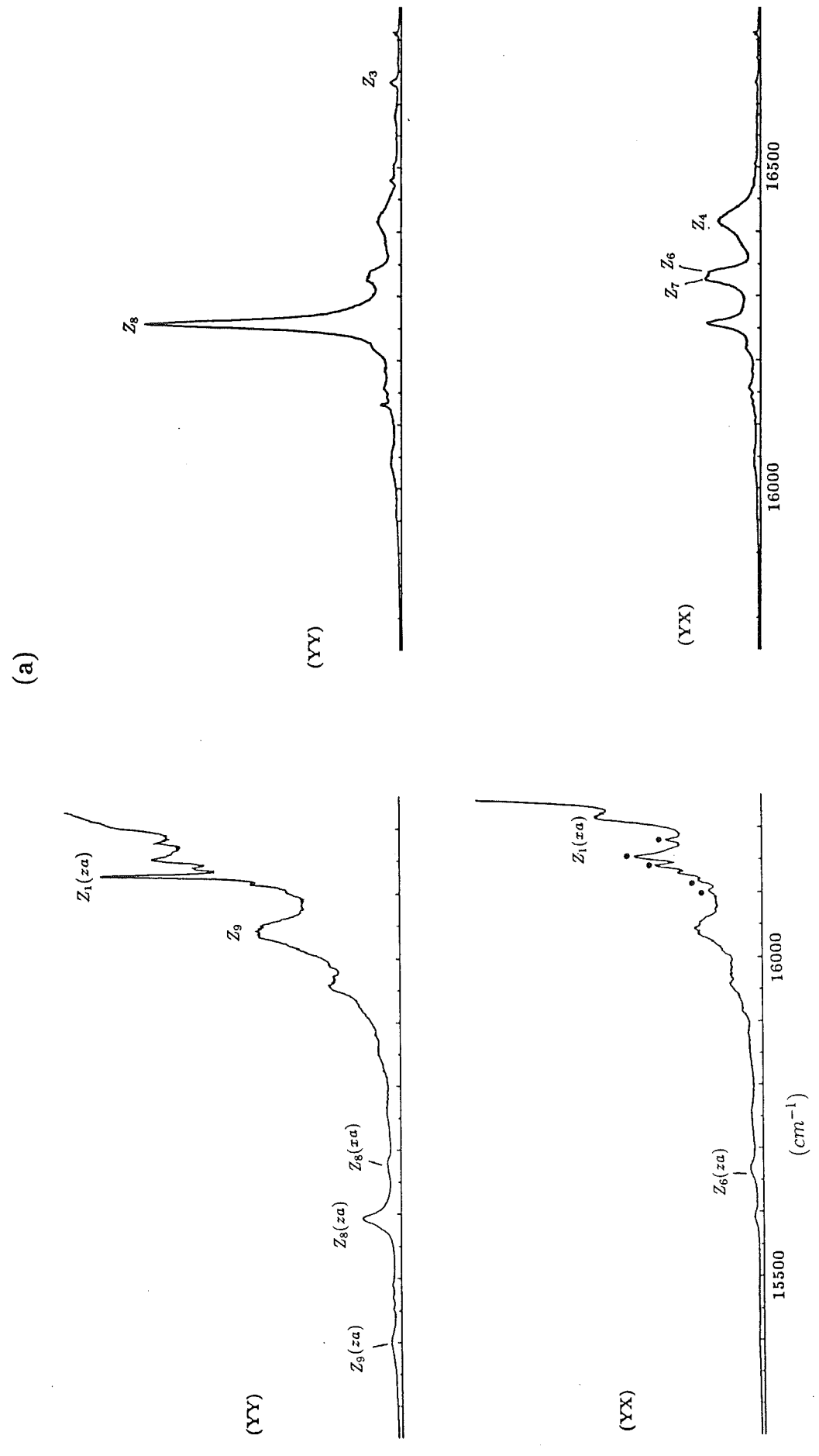
(a)
(YY)
Z_8
Z_3
(YX)
Z_7
Z_6
Z_4
16000
16500
(YY)
$Z_1(za)$
Z_9
$Z_8(xa)$
$Z_8(za)$
$Z_9(za)$
(YX)
$Z_1(xa)$
$Z_6(za)$
15500
16000
(cm^{-1})

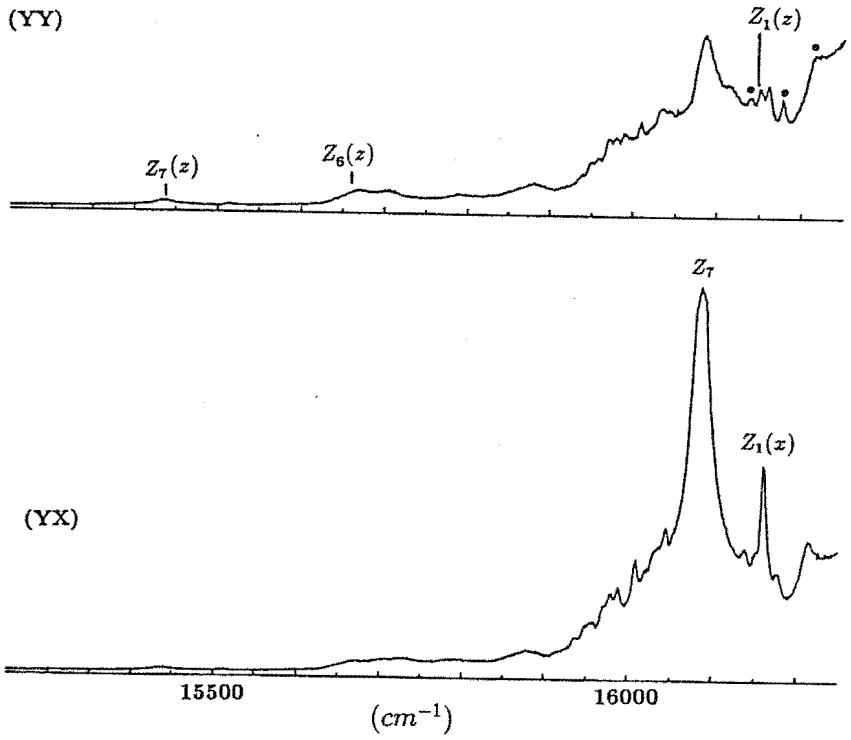
(YY)
$Z_1(z)$
$Z_7(z)$
$Z_6(z)$
Z_7
$Z_1(x)$
(YX)
15500
16000
(cm^{-1})

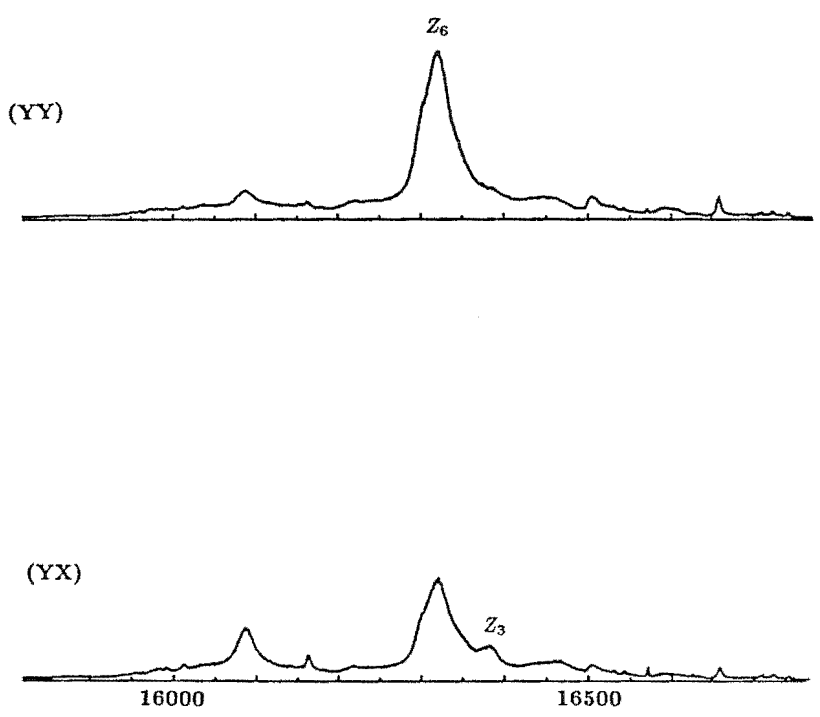
Z_6
(YY)
(YX)
Z_3
16000
16500

Chapter 6

Time Resolution and Lifetime Studies

The idea of using a mechanical chopper for time resolved laser spectroscopy was suggested by my supervisor Dr. GD Jones. The techniques for this experiment as outlined in chapter 3 were applied to the transitions of the fluorine mixed crystal centers with some success, firstly, in getting a qualitative appreciation of the relative transition lifetimes of the centers present and secondly, in revealing underlying mixed crystal center lines previously unresolved in the frequency domain. These are discussed in section 6.1 which also presents the spectra of the broadband excitation measurements performed in conjuction with the mechanical chopper on the $Ca_{1-x}Sr_xF_2 : Pr^{3+}$, $Ca_{1-x}Ba_xF_2 : Pr^{3+}$, $Sr_{1-x}Ca_xF_2 : Pr^{3+}$ and $Sr_{1-x}Ba_xF_2 : Pr^{3+}$ crystal systems.

To quantify the transition lifetimes of particular centers more accurately however required the use of the nitrogen pulse dye laser. These lifetimes were measured for the centers of the four crystal systems mentioned above and their deuterated analogues. The lifetimes of the centers studied are largely radiative and the different lifetimes of the mixed crystal centers are a consequence of the changes in crystal field between the different centers. The discussion on the results of the lifetime

measurements performed is presented in section 6.2.

6.1 Time Resolved Excitation using a Mechanical Chopper

The analyses of the time resolved broadband excitation spectra basically involve comparing the intensities of the lines present. The transitions with the fastest lifetimes will decrease in intensity more rapidly relative to the transitions with slower lifetimes as the chopper spped is reduced.

Figures 6.1(a) and (b) show the broadband excitation spectra of the $Ca_{1-x}Sr_xF_2 : Pr^{3+}$ crystal when the chopper was rotating at 200Hz and 30 Hz respectively. When the chopper speed was lowered, the intensities of the $A1$ and $A2$ centers has gone up roughly 30 and 6 times relative to the parent C_{4v} center respectively. Hence, it can be deduced that in this crystal the $D \rightarrow Z$ transitions of the $A2$ center have the longest lifetimes, followed by the $A1$ center and last of all, the parent C_{4v} center. Some weak lines at the shoulder of the $A2$ center D_2 transition, which could not be observed in the ordinary broadband excitation spectra taken without the chopper, appeared in the spectrum acquired at a lower chopper speed, indicating the presence of further centers.

Similar spectra for the 1% Ba^{2+} doped $CaF_2 : Pr^{3+}$ crystal taken in conjuction with the chopper is shown in figures 6.2(a) and (b). The lines belonging to the $A1(I)$, $A1(II)$ and $A2$ centers have all gone up relative to the parent C_{4v} center, hence the parent C_{4v} center has the fastest radiative decay times in this crystal. The intensities of the $A2$ center D_1 and D_2 lines have gone up fastest relative to the lines of the other centers, hence the $A2$ center has the longest decay lifetimes. The next longest fluorescence lifetimes belong to the transitions of the $A1(II)$ center since the intensity of its D_1 level has risen by about twice relative to the intensity of the $A1(I)$ center. Thus in descending order are the lifetimes belonging to the $A2$,

$A1(II)$, $A1(I)$ and the parent C_{4v} center.

The usefulness of using the chopper system for observing lines not resolved in the frequency domain is demonstrated in the spectra shown in figure 6.3. The broadband excitation spectrum of the $Sr_{1-x}Ca_xF_2 : Pr^{3+}$ crystal at the chopper speed of 200Hz (fig. 6.3(a)) looks similar to the spectrum taken without the chopper system. When the chopper speed was reduced to 30Hz, new lines were observed at the shoulder of the parent C_{4v} D_1 and D_2 levels. It is apparent that further centers are present in the Ca^{2+} doped SrF_2 crystal with transitions close to that of the parent C_{4v} center but selective excitation of these centers are not possible because of the proximity of their $Z \rightarrow D$ transition frequencies to each other.

The relatively larger SrF_2 crystal lattice constant (5.79Å) compared to that of the CaF_2 crystal (5.46Å) would account for the smaller departure of the energy levels of the mixed crystal centers from the levels of the parent C_{4v} center in the SrF_2 host crystal. In the superposition model of crystal fields, the crystal field V acting on the open-shell electrons of a paramagnetic ion is the resultant of the total contributions from individual ions in the crystal, with each of the single ions contributing an axial field $V(L)$ independent of the other ions [Newman and Ng, 1989]. Associated with the crystal field from each individual ion is an *intrinsic paramcter* $\overline{B_q^k}(R_L)$ which is geometrically independent and is a function of R_L only, the axial distance of the ligand ion from the paramagnetic ion. A review of the superposition model can be found in the work of Newman and Ng [1989]. Here the important point is that the intrinsic parameters have an inverse power relationship with the distance between the ligand and paramagentic ion i.e :

$$\overline{B_q^k}(R_L) \propto \left(\frac{1}{R}\right)^{t_k}, \tag{6.1}$$

where the t_k values are empirically determined. Applying this to the separations of the mixed crystal center energy levels from the levels of the parent center, any small shift in the positions of the lattice or interstitial fluorines induced by the alkaline earth dopant in a crystal host with a bigger lattic constant like the SrF_2, is expected to produce a smaller change in the crystal field experienced by the RE ion than it would in CaF_2. Further, the rate of change in the values of the intrinsic

parameters with respect to the shift of the F^- ions from the equilibrium positions would be smaller for the bigger R_L values of the SrF_2 compared the R_L values of CaF_2. Hence the energy levels of the different mixed crystal centers are observed to be very close to the levels of the parent C_{4v} center in the SrF_2 lattice.

Figure 6.4 gives the time resolved broadband excitation spectra of the $Sr_{1-x}Ba_xF_2 : Pr^{3+}$ crystal system. The line structures at the shoulders of the parent C_{4v} D_1 and D_2 lines with the chopper slowed down to 30Hz are different from those of the Ca^{2+} doped SrF_2, indicating further Ba^{2+} or mixed Ba^{2+} and Ca^{2+} dopant centers. An additional line structure was also observed close to the $Z_1 \rightarrow D_1$ line of the $A4$ center (fig. 6.4(b)) for the scan done at the reduced chopper speed. This line was not previously apparent in the spectrum measured and is presumed to be weak under normal excitation conditions without the chopper. Hence, its contribution to the fluorescence spectra of the $A4$ center should be minimal.

6.2 Lifetime Measurements using the N_2 Pulsed Laser

The centers excited optically in the CaF_2 and SrF_2 hosts undergo relaxation both radiatively and non-radiatively and the measured fluorescent lifetimes would comprise the sum of these two different contributions. For the fluorine centers, radiative decay is the main mechanism of de-excitation. The relaxation of excitation of the hydrogenic type centers has a greater contribution from the non-radiative decay processes due to the local mode phonons of the lighter hydrogenic ions [Reeves,1987] and as a result, the lifetimes of the D^- centers are invariably shorter than their F^- center counterparts.

The data points of the fluorescence decay of each center studied and the exponential curve as obtained from the fit of the data points of a particular center are superposed on the same diagram and presented in figures 6.5 to 6.9 with table 6.1

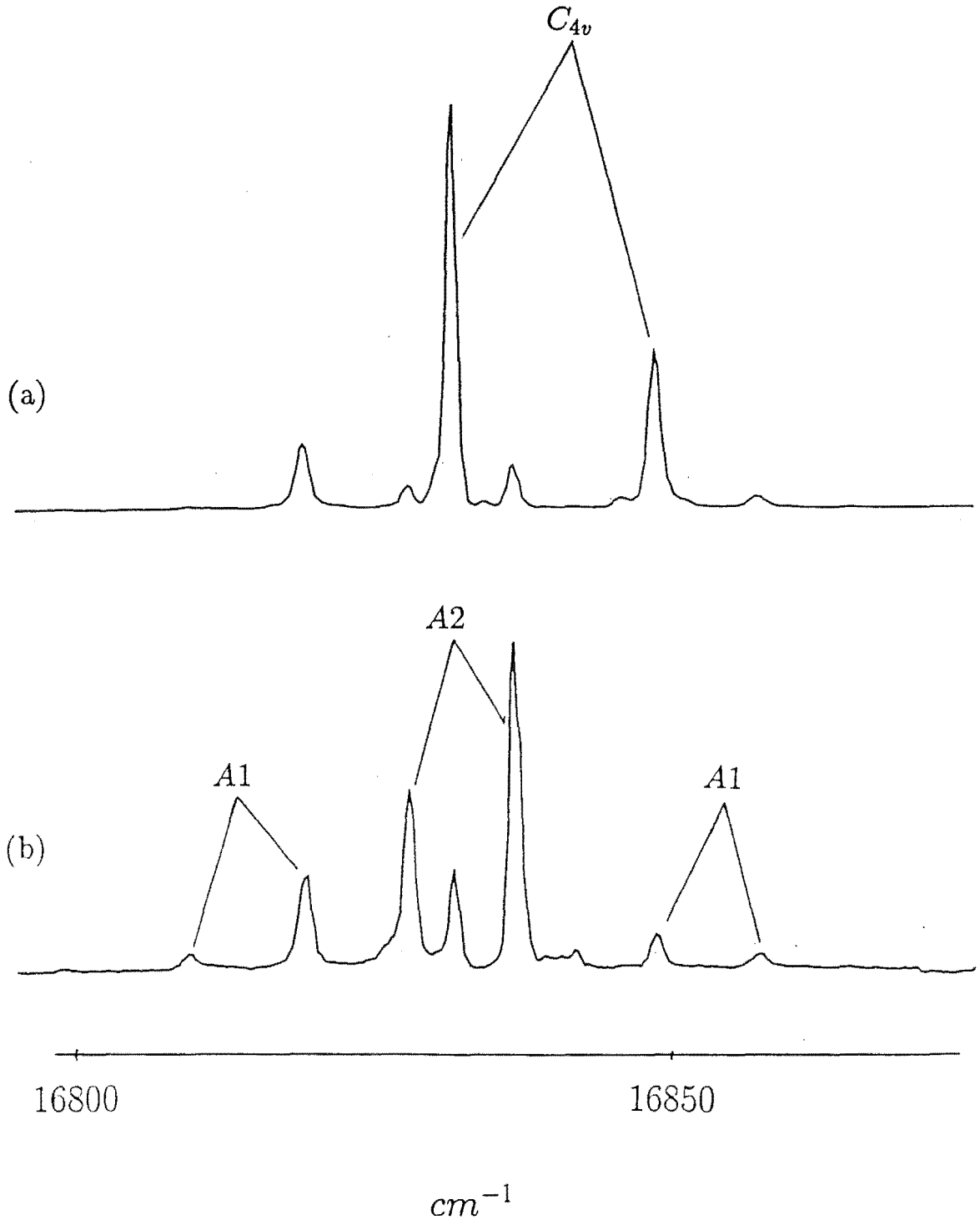

Figure 6.1 Broadband excitation spectra of the $Ca_{0.995}Sr_{0.005}F_2 : Pr^{3+}$ crystal at 11K. Chopper speed is approximately (a) 200Hz (b) 30Hz with the gate delay between excitation and observation of fluorescence approximately 1msec and 7msec and the gate width 0.8msec and 5msec for (a) and (b) respectively.

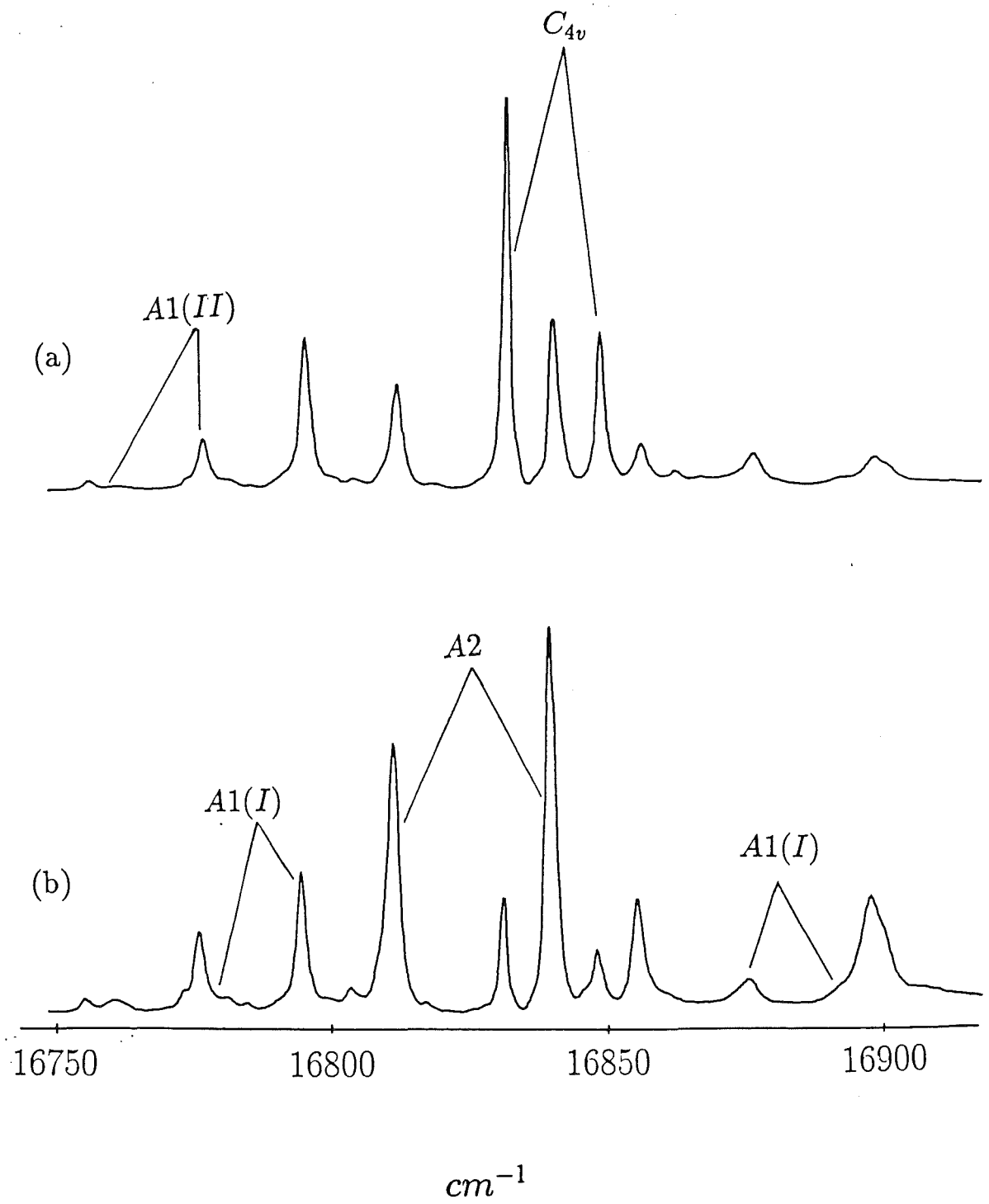

Figure 6.2 Same as figure 6.1 except for crystal $Ca_{0.995}Ba_{0.005}F_2 : Pr^{3+}$

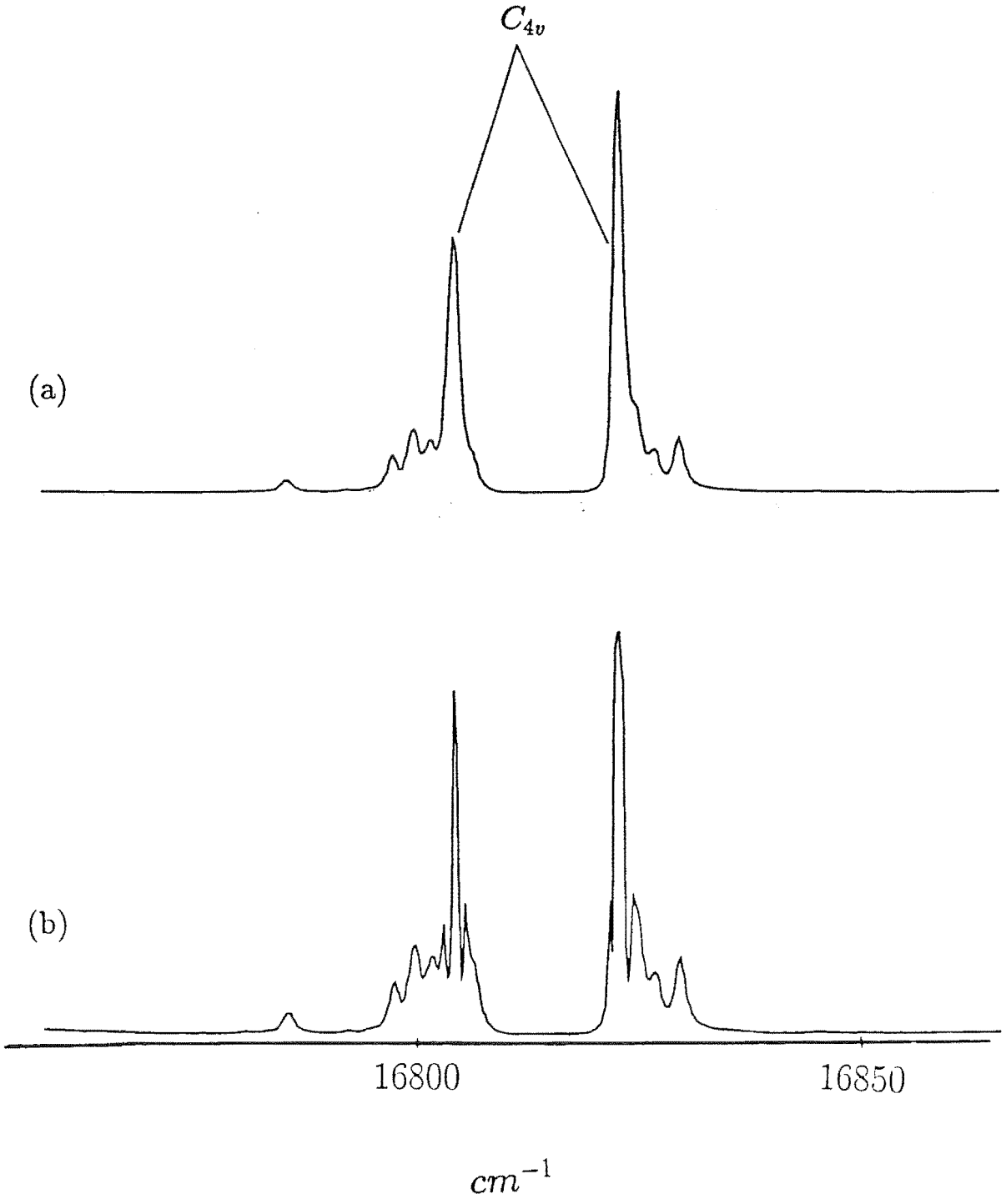

Figure 6.3 Same as figure 6.1 except for crystal $Sr_{0.995}Ca_{0.005}F_2 : Pr^{3+}$

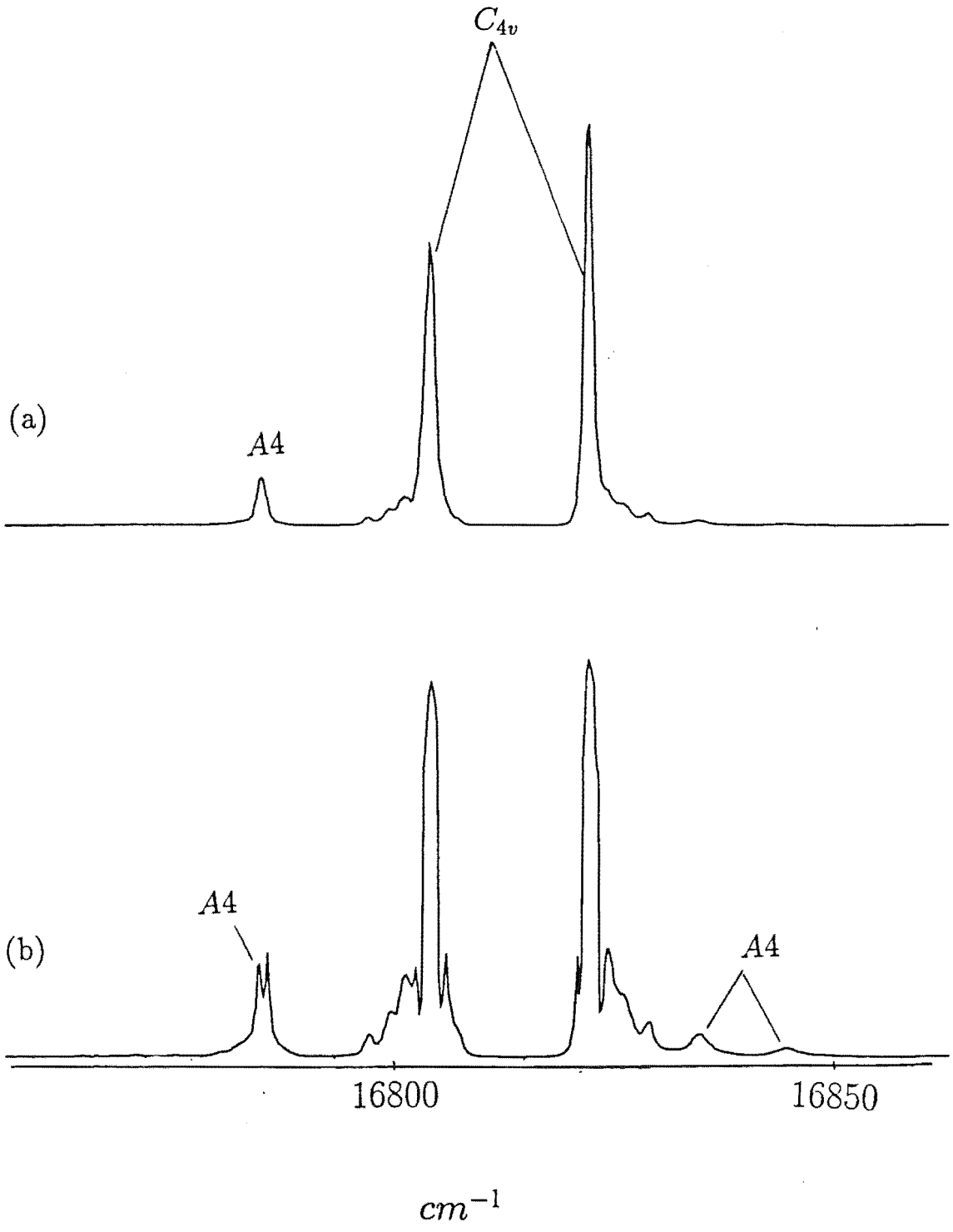

Figure 6.4 Same as figure 6.1 except for crystal $Sr_{0.995}Ba_{0.005}F_2 : Pr^{3+}$

listing the lifetimes as determined from the exponential fits.

6.2.1 Dependence of the CaF_2 C_{4v} center lifetime on the Pr^{3+} concentration

As listed in table 6.1, the lifetime of the parent C_{4v} center is dependent on the concentration of the Pr^{3+} dopant. When the concentration of the Pr^{3+} doping was raised, the density of sites in the crystal increased and this enhances the energy transfer activity among the centers via either ion pair relaxation or upconversion. Ion pair relaxation occurs when donor ions are excited and on de-excitation, transfer their energy to acceptor ions. If the acceptor ions are also in the excited state, the energy exchange would cause the acceptor ions to be at an even higher excited state and thus the upconversion process. Any energy deficit or credit in the ion pair relaxation process could be compensated by absorption or emission of lattice phonons.

The investigations of the upconversion transfer rates by Lezama et al [1986] of the C_{4v} center in CaF_2 and Reeves [1987] of the same center in SrF_2, reached the same conclusion that the predominant transfer mechanism between the C_{4v} centers in these crystals is long range dipole-dipole interaction.

The leading term of this multipole coupling is predicted to have a radial dependence of R^{-3} [Dexter,1953] where R is the distance between the acceptor and donor ions. As the mean distance between ions is inversely proportional to the cube root of the dopant concentration, a plot of the decay rate of the C_{4v} center which is the reciprocal value of the lifetime measured, against the inverse cube root of the Pr^{3+} concentration should yield values close to the predicted radial dependence. The three lifetime values of the C_{4v} center in the CaF_2 host measured in this work at Pr^{3+} concentrations of 0.001, 0.01 and 0.1 % and the other two at 0.2 and 0.9 % measured by Kliava et al [1978] were fitted to a curve with the formula:

$$W_R(R) = aR^{\beta} + c. \tag{6.2}$$

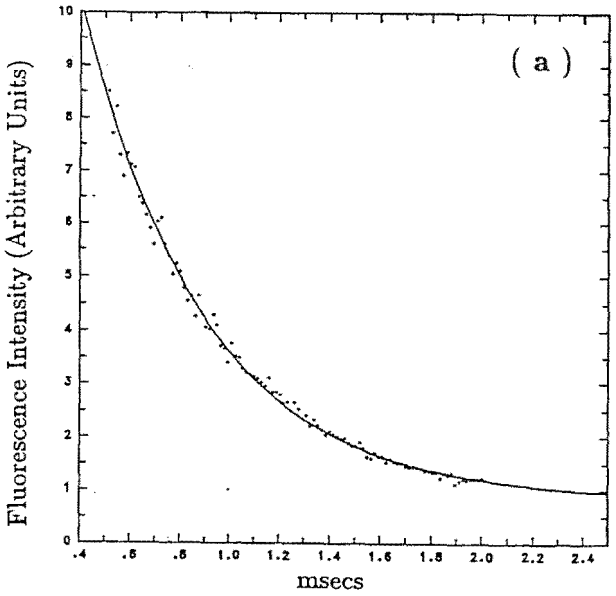

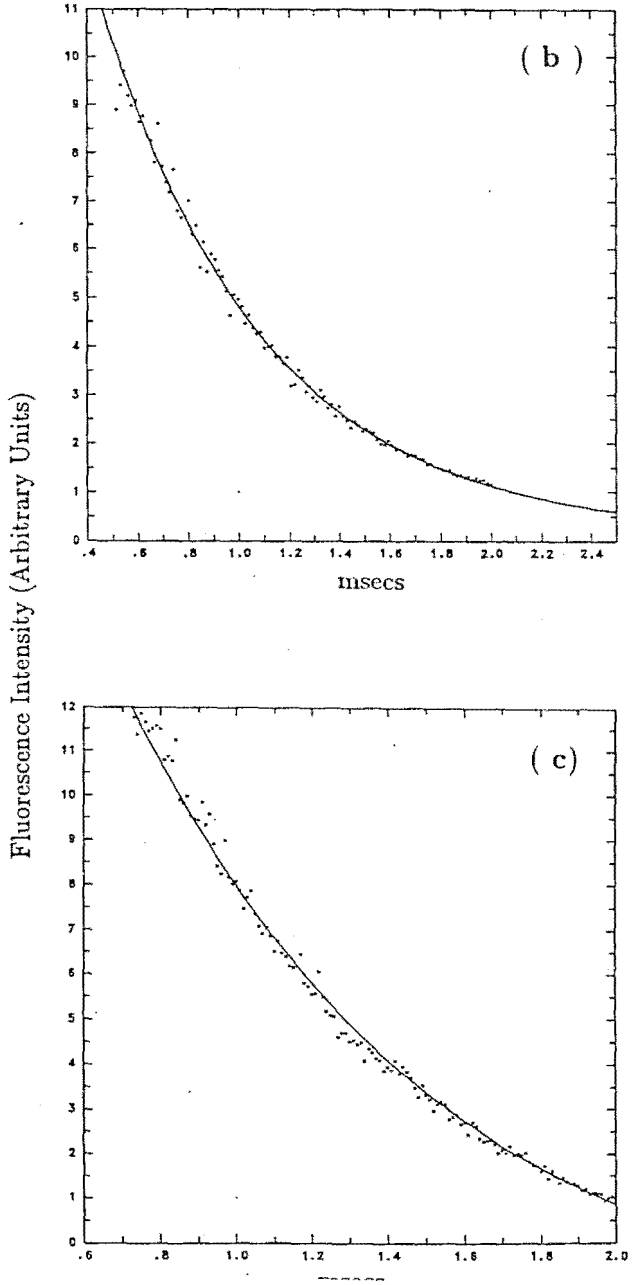

Figure 6.5 The ${}^1D_2 \rightarrow {}^3H_4$ fluorescent decay of the centers in the parent $CaF_2 : Pr^{3+}$ crystal with (**a**) 0.1% (**b**) 0.01% and (**c**) 0.001% dopant concentration of Pr^{3+}, measured at 11K. The solid lines overlayed on the data points are the fitted exponential curves.

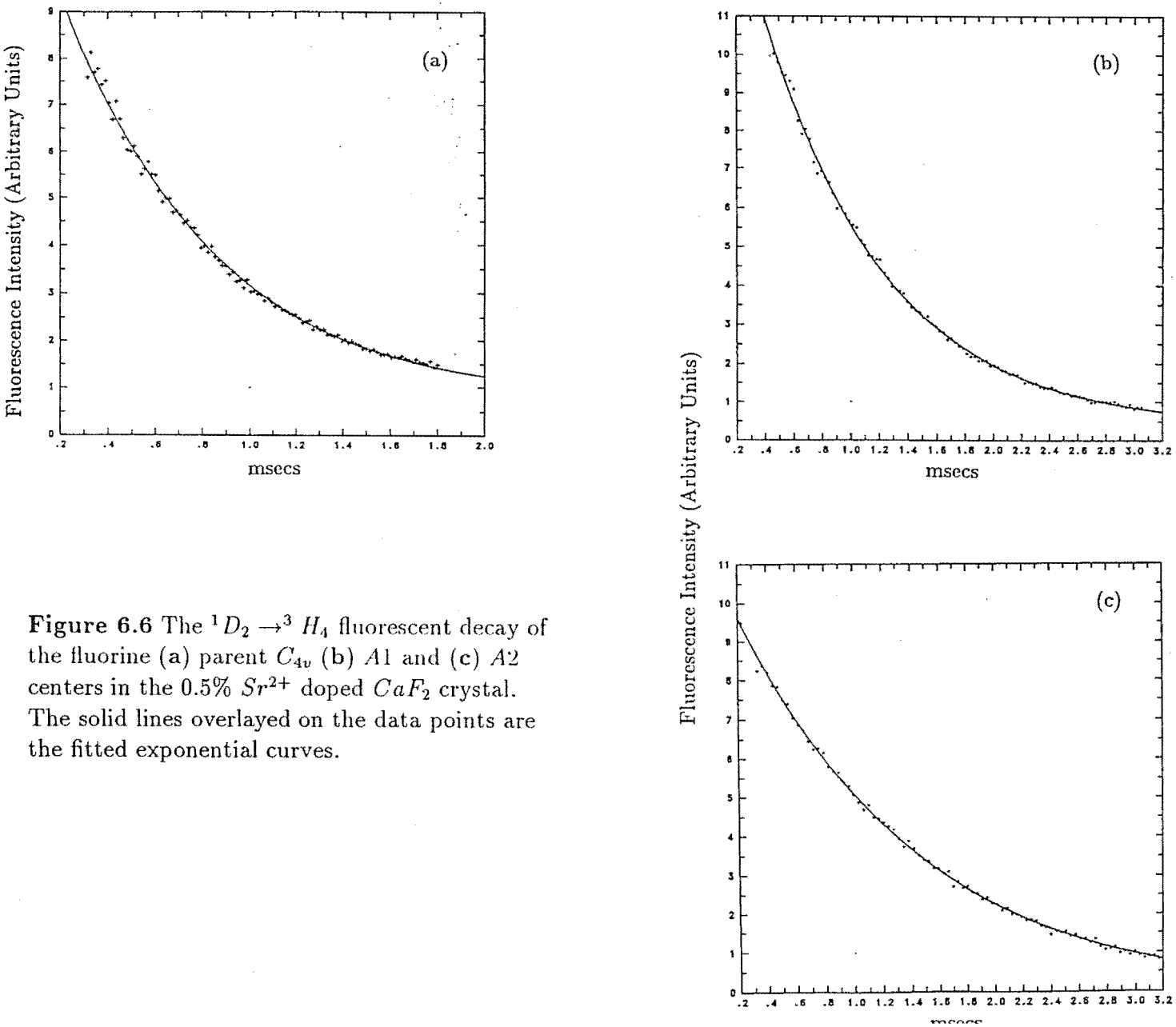

Figure 6.6 The ${}^1D_2 \rightarrow {}^3H_4$ fluorescent decay of the fluorine (a) parent C_{4v} (b) $A1$ and (c) $A2$ centers in the 0.5% Sr^{2+} doped CaF_2 crystal. The solid lines overlayed on the data points are the fitted exponential curves.

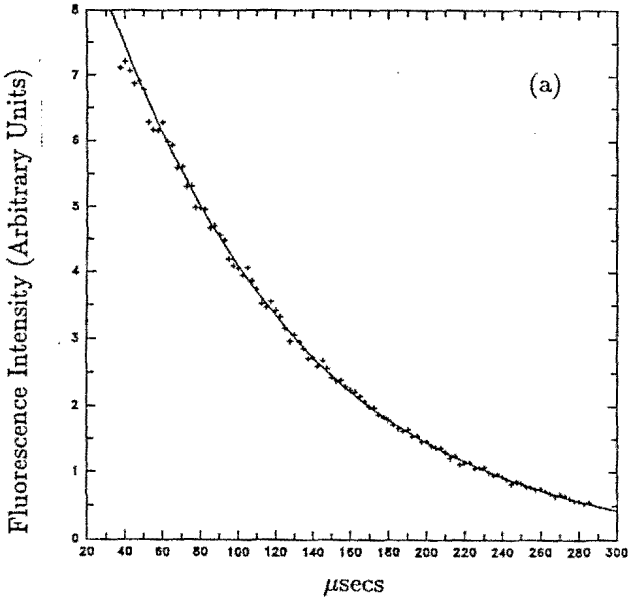

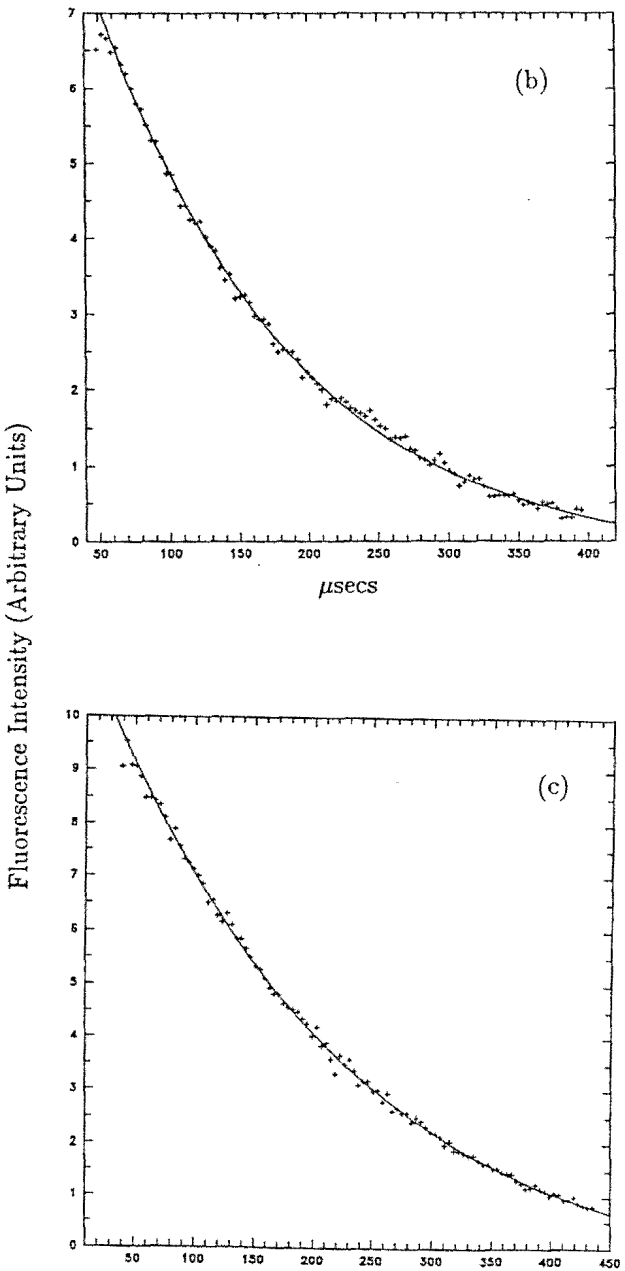

Figure 6.7 The ${}^1D_2 \rightarrow {}^3H_4$ fluorescent decay of the deuterium (a) parent C_{4v} (b) $A1$ and (c) $A2$ centers in the 0.5% Sr^{2+} doped CaF_2 crystal deuterated for 60hrs. The solid lines overlayed on the data points are the fitted exponential curves.

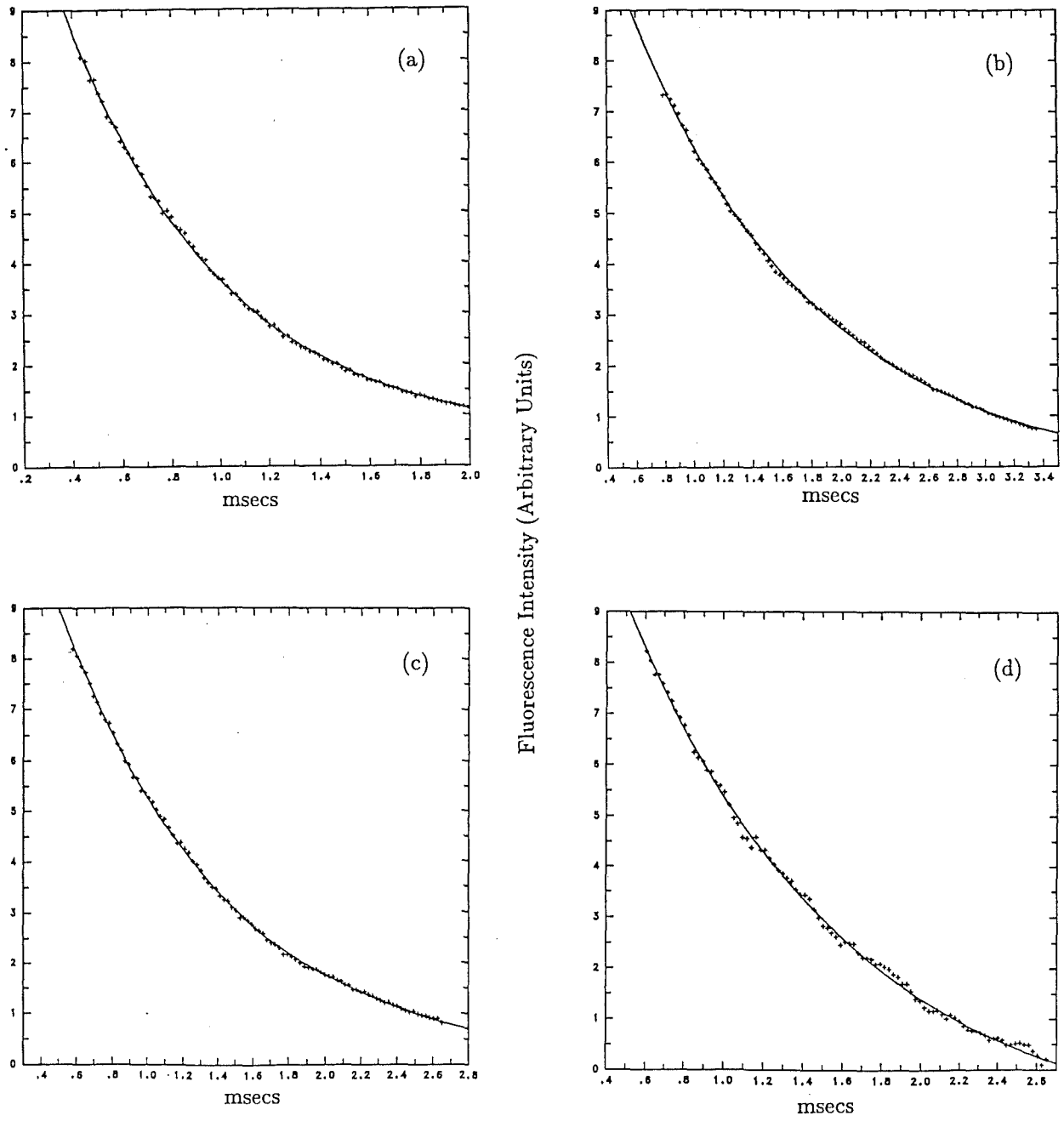

Figure 6.8 The $^1D_2 \rightarrow ^3 H_4$ fluorescent decay of the fluorine (**a**) parent C_{4v} (**b**) $A1(I)$ (**c**) $A1(II)$ and (**d**) $A2$ centers in the 0.5% Ba^{2+} doped CaF_2 crystal. The solid lines overlayed on the data points are the fitted exponential curves.

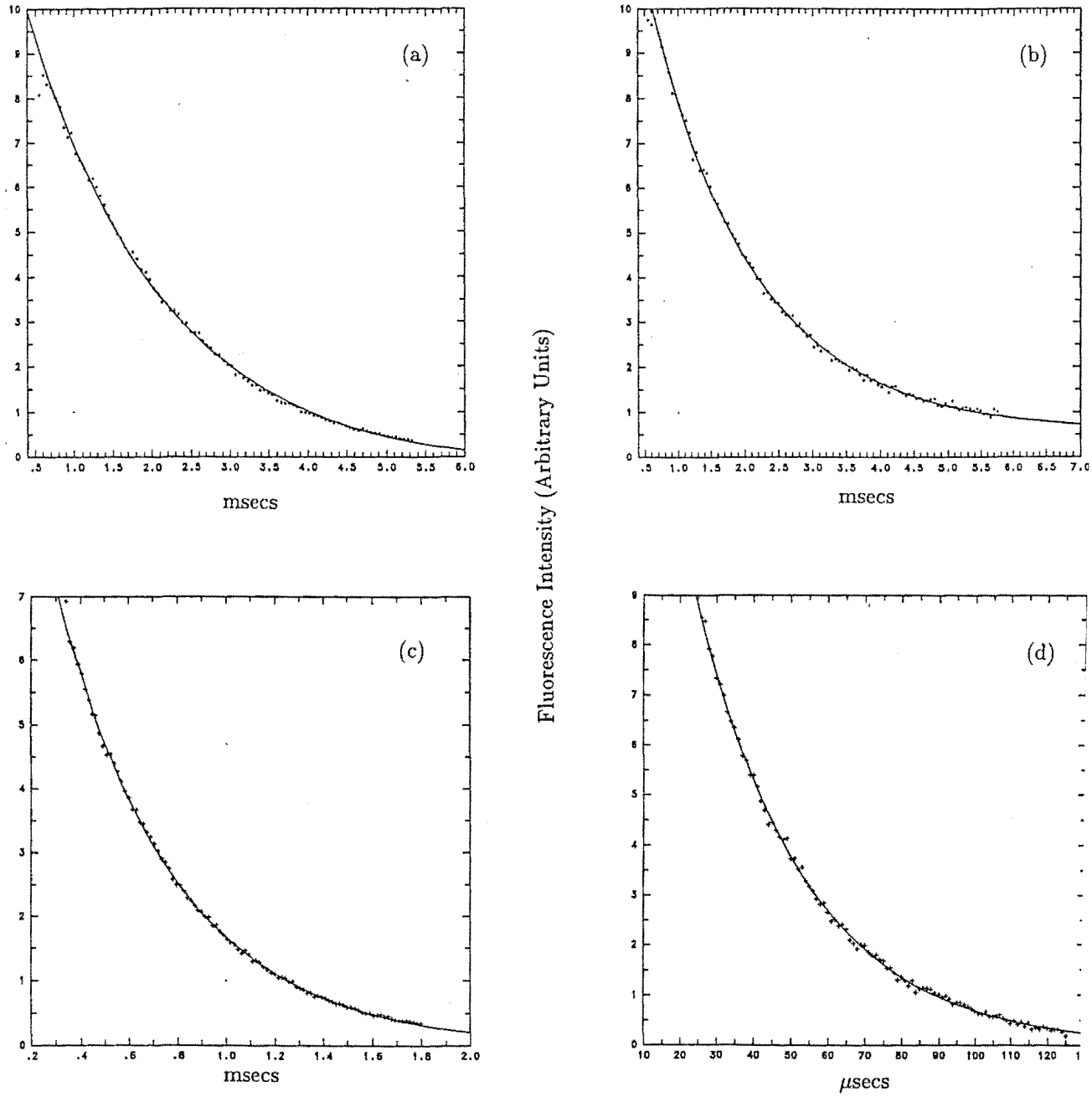

Figure 6.9 The ${}^1D_2 \rightarrow {}^3H_4$ fluorescent decay of the fluorine (**a**) parent C_{4v} (**b**) $A4$ and deuterium (**c**) C_{4v} (**d**) $A4$ center in the 0.5% Ba^{2+} doped SrF_2 crystal. The solid lines overlayed on the data points are the fitted exponential curves.

where $W_R(R)$ is the inverse of the lifetime, R the mean radial distance, or in this case the inverse cube root of the Pr^{3+} concentration, with a, c and β being constants determined from the fit. The result of the fit is shown in figure 6.10 and a β value of -2.7 ± 0.1 was obtained, in good agreement with the theoretical prediction of $\beta = -3$ by Dexter [1953] for a dipole-dipole coupling case.

Reeves [1987] comparing the upconversion transfer rate of the C_{4v} center in 0.5% and 0.05% Pr^{3+} doped SrF_2 crystals calculated a β value of -2.3. The transfer rate varies as $(R^{-3})^2$ for a dipole -dipole coupling mechanism and on the basis of his calculations, he concluded that this is the dominant mechanism of interaction for energy transfer between the C_{4v} centers. Lezama et al [1986] observed that the lifetime of the upconverted fluorescence from the $^3P_0$ level is 240μsecs while pumping the D_1 level and the lifetime of the direct fluorescence from the D_1 level is 480μsec in a 0.1% Pr^{3+} doped CaF_2 crystal. This situation is attributed to a small transfer rate due to weak long range interaction between the isolated C_{4v} centers. The result in this work is in agreement with the conclusions of Lezama et al [1986] and Reeves [1987]

6.2.2 Comparison of the mixed crystal center lifetimes

A detail comparative lifetime analysis of the centers would require extensive knowledge of the wavefunctions of the states involved in the transitions. These are not accurately known at present. However, the transition probabilities and hence the lifetimes are related to the square of the crystal field parameters $|B_q^k|^2$, thus allowing some general deductions about the crystal fields of the various centers to be made from the lifetime values measured without going into the specifics of the wavefunctions. The discussion in this section is not intended to be a substituted for a thorough crystal field analysis.

A pitfall in comparing the lifetimes of the various centers is to assume that they have similar population densities in a mixed crystal. This assumption is probably

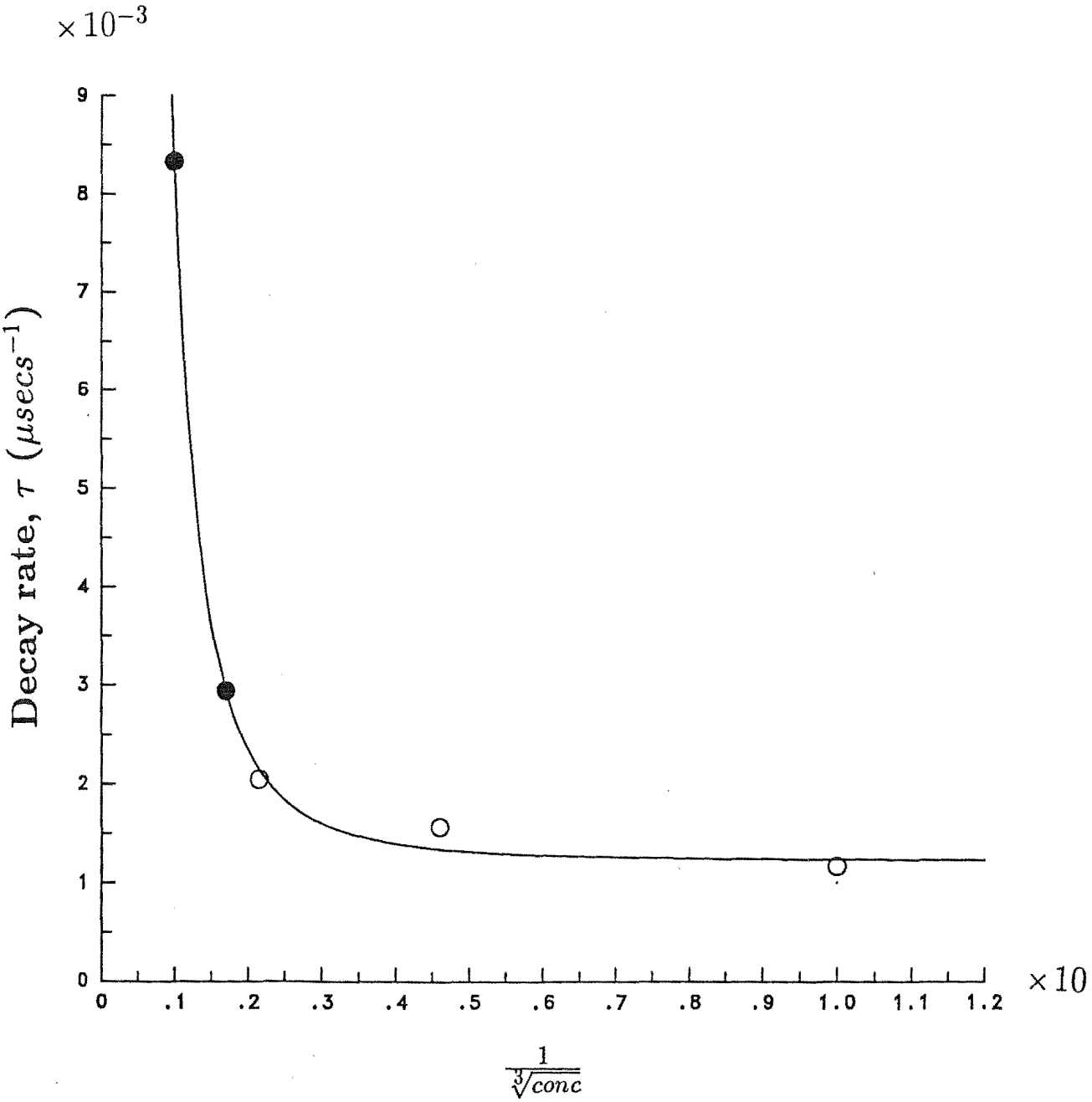

Figure 6.10 The plot of the decay rate τ versus the inverse cube root of the Pr^{3+} concentration. The open and blacken circles are the data points from this work and the work of Kliava et al [1978] respectively. The fit of the data points using $W_R(R) = aR^{\beta} + c$ (see text) produced the solid curve shown.

true for the mixed crystal centers with the same number of dopant cations. In a 0.01% Pr^{3+} crystal doped with 0.005% Sr^{2+}, there would be in the order of ten times as many parent C_{4v} centers as there are mixed crystal centers. Because of the concentration dependence of the lifetimes, a comparison between the lifetimes of the parent and mixed crystal centers in this crystal would not be valid for the purpose of getting a general idea of trends in the crystal field. Hence the lifetimes of the mixed crystal centers measured in this mixed crystal system should be compared with the lifetime of the parent C_{4v} center in a 0.001% Pr^{3+} crystal which is 857μsecs.

The lifetimes of the flourine $A1$ and $A2$ mixed crystal centers in the $Ca_{0.995}Sr_{0.005}F_2$: Pr^{3+} crystal are 841μsecs and 1275μsecs respectively. Recall that the $A2$ center has a C_{4v} symmetry with an on-axis cation substitution, which induces re-positioning of the interstitial F^- anion along the C_4 axis, while the proposed model for the $A1$ center suggests off-axis re-positioning of the same anion. It appears that the change in the axial field is significant going from a parent C_{4v} center to the $A2$ center, consistent with the 50% increase in the lifetime observed. This increase in lifetime of the $A2$ center corresponds to a lower transition probability and thus smaller crystal field parameters, hinting that the interstitial F^- ions have repositioned further away from the Pr^{3+} ions reducing the axial field they exert on the rare earth ion.

The lifetime of the $A1$ center is however not very different from that of the parent C_{4v} center. The transition probability for the $A1$ center would have the usual contribution from the cubic and axial crystal field terms with the addition of the transverse field terms from the B_2^k parameters where the B_2^2 term is expected to give the dominant contribution. The similarity of the $A1$ and parent C_{4v} center lifetimes suggests that the cubic and axial terms of the $A1$ center are probably not very different between these two centers and the contribution of the transverse field terms is not expected to be very significant. The latter contribution is consistent with the small splittings of the parent center γ_5 levels observed in the lower symmetry $A1$ center of $8cm^{-1}$.

The lifetime trend of the fluorine $A1$ and $A2$ centers is also present in the deuterium analogues of these centers. The $A2$ center lifetime is roughly 50% greater than that for the $A1$ center for both the F^- and D^- ion charge compensator centers.

This similar proportional difference is evidence that the corresponding fluorine and deuterium $A1$ and $A2$ centers are analogues.

One surprising result is that the lifetime of the $A2(F^-)$ center in the $Ca_{0.995}Ba_{0.005}F_2 : Pr^{3+}$ crystal is not very much different from the equivalent center in the Sr doped crystal, in spite of the Ba^{2+} ion having a larger ionic radius which is expected to give a greater change in the axial crystal field. It is likely that the F^- interstitials have reached the maximum axial distance away from the Pr^{3+} ion in the Sr^{2+} $A2$ center, with further movement being restricted by the repulsive forces of the four lattice fluorines between the interstial F^- and the alkaline earth dopant cation. This would give similar crystal field values and hence transition probability for $A2$ centers in both the Sr^{2+} and Ba^{2+} doped crystals.

The $A1(I)$ center has a greater lifetime than the $A1$ center of the Sr^{2+} doped crystal. The decreased transition probability of the $A1(I)$ center probably arose out of the decrease in the values of the cubic or axial terms, as the dominant transverse field term B_2^2 is likely to be larger for the $A1(I)$ center than the $A1$ center, judging from the ground state splittings of $15cm^{-1}$ and $8cm^{-1}$ for the $A1$ and $A1(I)$ centers respectively. If the splitting of the C_{4v} γ_5 ground state is assumed to come mainly from the B_2^2 term, then this term contributes $|B_2^2|^2$ of approximately four times more to the transition probability in the $A1(I)$ center than the $A1$ center.
There is about a 10% increased in the lifetime of the $A1(II)$ center compared to the $A1(I)$ center. Following the same line of argument as for the comparison of the $A1(I)$ and $A1$ centers, this increase of the $A1(II)$ center lifetime from that of the $A1(I)$ center probably represents further reduction in the values of the cubic and axial parameters in going from the $A1(I)$ to $A1(II)$ centers.

The $A4$ center of the Ba^{2+} doped SrF_2 crystal has unique polarisation ratios which suggests the lowest symmetry group for this center. This center also goes against the trend of increasing lifetimes for lower symmetry centers derived from the parent C_{4v} center. In the .001% Pr^{3+} doped crystal, the parent C_{4v} center has a lifetime of $1.99msec$ while that of the $A4$ center in the $Sr_{0.995}Ba_{0.005}F_2 : Pr^{3+}$ crystal is $1.56msec$, a decay time decrease of about 20%. A detail understanding of

the reason for this would come about when reliable crystal field parameters becomes available.

The lifetime of the $A4(D^-)$ center at 29.7μsec is about 6% that of the parent $C_{4v}(D^-)$ center at 484μsec. An increase in the values of the crystal field parameters or the effectiveness of the local modes to dissipate the excitation energy would account for the observed lifetime of the $A4(D^-)$ center.

The lifetimes of the other mixed crystal $A3$ centers in the Ca^{2+} doped SrF_2 and Sr^{2+} doped CaF_2 were not studied as the lower resolution and power of the pulsed dye laser made it impossible to do so. The lifetimes of the D^- mixed crystal centers in the Ba^{2+} doped CaF_2 crystal could not be obtained for the same reasons.

Table 6.1: Lifetimes of the various parent and mixed crystal centres.

		μsecs
CaF_2:Pr^{3+}(0.1)	$C_{4v}(F^-)$	489 ± 17
CaF_2:Pr^{3+}(0.01)	$C_{4v}(F^-)$	640 ± 27
CaF_2:Pr^{3+}(0.001)	$C_{4v}(F^-)$	857 ± 40
$Ca_{1-x}Sr_xF_2$:Pr^{3+}(0.01)	$C_{4v}(F^-)$	632 ± 23
	$A1(F^-)$	841 ± 27
	$A2(F^-)$	1275 ± 40
	$C_{4v}(D^-)$	104 ± 12
	$A1(D^-)$	137 ± 12
	$A2(D^-)$	210 ± 15
$Ca_{1-x}Ba_xF_2$:Pr^{3+}(0.01)	$C_{4v}(F^-)$	644 ± 15
	$A1(I)(F^-)$	944 ± 31
	$A1(II)(F^-)$	1119 ± 40
	$A2(F^-)$	1269 ± 50
$Sr_{1-x}Ba_xF_2$:Pr^{3+}(0.01)	$C_{4v}(F^-)$	1735 ± 40
	$A4(F^-)$	1556 ± 30
	$C_{4v}(D^-)$	484 ± 30
	$A4(D^-)$	29.7 ± 0.2

Chapter 7

Crystal Field Analysis of the C_{4v} centers in the CaF_2 and SrF_2 hosts.

7.1 Introduction

The prominent spectral features of the Pr^{3+} doped CaF_2 and SrF_2 crystals are those belonging to the C_{4v} center, hence it is not surprising that there are more crystal field levels established for this center than the other centers. Various crystal field fits have been attempted for the Pr^{3+} C_{4v} centers in these hosts but, to the knowledge of the author, a definitive set of crystal field parameters have yet to emerge from these efforts. The earliest crystal field fit peformed on the F^- tetragonal center in the $CaF_2 : Pr^{3+}$ crystal was by Hargreaves [1972], though gross mis-assignment of many of the levels casts serious doubts on the reliability of the fit. Another attempt was made by Reeves [1987] to fit the $C_{4v}(F^-)$ levels in the $SrF_2 : Pr^{3+}$ crystal. The standard deviation of the difference between the calculated and experimental values in that fit was $69cm^{-1}$ with the worst deviation of an individual level reaching $130cm^{-1}$.

Crystal field fits for the parent F^- and D^- C_{4v} centers and the $A2$ center in the Sr^{2+} doped $CaF_2 : Pr^{3+}$ crystal were attempted in this work. The results can still be considered only tentative, however the major problems preventing a fit with a convincing set of parameters are identified. These are summarized as follows:

1) The lack of rationale for unique assignments to components of the $^1I_6$ states which are required to define the free-ion two-body operator parametrized by α .
2) The need for further $^3P_2$ levels to be positively identified.
3) The need to establish the $^1S_0$ level to specify the free-ion two-body parameter γ associated with the $G(R_7)$ Casimir operator.
4) The larger standard deviation observed in the $^1D_2$ multiplet compared to the other multiplets.

The first problem mentioned above was encountered in the crystal field fit of $LaF_2 : Pr^{3+}$ by Carnall et al [1988]. Though four levels were assigned to the $^1I_6$ multiplet on the basis of the fluorescence from the $^1S_0 \rightarrow ^1 I_6$ transitions, these were not altogether unambigous. As it turned out, the value of the α parameter for the Pr^{3+} ion obtained from the fit using those four $^1I_6$ levels went against the systematic α value trend of the other rare earths (Fig.2, Carnall et al [1988]).

Considerable efforts were made in this work to unravel the C_{4v} levels of the upper $^3P_2$, $^3P_1$ and $^1I_6$ multiplets using the pulsed dye laser, to address point 1 and 2 above. With a lower power and a resolution of about $1.5cm^{-1}$, the pulsed dye laser system used was not ideal for acquiring the spectra of these systems. The wider beam divergence of the pulsed laser compared to the CW dye laser made polarisation measurements difficult. Due to these limitations, only the F^- C_{4v} centers were investigated and the broadband spectra of these are shown in figures 7.1, 7.2 and 7.3 for the CaF_2 $C_{4v}(F^-)$, SrF_2 $C_{4v}(F^-)$ and $Ca_{1-x}Sr_xF_2$ $A2(F^-)$ centers.

The principal contribution from the excitation using the pulsed dye laser is the positive identification of a γ_5 level belonging to the $^1I_6$ multiplet in the $SrF_2 : Pr^{3+}$ and $CaF_2 : Pr^{3+}$ crystals at $21612cm^{-1}(462.7nm)$ and $21615cm^{-1}(462.6nm)$

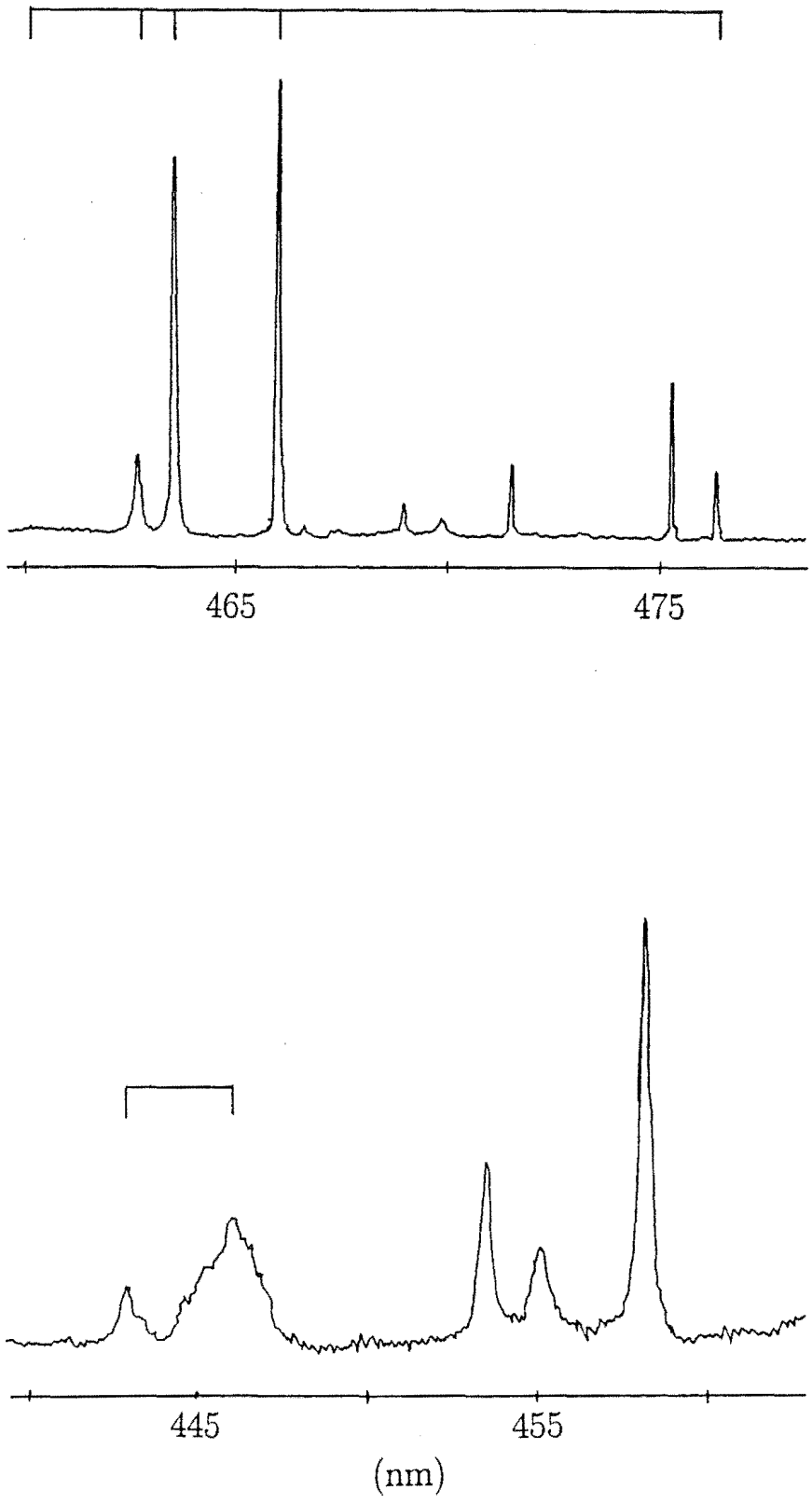

Figure 7.1 The broadband excitation of the $C_{4v}(F^-)$ center in the $CaF_2 : Pr^{3+}$ crystal at 11K using the pulsed dye laser. The transitions assigned to the C_{4v} center are indicated by the ticks at the top of the spectra.

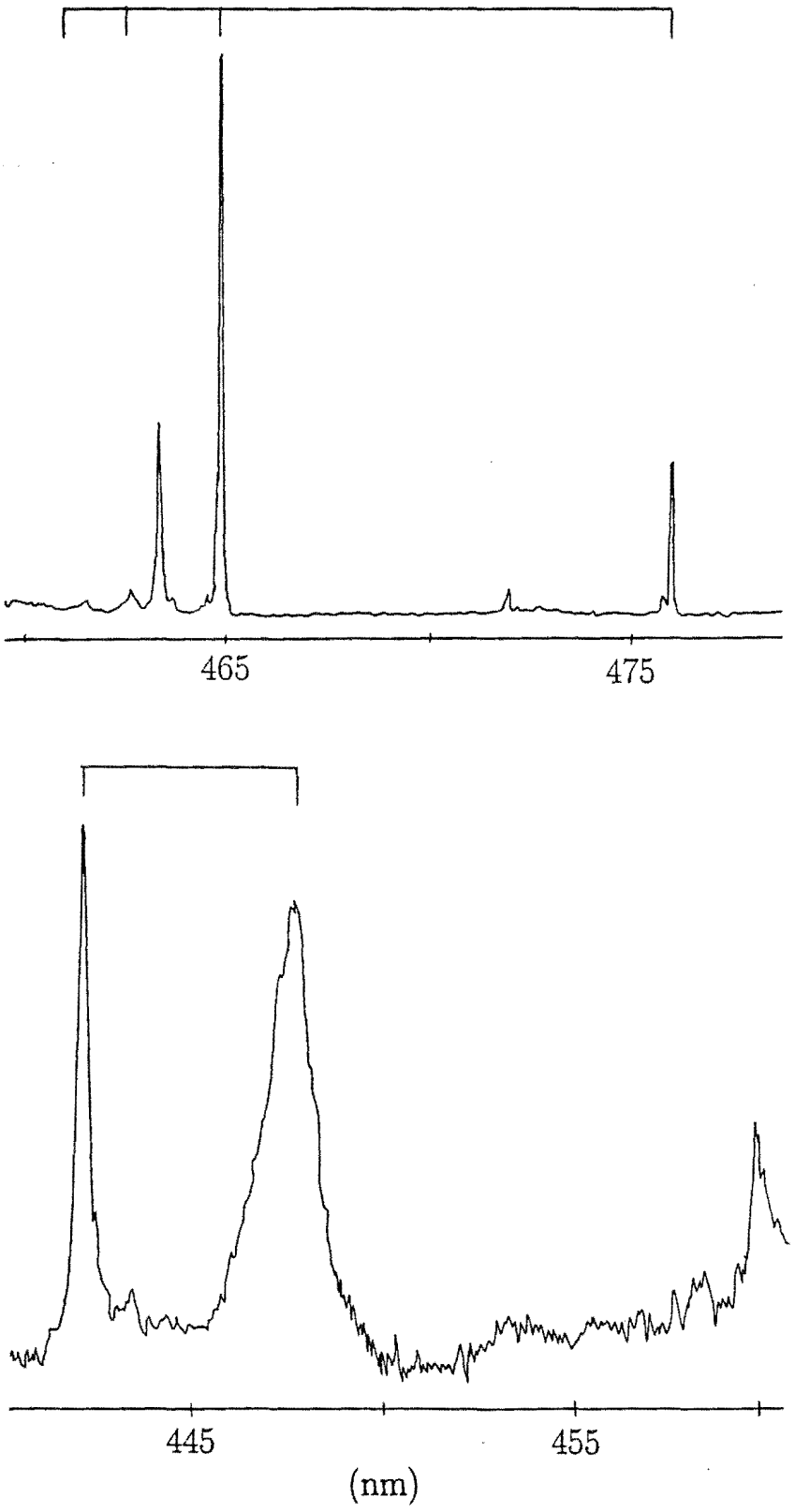

Figure 7.2 The broadband excitation of the $C_{4v}(F^-)$ center in the $SrF_2 : Pr^{3+}$ crystal at 11K using the pulsed dye laser. The transitions assigned to the C_{4v} center are indicated by the ticks at the top of the spectra.

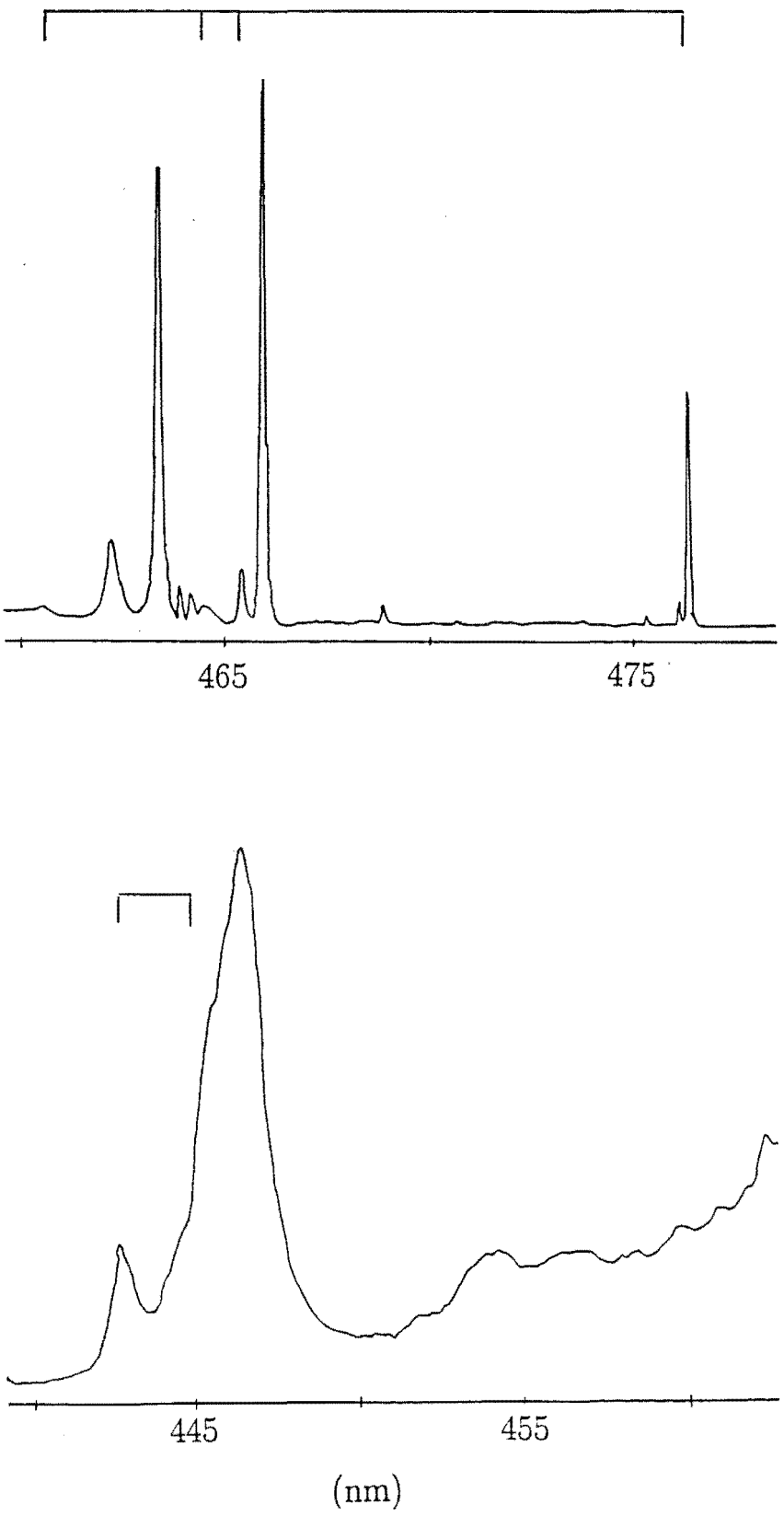

Figure 7.3 The broadband excitation of the $A2(F^-)$ center in the $Ca_{1-x}Sr_xF_2 : Pr^{3+}$ crystal using the pulsed dye laser. The transitions assigned to the C_{4v} center are indicated by the ticks at the top of the spectra.

respectively. Tentatively, two other levels, one in the $^1I_6$ and the other in the $^3P_2$ multiplet were also assigned for each of the three crystal systems studied. These are indicated in the tables 7.1, 7.2 and 7.5 by asterisks for the SrF_2 $C_{4v}(F^-)$, CaF_2 $C_{4v}(F^-)$ and $Ca_{1-x}Sr_xF_2$ $A2(F^-)$ centers. It was also found that the levels excited in the $^3P_1$, $^1I_6$ and $^3P_2$ multiplets do not radiatively emit directly from these excited levels but decay to the single $^3P_0$ level. This is unfortunate since the lowest level of the $^3P_1$ multiplet has a γ_5 irrep and if radiative transitions from this level to the levels of the other lower multiplets were stronger, it would have allowed many more levels to be assigned since the selection rules allow transitions from a γ_5 level to all other levels.

The $^1S_0$ levels of the C_{4v} centers will remain elusive with the present instrumentations. At an expected wavenumber of approximately $50{,}000cm^{-1}$ i.e at a wavelength of roughly 200nm, this level is out of the excitation range of the current laser sources and the detection range of the photmultiplier tubes used in this work.

The levels of the Pr^{3+} $^1D_2$ multiplet in the alkaline earth host crystals present some special difficulties in that a larger standard deviation was observed for this multiplet than for other multiplets. As was pointed out in chapter 2, this problem has also been encountered for the Pr^{3+} ion in other host crystals. A preliminary attempt was made towards resolving this anamoly by adding three extra SCCF [1] parameters which improved the fit considerably for the $^1D_2$ levels.

The program for fitting the C_{4v} centers in this work was the *F-shell Empirical* program developed by Dr. Mike Reid which uses the matrix elements constructed out of the Hamiltonian

$$\begin{aligned} H &= H_0 + \sum_{k=0,2,4,6} F^k(nf,nf)f_k + \zeta_f A_{SO} \\ &+ \alpha L(L+1) + \beta G(G_2) + \gamma G(G_7) \\ &+ \sum_{i=0,2,4} m_h M^h + \sum_{f=2,4,6} p_f P^f \\ &+ H_{C_{4v}} + H_{SCCF}, \end{aligned} \tag{7.1}$$

[1] Spin Correlated Crystal Field

where H_0 is the spherically symmetric one-electron part of the Hamiltonian. The F^k and ζ_f terms are the electrostatic and spin orbit parameters with f_k and A_{SO} representing the angular parts of the electrostatic and spin-orbit interactions. The two body correction terms are designated α, β and γ; $G(G_2)$ and $G(R_7)$ are the Casimir operators for the groups G_2 and R_7 and L is the total angular momentum. Magnetically correlated corrections are parametrised by the M^h (Marvin integrals) and P^f with the corresponding operators m_h and p_f, where the latter represents the two-body magnetic corrections.

The crystal field Hamiltonian, $H_{C_{4v}}$, for the tetragonal symmetry in the JM basis as converted from the point group basis (see table 2.1 or Han [1987]), used in the fit is

$$\begin{aligned} H_{C_{4v}} &= -B^2_{tet}C^2_0 \\ &+ B^4_{tet}\left[\sqrt{\frac{5}{12}}C^4_0 - \sqrt{\frac{7}{24}}(C^4_4 + C^4_{-4})\right] \\ &+ B^6_{tet}\left[\sqrt{\frac{7}{8}}C^6_0 + \frac{1}{4}(C^6_4 + C^6_{-4})\right] \\ &+ B^4_{cub}\left[\sqrt{\frac{7}{12}}C^4_0 + \sqrt{\frac{5}{24}}(C^4_4 + C^4_{-4})\right] \\ &+ B^6_{cub}\left[-\sqrt{\frac{1}{8}}C^6_0 + \sqrt{\frac{7}{4}}(C^6_4 + C^4_{-4})\right] \end{aligned} \tag{7.2}$$

A full parametrisation of the SCCF would require each crystal field parameter to have an associated SCCF parameter, effectively doubling the number of crystal field parameters which is unwarranted at present given the limited number of levels assigned. Hence only a partial parametrisation of the SCCF was attempted with

$$H_{SCCF} = b^k_0(\mathbf{S}\cdot\mathbf{s_i})C^k_0 \tag{7.3}$$

and k=2,4,6. The values of the SCCF parameters so obtained would not be particularly useful, however the aim of including the SCCF at present is not to arrive at

some definitive conclusion about the SCCF effects in the C_{4v} centers studied but to see if the inclusion of the SCCF does improve the fit for the problematic Pr^{3+} $^1D_2$ levels.

All the parameters in the fits performed were varied except for two exceptions. Firstly, the parameters associated with the free ion magnetically correlated correction terms are fixed to the values obtained from the fit of Nd^{3+} in LaF_3 [Reid, 1990]. This is to reduce the number of parameters and should not affect the final outcome significantly as the contributions of these terms are very small, in the order of a few cm^{-1}. These parameters are also constrained according to the relationships: $M^2 = 0.5M^0$, $M^4 = 0.38M^0$, $P^2 = 0.75P^0$, $P^4 = 0.5P^0$ and $M^0 + M^2 + M^4 = 1.75$ and $P^0 + P^2 + P^4 = 275$. Secondly, for the fit of the $A2$ center in the $Ca_{1-x}Sr_xF_2 : Pr^{3+}$ crystal, the α, β and γ parameters were fixed at 21.5, -600 and 2200 cm^{-1} respectively since insufficient experimental levels were available. These parameter values are approximately those obtained from the fit of the $C_{4v}(F^-)$ center in $CaF_2 : Pr^{3+}$.

The most controversial aspect of this section would be the reassignment of the second level of the $^3P_1$ multiplet to a level belonging to the $^1I_6$ multiplet of the C_{4v} centers. The two most intense absorption lines around the $465nm$ or $21500cm^{-1}$ region were previously assigned as the two levels in the $^3P_1$ mulitplet of the C_{4v} center on the basis of their absorption strength. This was reasonable as transitions from the ground state to the the levels of the $^1I_6$ multiplet, which overlap the levels of the $^3P_1$ multiplet, were expected to be weak, being spin forbidden in the first order. However, with this assignment, the *F-shell Empirical* program gave a very poor fit to the experimental levels. By reassigning the previously assigned second excited level of the $^3P_1$ multiplet to the $^1I_6$ multiplet [2], the fit improved considerably. Admittedly, the improvement of a fit alone is insufficient justification for this reassignment and how a $^1I_6$ level could have such a strong absorption intensity relative to that of a $^3P_1$ level is yet to be properly addressed. However, the mixing of states by the crystal field may account for stronger intensities in some levels of the $^1I_6$ multiplet relative to the $^3P_1$ multiplet and simulated intensities using the crystal field parameters obtained from the fit of the $CaF_2 : Nd^{3+}$ C_{4v} center, show that it is possible for

[2] marked with † in table 7.1 and 7.2

some absorption lines of the $^1I_6$ multiplet in the $CaF_2 : Pr^{3+}$ C_{4v} center to have comparable strengths to those of the $^3P_1$ multiplet [Reid, 1990].

7.2 Results and discussions

Apart from the few levels of multiplets above the $^3P_0$ multiplet discussed previously, the levels of the F^- and D^- C_{4v} centers in the CaF_2 and SrF_2 crystal hosts were obtained from the work of Reeves[1987]. The levels of the mixed crystal $A2$ center were assigned in this work.

The parameters from the attempted fits of the $C_{4v}(F^-)$ centers in the SrF_2 and CaF_2 hosts are presented in tables 7.1 and 7.2 respectively. The $^1D_2$ levels have some significant bearing on the overall standard deviation of the fits in these hosts with the overall standard deviation doubling when the three $^1D_2$ levels were included. A marked improvement to the fit of the $^1D_2$ levels was observed when the modified SCCF was applied. The trend of the results from the fits including the SCCF are similar to those observed for NdF_3, $Nd^{3+} : LaF_3$ and $Nd^{3+} : LiYF_4$ by Jayanaskar et al [1987] i.e the SCCF affects the values of sixth degree crystal field parameters most. In the case of the alkaline earth fluoride hosts studied here, the values of the sixth degree axial field terms are most dramatically altered by the SCCF while those of the cubic terms are less so. The reason for this is not apparent at this stage.

The tentative fits of the $C_{4v}(D^-)$ centers are listed in tables 7.3 and 7.4 for the SrF_2 and CaF_2 hosts respectively. When the SCCF was introduced, the SCCF sixth degree terms again dominate and the alteration of the cubic terms is more than those observed for the case of the $C_{4v}(F^-)$ centers. The standard deviations of the $^1D_2$ levels in both CaF_2 and SrF_2 improved remarkably when the SCCF was considered in the fit.

The values of the parameters from the fits of the F^- and D^- C_{4v} centers are comparable to those of the $CaF_2 : Nd^{3+}$ and $SrF_2 : Nd^{3+}$ C_{4v} centers [Han, 1988,

Table 7.5] both in terms of sign and magnitude which is encouranging for a tentative attempt.

Though only a limited number of experimental values are available for the mixed crystal $A2$ C_{4v} center in the $Ca_{1-x}Sr_xF_2 : Pr^{3+}$ host, a fit was performed and the second degree axial term was found to decrease by 15% from that of the parent $C_{4v}(F^-)$ center, consistent with the interstitial F^- moving away from the Pr^{3+} ion as originally proposed.

In conclusion, improvement to the crystal field fit of the C_{4v} centers in the $CaF_2 : Pr^{3+}$ and $SrF_2 : Pr^{3+}$ crystals would require positive identification of more levels in the upper multiplets particularly those of the $^1I_6$ and $^3P_2$ mulitplets. There appears to be a need to consider the SCCF if a 'proper' fit is to be achieved for the $^1D_2$ multiplet.

Table 7.1(a) Energy level parameters (in cm^{-1}) for the $C_{4v}(F^-)2$ center in $SrF_2 : Pr^{3+}$. $\sigma^d = \sum \left[\frac{(\delta_i)^2}{n-p}\right]^{1/2}$ where δ_i is the difference between the experimental and calculated energies, n is the number of levels fitted and p the number of parameters varied.

Parameters	Conventional fit excluding $^1D_2$ levels	Conventional fit including $^1D_2$ levels	Fit with SCCF
F^2	68741 ± 63	68226 ± 117	68232 ± 86
F^4	49205 ± 98	49236 ± 189	49725 ± 141
F^6	32807 ± 111	30956 ± 202	31147 ± 149
α	15 ± 4	21 ± 3	21 ± 3
β	-462 ± 21	-590 ± 23	-596 ± 18
γ	1992 ± 58	2183 ± 112	2186 ± 83
ζ	746 ± 3	745 ± 7	746 ± 5
B^4_{cub}	-2251 ± 18	-2215 ± 36	-2166 ± 39
B^6_{cub}	-1101 ± 15	-1095 ± 31	-986 ± 31
B^2_{tet}	-562 ± 14	-535 ± 25	-378 ± 32
B^4_{tet}	705 ± 21	840 ± 40	798 ± 44
B^6_{tet}	727 ± 24	794 ± 47	17 ± 68
b^2_0	NA	NA	-247 ± 38
b^4_0	NA	NA	-130 ± 52
b^6_0	NA	NA	-907 ± 78
σ^d	9	18	13
$\sigma(^1D_2)$	NA	27	9

Table 7.1 (b) Comparison of experimental and theoretically calculated levels for the $C_{4v}(F^-)$ center in $SrF_2 : Pr^{3+}$

	Conventional fit excluding $^1D_2$ levels			Conventional fit including $^1D_2$ levels			Fit with SCCF		
	Theory (T)	Expt. (E)	E - T	Theory (T)	Expt. (E)	E - T	Theory (T)	Expt. (E)	E - T
$^3H_4$	-4	0	4	-4	0	4	-5	0	5
	86	-	-	94	-	-	89	-	-
	234	-	-	239	-	-	236	-	-
	236	-	-	241	-	-	238	-	-
	456	461	5	436	461	25	451	461	10
	494	490	-4	497	490	-7	495	490	-5
	636	-	-	661	-	-	645	-	-
$^3H_5$	2181	-	-	2188	-	-	2182	-	-
	2214	2221	7	2228	2221	-7	2216	2221	5
	2292	2285	-7	2292	2292	0	2292	2285	-7
	2299	2292	-7	2298	2285	-13	2297	2292	-5
	2237	2334	-3	2334	2334	0	2336	2334	-2
	2567	-	-	2556	-	-	2556	-	-
	2614	-	-	2621	-	-	2616	-	-
	2691	-	-	2711	-	-	2694	-	-
$^3H_6$	4260	4250	-10	4270	4250	-20	4263	4250	-13
	4342	-	-	4341	-	-	4343	-	-
	4399	4405	6	4397	4405	8	4400	4405	5
	4461	4471	10	4452	4471	19	4460	4471	11
	4514	-	-	4515	-	-	4516	-	-
	4544	-	-	4552	-	-	4548	-	-
	4562	-	-	4567	-	-	4562	-	-
	4800	-	-	4801	-	-	4804	-	-
	4876	-	-	4884	-	-	4877	-	-
	4985	-	-	4993	-	-	4988	-	-
$^3F_2$	5266	5275	9	5262	5275	13	5259	5275	16
	5314	5308	-6	5312	5308	-4	5308	5308	0
	5329	-	-	5318	-	-	5322	-	-
	5379	-	-	5370	-	-	5369	-	-
$^3F_3$	6483	6484	1	6484	6484	0	6481	6484	3
	6557	6565	7	6560	6565	5	6563	6565	2
	6666	-	-	6670	-	-	6667	-	-
	6729	-	-	6726	-	-	6729	-	-
	6829	-	-8	6826	6821	-5	6833	6821	-12

	Theory (T)	Expt. (E)	E - T	Theory (T)	Expt. (E)	E - T	Theory (T)	Expt. (E)	E - T
$^3F_4$	7001	-	-	7000	-	-	7027	7024	-3
	7025	7024	-1	7021	7024	3	7028	-	-
	7036	-	-	7023	-	-	7067	-	-
	7204	-	-	7194	-	-	7232	-	-
	7232	-	-	7245	-	-	7271	7260	-11
	7267	7260	-7	7276	7260	-16	7305	-	-
	7314	-	-	7310	-	-	7320	-	-
$^1G_4$	9833	-	-	9816	-	-	9830	-	-
	9845	-	-	9828	-	-	9957	9963	6
	9960	9963	3	9958	9963	5	9986	-	-
	9982	-	-	9992	-	-	10121	-	-
	10225	-	-	10209	-	-	10290	-	-
	10346	-	-	10356	-	-	10363	-	-
	10843	-	-	10803	-	-	10842	-	-
$^1D_2$	17148	-	-	16847	16872	25	16863	16854	-9
	17232	-	-	16891	16854	-37	16875	16872	-3
	17460	-	-	17137	-	-	17142	-	-
	17752	-	-	17447	17459	11	17447	17459	11
$^3P_0$	20980	20980	0	20980	20980	0	20980	20980	0
$^3P_1$	21500	21504	4	21501	21504	-6	21508	21504	-4
	21689	21686	-3	21692	21686	-6	21696	21686	-10
$^1I_6$	21198	-	-	21245	-	-	21396	-	-
	21199	-	-	21247	-	-	21398	-	-
	21588	21578†	-10	21581	21578†	-4	21591	21578†	-13
	21610	21612	2	21604	21612	8	21600	21612	12
	21659	-	-	21657	-	-	21624	-	-
	21904	-	-	21911	-	-	21942	-	-
	22029	-	-	22019	-	-	22051	-	-
	22311	-	-	22327	-	-	22318	-	-
	22318	-	-	22332	-	-	22321	-	-
	22339	23347*	8	22351	23347*	-4	22345	23347*	2
$^3P_2$	22614	22613*	-1	22599	22613*	14	22597	22613*	16
	22780	-	-	22746	-	-	22754	-	-
	22805	-	-	22779	-	-	22782	-	-
	22995	-	-	22961	-	-	22916	-	-
$^1S_0$	46027	-	-	45185	-	-	45334	-	-

* - Levels tentatively assigned to the $^3P_2$ and $^1I_6$ multiplet.

† - previously assigned as the second excited level in the $^3P_1$ multiplet.

Table 7.2(a) Same table 7.1(a) except for $C_{4v}(F^-)$ center in $CaF_2 : Pr^{3+}$

Parameters	Conventional fit excluding $^1D_2$ levels	Conventional fit including $^1D_2$ levels	Fit with SCCF
F^2	68345 ± 75	67952 ± 151	68044 ± 77
F^4	48542 ± 118	48453 ± 245	49134 ± 126
F^6	31908 ± 133	30384 ± 261	30758 ± 133
α	17 ± 5	22 ± 4	22 ± 2
β	-508 ± 21	-616 ± 33	-635 ± 17
γ	2078 ± 70	2257 ± 146	2214 ± 74
ζ	745 ± 4	743 ± 10	745 ± 5
B^4_{cub}	-2435 ± 22	-2374 ± 47	-2327 ± 33
B^6_{cub}	-1385 ± 21	-1393 ± 45	-1227 ± 29
B^2_{tet}	-804 ± 15	-759 ± 30	-518 ± 30
B^4_{tet}	858 ± 22	1008 ± 46	936 ± 40
B^6_{tet}	949 ± 30	1022 ± 64	109 ± 55
b^2_0	NA	NA	-395 ± 37
b^4_0	NA	NA	-126 ± 52
b^6_0	NA	NA	-1088 ± 65
σ^d	11	23	12
$\sigma(^1D_2)$	NA	35	3

Table 7.2(b) Comparison of experimental and theoretically calculated levels for the $C_{4v}(F^-)$ center in $CaF_2 : Pr^{3+}$

	Conventional fit excluding $^1D_2$ levels			Conventional fit including $^1D_2$ levels			Fit with SCCF		
	Theory (T)	Expt. (E)	E - T	Theory (T)	Expt. (E)	E - T	Theory (T)	Expt. (E)	E - T
$^3H_4$	-1	0	1	12	0	-12	-1	0	1
	131	-	-	140	-	-	141	-	-
	203	-	-	211	-	-	203	-	-
	203	-	-	213	-	-	205	-	-
	533	534	1	506	534	27	528	534	5
	557	552	-5	555	552	-3	557	552	-5
	757	-	-	789	-	-	768	-	-
$^3H_5$	2182	2189	7	2181	2189	-2	2184	2189	5
	2210	2211	1	2225	2211	-14	2210	2211	1
	2277	2270	-7	2280	2270	-10	2276	2270	-6
	2335	-	-	2321	-	-	2336	-	-
	2394	2399	5	2391	2399	8	2396	2399	3
	2638	-	-	2615	-	-	2637	-	-
	2696	-	-	2701	-	-	2697	-	-
	2803	-	-	2823	-	-	2806	-	-
$^3H_6$	4212	4205	-7	4218	4205	-13	4213	4205	-8
	4304	-	-	4294	-	-	4307	-	-
	4449	-	-	4440	-	-	4452	-	-
	4471	-	-	4465	-	-	4472	-	-
	4509	4508	-1	4491	4508	17	4511	4508	-3
	4559	-	-	4544	-	-	4561	-	-
	4621	-	-	4646	-	-	4626	-	-
	4867	-	-	4861	-	-	4868	-	-
	4942	4954	12	4945	4954	9	4942	4954	12
	5076	-	-	5081	-	-	5078	-	-
$^3F_2$	5319	5332	13	5318	5332	13	5316	5332	16
	5406	5387	-19	5408	5387	-21	5403	5387	-16
	5437	-	-	5427	-	-	5435	-	-
	5485	-	-	5479	-	-	5479	-	-
$^3F_3$	6501	6500	-1	6501	6500	-1	6502	6500	-2
	6611	-	-	6611	-	-	6622	-	-
	6731	-	-	6737	-	-	6735	-	-
	6833	6835	1	6830	6835	5	6837	6835	-2
	6945	-	-	6945	-	-	6957	-	-

	Theory (T)	Expt. (E)	E - T	Theory (T)	Expt. (E)	E - T	Theory (T)	Expt. (E)	E - T
$^3F_4$	7034	-	-	7014	-	-	7021	-	-
	7040	-	-	7039	-	-	7063	7068	5
	7059	7068	9	7052	7068	15	7116	-	-
	7250	-	-	7234	-	-	7284	-	-
	7328	-	-	7337	-	-	7355	7350	-5
	7358	7350	-9	7362	-	-	7380	-	-
	7370	-	-	7367	7350	-17	7409	-	-
$^1G_4$	9762	-	-	9730	-	-	9755	-	-
	9822	-	-	9800	-	-	9956	-	-
	9942	-	-	9940	-	-	9978	-	-
	9964	-	-	9953	-	-	9977	-	-
	10216	-	-	10189	-	-	10083	-	-
	10375	-	-	10377	-	-	10287	-	-
	10950	-	-	10929	-	-	10378	-	-
$^1D_2$	17010	-	-	16788	16828	40	16830	16828	-2
	17160	-	-	16844	16889	-45	16847	16844	-3
	17326	-	-	17073	-	-	17088	-	-
	17712	-	-	17473	17479	5	17475	17479	4
$^3P_0$	20958	20958	0	20959	20958	-1	20958	20958	0
$^3P_1$	214521	21452	1	21461	21452	-9	21456	21452	-4
	21733	21733	0	21731	21733	2	21740	21733	-8
$^1I_6$	21004	-	-	21073	-	-	21297	-	-
	21005	-	-	21074	-	-	21298	-	-
	21583	21575†	-8	21576	21575†	-1	21583	21575†	-9
	21610	21615	5	21607	21615	8	21604	21615	10
	21682	-	-	21681	-	-	21641	-	-
	21862	-	-	21874	-	-	21934	-	-
	22009	-	-	21998	-	-	22053	-	-
	22393	-	-	22408*	-	-	22394	-	-
	22404	22408*	4	22416	22408*	-8	22403	-	-
	22408	-	-	22419	-	-	22409	22408	-1
$^3P_2$	22571	22571*	0	22562	22571*	9	22558	22571*	13
	22784	-	-	22753	-	-	22768	-	-
	22837	-	-	22809	-	-	22819	-	-
	23090	-	-	23059	-	-	22989	-	-
$^1S_0$	45500	-	-	44770	-	-	45084	-	-

* - Levels tentatively assigned to the $^3P_2$ and $^1I_6$ multiplet.

† - previously assigned as the second excited level in the $^3P_1$ multiplet.

Table 7.3(a) Same as table 7.1(a) except for $C_{4v}(D^-)$ center in $SrF_2 : Pr^{3+}$

Parameters	Conventional fit, no SCCF	Fit with SCCF
F^2	67757 ± 106	67501 ± 81
F^4	47794 ± 171	48537 ± 148
F^6	30010 ± 183	29867 ± 147
α	21 ± 3	21 ± 5
β	-594 ± 21	-592 ± 23
γ	2388 ± 102	2453 ± 78
ζ	746 ± 6	747 ± 4
B^4_{cub}	-2013 ± 34	-1843 ± 53
B^6_{cub}	-1214 ± 28	-940 ± 58
B^2_{tet}	-730 ± 21	-515 ± 57
B^4_{tet}	846 ± 32	1006 ± 47
B^6_{tet}	797 ± 40	-626 ± 135
b^2_0	NA	-314
b^4_0	NA	-379
b^6_0	NA	-1719
σ^d	15	11
$\sigma(^1D_2)$	16	0.4

Table 7.3(b) Comparison of experimental and theoretically calculated levels for the $C_{4v}(D^-)$ center in $SrF_2 : Pr^{3+}$

	Conventional fit,no SCCF			Fit with SCCF		
	Theory (T)	Expt. (E)	E - T	Theory (T)	Expt. (E)	E - T
$^3H_4$	5	0	-5	-3	0	3
	112	-	-	109	-	-
	156	-	-	161.9	-	-
	157	-	-	162.2	-	-
	459	467	8	470	467	-3
	491	499	8	498	499	1
	679	-	-	674	-	-
$^3H_5$	2177	2175	-2	2171	2175	4
	2199	2199	0	2194	2199	5
	2241	2236	-5	2241	2236	-5
	2302	2305	3	2307	2305	-2
	2353	2339	-14	2348	2339	-9
	2569	-	-	2581	-	-
	2635	-	-	2634	-	-
	2727	-	-	2714	-	-
$^3H_6$	4230	4218	-12	4231	4218	-13
	4291	-	-	4296	-	-
	4431	-	-	4429	4441	12
	4436	4441	4	4433	-	-
	4483	4480	-3	4483	4480	-3
	4527	-	-	4532	-	-
	4586	-	-	4568	-	-
	4806	4831	24	4819	4831	12
	4891	-	-	4890	-	-
	5016	-	-	5012	-	-
$^3F_2$	5228	5246	18	5227	5246	19
	5310	5290	-20	5303	5290	-13
	5338	-	-	5334	-	-
	5383	5380	-3	5380	5380	0
$^3F_3$	6459	6461	2	6457	6461	4
	6559	6556	-3	6566	6556	-10
	6650	-	-	6647	-	-
	6741	6740	-1	6741	6740	-1
	6824	-	-	6833	-	-

	Theory (T)	Expt. (E)	E - T	Theory (T)	Expt. (E)	E - T
$^3F_4$	6953	6938	-15	6938	6938	0
	6965	-	-	6994	6999	5
	6981	6999	18	7096	-	-
	7152	-	-	7214	-	-
	7212	-	-	7250	7245	-5
	7246	7245	-1	7294	-	-
	7269	-	-	7350	-	-
$^1G_4$	9711	-	-	9708	-	-
	9800	-	-	9920	-	-
	9898	-	-	10092	-	-
	9915	-	-	10175	-	-
	10121	-	-	10246	-	-
	10270	-	-	10303	-	-
	10761	-	-	10771	-	-
$^1D_2$	16799	16815	16	16797	-	-
	16923	-	-	16816	16815	-1
	17054	-	-	16985	-	-
	17428	17412	-16	17411	17412	1
$^3P_0$	20877	20877	0	20877	20877	0
$^3P_1$	21392	21393	1	21393	21393	0
	21649	-	-	21654	-	-
$^1I_6$	21032.6	-	-	21258.9	-	-
	21032.8	-	-	21259.3	-	-
	21540	21541	1	21541	21541	0
	21557	-	-	21514	-	-
	21614	-	-	21528	-	-
	21744	-	-	21719	-	-
	21867	-	-	21841	-	-
	22240	-	-	22191	-	-
	22245	-	-	22221	-	-
	22273	-	-	22246	-	-
$^3P_2$	22500	-	-	22504	-	-
	22669	-	-	22667	-	-
	22745	-	-	22748	-	-
	22930	-	-	22852	-	-
$^1S_0$	44282	-	-	44248	-	-

Table 7.4(a) Same as table 7.1(a) except for $C_{4v}(D^-)$ center in $CaF_2 : Pr^{3+}$

Parameters	Conventional fit, no SCCF	Fit with SCCF
F^2	67026 ± 236	66978 ± 87
F^4	47839 ± 385	47980 ± 140
F^6	29612 ± 412	29246 ± 149
α	19 ± 7	21 ± 3
β	-569 ± 52	-591 ± 20
γ	2409 ± 228	2659 ± 82
ζ	747 ± 13	745 ± 5
B^4_{cub}	-2136 ± 82	-2110 ± 49
B^6_{cub}	-1412 ± 69	-916 ± 33
B^2_{tet}	-930 ± 48	-520 ± 35
B^4_{tet}	1209 ± 65	898 ± 41
B^6_{tet}	1221 ± 92	-779 ± 57
b^2_0	NA	-672 ± 41
b^4_0	NA	440 ± 58
b^6_0	NA	-3049 ± 69
σ^d	35	13
$\sigma(^1D_2)$	37	13

Table 7.4(b) Comparison of experimental and theoretically calculated levels for the $C_{4v}(D^-)$ center in $CaF_2 : Pr^{3+}$

	Conventional fit,no SCCF			Fit with SCCF		
	Theory (T)	Expt. (E)	E - T	Theory (T)	Expt. (E)	E - T
$^3H_4$	0	0	0	4	0	-4
	128	-	-	130	-	-
	129	-	-	130	-	-
	169	-	-	282	-	-
	478	463	-15	460	463	3
	544	559	15	553	559	6
	823	-	-	878	-	-
$^3H_5$	2169	2164	-6	2163	2164	1
	2203	2183	-20	2187	2183	-4
	2213	2206	-7	2206	2206	-0
	2323	-	-	2367	-	-
	2405	2425	20	2439	2425	-14
	2606	-	-	2605	-	-
	2715	2723	8	2717	2723	6
	2863	-	-	2895	-	-
$^3H_6$	4192	4163	-29	4160	4163	3
	4273	-	-	4313	-	-
	4396	-	-	4406	-	-
	4460	4476	16	4478	4476	-2
	4508	4528	20	4523	-	-
	4509	-	-	4538	4528	-10
	4697	-	-	4731	-	-
	4870	4869	-1	4851	4869	18
	4965	4967	2	4967	4967	-0
	5102	-	-	5077	-	-
$^3F_2$	5282	5293	11	5278	5293	15
	5386	5357	-29	5368	5357	-11
	5423	5448	25	5447	5448	1
	5479	-	-	5494	-	-
$^3F_3$	6477	6473	-4	6474	6473	-1
	6618	-	-	6642	-	-
	6715	6719	4	6718	6719	1
	6832	6820	-12	6832	6820	-12
	6910	-	-	6895	-	-

	Theory (T)	Expt. (E)	E - T	Theory (T)	Expt. (E)	E - T
$^3F_4$	6981	6947	-34	6965	6947	-18
	7027	-	-	7033	7040	7
	7038	7040	1	7177	-	-
	7218	7307	89	7290	7307	17
	7345	-	-	7345	7343	-2
	7373	-	-	7351	-	-
	7399	7343	-56	7534	-	-
$^1G_4$	9723	-	-	9761	-	-
	9812	-	-	9954	-	-
	9964	-	-	10142	-	-
	9992	-	-	10252	-	-
	10175	-	-	10330	-	-
	10428	-	-	10374	-	-
	10924	-	-	10856	-	-
$^1D_2$	16709	16755	46	16757	16755	-2
	16841	16794	-47	16778	16794	16
	16934	-	-	17019	-	-
	17412	17413	1	17428	17413	-15
$^3P_0$	20816	20815	-1	20815	20815	-0
$^3P_1$	21305	21301	-4	21304	21301	-3
	21648	-	-	21676	-	-
$^1I_6$	20796	-	-	21204	-	-
	20797	-	-	21205	-	-
	21417	-	-	21492	-	-
	21420	-	-	21501	21501	-0
	21501	21501	-0	21526	-	-
	21612	-	-	21736	-	-
	21714	-	-	21887	-	-
	22227	-	-	22217	-	-
	22242	-	-	22242	-	-
	22276	-	-	22255	-	-
$^3P_2$	22448	22453	5	22449	22453	4
	22629	-	-	22645	-	-
	22740	-	-	22768	-	-
	22986	-	-	22869	-	-
$^1S_0$	44006	-	-	43642	-	-

Table 7.5(a) Same as table 7.1(a) except for $A2$ center in $Ca_{1-x}Sr_xF_2 : Pr^{3+}$

Parameters	Conventional fit, no SCCF	Fit with SCCF
F^2	68090 ± 37	68344 ± 87
F^4	48990 ± 94	49719 ± 140
F^6	30752 ± 67	31539 ± 149
α	[21.5]	[21.5]
β	[−600]	[−600]
γ	[2200]	[2200]
ζ	[746]	[746]
B^4_{cub}	-2538 ± 51	-3093 ± 29
B^6_{cub}	-1422 ± 42	-1273 ± 33
B^2_{tet}	-644 ± 33	-213 ± 31
B^4_{tet}	1086 ± 48	468 ± 38
B^6_{tet}	986 ± 63	649 ± 72
b^2_0	NA	-663 ± 38
b^4_0	NA	870 ± 47
b^6_0	NA	-416 ± 82
σ^d	22	13
$\sigma(^1D_2)$	18	0.1

Table 7.5(b) Comparison of experimental and theoretically calculated levels for the $A2$ center in $Ca_{1-x}Sr_xF_2 : Pr^{3+}$

	Conventional fit,no SCCF			Fit with SCCF		
	Theory (T)	Expt. (E)	E - T	Theory (T)	Expt. (E)	E - T
$^3H_4$	-2	0	2	-6	0	6
	98	-	-	118	-	-
	237	-	-	237	-	-
	240	-	-	240	-	-
	479	509	30	502	509	7
	544	532	-12	555	532	-23
	785	-	-	762	-	-
$^3H_5$	2197	-	-	2187	-	-
	2240	2225	-15	2228	2225	-3
	2292	-	-	2298	2301	4
	2299	2301	2	2318	-	-
	2372	2371	-1	2373	2371	-2
	2596	-	-	2614	-	-
	2698	-	-	2690	-	-
	2817	-	-	2803	-	-
$^3H_6$	4236	4223	-13	4234	4223	-11
	4284	-	-	4319	-	-
	4415	-	-	4422	-	-
	4462	4484	22	4481	4484	3
	4495	-	-	4498	-	-
	4549	-	-	4553	-	-
	4684	-	-	4626	-	-
	4866	4873	7	4863	4873	10
	4944	4958	14	4940	4958	18
	5084	-	-	5071	-	-
$^3F_2$	5337	5332	-5	5325	5332	7
	5422	-	-	5401	5387	-14
	5423	5387	-34	5412	-	-
	5475	-	-	5462	-	-
$^3F_3$	6509	-	-	6503	-	-
	6605	-	-	6607	-	-
	6756	-	-	6740	-	-
	6831	-	-	6819	-	-
	6969	-	-	6946	-	-

	Theory (T)	Expt. (E)	E - T	Theory (T)	Expt. (E)	E - T
$^3F_4$	7036	-	-	7074	-	-
	7071	-	-	7080	-	-
	7076	-	-	7119	-	-
	7255	-	-	7323	-	-
	7365	-	-	7369	-	-
	7389	-	-	7372	-	-
	7392	-	-	7418	-	-
$^1G_4$	9748	-	-	9869	-	-
	9823	-	-	9902	-	-
	9968	-	-	9961	-	-
	9987	-	-	10031	-	-
	10235	-	-	10387	-	-
	10428	-	-	10453	-	-
	11002	-	-	11088	-	-
$^1D_2$	16807	16830	23	16830	16830	0
	16846	16839	-7	16839	16839	0
	17093	-	-	17314	-	-
	17478	17460	-18	17460	17460	0
$^3P_0$	20976	20968	-8	20969	20968	1
$^3P_1$	21492	21485	-7	21477	21485	7
	21718	21713	-5	21720	21713	-7
$^1I_6$	21184	-	-	21418	-	-
	21185	-	-	21422	-	-
	21560	21539	-21	21540	21539	-1
	21601	-	-	21555	-	-
	21677	-	-	21584	-	-
	21955	-	-	22206	-	-
	22066	-	-	22346	-	-
	22446	-	-	22395	-	-
	22456	22476*	20	22474	22476 *	2
	22481	-	-	22619	22618*	-1
$^3P_2$	22588	22618*	29	22568	-	-
	22779	-	-	22796	-	-
	22794	-	-	22816	-	-
	23067	-	-	23020	-	-
$^1S_0$	45079	-	-	45513	-	-

* - Levels tentatively assigned to the $^3P_2$ and $^1I_6$ multiplet.

Chapter 8

Spectroscopy of Bleaching Centers

In the study of deuterated and hydrogenated samples of RE ions doped in alkaline earth flouride hosts, it was discovered that some centers are unstable under optical excitation (Cockroft[1987] , Reeves et al [1989] , Han[1988]). These are referred to as *bleaching centers.* With a laser frequency tuned to a transition belonging to a bleaching center, it was found that the emission intensity from that transition decreases over time. After bleaching some of these centers, new transitions could be observed in the broadband excitation corresponding to the formation of new centers distinct from the center being bleached. There are also bleaching centers that exhibit *reversible bleaching* i.e by merely switching the laser polarisation by 90° the partial or complete restoration of the emission intensity was observed.

These bleaching phenomena are understood to be the result of the excited hydrogenic ions gaining sufficient energy to overcome the potential barriers they are in to migrate to another lattice or interstitial site. A *photoproduct* is created if the new center formed as a result of the hydrogenic ions migrating is inequivalent to the original center. No photoproduct would be produced if the ions present migrate to give different orientations of the same center and in such circumstances, reversible

bleaching with complete recovery of the bleached emission intensity would be observed.

The low symmetry bleaching deuterium centers of Pr^{3+} in alkaline earth fluorides have been characterised by Reeves[1987]. Four of these centers giving the strongest transitions were studied and given the labels $C_s(1)$, $C_s(2)$, $C_s(3)$ and $C_s(4)$. A fifth bleaching center was studied in this work and is labelled the $C_s(5)$ center. Additionally, new polarisation results for these centers will be presented and compared with models previously assigned to them. The rest of this chapter then discusses the bleaching behaviour of the weak satellite structures found in the mixed crystal systems $Ca_{1-x}Sr_xF_2 : Pr^{3+}$ and $Sr_{1-x}Ca_xF_2 : Pr^{3+}$.

8.1 LSE of the parent bleaching centers

8.1.1 Excitation

In order to choose a suitable line to monitor, the emission spectrum of a center was first measured. The center was allowed to bleach for a few minutes beforehand so that the rate of decrease in emission was appreciably reduced while the emission spectrum was being acquired. While this procedure greatly sacrificed signal intensity , the strongest line for monitoring could be chosen more accurately as some transitions could lose up to 90% of their intensity over the few minutes they were being bleached. Typically, there was an emission intensity drop of less than 5% as measured on the Baucsh and Lomb 1/4 metre monochromator, while an emission spectrum was recorded.

Figures 8.1 and 8.2 present the selective excitation spectra of the $C_s(i)$ centers in deuterated CaF_2 and SrF_2 respectively, monitoring specific transitions between the $^1D_2 \rightarrow ^3 H_5$ multiplet on the SPEX1403. It was not possible to obtain the excitation of the $C_s(5)$ center in SrF_2 as the fluorescence of its transitions to the $^3H_5$ multiplet

was buried by the much stronger fluorescence of the Sm^{2+} $(^5D_0)^1\Gamma_{1g} \rightarrow (^7F_1)^3\Gamma_{4g}$ transition at $14353cm^{-1}$ [Wood et al, 1962] and the broad background from 12500 to $14500cm^{-1}$ produced by the same ion.

The $^3H_5$ multiplet was chosen as the terminating multiplet as the others were found to be less favourable. While the $^3H_4$ multiplet could be used and would give stronger signals, the transitions to this multiplet are broad making it impossible to monitor a level that would satisfactorily discriminate one center against another. Emission to the $^3H_6$ and $^3F_2$ multiplets was substantially weaker and it was therefore less useful monitoring transition to these multiplets to get the LSE spectra.

The excitation spectra of the $C_s(2)$, $C_s(3)$,$C_s(5)$ centers in CaF_2 revealed some broad transition structures at $16736cm^{-1}$, $16697cm^{-1}$ and $16682cm^{-1}$ respectively (fig 8.1(c),(d),(f)). These are assigned as the second excited state of the $^1D_2$ multiplet of the three centers. An increased in the line broadening of the transitions to the D_2 level from roughly $1cm^{-1}$ observed in the fluorine and deuterium C_{4v} centers to $15cm^{-1}$ in the bleaching centers was apparent. The homogenous broadening by spontaneous phonon emission of the upper levels within a multiplet is expected to be larger [MacFarlane and Shelby, 1987] and this was observed to be the case for centers studied in the CaF_2 host. The substitution of the lattice F^- by D^- anions produce a greater change in crystal field experienced by the Pr^{3+} ion which is reflected in the increased seperation of the D_1 and D_2 levels from 17 and $40cm^{-1}$ for the C_{4v} F^- and D^- centers respectively to approximately $200cm^{-1}$ for the bleaching centers.

8.1.2 Polarised Emission

Through polarised emission measurements, some insight into the symmetry of these bleaching centers may be gained. The motivation behind these measurements is to compare the symmetries deduced from the polarised emission with those previously assigned to the $C_s(1)$, $C_s(2)$, $C_s(3)$ and $C_s(4)$ centers by Reeves[1987].

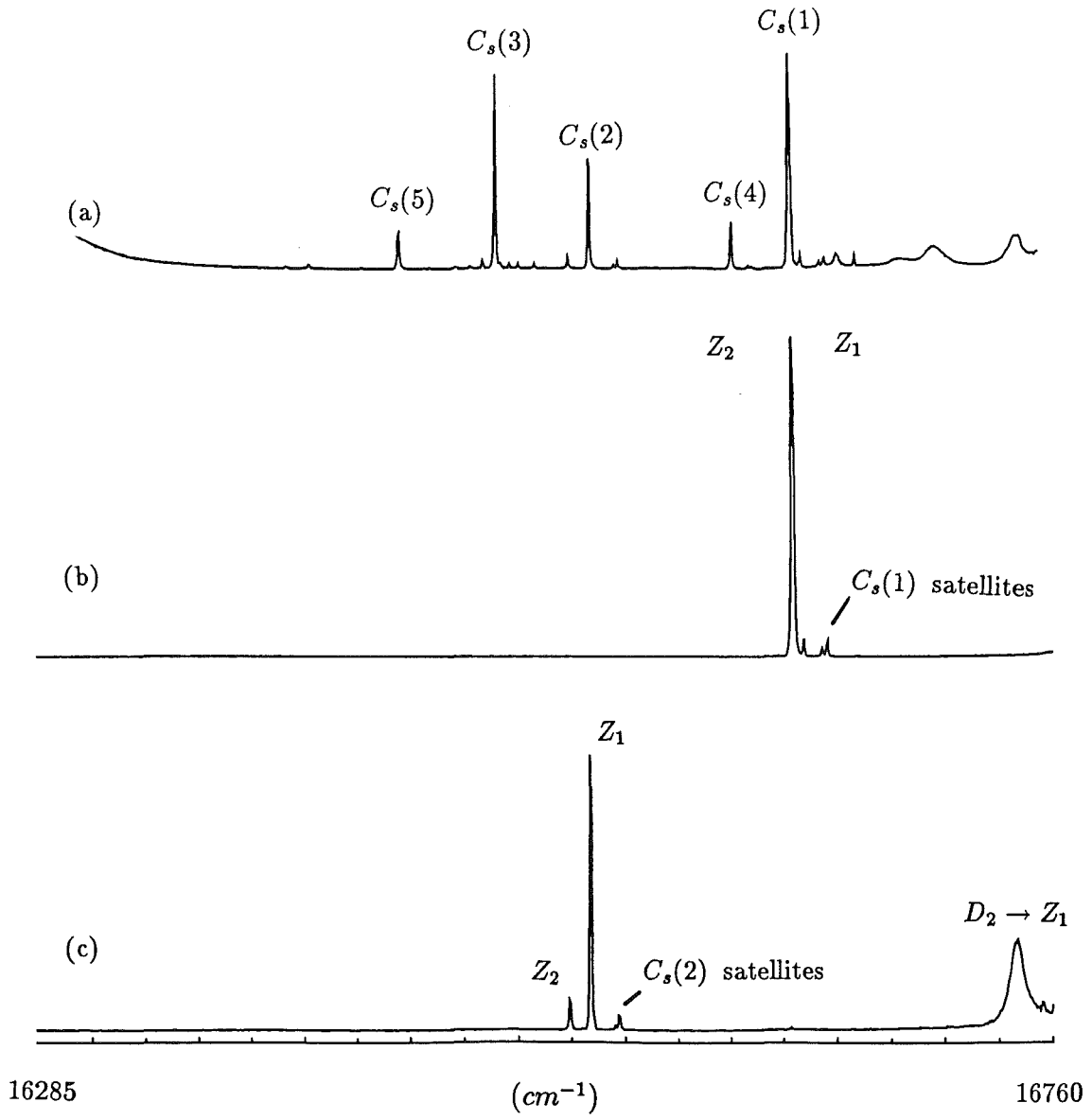

Figure 8.1 Excitation spectra of bleaching centers in deuterated CaF_2 at 11K.

(a) Broadband excitation. (b),(c),(d),(e)and (f) Selective excitation of the $C_s(1)$, $C_s(2)$, $C_s(3)$, $C_s(4)$ and $C_s(5)$ centers monitoring $14473cm^{-1}$, $14381cm^{-1}$, $14342cm^{-1}$, $14442cm^{-1}$ and $14324cm^{-1}$ respectively.

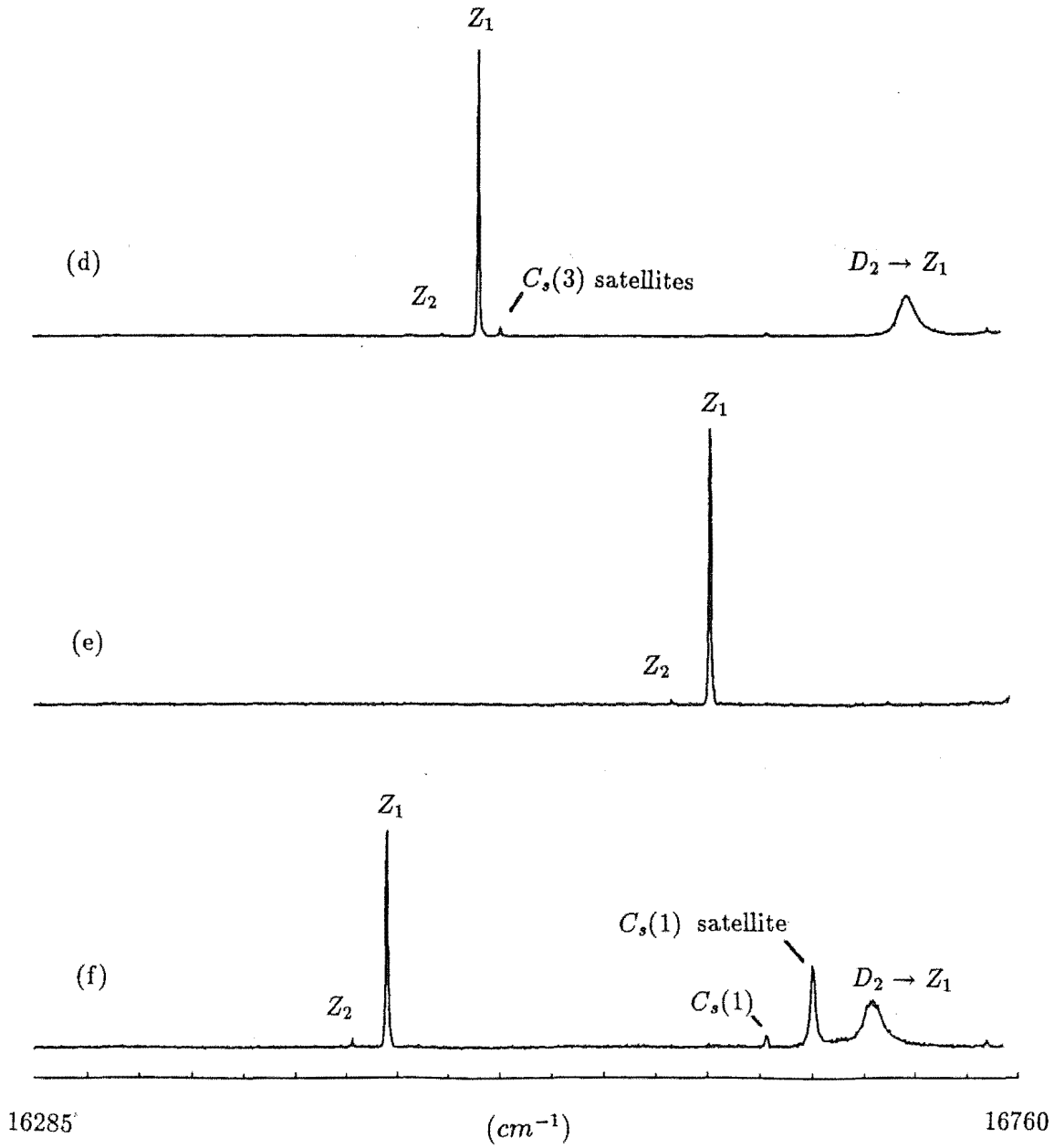
Z_1
(d)
Z_2
$C_s(3)$ satellites
$D_2 \rightarrow Z_1$
Z_1
(e)
Z_2
Z_1
$C_s(1)$ satellite
(f)
Z_2
$C_s(1)$
$D_2 \rightarrow Z_1$
16285
(cm^{-1})
16760

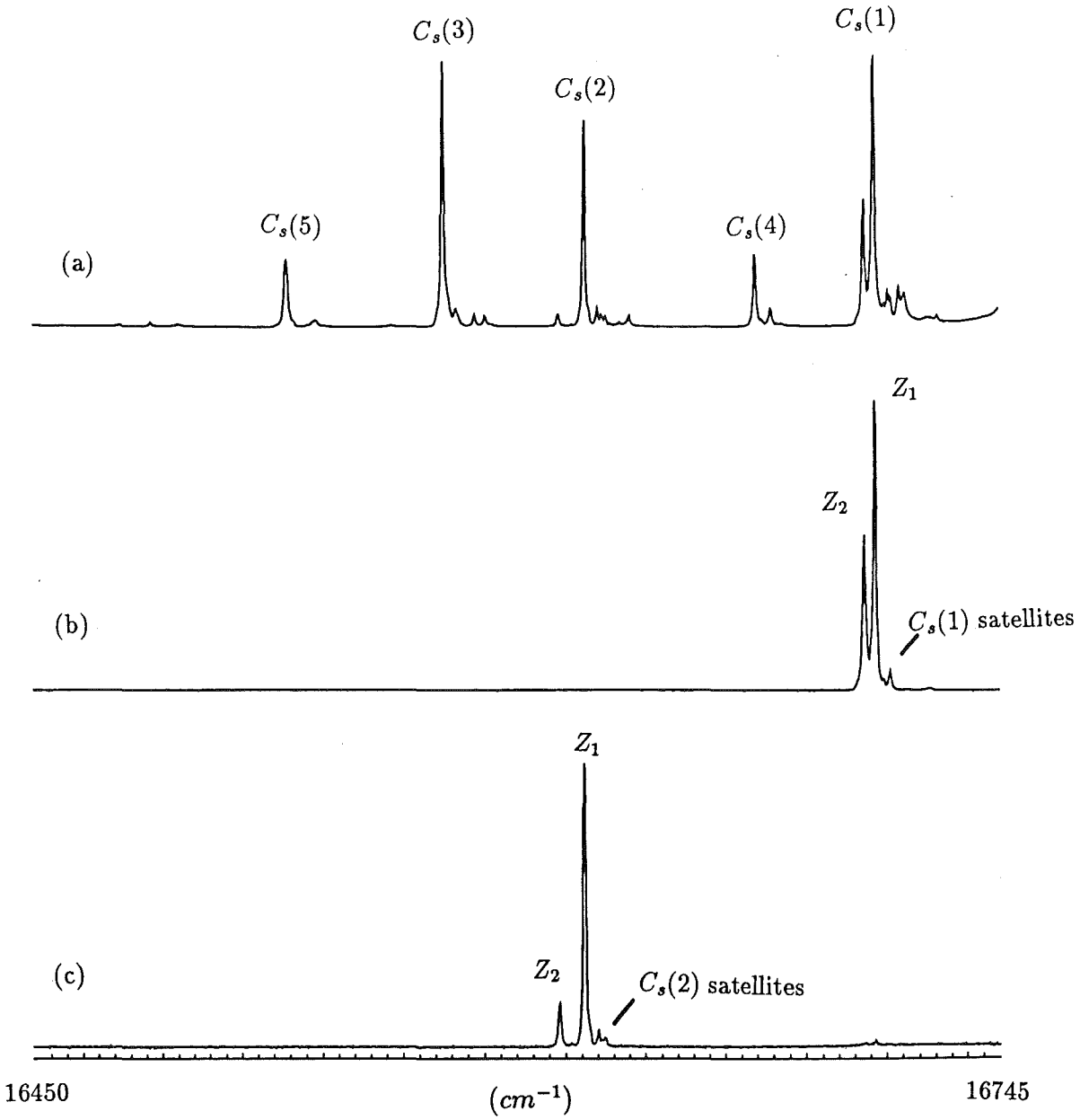

Figure 8.2 Excitation spectra of bleaching centers in deuterated SrF_2 at 11K.

8.2(a) Broadband excitation. (b),(c),(d),(e) Selective excitation of the $C_s(1)$, $C_s(2)$, $C_s(3)$ and $C_s(4)$ centers monitoring $14535cm^{-1}$, $14454cm^{-1}$, $14414cm^{-1}$ and $14495cm^{-1}$ respectively.

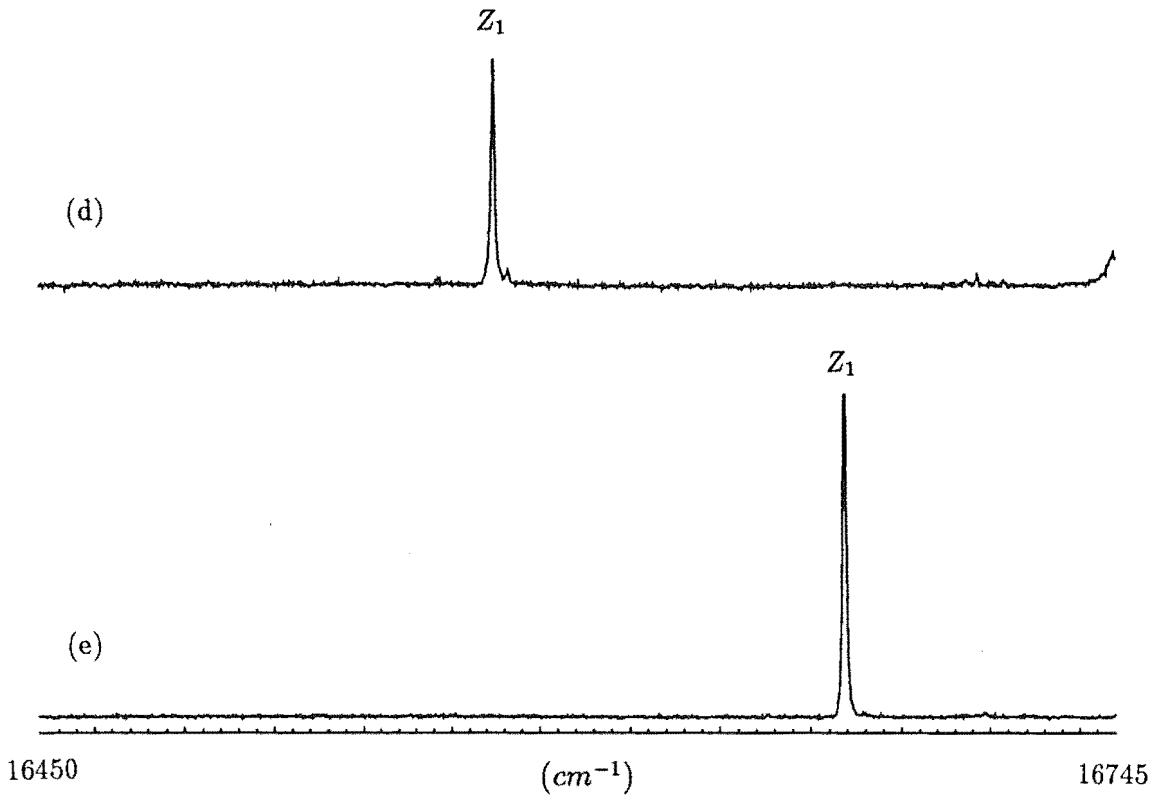
Z_1
(d)
Z_1
(e)
16450
(cm^{-1})
16745

For reasons mentioned in section 8.1.1, if the relative intensities of transitions in the emission spectra of bleaching centers are to be compared, it was particularly important to pre-bleach a center. This had to be carried out before each polarised emission spectrum was taken, otherwise inaccurate polarisation ratios of the transitions would be obtained. The introduction of the analyzer further diminished the already weak emission from a pre-bleached center, hence integration times of 10 to 20 seconds per data point were necessary to discriminate the signal from the background noise. With these adverse factors, only a few transitions from the D_1 level to the lower levels of the $^3H_5$ multiplet were recorded. Polarised emission of these are shown in figures 8.3 and 8.4 for the bleaching centers in CaF_2 and SrF_2 respectively. The corresponding bleaching centers in CaF_2 and SrF_2 display the same polarisation ratios, which suggests structural similarity between equivalent bleaching centers in both these hosts. Figure 8.5 displays the models proposed by Reeves[1987] for the various bleaching centers and the possible migration paths of the hydrogenic ions.

The $C_s(1)$ center

The model assigned by Reeves[1987] to the $C_s(1)$ center has a C_s symmetry with the reflection plane at 45° to the (100) planes parallel to the C_4 axis of the parent C_{4v} center. The polarisation ratios obtained are roughly 1:1 for the transitions observed (figs.8.3(a),8.4(a)) , and these are consistent with the polarisation ratios which could be observed for this $C_s(a)$ configuration [1] under γ_1(x or y) absorption of the laser radiation assuming the population in each orientation of this center is equal. However, on bleaching this $C_s(1)$ center, the hydrogenic ions in the $C_s(1)$ center reorient themselves to an equivalent position since this center demonstrates reversible bleaching with complete recovery of the emission intensity. Therefore, when this center is bleached, the population of certain orientations will increase while others decrease and the analysis now has to take this into account.

Assume firstly, a $\gamma_2 \rightarrow \gamma_1$ or $\gamma_1 \rightarrow \gamma_2$ absorbtion transition for the $C_s(1)$ center. Under the polarisation selection rules for a C_s center[2], only the z-component of the

[1]See chapter 2 or appendix A

[2]See table 2.3

Figure 8.3 Polarised spectra of the **(a)** $C_s(1)$, **(b)** $C_s(2)$, **(c)** $C_s(3)$, **(d)** $C_s(4)$ and **(e)** $C_s(5)$ centers in CaF_2.

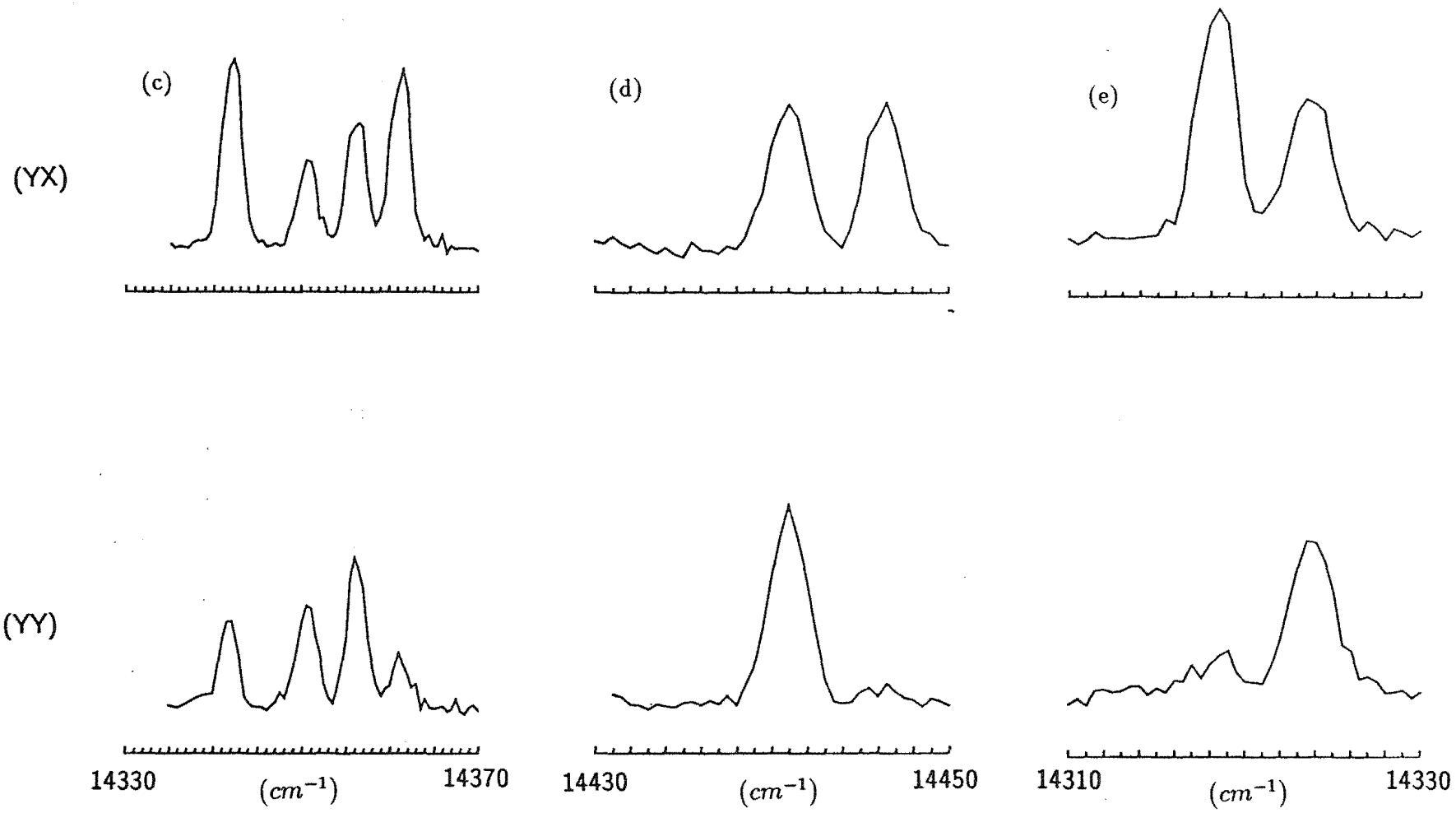
(c)
(d)
(e)
(YX)
(YY)
14330
(cm^{-1})
14370
14430
(cm^{-1})
14450
14310
(cm^{-1})
14330

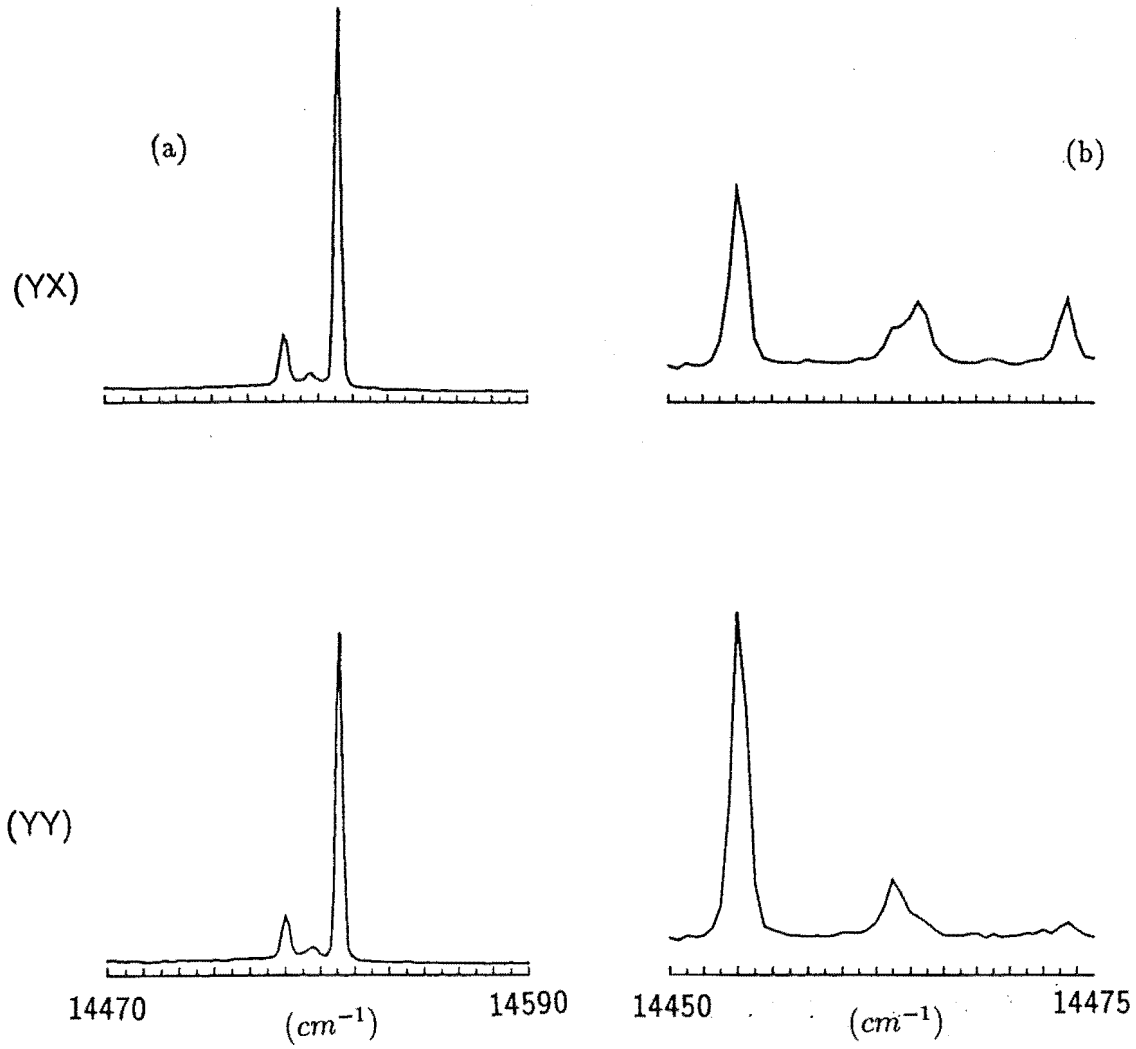

Figure 8.4 Polarised spectra of the **(a)** $C_s(1)$, **(b)** $C_s(2)$, **(c)** $C_s(3)$ and **(d)** $C_s(4)$ centers in SrF_2.

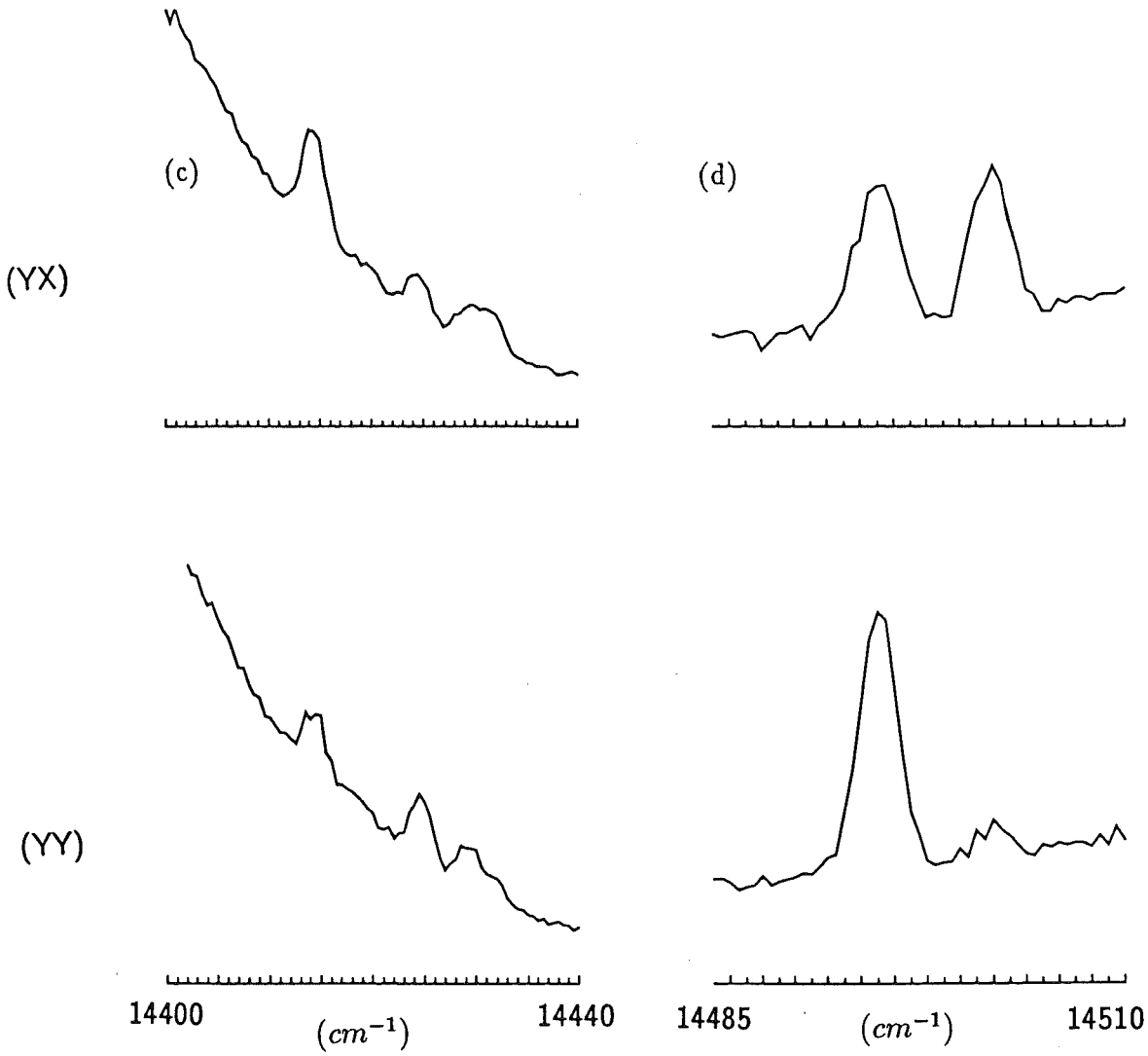
(c)
(d)
(YX)
(YY)
14400
(cm^{-1})
14440
14485
(cm^{-1})
14510

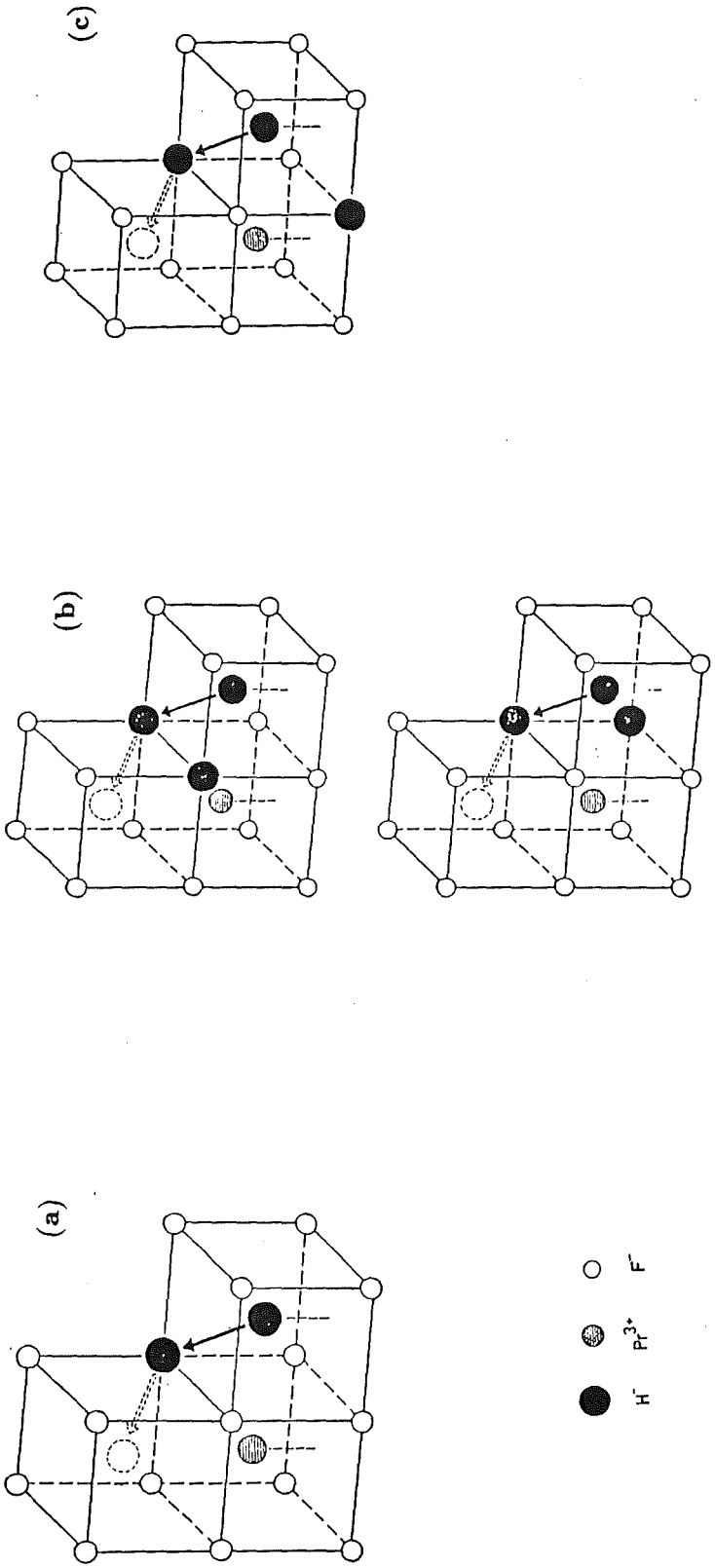

Figure 8.5 Previous models proposed by for the (a) $C_s(1)$, (b) $C_s(2)$ and (c) $C_s(4)$ bleaching centers [chap.6, Reeves, 1987]. The arrows indicate the migration paths of the hydride ions.

electric dipole absorbs for $C_s(1)$. If the laser is polarised E_Y, then according to figure A.2 or table A.1(a) (Appendix A), orientations 1,2,3 and 4 (set A) will be depleted and orientations 5 and 6 (set B) increased since components of the laser E-vector polarised in the Y-direction exist along the z-axes for orientations in set A but not for the orientations of set B. The depleted orientations in set A would give expected (YX):(YY) ratios of 1:2 and between 1:2 and 1:0 for a γ_2 and γ_1 emission respectively while the orientations in set B do not contribute to the observed polarised emission as they do not absorb with the laser polarised in the Y-direction. Polarisation ratios of between 1:2 to 1:0 were observed for the case of $C_s(1)$ center though not the ratio of 1:2.

Consider now the case of a $\gamma_1 \rightarrow \gamma_1$ or $\gamma_2 \rightarrow \gamma_2$ absorption transition of the $C_s(1)$ center, which now requires the x and y-components of the electric dipole to absorb. Figure A.2 shows that all six different orientations can now absorb. For bleaching to be observed in this case, the absorption strength for one of the x or y electric dipole components must be greater than the other. If the absorption by the x-component is stronger, then population set A will be depleted and set B enhanced and if the absorption by the y-component is stronger, the population set A will be enhanced and set B depleted. A depleted set A or set B could still give a significant contribution since the emission strength of one of the x or y-components will be stronger than the other.

Examination of figure VI.2.5 Reeves[1987] reveals that both the $Z_1 \rightarrow D_1$ and $Z_2 \rightarrow D_1$ transitions of the $C_s(1)$ center bleach together, this being consistent with a depletion of population set A after the $C_s(1)$ center was bleached. If set A was enhanced instead of depleted, the $Z_2 \rightarrow D_1$ transition would increase in intensity relative to the $Z_1 \rightarrow D_1$ transition after the $Z_1 \rightarrow D_1$ is bleached. The depletion of the population set A can occur as a result of absorption by the z-component of the electric dipole or the x-component absorbing more strongly than the y-component. With the caveat that only a limited number of polarised transitions were recorded, the lack of a (YX):(YY) polarisation ratio of 1:2 observed for the $C_s(1)$ center, favours the latter mechanism for depletion of population set A.

The $C_s(2)$ center

The bleaching behaviour of the $C_s(2)$ center was found to be more varied and to display the following behaviour:

1) on pumping the $Z_1 \rightarrow D_1$ transition, the bleaching is reversible though the intensity recovery is not as complete as that of the $C_s(1)$ center;
2) after bleaching the $Z_1 \rightarrow D_1$ transition for 30 minutes, the bleaching cycle becomes completely recoverable;
3) photoproducts are formed when the $Z_1 \rightarrow D_1$ transition is bleached and bleaching of these photoproducts restores the $Z_1 \rightarrow D_1$ transition;
4) on exciting the $Z_2 \rightarrow D_1$ transition, the bleaching cycle was found to be non-reversible;
5) bleaching of the $Z_1 \rightarrow D_1$ transition does not affect the $Z_2 \rightarrow D_1$ transition.

The model proposed for the $C_s(2)$ center is shown in figure 8.5(b) and has a configuration of the type $C_s(b)$ (see appendix A) with the reflection plane parallel to the [100] axis. This model is sufficient to explain points 1,2 and 3. No explanation was offered for points 4 and 5 in previous work. To explain point 5, it is necessary to examine the six possible orientations of the $C_s(b)$ configuration. The orientations excited when the laser is polarised E_Y are 1,2,3 and 6 when the radiation is absorbed by the x or y component of the electric dipole and 4 and 5 when the z-component absorbs[3]. There are only two possible irreps for levels of a C_s symmetry i.e γ_1 or γ_2. The Z_1 and Z_2 ground state level can not have the same irrep since these levels originated from the lifting of degeneracy of a C_{4v} γ_5 level. Therefore a $Z_1 \rightarrow D_1$ transition can only affect one set of the possible $C_s(b)$ orientations and the $Z_2 \rightarrow D_1$ a different set. As was observed, the Z_1 and Z_2 levels of this center bleach independently.

Since the laser E-vector is either parallel or perpendicular to the C_s plane, different alignments of the E-vector will favour migration of ions to form different

[3]see figure A.3

orientations or different types of centers. For the bleaching of the $Z_2 \rightarrow D_1$ transition the E-vector alignment only allows formation of inequivalent centers and hence the non-reversible behaviour of point 4 was observed.

The observed polarised emission (figs 8.3(b) and 8.4(b)) for the $C_s(2)$ center is explained by this model. However, the $C_s(a)$ and $C_{2v}(a)$ configurations could also account for the polarisation ratios observed, though it is not obvious how these two configurations would explain point 5.

The $C_s(3)$ center

The following features were observed in the LSE of the $C_s(3)$ center:

(i) formation of photoproducts when bleached;
(ii) a very fast bleaching rate, of the order of a few seconds in SrF_2 compared to several minutes for the other $C_s(i)$ centers;
(iii) a greater number of local mode vibronic lines in its emission spectra compared to the other $C_s(i)$ centers;
(iv) absence of distinct (YX):(YY) polarisation ratios of 1:2, 1:0 or 0:1(figs. 8.3(c) and 8.4(c)).

No model was assign in previous work to this center but it was concluded that the $C_s(3)$ center should comprise a bleaching center with more than two hydrogenic ions in the local environment of the Pr^{3+} ion. Point (iv) suggests that the lowest symmetry group of C_1 is appropriate for this center. Several D^- substituitonal arrangements with a C_1 symmetry are possible but the present set of polarised emisison spectra is unable to distinguish between them.

The $C_s(4)$ center

Figure 8.5(c) shows the model assigned to the $C_s(4)$ center. Strictly speaking, the model does not have a C_s but a C_{2v} symmetry. The observed polarisation ratios

(figs. 8.3(d) and 8.4(d)) are consistent with those originating from a C_{2v} center and support the previous model assignment. Two new lines P1 and P2 arose when the $C_s(4)$ center was bleached (figure VI.2.10 of Reeves[1987]) and were assigned as the Z_1 and Z_2 levels of the same photoproduct. Bleaching both the P1 and P2 lines restores only about half the $C_s(4)$ intensity which means not all the ions of the photoproducts migrate to reform the parent $C_s(4)$ center. There are no new lines to suggest they form other centers around the RE ion so they must have migrated further away from the RE ion.

The $C_s(5)$ center

The parent $C_s(5)$ center has not been studied previously. When this center in the CaF_2 host is bleached (fig. 8.6(a)) only the transition at $16403cm^{-1}$ appeared weakly. It appears that the photoproduct transition of the $C_s(5)$ center belonging to this transition lies very close to the Z_2 transition of the parent $C_s(5)$ center at $16403cm^{-1}$. A distinct photoproduct corresponding to the transition at $16506cm^{-1}$ was evident when the $C_s(5)$ center was bleached in the SrF_2 crystal (fig. 8.7(b)). Tuning the laser to the photoproduct absorption line restores the $C_s(5)$ center for both the CaF_2 and SrF_2 hosts.

The polarised emission for the $C_s(5)$ (fig. 8.3(e)) was only measured for the $C_s(5)$ center in CaF_2 because of the difficulties mentioned section 8.1.1. No combination of the absorption or emission strengths **a**,**b** or **c** of the x, y or z electric dipole components of the C_s or C_{2v} center configurations presented in appendix A would give the polarisation ratios of 1:1 and 1:0 observed for this center. Therefore it was not possible to assign a model based the geometries of the C_s and C_{2v} configurations investigated here.

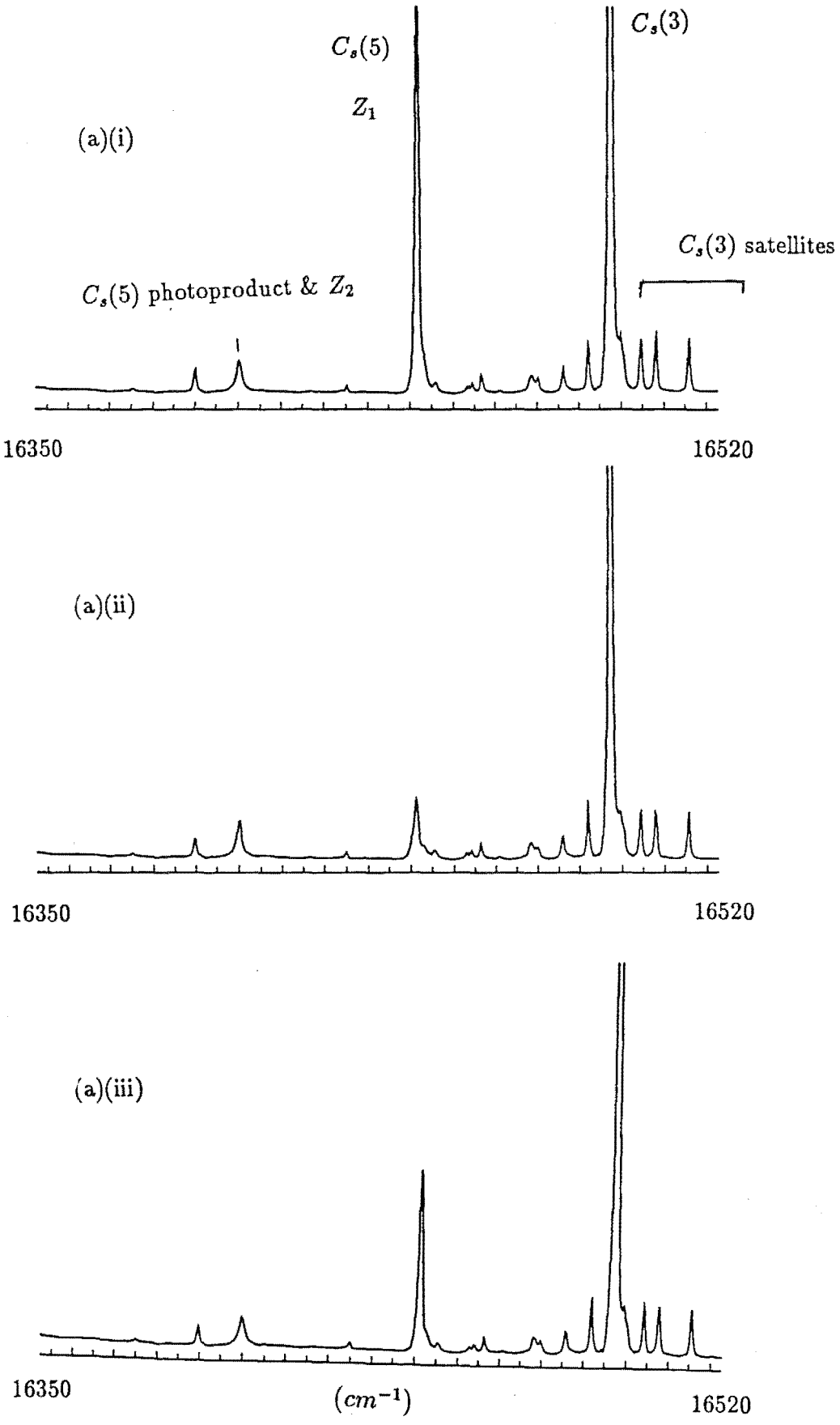
$C_s(5)$
Z_1
$C_s(3)$
(a)(i)
$C_s(3)$ satellites
$C_s(5)$ photoproduct & Z_2
16350
16520
(a)(ii)
16350
16520
(a)(iii)
16350
(cm^{-1})
16520

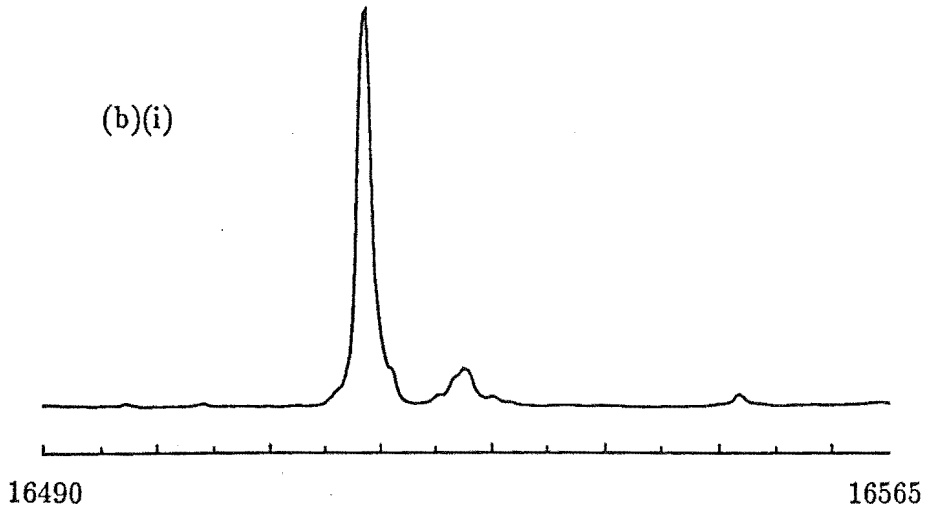
(b)(i)
16490
16565

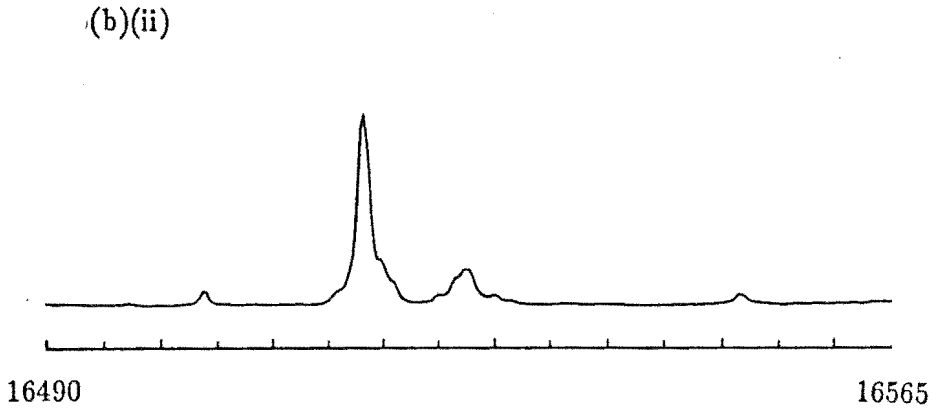
(b)(ii)
16490
16565

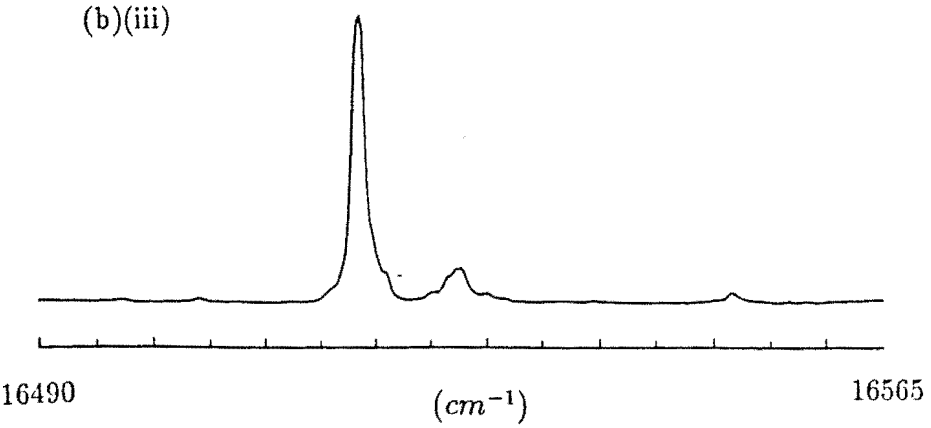
(b)(iii)
16490
16565
(cm^{-1})

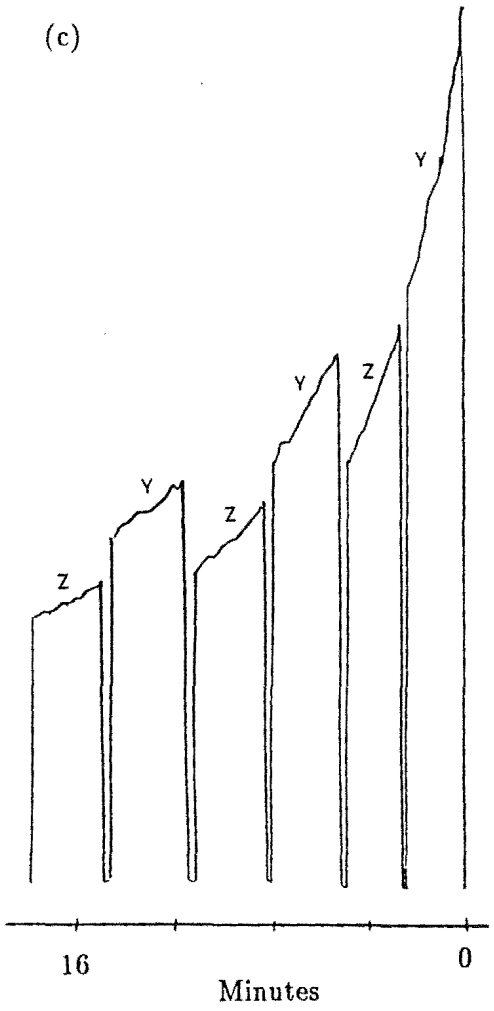

Figure 8.6 Excitation spectra of the $C_s(5)$ centers in deuterated **(a)** CaF_2 **(b)** SrF_2 at 11K.

(i) before bleaching (ii) after bleaching the $C_s(5)$ center (iii) after bleaching the $C_s(5)$ center photoproduct. Some recovery is apparent.

(c) Bleaching curve of the $C_s(5)$ center

8.2 LSE of Bleaching Centers in Deuterated Mixed Crystals

In the mixed crystals, weak satellite line structures around the main transitions of the bleaching centers were observed in the excitation spectra. The emission strengths of the lines from these centers were typically in the order of ten to a few hundred times less intense than the electronic transitions of the main bleaching centers in the mixed crystals, while in the parent crystals, these satellite lines were several thousand times weaker than the parent $C_s(i)$ transitions. The results from the study of these mixed crystal bleaching centers in $Ca_{1-x}Sr_xF_2 : Pr^{3+} : D^-$ and $Sr_{1-x}Ca_xF_2 : Pr^{3+} : D^-$ are reported in section 8.2.1 and 8.2.2 respectively. Some discussion about possible models for these centers is given section 8.2.3. Throughout the discussion of this section, the labels $C_s(i)K$ will be used , where i is 1,2,3,4,5 identifying the parent center and K is an alphabetic label of a particular satellite center associated with the parent center.

Typically, each center was bleached for 15 to 30 minutes at 50 to 100mW of laser power. The broadband excitation scans were performed at a lower power setting of 10 to 25mW to reduce unintentional bleaching of the centers which have transitions within the frequency range of the scans. As the signal levels from the emission of the satellite centers are extremely low, the gain of the Keithley electrometer used was adjusted to a higher setting. The increased sensistivity of the electrometer however produced an undesirable effect of amplifying the minute variations in light intensity as the image tended to oscillate slightly about the Bausch and Lomb monochromator entrance slit when the laser frequency was being varied. This signal artifact which may show up as ripples in the background of a spectrum originates from the birefringent tuning mechanism of the dye laser and can be eliminated by optimizing the light collection optics to minimize the oscillations of the image at the slit and ensuring that the monochromator entrance slits are opened wider.

8.2.1 Bleaching Centers in $Ca_{1-x}Sr_xF_2 : Pr^{3+} : D^-$

Extra transitions were observed around transitions of all the $C_s(i)$ centers in $Ca_{1-x}Sr_xF_2 : Pr^{3+} : D^-$ and these will be discussed in turn. Only satellites with transitions which are distinct and sufficiently intense were studied and there are 4,2,3,2 and 5 of these asssociated with the $C_s(1)$, $C_s(2)$, $C_s(3)$, $C_s(4)$ and $C_s(5)$ parent centers respectively.

The $C_s(1)$ satellites

Figure 8.7(a) displays the excitation spectra of the region around the $C_s(1)$ satellite lines. The satellite features are labelled $C_s(1)A$, $C_s(1)B$,$C_s(1)C$ and $C_s(1)D$. The spectrum in figure 8.7(a) is a reference to compare the the excitation spectrum before and after the bleaching of the satellite lines.

The $C_s(1)A$ center

After bleaching the $C_s(1)A$ center, two photoproduct transitions at $16621cm^{-1}$ and $16640cm^{-1}$ which are labelled $A1$ and $A2$ in figure 8.7(b)(i) were produced. Bleaching the weak $A1$ line partially restores the $C_s(1)A$ transition and bleaching the line $A2$ restores it even further (figs. 8.7(b)(ii & iii)) though not completely. Another transition at $16625cm^{-1}$ seems to be a photoproduct transition of the $C_s(1)A$ center but it does not affect the intensity of $C_s(1)A$ center when bleached. Repeated scanning over different regions of the crystal and at different times revealed that the intensity of the transition at $16625cm^{-1}$ appears to be random. It is rather stable under bleaching and dropped in intensity by about only 10% after 15 minutes of bleaching at 100mW of laser power. No further investigation was carried out on this center because of its weak emission. The bleaching curve of the $C_s(1)A$ center is shown figure 8.7(f)(i) and is completely reversible after a few cycles of bleaching

The $C_s(1)B$,$C_s(1)C$ and $C_s(1)D$ centers

Table 8.1 Summary of the results from the study of the satellite bleaching centers in $Ca_{1-x}Sr_xF_2 : Pr^{3+}$.

Centers	$Z_1 \rightarrow D_1$ ($Z_2 \rightarrow D_1$) $\pm 1 cm^{-1}$	Description of emission intensity under a bleaching cycle where the laser polarisation was switched between E_Y and E_Z	Frequency of Photoproducts $\pm 1 cm^{-1}$
$C_s(1)$	16631 (16630.5)	Fully Recoverable	-
$C_s(1)A$	16638	Fully recoverable after a few cycles	16621 16640
$C_s(1)B$	16648 (16646)	Non recoverable	-
$C_s(1)C$	16654	Non recoverable	-
$C_s(1)D$	16662	Non recoverable	-
$C_s(2)$	16533 (16524)	Partially recoverable	16575
$C_s(2)A$	16545	Non recoverable	-
$C_s(2)B$	16654	Non recoverable	16586

$C_s(3)$	16489 (16470)	Non recoverable	16482
$C_s(3)A$	16497	Non recoverable	-
$C_s(3)B$	16501	Non recoverable	-
$C_s(3)C$	16509	Non recoverable	-
$C_s(4)$	16603 (16585)	Non recoverable	-
$C_s(4)A$	16611	Non recoverable	16609
$C_s(4)B$	16613	Non recoverable	-
$C_s(5)$	16443	Non recoverable	16403
$C_s(5)A$	16392 (16378)	Non recoverable	16370
$C_s(5)B$	16426	-	-
$C_s(5)C$	16455	-	-
$C_s(5)D$	16463	-	-
$C_s(5)E$	16475	-	-

The two lines at $16646cm^{-1}$ and $16648cm^{-1}$ are the $Z_2 \rightarrow D_1$ and $Z_1 \rightarrow D_1$ transitions respectively of the $C_s(1)B$ center. The laser tuned to either of these two lines will bleach both the lines simultaneously. No photoproducts were apparent after bleaching this center (fig. 8.7(c)) even though it did exhibit a non-reversible bleaching cycle (figs. 8.7f(ii)).

The lines at 16654 and $16662cm^{-1}$ belong to the $C_s(1)C$ and $C_s(1)D$ centers respectively. As for the case of the $C_s(1)B$ center, the bleaching cycles of the $C_s(1)C$ and $C_s(1)D$ centers are non reversible (fig. 8.7(f)(iii) & (iv)) and no apparent photoproducts were present after bleaching (fig. 8.7(d) & (e)). The $C_s(1)C$ center transition also appeared in the excitation spectra while monitoring the $14495cm^{-1}$ line of the $C_s(5)$ center (fig. 8.1(f)). An emission spectrum, scanning through the $D_1 \rightarrow Z_1$ frequency region of the $C_s(5)$ center while pumping the $16654cm^{-1}$ line , would confirm whether the line labelled $C_s(1)C$ does belong to $C_s(5)$ or not. However, since the $16654cm^{-1}$ line appears to be out of place when the excitation spectrum of the $C_s(5)$ center is compared to the excitation spectrum pattern of the $C_s(2)$ and $C_s(3)$ centers, it is highly unlikely this line does belong to the $C_s(5)$ center and it is tentatively assigned as a line of the $C_s(1)$C satellite center.

The excitation spectra after bleaching $C_s(1)D$ show that there are further structures at the shoulder of this center. These were however too weak to be investigated further.

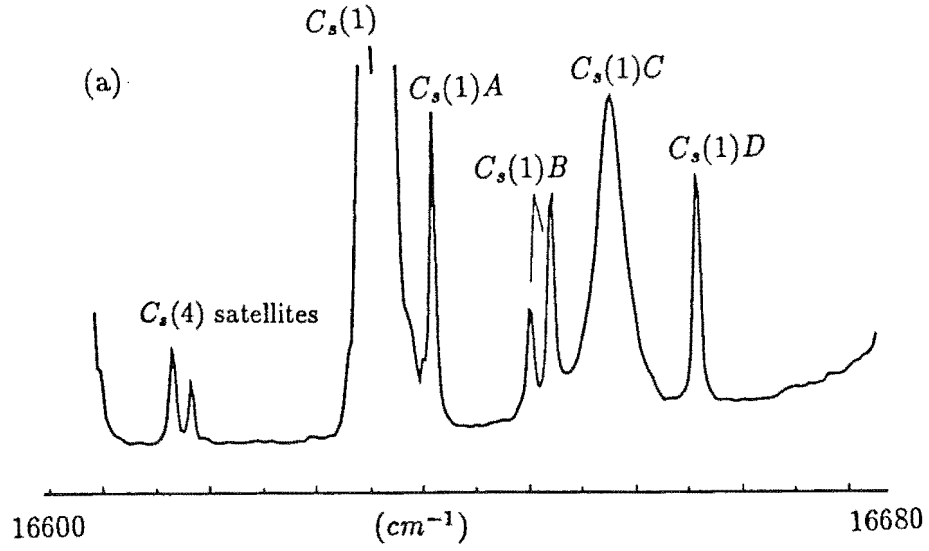

Figure 8.7 Broadband excitation spectrum of the $C_s(1)$ center and its satellites in the $Ca_{1-x}Sr_xF_2 : Pr^{3+}$ mixed crystal at 11K

(a) Before bleaching.
(b)(i) After bleaching the $C_s(1)A$ satellite two photoproducts transitions at $16621cm^{-1}$and $16640cm^{-1}$labelled A1 and A2 respectively. (ii) & (iii) Exciting the photproduct transitions A1 and A2 respectively partially restores some of the lost intensity in the $C_s(1)A$ center.
(c),**(d)**,**(e)** After bleaching the satellites $C_s(1)B$, $C_s(1)C$ and $C_s(1)D$ respectively. There were no obvious photoproducts after bleaching these centers.
(f)(i)-(iv) The bleaching curves of the $C_s(1)A$, $C_s(1)B$, $C_s(1)C$ and $C_s(1)D$ respectively. The **Z** and **Y** labels refer to the two orthogonal polarisation direction of the laser polarisation.

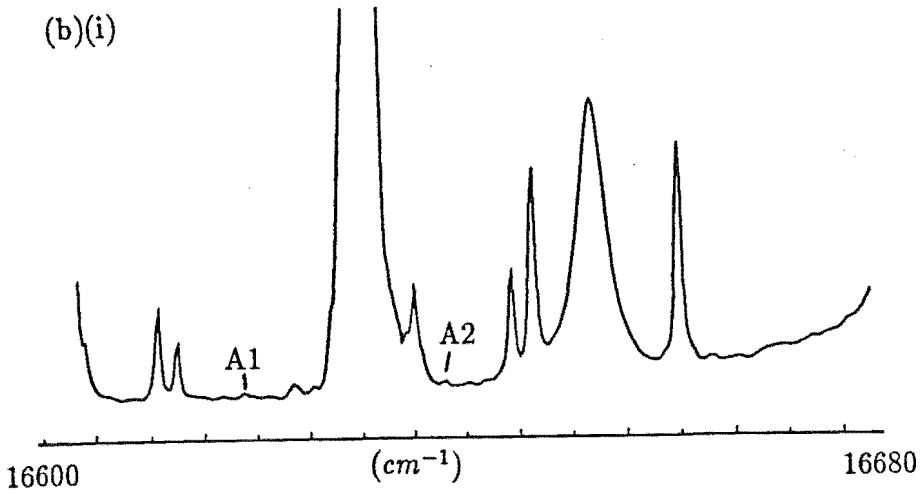
(b)(i)
A1
A2
16600
(cm^{-1})
16680

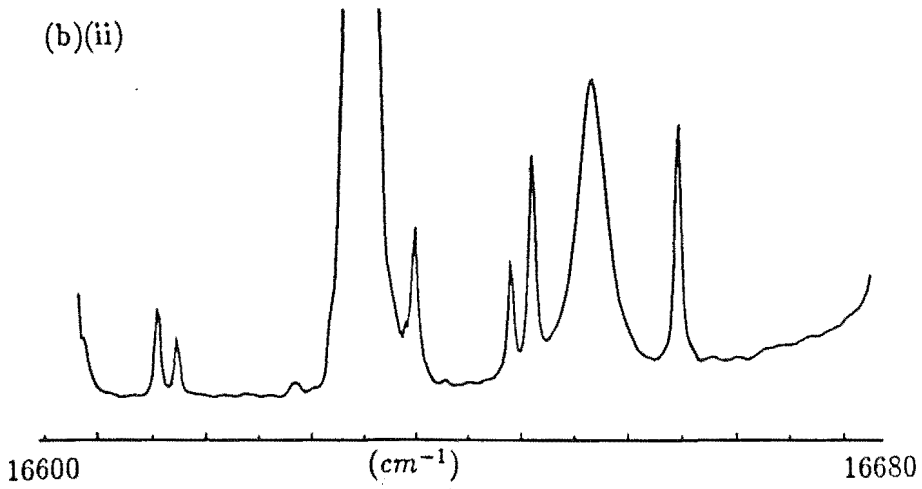
(b)(ii)
16600
(cm^{-1})
16680

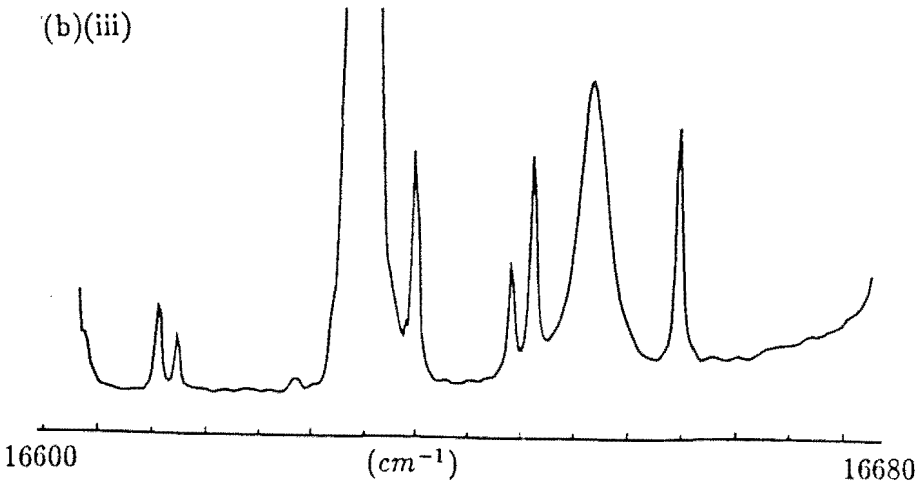
(b)(iii)
16600
(cm^{-1})
16680

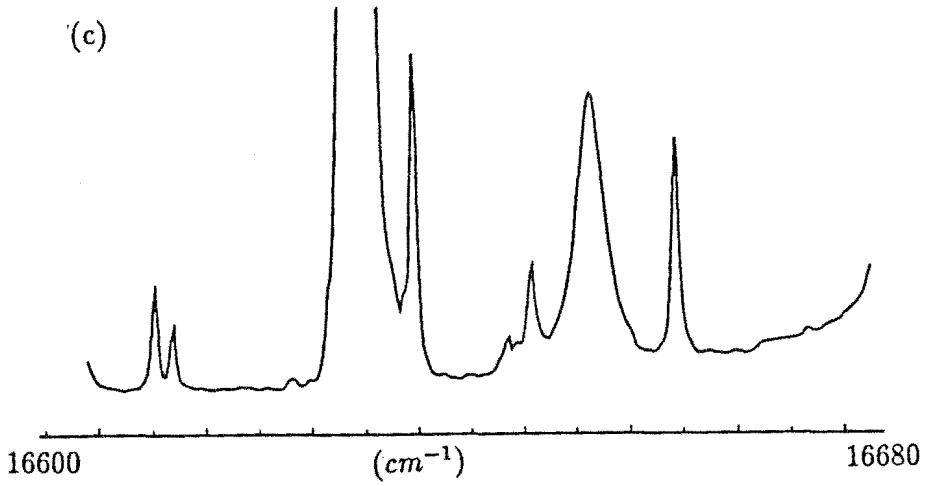
(c)
16600
(cm^{-1})
16680

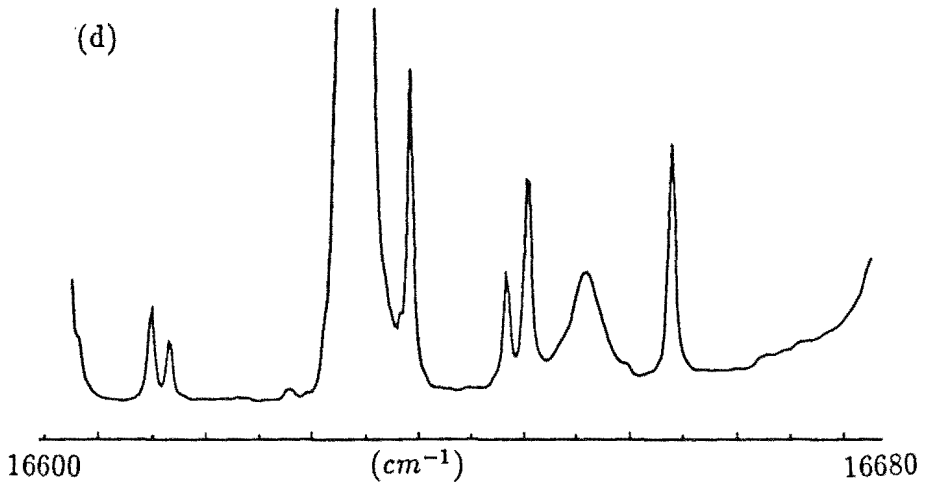
(d)
16600
(cm^{-1})
16680

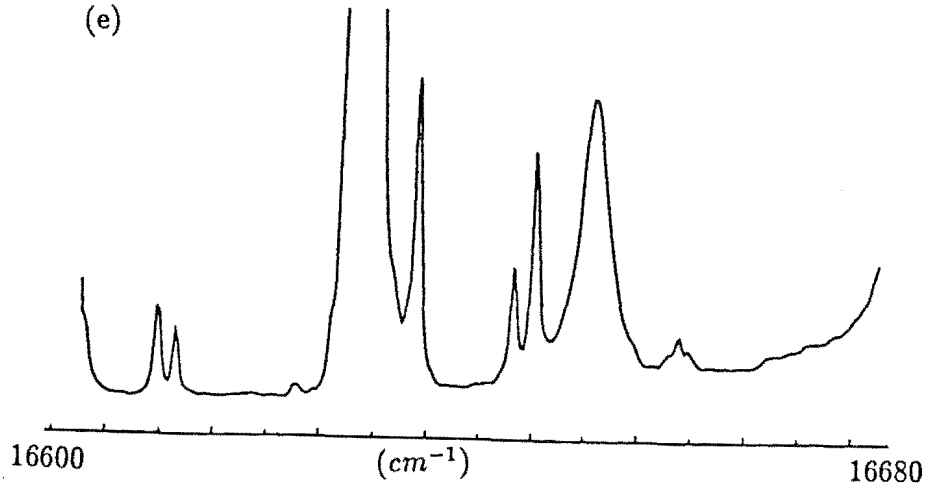
(e)
16600
(cm^{-1})
16680

(f)(i)

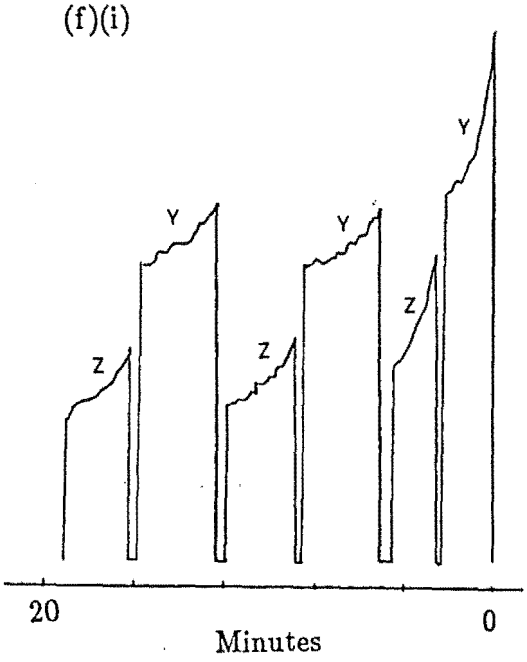

(f)(ii)

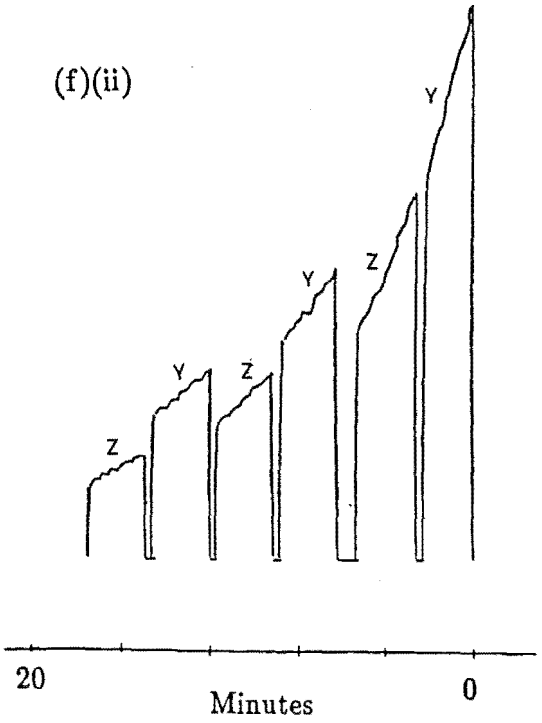

(f)(iii)

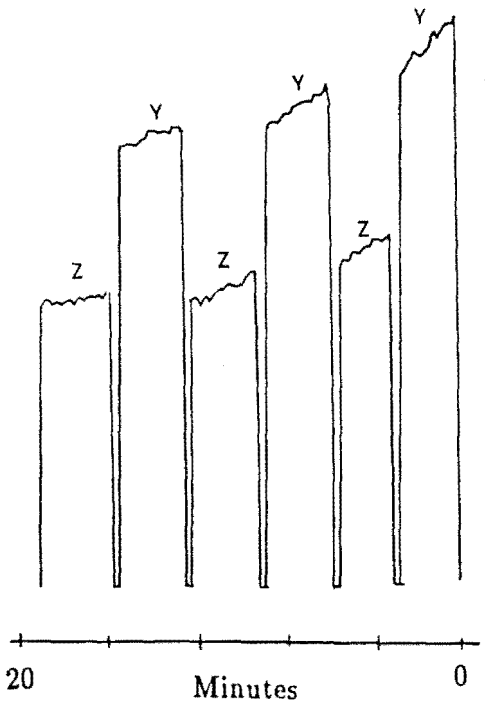

(f)(iv)

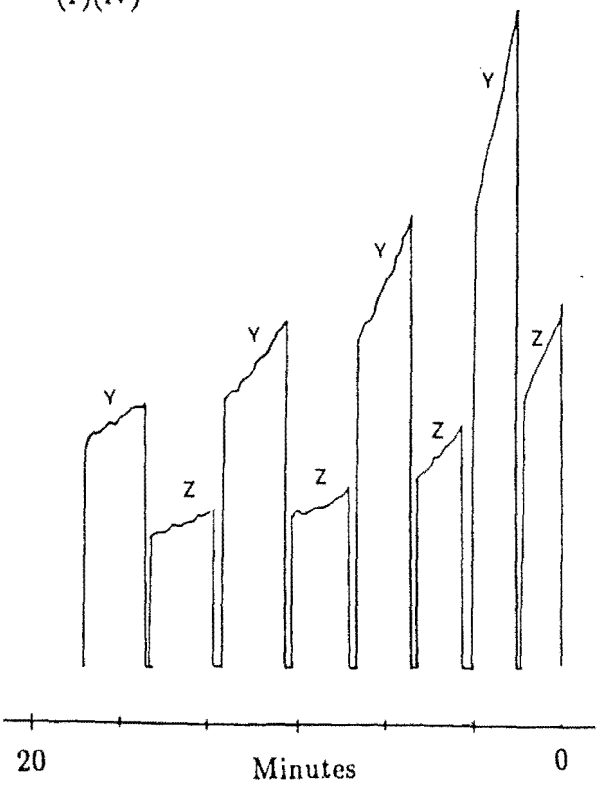

The $C_s(2)$ satellites

The $C_s(2)A$ and $C_s(2)B$ centers

The excitation spectra of the $C_s(2)$ center and its satellite transitions are shown in figure 8.8. Only the two strongest satellite lines, belonging to the $C_s(2)A$ and $C_S(2)B$ centers at $16545cm^{-1}$ and $16547cm^{-1}$ were studied. They both display non reversible bleaching (fig. 8.8(d)) with only the $C_s(2)B$ center giving an obvious photoproduct transition at $16586cm^{-1}$ (fig. 8.8(c)(i)). No new transitions were observed for the $C_s(2)A$ center after bleaching (fig. 8.8(b)).

The $C_s(3)$ satellites

The $C_s(3)A$, $C_s(3)B$ and $C_s(3)C$ centers

Figure 8.9(a) shows the spectral region around the transition belonging to the $C_s(3)$ center. The satellite structures investigated in this study associated with the $C_s(3)$ center are labelled $C_s(3)A$, $C_s(3)B$ and $C_s(3)C$. Like their parent $C_s(3)$ center , the three satellites bleach non reversibly (fig. 8.9(e)). After bleaching each of these three satellite centers, careful scrutiny of the excitation spectra (figs. 8.9(b),(c) & (d)) did not reveal any new transitions belonging to photoproducts.

The line at $16477cm^{-1}$ does not bleach which is most uncharacteristic of transitions in this region of the spectra. The location of this line fits in with the overall energy scheme of a $Z_2(\gamma_4) \rightarrow D_2(\gamma_3)$ magnetic dipole transition of the D^- or F^- C_{4v} centers. The Z_2 level was not observed directly in the work of Reeves[1987] but was inferred from the Z_2 vibronic levels to be $195cm^{-1}$. The line at $16477cm^{-1}$ would give an assignment of $237cm^{-1}$ for the D^- C_{4v} Z_2 level. If the line at $16477cm^{-1}$ is considered as the F^- C_{4v} center transition, then the Z_2 level of this center would be assigned at $338cm^{-1}$.

Figure 8.8 Bleaching of the $C_s(2)$ center satellites in the $Ca_{1-x}Sr_xF_2 : Pr^{3+}$ mixed crystal at 11K.

(a) Before bleaching.
(b) After bleaching the $C_s(2)A$ center, no photoproduct formation apparent.
(c)(i) A single photoproduct formation was apparent after bleaching the $C_s(2)B$ center. The photoproduct transition, at $16586cm^{-1}$is marked with an asterisk. (ii) On pumping the photoproduct, the bleached intensity of the $C_s(2)B$ center was partially restored.
(d)(i) & (ii) The bleaching curves of the $C_s(2)A$ and $C_s(2)B$ center respectively.

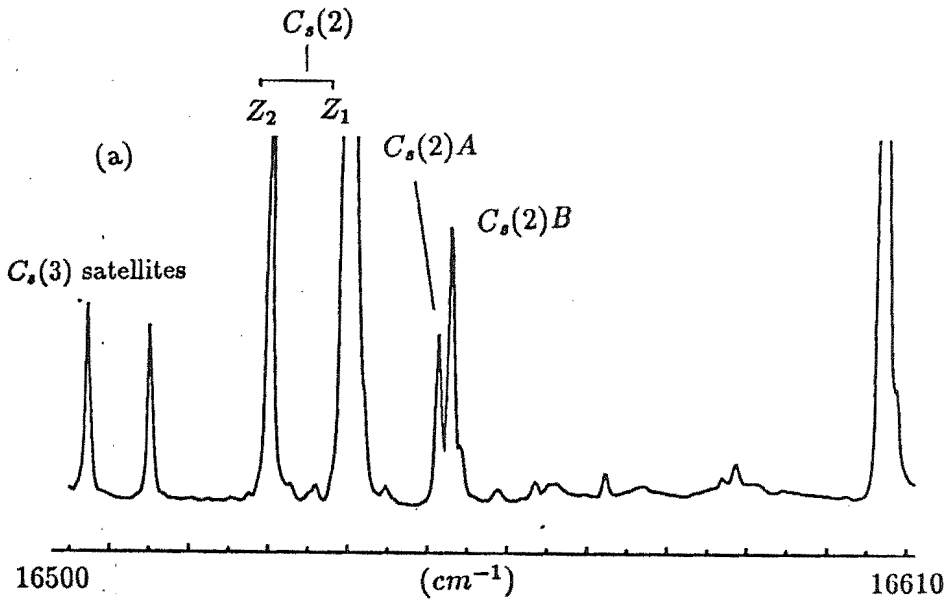
$C_s(2)$
Z_2
Z_1
(a)
$C_s(2)A$
$C_s(2)B$
$C_s(3)$ satellites
16500
(cm^{-1})
16610

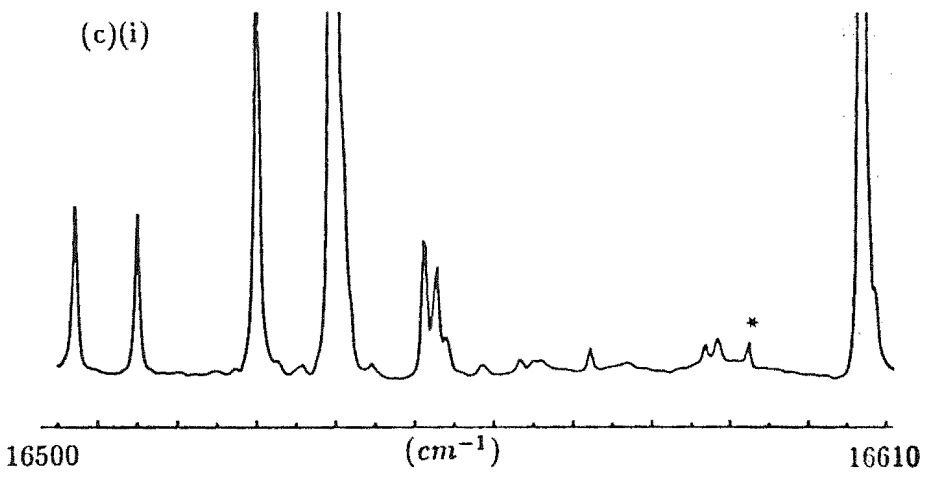
(c)(i)
*
16500
(cm^{-1})
16610

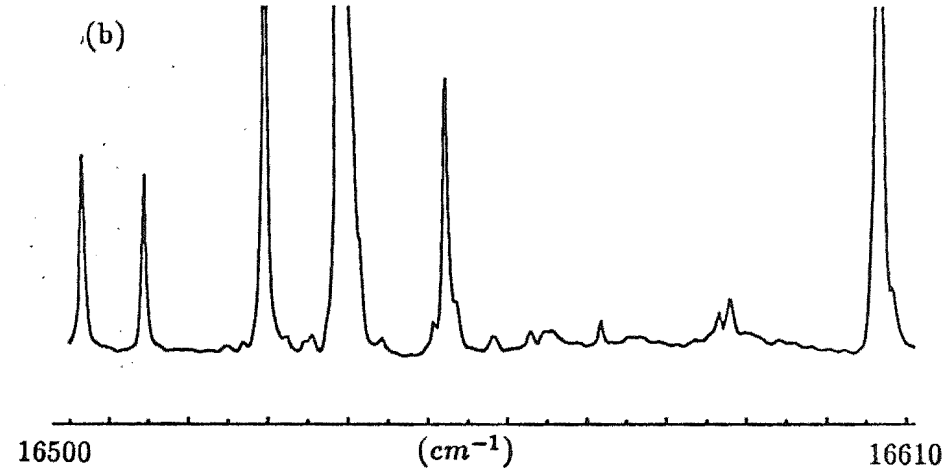
(b)
16500
(cm^{-1})
16610

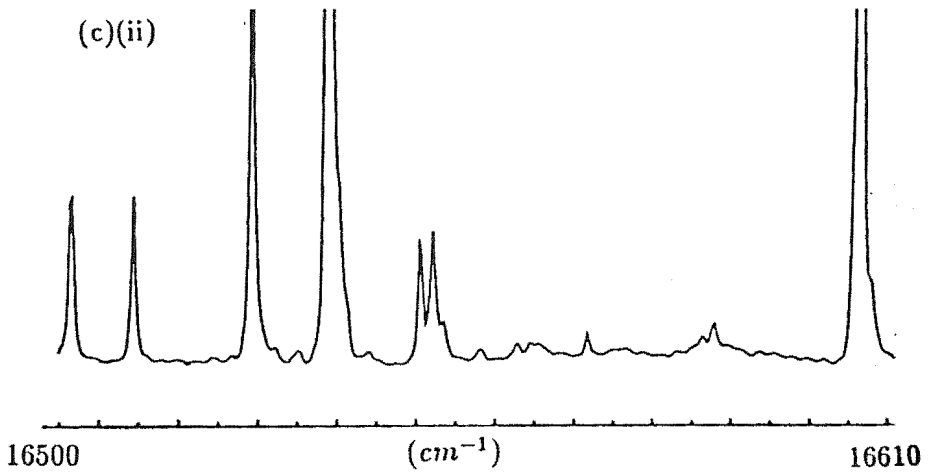
(c)(ii)
16500
(cm^{-1})
16610

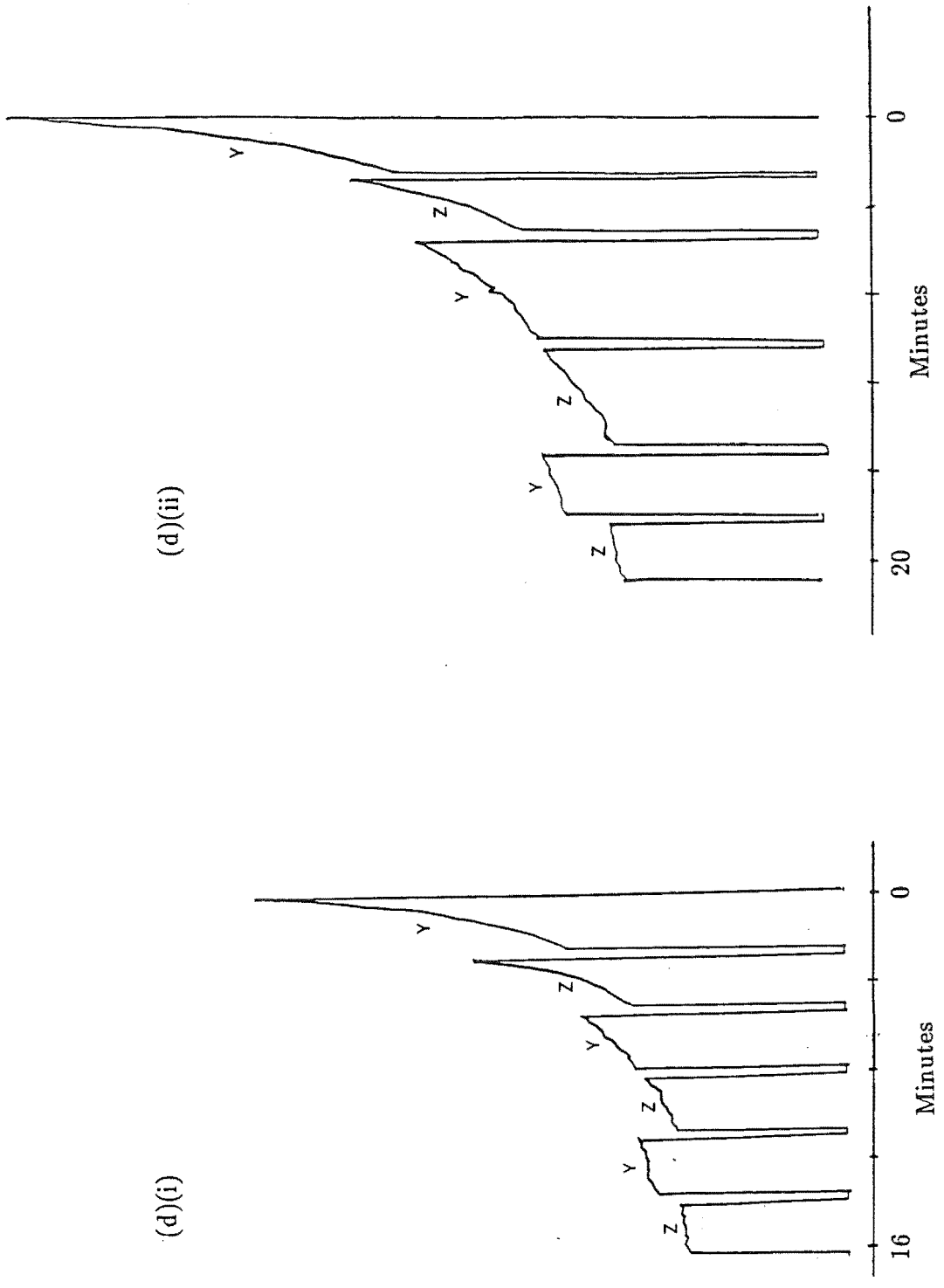
(d)(ii)
Y
Z
Y
Z
Y
Z
0
Minutes
20
(d)(i)
Y
Z
Y
Z
Y
Z
0
Minutes
16

A few other lines in figure 8.9(a) are observed from $16450cm^{-1}$ to $16475cm^{-1}$. These were taken to be the satellite lines associated with the $C_s(5)$ center though this association is somewhat arbitrary given that these lines are almost as close to the main transitions of the $C_s(3)$ center as to those of the $C_s(5)$ center. Their relative intensities appeared to have altered after the first scan of figure 7.12(a) but remained constant after subsequent scans. At present, the cause of this behaviour remains unexplained.

The $C_s(4)$ satellites

The $C_s(4)A$ and $C_s(4)B$ centers

Examination of the excitation spectra reveals that the line belonging to the $C_s(4)A$ center is the strongest satellite line associated with the $C_s(4)$ center (fig. 8.10(a)). One distinct photoproduct transition was produced when this satellite was bleached. On exciting the photoproduct not only is the intensity of the $C_s(4)A$ satellite restored but a new transition peak arose at $16582cm^{-1}$ (fig. 8.10(d)). Bleaching the $16582cm^{-1}$ peak produced no change to the excitation spectra apart from the diminished intensity of the line being bleached. The non reversible bleaching cycle observed for the $C_s(4)A$ center (fig. 8.10(e)) is consistent with photoproduct formation.

Satellite $C_s(4)B$ bleaches non reversibly (fig.8.10(e)) as well but no clear photoproducts were observed (fig.8.10(b)). The other weaker satellites centered around $16853cm^{-1}$ were not studied in detail but they did bleach under excitation.

The $C_s(5)$ satellites

The $C_s(5)A$,$C_s(5)B$, $C_s(5)C$, $C_s(5)D$, $C_s(5)E$ centers

Figure 8.9 Bleaching of the $C_s(3)$ center satellites in the $Ca_{1-x}Sr_xF_2 : Pr^{3+}$ mixed crystal at 11K

(a) Before bleaching.
(b) After bleaching the $C_s(3)A$ center.
(c) After bleaching the $C_s(3)B$ center.
(d) After bleaching the $C_s(3)C$ center.
No obvious transitions of photoproduct were observed after bleaching each of the three centers.
(e)(i)-(iii) The non-reversible bleaching cycles of the $C_s(3)A$, $C_s(3)B$ and $C_s(3)C$ centers respectively.

The transition labelled with asterisks are satellite lines associated with the $C_s(5)$ center.
The lines labelled 1 is the photoproduct of the $C_s(3)$ center. The line labelled 2 at $16477cm^{-1}$ is discussed in the text.

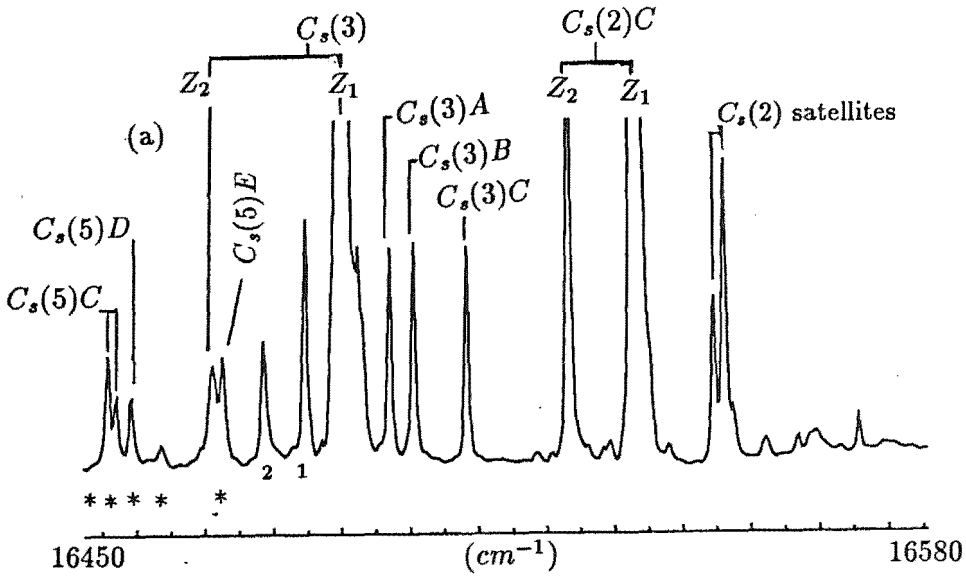
(a)
$C_s(3)$
Z_2
Z_1
$C_s(2)C$
Z_2
Z_1
$C_s(3)A$
$C_s(3)B$
$C_s(3)C$
$C_s(2)$ satellites
$C_s(5)D$
$C_s(5)C$
$C_s(5)E$
2
1
* * * * *
16450
(cm^{-1})
16580

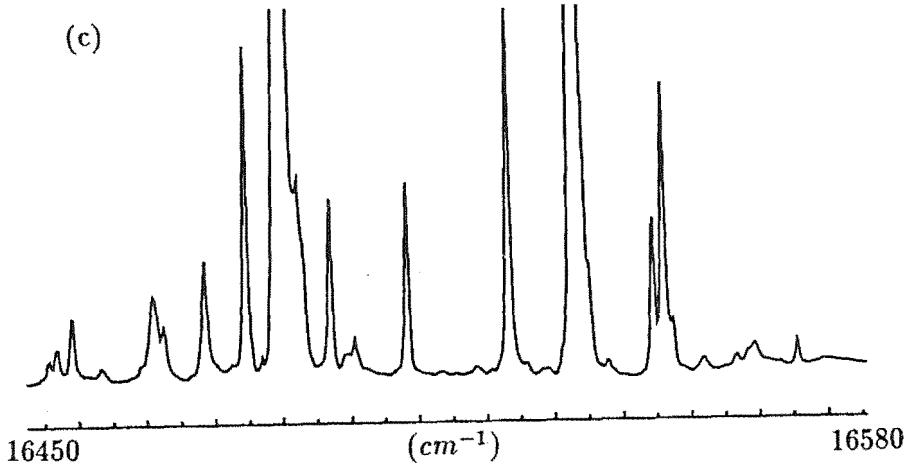
(c)
16450
(cm^{-1})
16580

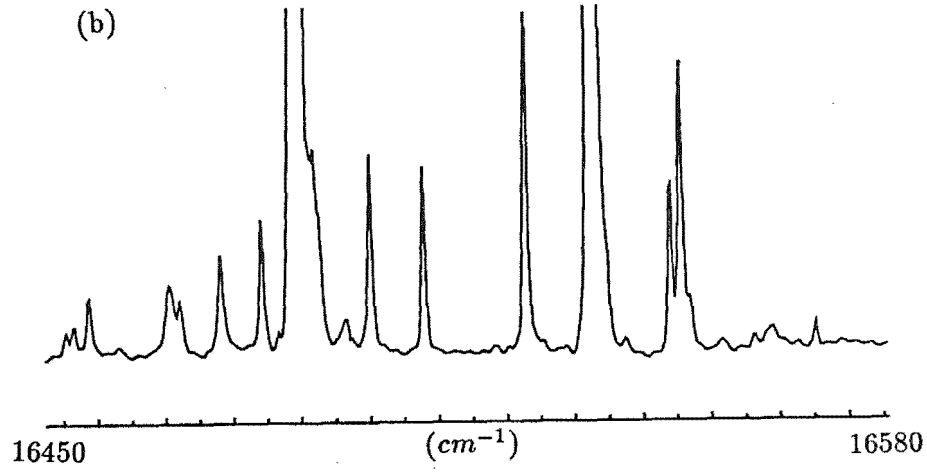
(b)
16450
(cm^{-1})
16580

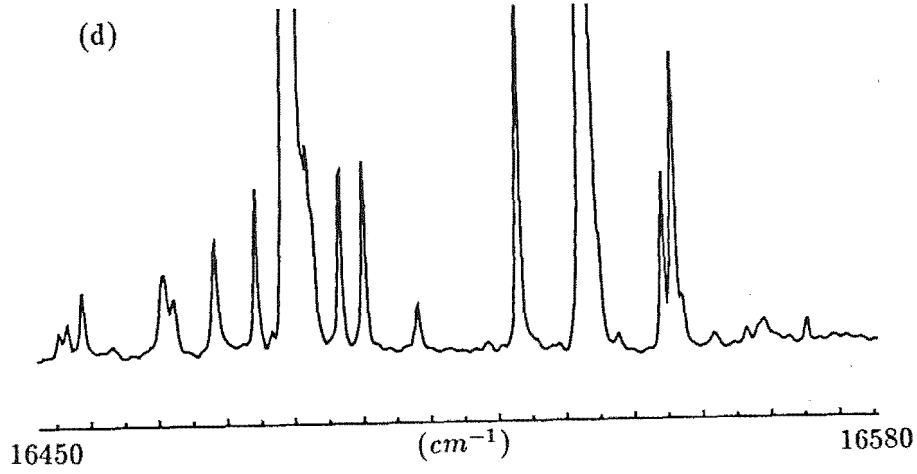
(d)
16450
(cm^{-1})
16580

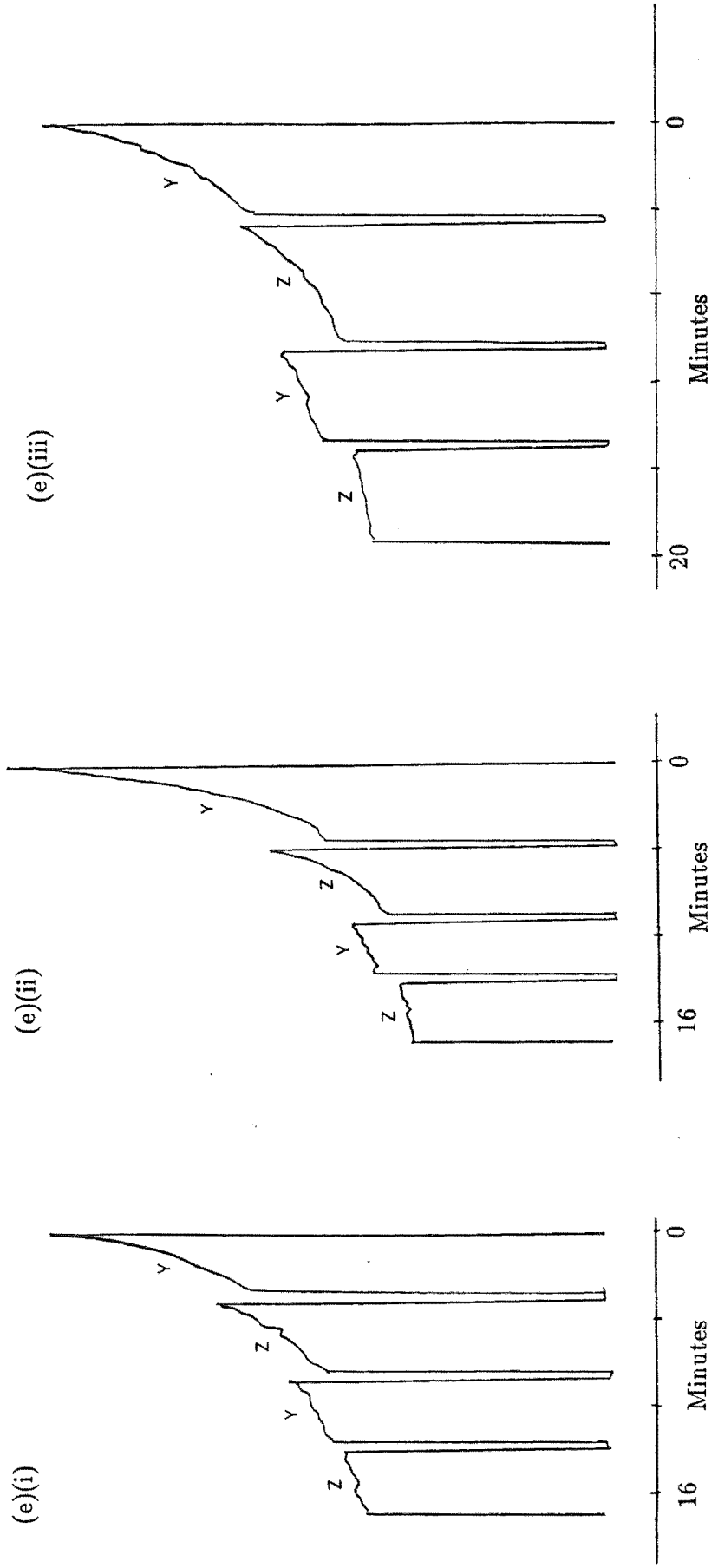
(e)(iii)
Y
Z
Y
Z
0
20
Minutes
(e)(ii)
Y
Z
Y
Z
0
16
Minutes
(e)(i)
Y
Z
Y
Z
0
16
Minutes

Figure 8.10 Bleaching of the $C_s(4)$ center satellites in the $Ca_{1-x}Sr_xF_2 : Pr^{3+}$ mixed crystal at 11K

(a) Before bleaching.
(b) After bleaching the $C_s(4)B$ center, no photoproduct observed.
(c) After bleaching the $C_s(4)A$ center, one photoproduct observed at $16608cm^{-1}$(the transition labelled with an asterisk).
(d) After exciting the photoproduct transition at $16608cm^{-1}$, some restoration of the $C_s(4)A$ center was observed and another peak was seen to appear at $16852cm^{-1}$(labelled with an asterisk).
(e)(i) & (ii) The non-reversible bleaching curves of the $C_s(4)A$ and $C_s(4)B$ respectively.

The line labelled 1 is the transition from the Z_2 level of the $C_s(4)$ center.

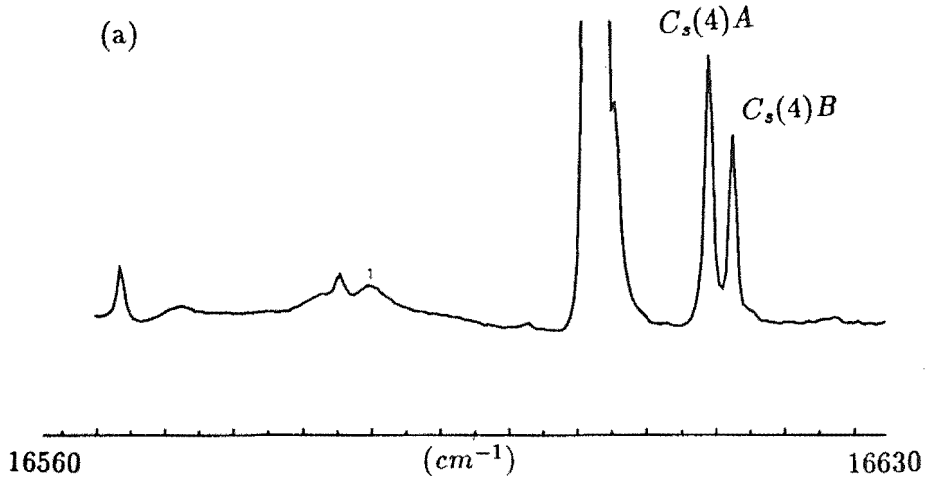
(a)
$C_s(4)A$
$C_s(4)B$
16560
(cm^{-1})
16630

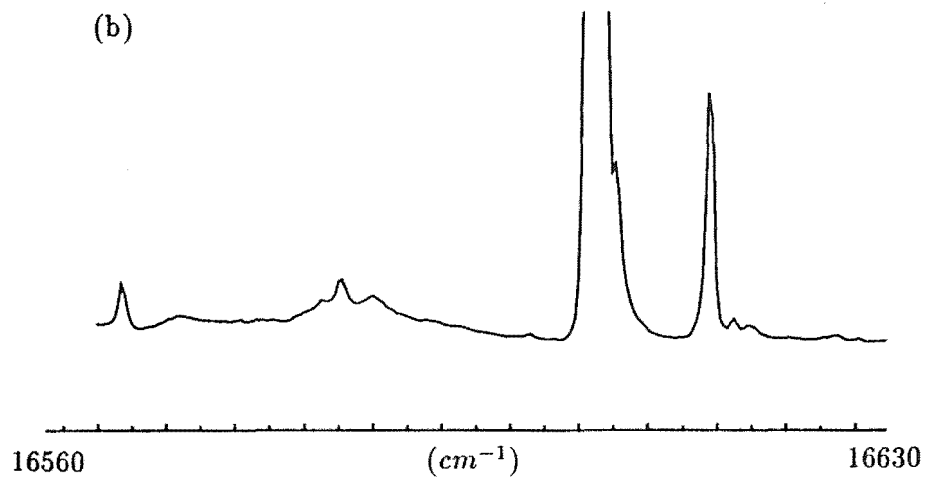
(b)
16560
(cm^{-1})
16630

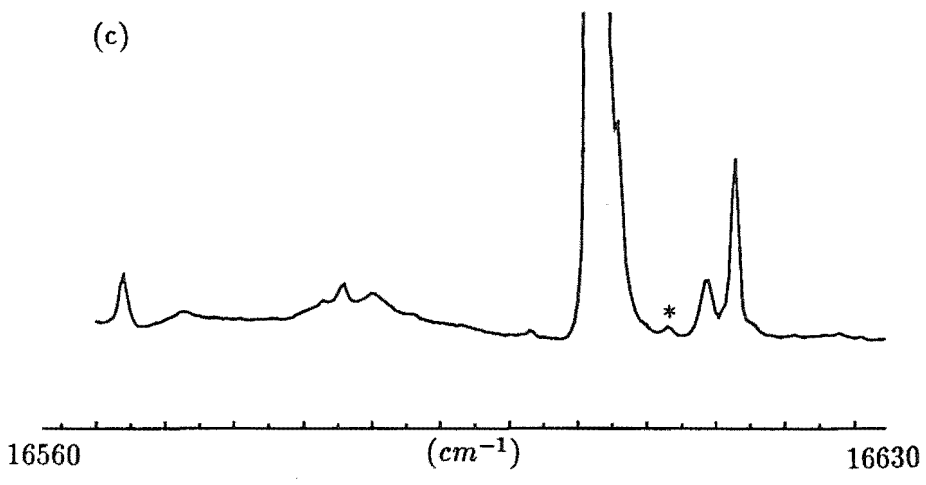
(c)
*
16560
(cm^{-1})
16630

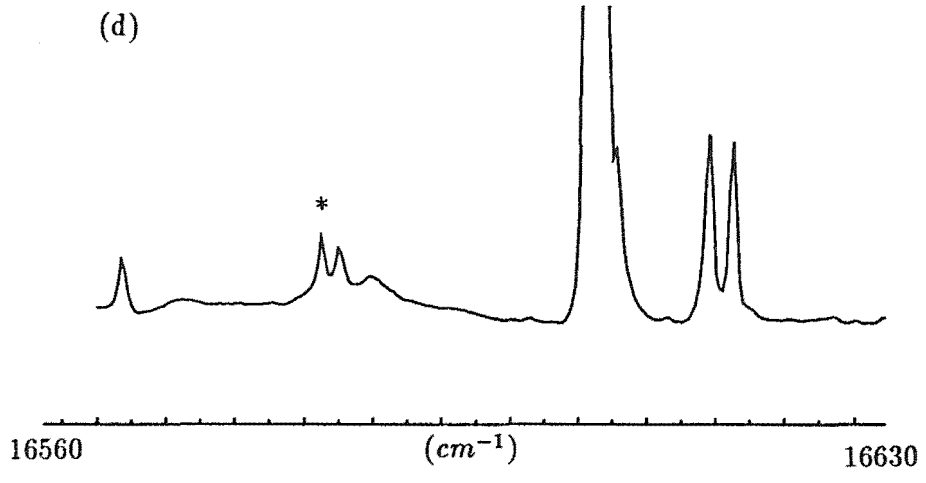
(d)
*
16560
(cm^{-1})
16630

(e)(i)

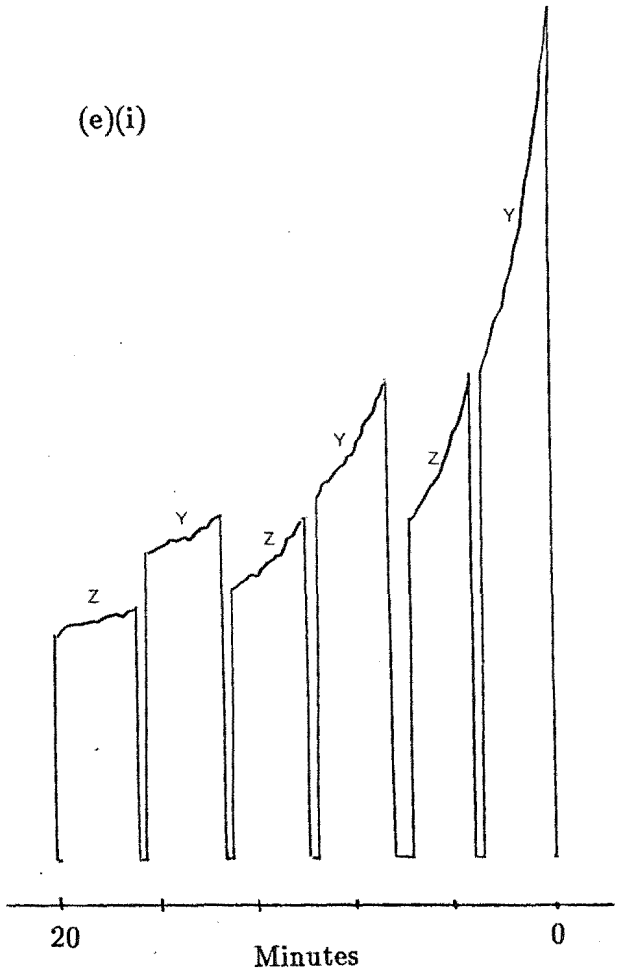

(e)(ii)

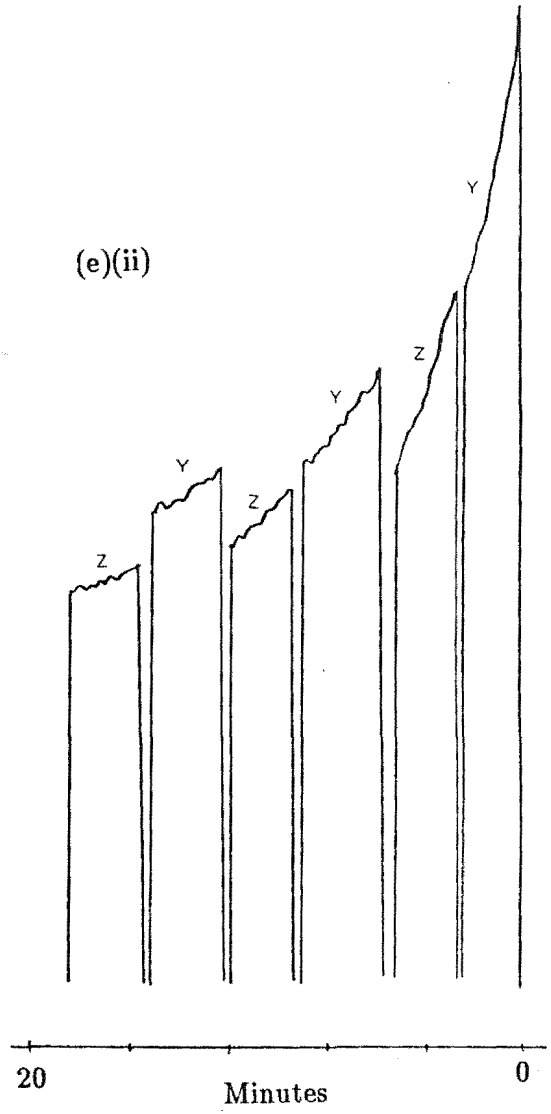

The Z_1 and Z_2 levels of $C_s(5)A$ center bleach together and after bleaching, a single photoproduct transition was observed at $16370cm^{-1}$ (fig.8.11). Pumping the photoproduct restores the bleached intensity of the $C_s(5)A$ center. There are other satellite structures associated with the $C_s(5)$ center from $16450cm^{-1}$ to $16475cm^{-1}$. They were bleached but no transitions belonging to photoproducts were apparent.

The satellite lines of the $C_s(5)B$, $C_s(5)C$, $C_s(5)D$ and $C_s(5)E$ centers (fig. 8.9(a)) were bleached but no obvious photoproducts were observed.

8.2.2 Bleaching Centers in $Sr_{1-x}Ca_xF_2 : Pr^{3+} : D^-$

While the parent $C_s(1)$ to $C_s(5)$ bleaching centers appear to be equivalent in both the CaF_2 and SrF_2 hosts, the same cannot be said of all their satellites which vary in number, spectral features in the broadband excitation and bleaching behaviour. This is further evidence that the mixed crystal centers in the $Sr_{1-x}Ca_xF_2 : Pr^{3+} : D^-$ and $Ca_{1-x}Sr_xF_2 : Pr^{3+} : D^-$ crystal systems have significantly different structures. This section present the results of the work done on the bleaching of the satellite structures in the $Sr_{1-x}Ca_xF_2 : Pr^{3+} : D^-$ crystal with 5, 5, 3 and 1 satellite centers studied for the $C_s(1)$, $C_s(2)$, $C_s(3)$ and $C_s(4)$ centers respectively. The satellite centers for the $C_s(5)$ center were too closely overlapped to be properly studied.

The $C_s(1)$ satellites

Figure 8.12(a) displaying the broadband excitation around the $C_s(1)$ region may be used as a reference to compare with a spectrum after a satellite center has been bleached. Five satellite centers associated with the $C_s(1)$ center labelled $C_s(1)A$ to $C_s(1)E$ are studied and the results from the LSE study of these centers are presented below.

The $C_s(1)A$ center

8.11(a)

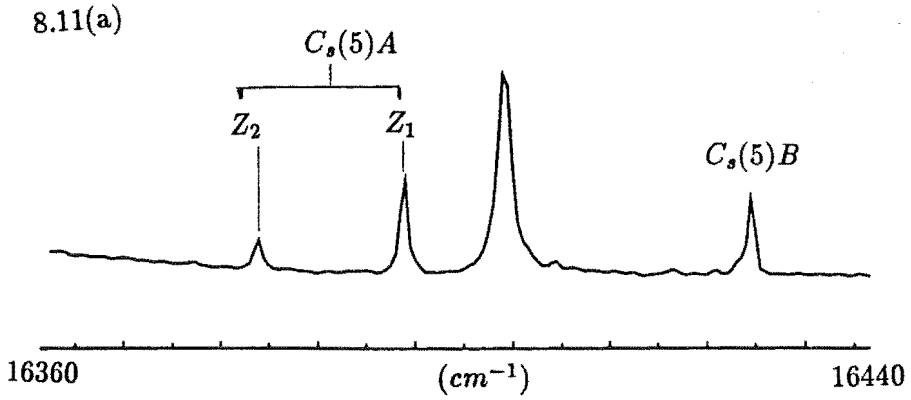

8.11(b)

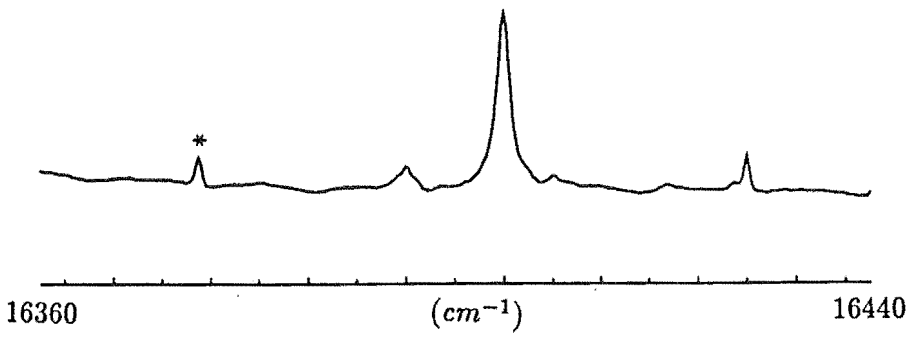

8.11(c)

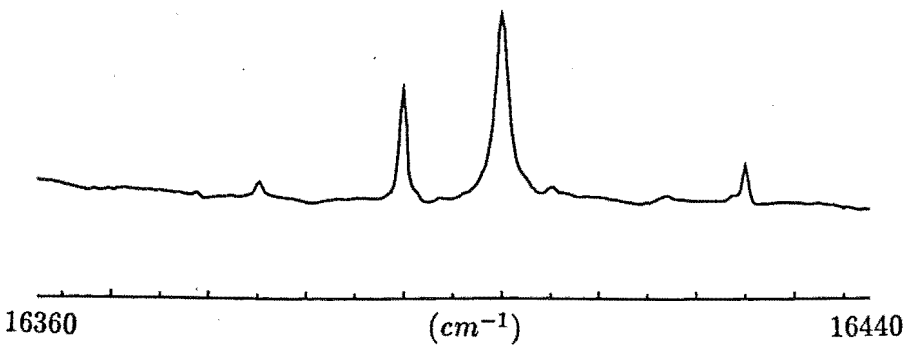

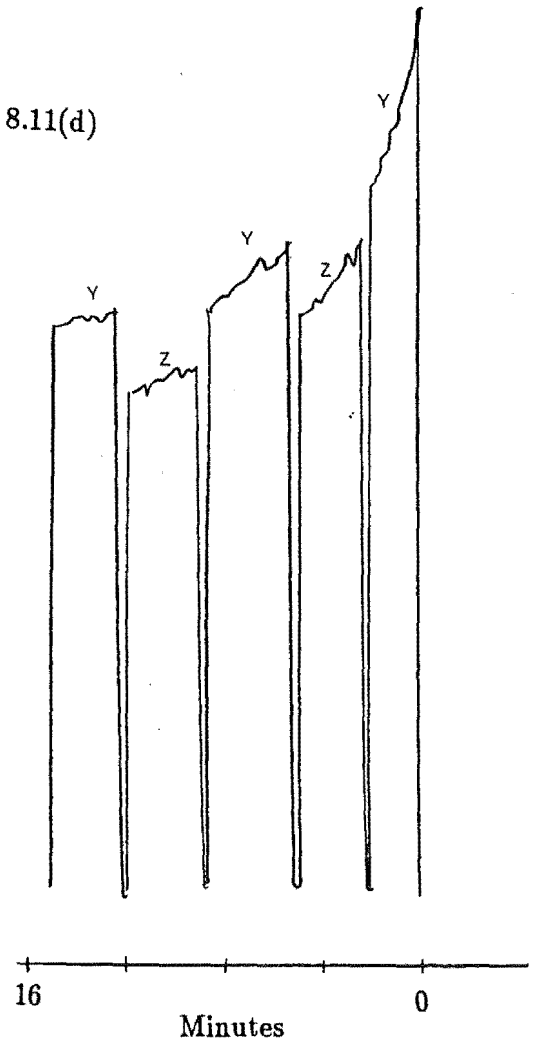

Figure 8.11 Bleaching of the $C_s(5)$ center satellites in the $Ca_{1-x}Sr_xF_2 : Pr^{3+}$ mixed crystal at 11K

(a) Before bleaching.
(b) After bleaching the Z_1 transition of the $C_s(5)A$ center, the Z_2 transition decreased in intensity as well and a single photoproduct was apparent at $16370cm^{-1}$.
(c) Bleaching the photoproduct restores both the Z_1 and Z_2 transtion.
(d) The bleaching curve of the $C_s(5)A$ center.

Table 8.2 Summary of the results from the study of the satellite bleaching centers in $Sr_{1-x}Ca_xF_2 : Pr^{3+}$.

Centers	$Z_1 \rightarrow D_1$ ($Z_2 \rightarrow D_1$) $\pm 1 cm^{-1}$	Description of emission intensity under a bleaching cycle where the laser polarisation was switched between E_Y and E_Z	Frequency of Photoproducts $\pm 1 cm^{-1}$
$C_s(1)$	16709 (16706)	Fully Recoverable	-
$C_s(1)A$	16713	partially recoverable	16685
$C_s(1)B$	16714	-	16717(?)
$C_s(1)C$	16717	Partially recoverable	16685
$C_s(1)D$	16719	Partially recoverable	-
$C_s(1)E$	16730	Partially recoverable	-
$C_s(2)$	16615 (16606)	Partially recoverable	16667
$C_s(2)A$	16619	Partial recoverable	16597
$C_s(2)B$	16620	Partial recoverable	16602
$C_s(2)C$	16621	Non recoverable	16602
$C_s(2)D$	16626	Non recoverable	16649
$C_s(2)E$	16629	Non recoverable	-

$C_s(3)$	16569 (16553)	Non recoverable	16572
$C_s(3)A$	16573	Non recoverable	16566
$C_s(3)B$	16579	Non recoverable	16555
$C_s(3)C$	16582 (16557)	Non recoverable	-
$C_s(4)$	16670	Non recoverable	16679 16668
$C_s(4)A$	16675	Partially recoverable	16686 16658

Figure 8.12 Bleaching of the $C_s(1)$ center satellites in the $Sr_{1-x}Ca_xF_2 : Pr^{3+}$ mixed crystal at 11K

(a) Before bleaching.
(b)(i) Bleaching the $C_s(1)A$ satellite produced one photoproduct apparent at $16685cm^{-1}$(labelled with an asterisk). (ii) Exciting the photoproduct, there was some recovery of the bleached intensity in the $C_s(1)A$ center.
(c) Bleaching sequence demostrating inter-conversion between satellite centers. (i) After bleaching the $C_s(2)B$ satellite, a small rise in the intensity of the $C_s(1)C$ transition was observed. (ii) Bleaching the $C_s(1)C$ transition restores the $C_s(1)B$ center as well as produces a photoproduct with a transition at $16685cm^{-1}$. (iii) Bleaching the photproduct restores the $C_s(1)C$ center.

(d) & **(e)** Bleaching of $C_s(1)D$ and $C_s(1)E$ centers respectively produced no obvious photoproduct.
(f)(i)-(v) The bleaching curves of the $C_s(1)A$, $C_s(1)B$, $C_s(1)C$, $C_s(1)D$ and $C_s(1)E$ centers respectively.

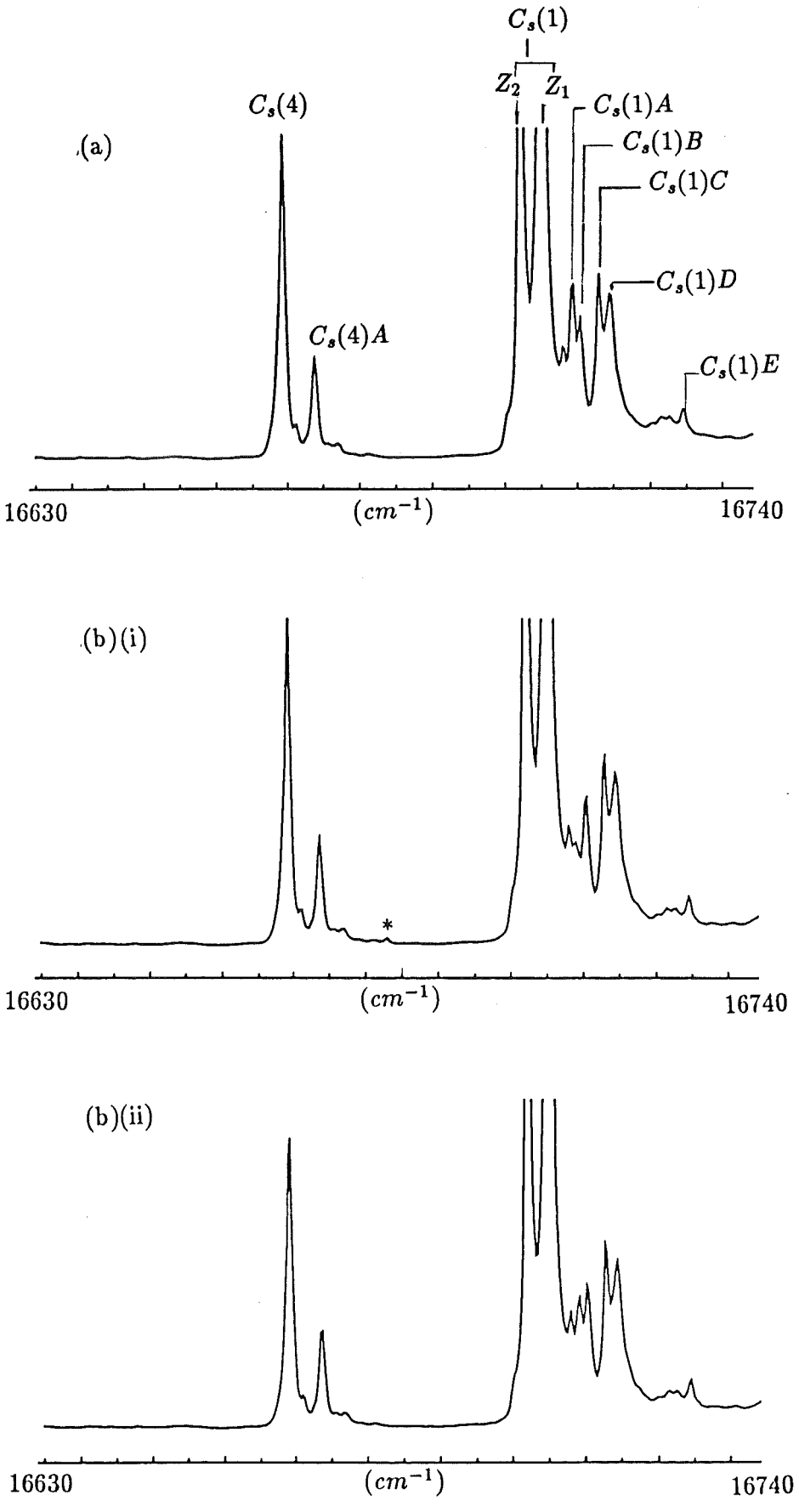
(a)
$C_s(1)$
Z_2
Z_1
$C_s(4)$
$C_s(1)A$
$C_s(1)B$
$C_s(1)C$
$C_s(1)D$
$C_s(4)A$
$C_s(1)E$
16630
(cm^{-1})
16740
(b)(i)
*
16630
(cm^{-1})
16740
(b)(ii)
16630
(cm^{-1})
16740

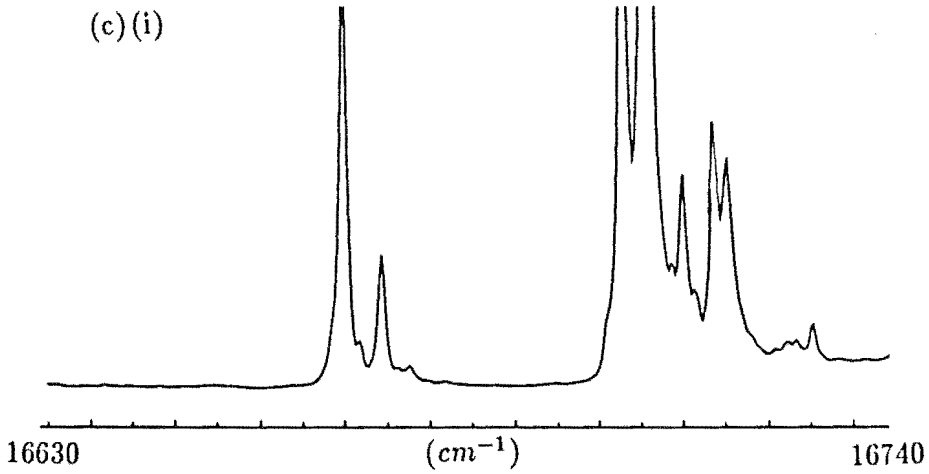
(c) (i)
16630
(cm^{-1})
16740

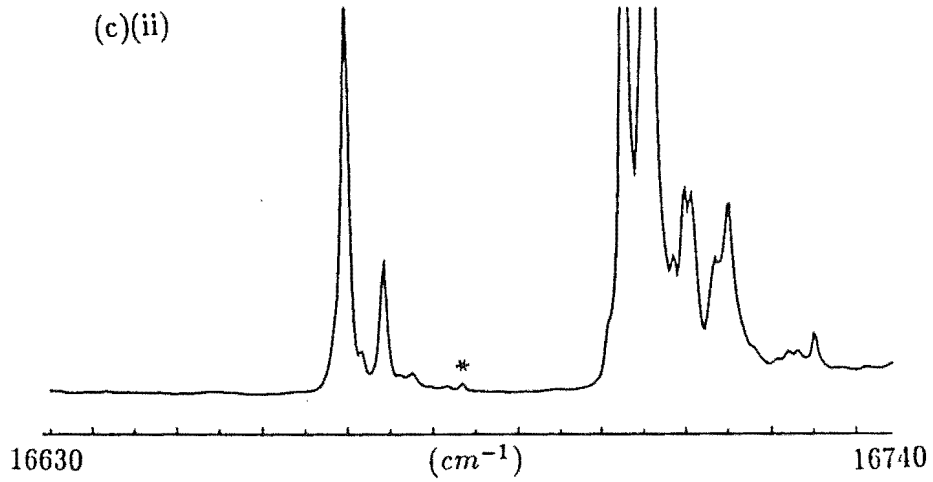
(c)(ii)
*
16630
(cm^{-1})
16740

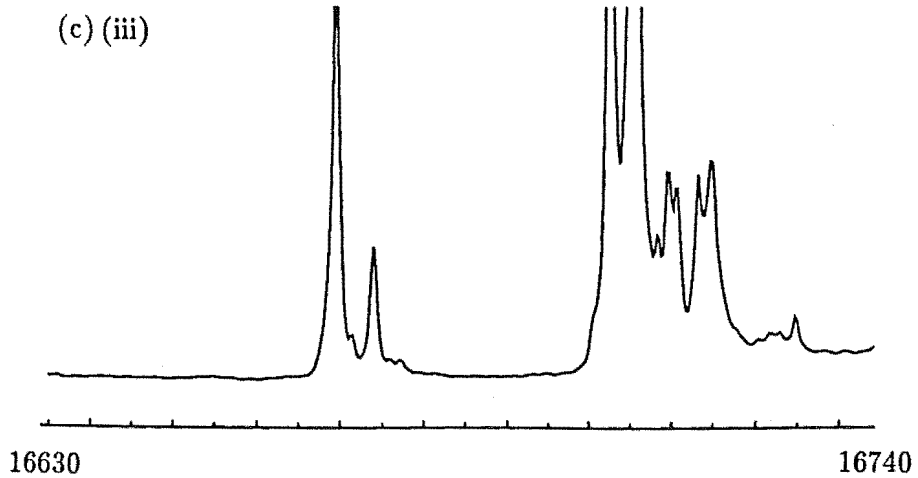
(c) (iii)
16630
16740

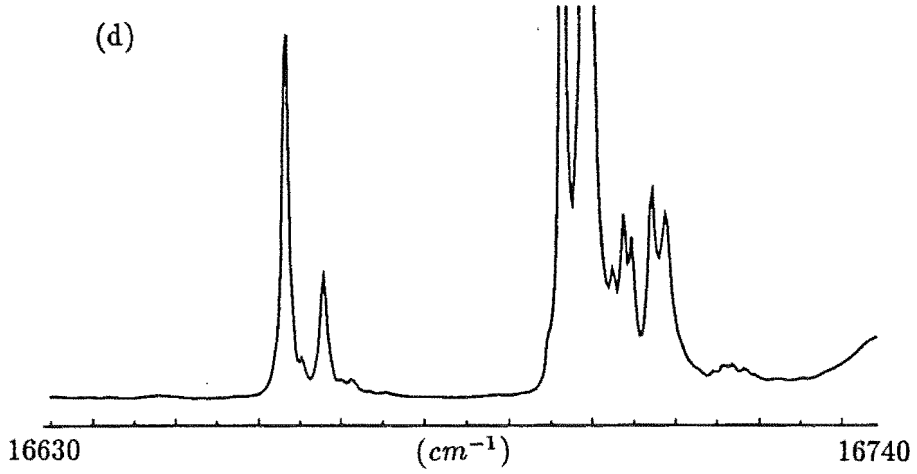
(d)
16630
(cm^{-1})
16740

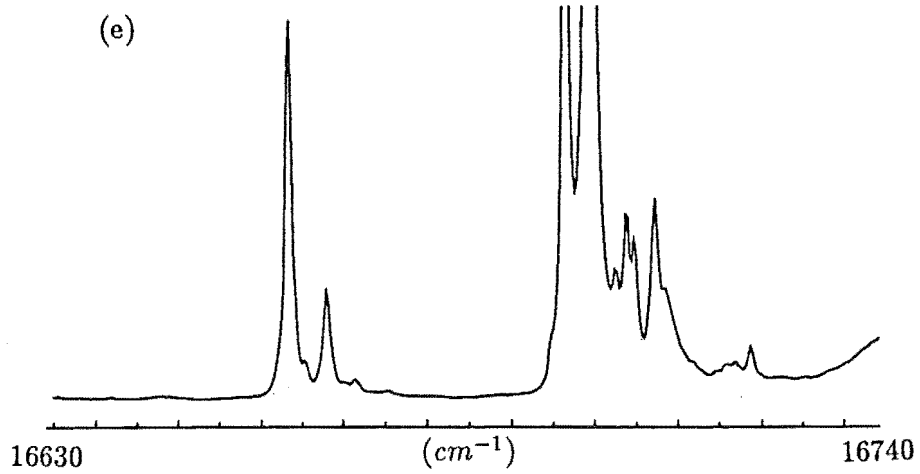
(e)
16630
(cm^{-1})
16740

(f)(i)

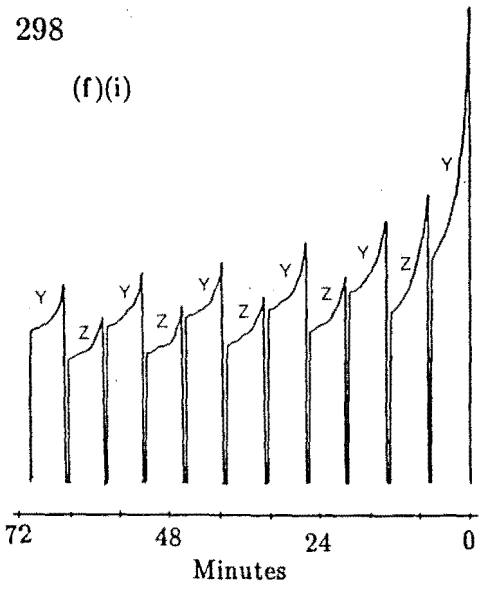

8.12(f)(ii)

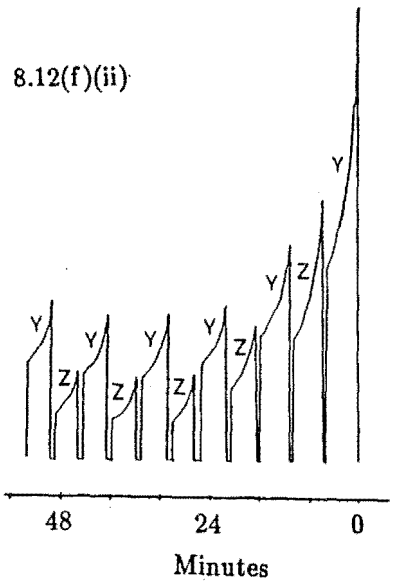

8.12(f)(iii)

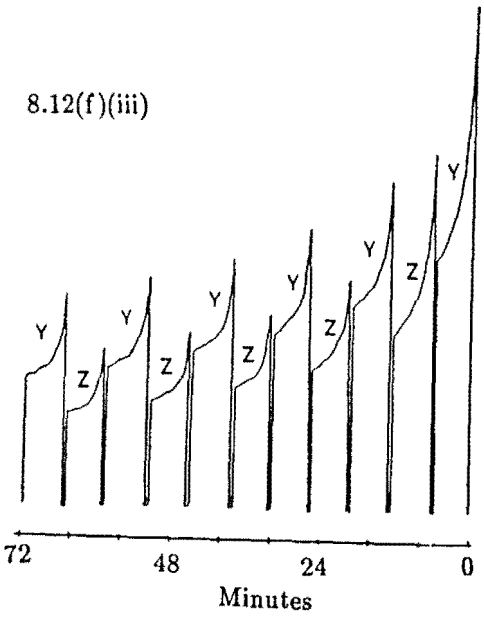

8.12(f)(iv)

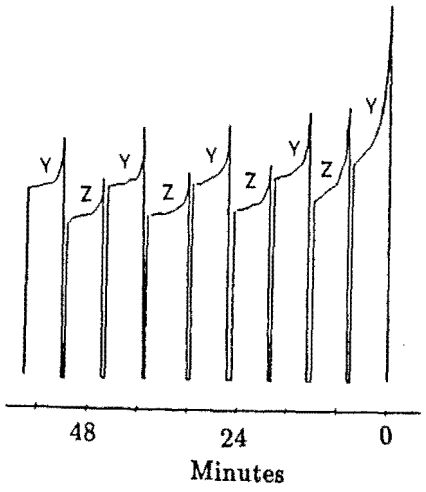

8.12(f)(v)

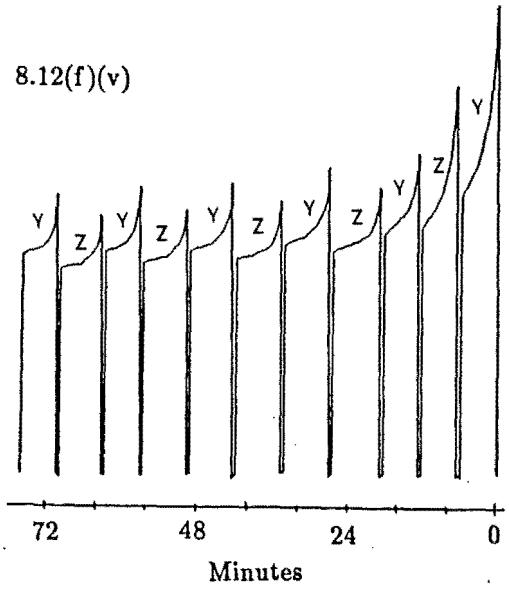

After bleaching the $C_s(1)A$ satellite line, a small rise of intensity at $16685cm^{-1}$ was found to be a photoproduct of the $C_s(1)A$ satellite (fig.8.12(b)). After bleaching the photoproduct, some partial recovery in the $C_s(1)A$ center was apparent. The bleaching cycle shows that this center bleaches reversibly after the first few cycles (fig.8.12(f)).

The $C_s(1)B$ and $C_s(1)C$ centers

Following the bleaching sequence shown in figures 8.12(c)(i) to (iii), the bleaching of $C_s(1)B$ center produces no photoproduct though a small rise in the intensity of the $C_s(1)C$ center transition was observed. When the laser was tuned to excite the $C_s(1)C$ center transition after bleaching the $C_s(1)B$ center, the $C_s(1)C$ center bleaches while the $C_s(1)B$ center recovers and exceeds its initial intensity. A photoproduct was also observed at $16685cm^{-1}$ at the exact position where the $C_s(1)A$ photoproduct was found, after bleaching the $C_s(1)C$ center. By exciting the photoproduct, it is possible to recover partially the $C_s(1)C$ satellite. The bleaching cycles of the $C_s(1)B$ and $C_s(1)C$ centers show that their intensity is partially recoverable (fig.8.12(f)).

The $C_s(1)D$ and $C_s(1)E$ centers

Both the $C_s(1)D$ and $C_s(1)E$ centers have bleaching cycles which are also partially recoverable (figs.8.12(f))). The excitation spectra after bleaching revealed no new transitions (fig.8.12(d) & (e)). The other transition at $16712cm^{-1}$ between the line of the $C_s(1)$ parent center and the $C_s(1)A$ center (fig.8.12(a)) bleaches as well with no photoproduct apparent after bleaching.

The $C_s(2)$ satellites

The broadband excitation spectrum around the $C_s(2)$ region before any bleaching is shown in figure 8.13(a). The $C_s(2)$ satellite structures investigated comprise the centers $C_s(1)A$ to $C_s(1)E$ which are discussed below.

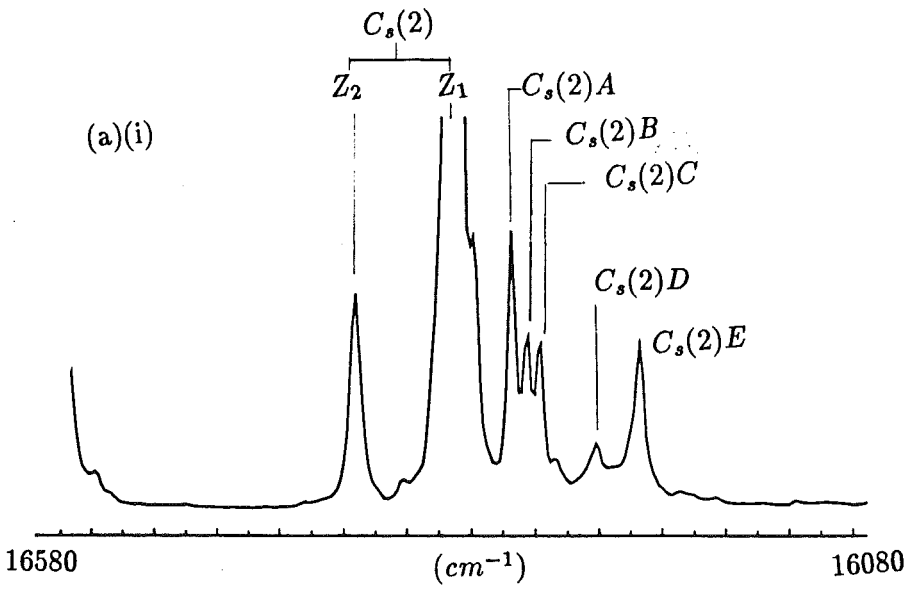

Figure 8.13 Broadband excitation spectrum of the $C_s(2)$ center and its satellites in the $Sr_{1-x}Ca_xF_2 : Pr^{3+}$ mixed crystal at 11K

(a) Before bleaching.
(b)(i) After bleaching the $C_s(2)A$ center. One photoproduct with a weak transition intensity is observed at $16597cm^{-1}$(marked with asterisk). (ii) After bleaching the photproduct, some restoration of the $C_s(2)A$ center occurred.
(c)(i)& (ii) As for **(b)** except now bleaching the $C_s(2)B$ center and the photproduct transtion is at $16602cm^{-1}$.
(d)(i)& (ii) As for **(b)** except now bleaching the $C_s(2)C$ center and the photproduct transtion is at $16603cm^{-1}$.
(e) Bleaching the $C_s(2)D$ center, a photproduct was formed with transition at $16649cm^{-1}$.
(f) Bleaching the $C_s(2)E$ center did not produce any obvious photoproduct. Further sturctures are apparent under the under the $C_s(2)E$ transition.
(g)(i)-(v) The bleaching cycles of the $C_s(2)A$, $C_s(2)B$, $C_s(2)C$, $C_s(2)D$ and $C_s(2)E$ centers respectively.

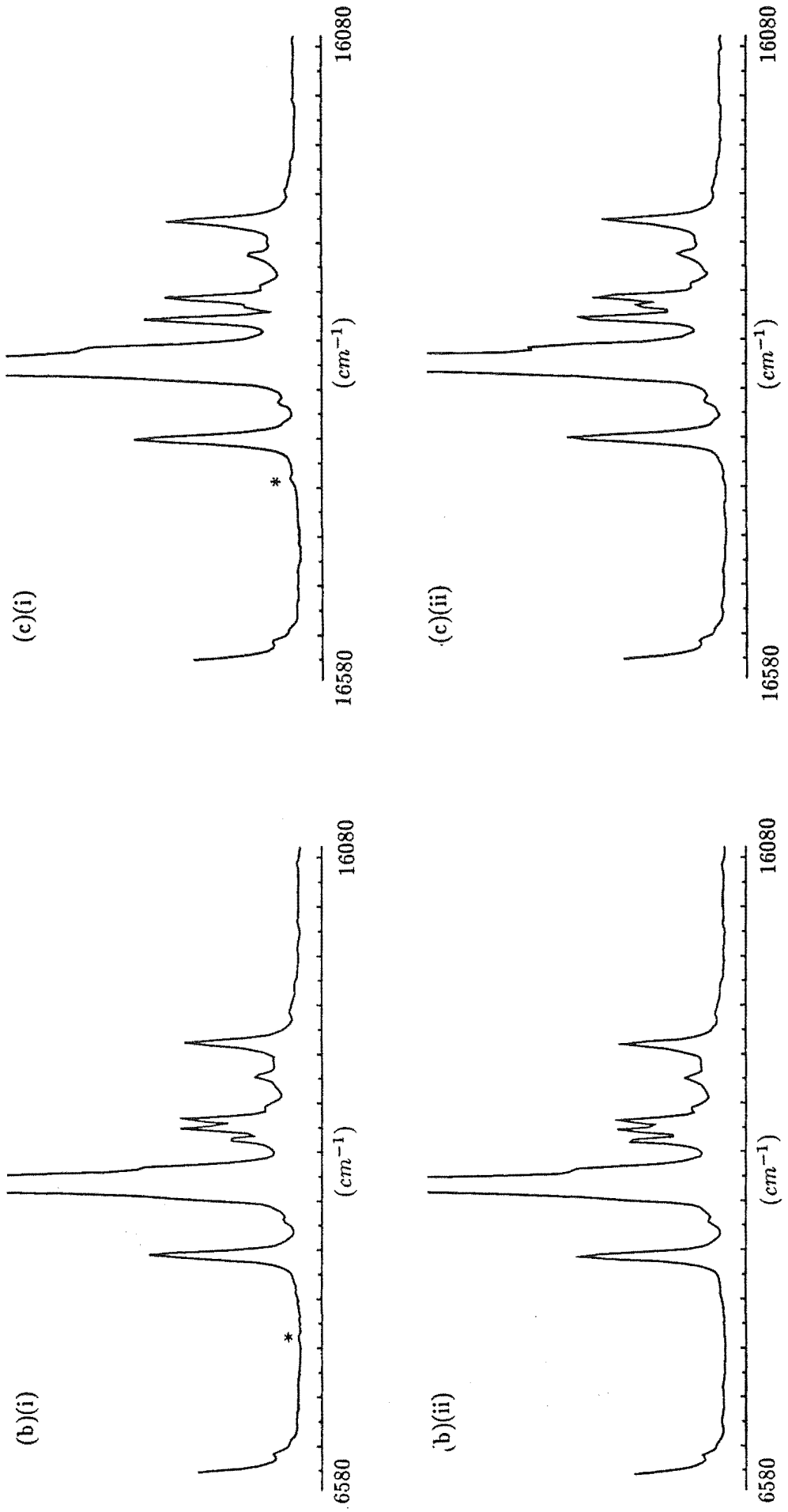
(c)(i)
16580
16080
(cm^{-1})
*
(c)(ii)
16580
16080
(cm^{-1})
(b)(i)
6580
16080
(cm^{-1})
*
(b)(ii)
6580
16080
(cm^{-1})

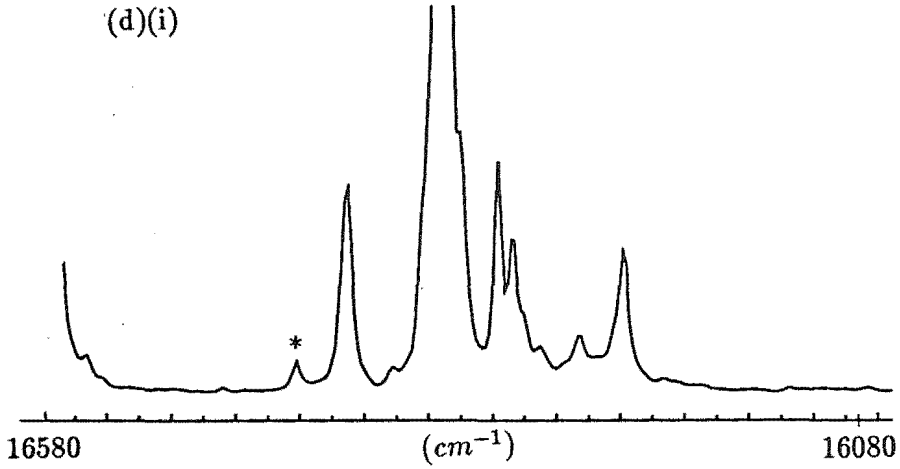
(d)(i)
*
16580
(cm^{-1})
16080

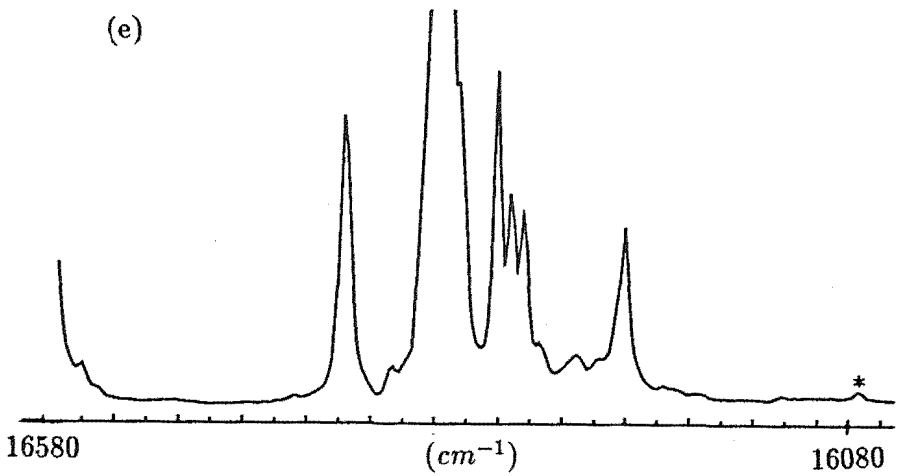
(e)
*
16580
(cm^{-1})
16080

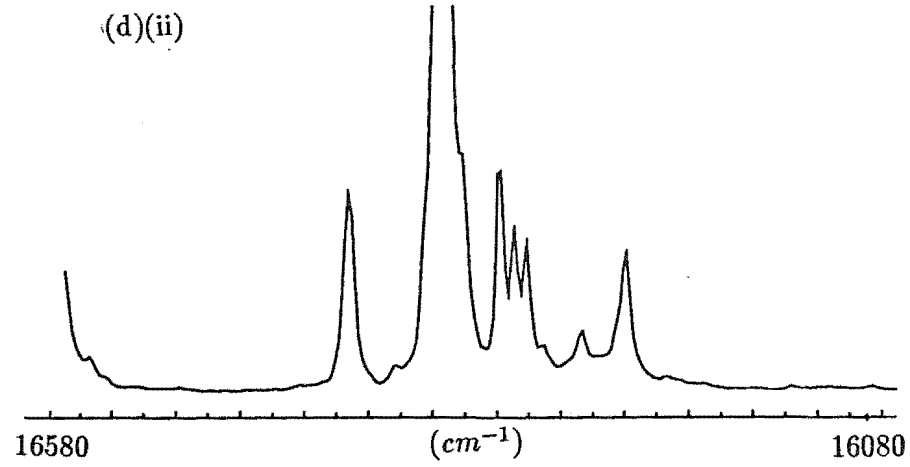
(d)(ii)
16580
(cm^{-1})
16080

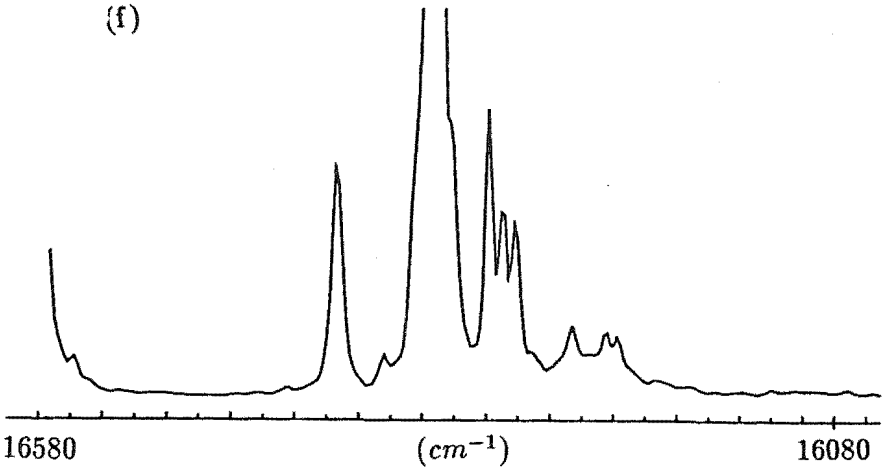
(f)
16580
(cm^{-1})
16080

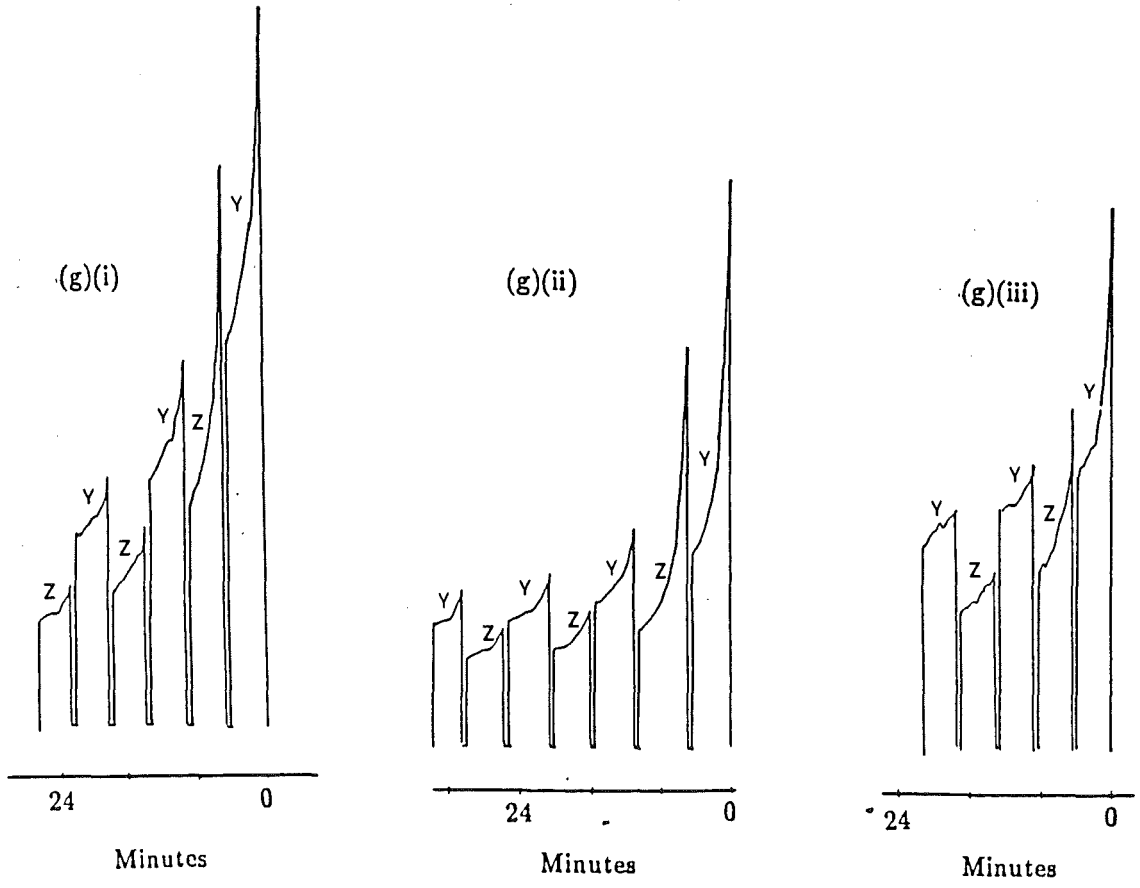
(g)(i)
Y
Y
Z
Y
Z
Z
24
0
Minutes
(g)(ii)
Y
Z
Y
Z
Y
Z
Y
24
0
Minutes
(g)(iii)
Y
Z
Y
Z
Y
24
0
Minutes

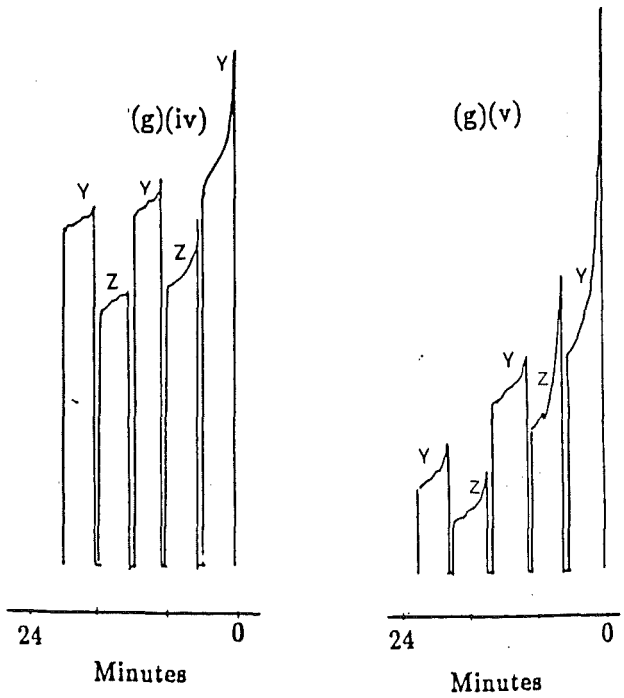
(g)(iv)
Y
Z
Y
Z
Y
24
0
Minutes
(g)(v)
Y
Z
Y
Z
Y
24
0
Minutes

The $C_s(2)A$ and $C_s(2)B$ centers

Like their parent center, the $C_s(2)A$ and $C_s(2)B$ centers undergo reversible bleaching with partial recovery of their intensity (fig. 8.13(g)) after a few bleaching cycles. Photoproduct transitions are just discernable at $16597cm^{-1}$ and $16602cm^{-1}$ after bleaching the centers $C_s(2)A$ and $C_s(2)B$ respectively. By exciting these photoproduct, it was possible to recover the $C_s(2)A$ and $C_s(2)B$ centers (fig. 8.13(b) & (c)).

The $C_s(2)C$, $C_s(2)D$ and $C_s(2)E$ centers

These three centers do not exhibit reversible bleaching (fig. 8.13 (g)) with photoproduct transitions apparent after the $C_s(2)C$ and $C_S(2)D$ centers were bleached (figs. 8.13(d) & (e)). The photoproduct transitions were recorded at $16602cm^{-1}$ and $16649cm^{-1}$ for the $C_s(2)C$ and $C_s(2)D$ centers respectively. No photoproduct transitions were observed after bleaching the $C_s(2)E$ center.

The $C_s(3)$ satellites

The $C_s(3)A$, $C_s(3)B$ and $C_s(3)C$ centers

Figure 8.14(a) shows the typical excitation spectrum before any of the $C_s(3)$ satellite centers were bleached. The bleaching cycles for all three centers are non-reversible (fig. 8.14(e)). After bleaching the $C_s(3)A$ and $C_s(3)B$ centers, photoproduct transitions were found at $16566cm^{-1}$ and $16555cm^{-1}$ respectively (fig. 8.14(b) & (c)). The bleached intensity of both the $C_s(3)A$ and $C_s(3)B$ centers can be restored by excitation of their photoproduct transitions. The $C_s(3)C$ center bleaches with no obvious photoproduct transitions being produced. The line at $15557cm^{-1}$ is assigned the Z_2 level of the $C_s(3)C$ center as it bleaches with the Z_1 level at $15582cm^{-1}$.

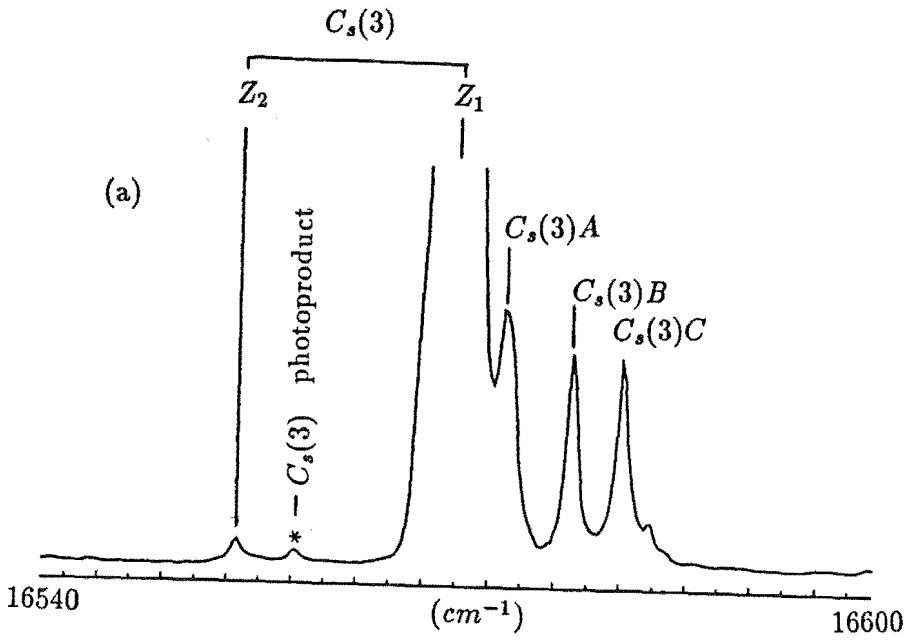

Figure 8.14 Bleaching of the $C_s(3)$ center satellites in the $Sr_{1-x}Ca_xF_2 : Pr^{3+}$ mixed crystal at 11K

(a) Before bleaching any of the satellites.
(b)(i) After bleaching the $C_s(3)A$ center. One photoproduct with a transition observed at $16566cm^{-1}$(marked with asterisk). (ii) After bleaching the photproduct, some restoration of the $C_s(3)A$ center occured.
(c) As for **(b)** except bleaching the $C_s(3)B$ center and the photproduct is at $16555cm^{-1}$
(d) Bleaching the $C_s(3)C$ center revealed further structures under this center as well. The arrow indicate the position of the Z_2 transition of the $C_s(3)C$ center which bleach with the Z_1 transition.
(e)(i)-(iii) The bleaching curves of the $C_s(3)A$, $C_s(3)B$ and $C_s(3)C$ centers respectively.

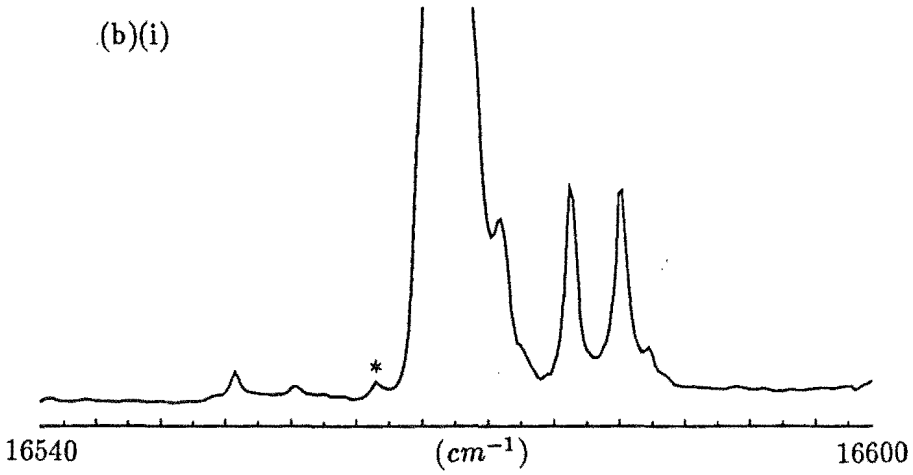
(b)(i)
*
16540
(cm^{-1})
16600

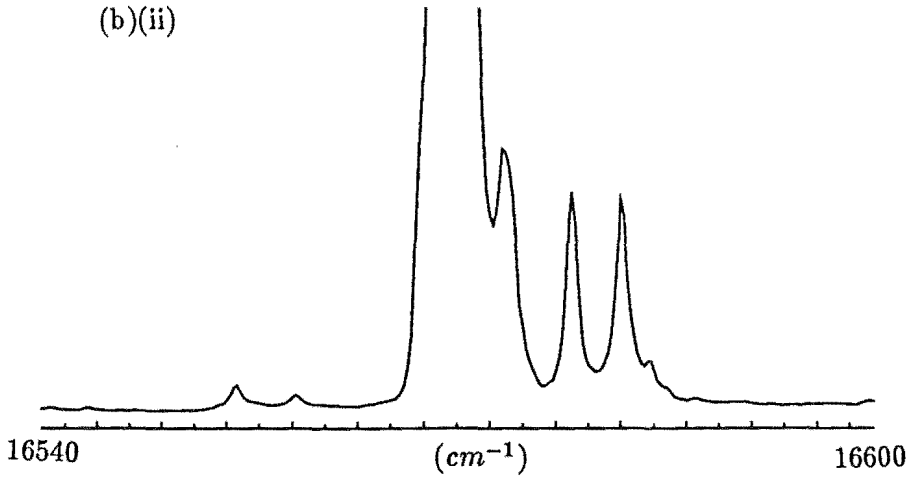
(b)(ii)
16540
(cm^{-1})
16600

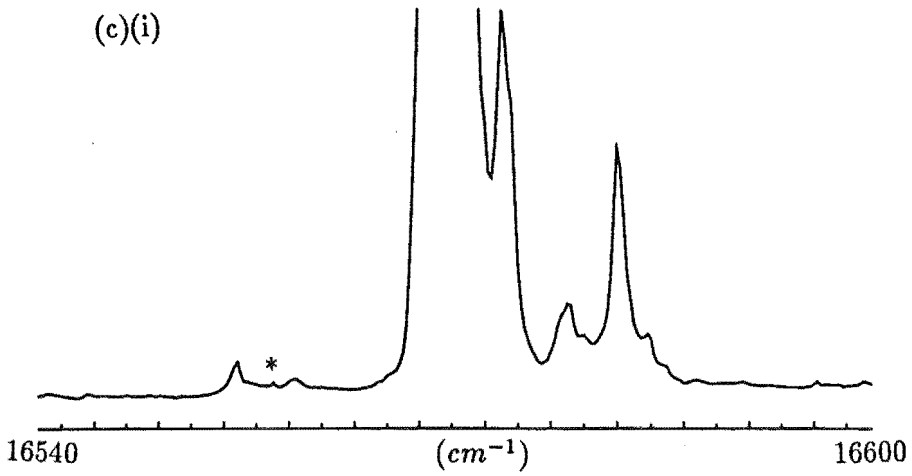
(c)(i)
*
16540
(cm^{-1})
16600

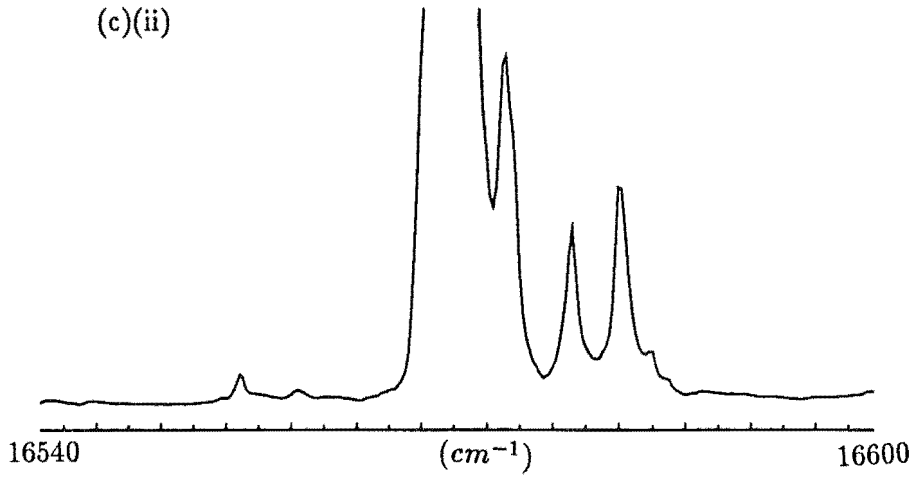
(c)(ii)
16540
(cm^{-1})
16600

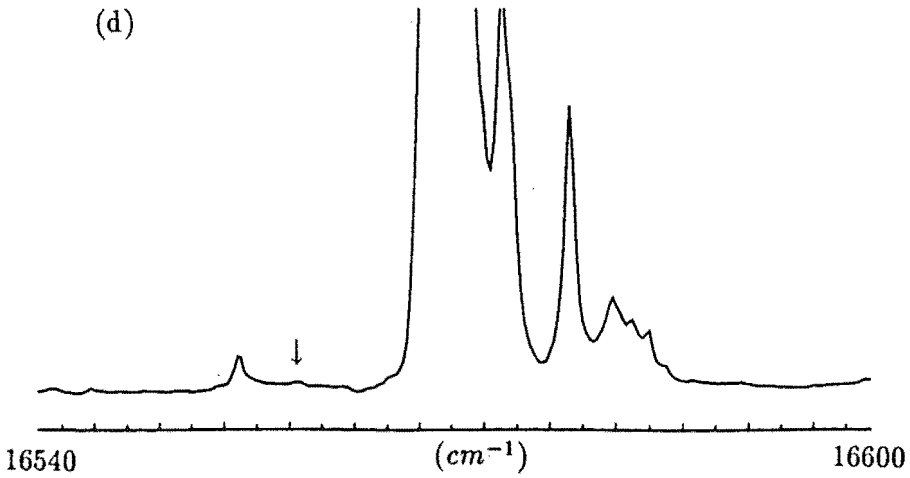
(d)
↓
16540
(cm^{-1})
16600

(e)(i)

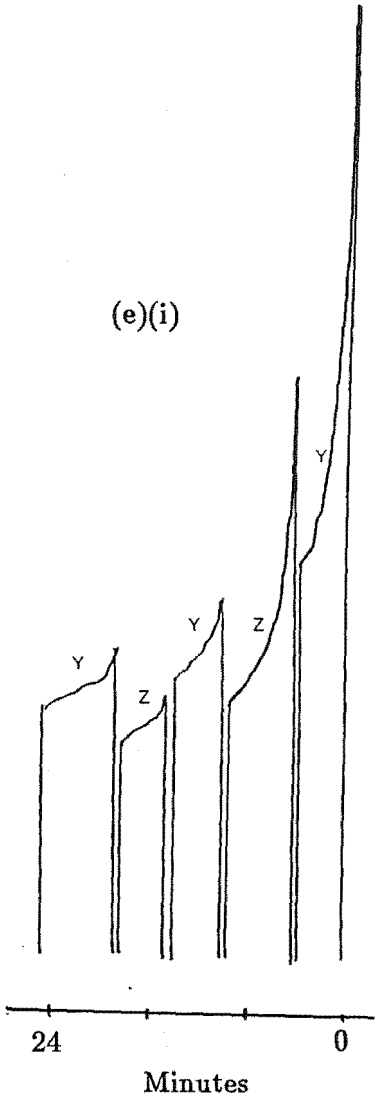

(e)(ii)

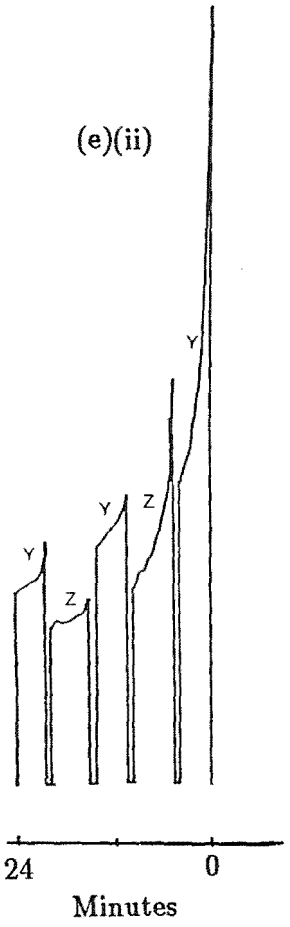

(e)(iii)

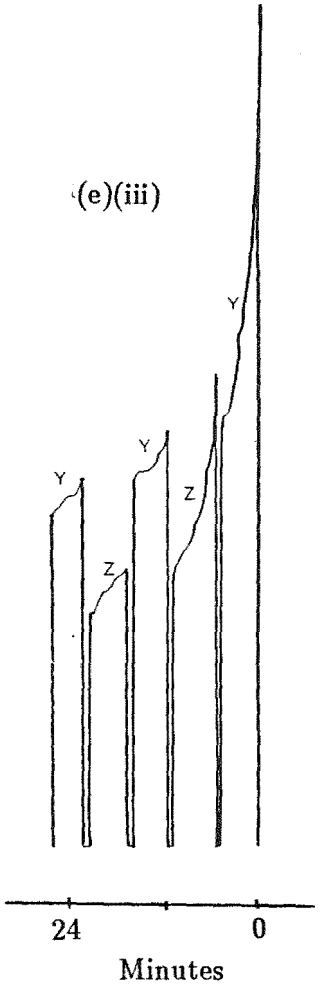

The $C_s(4)$ satellite

The $C_s(4)A$ center

Only one $C_s(4)$ satellite was studied and is labelled $C_s(4)A$ in figure 8.15(a). The bleaching cycle of this center (fig. 8.15(c)) shows that it is not completely reversible. After bleaching, it also has two photoproducts like its parent , labelled P1 and P2 , and exciting both the P1 and P2 photoproducts of this center partially recovers the bleached intensity of the $C_s(4)A$ center.

There are also weaker transitions around the $C_s(4)A$ center. These were not studied in detail since they were too closely overlapped by each other and the $C_s(4)A$ center.

The $C_s(5)$ satellites

The prominent $C_s(5)$ satellites in this host consist of a band centered on $16529cm^{-1}$ and it appears that the transitions around this band consist of a few closely overlapping transitions. On tuning the laser to coincide with the peak frequency of this band, the intensity of the peak diminished revealing futher overlapping transitions (fig. 8.16). These were too weak and closely overlapped to be successfully studied.

8.2.3 Summary, Discussion and Possible Models

The frequencies, bleaching behaviour and photoproducts of the mixed crystal centers studied are summarized in tables 8.1 and 8.2. Apart from the simplest cases, modelling the mixed crystal bleaching centers is difficult because of the number of possibilities available with the increase in the type and number of ions that constitute the mixed crystal bleaching centers.

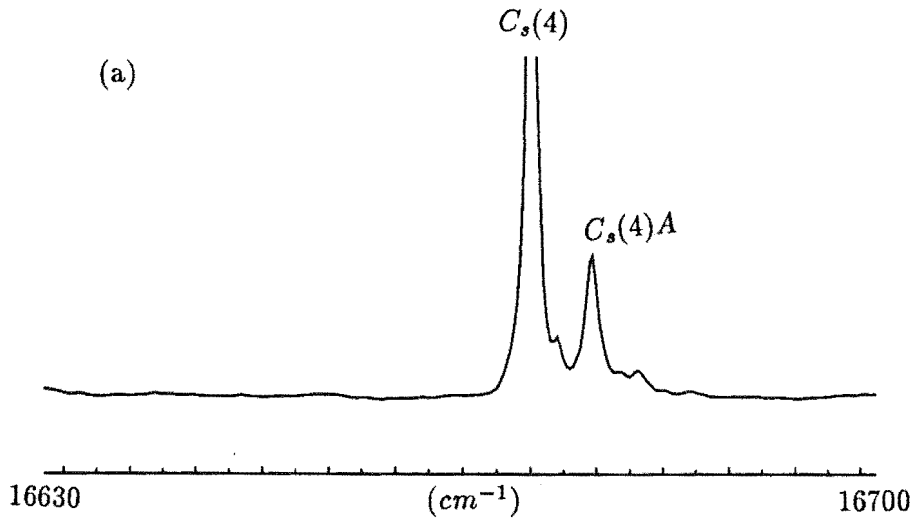
(a)
$C_s(4)$
$C_s(4)A$
16630
(cm^{-1})
16700

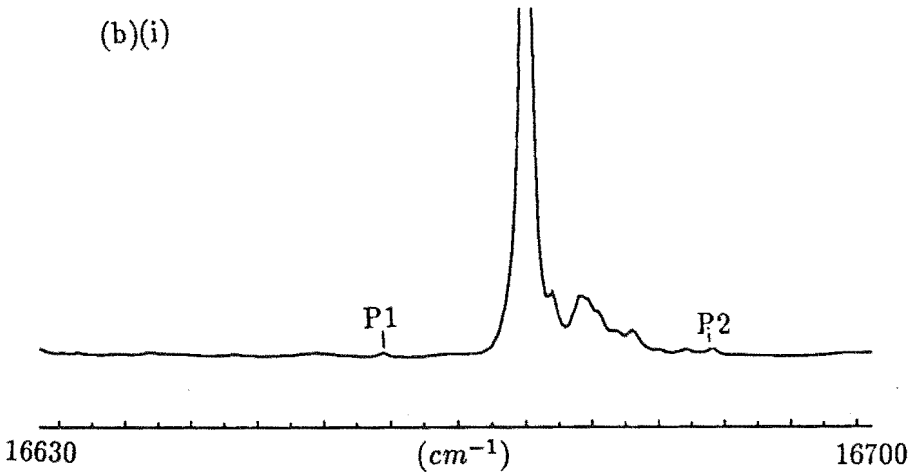
(b)(i)
P1
P2
16630
(cm^{-1})
16700

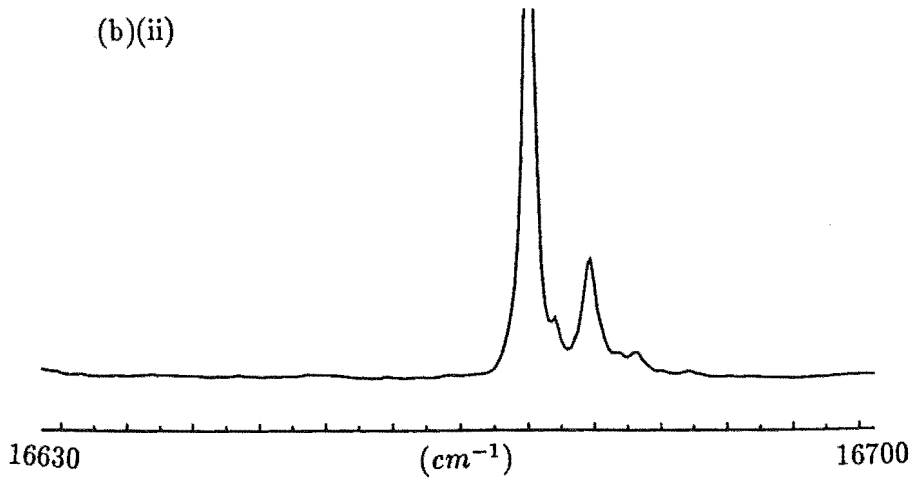
(b)(ii)
16630
(cm^{-1})
16700

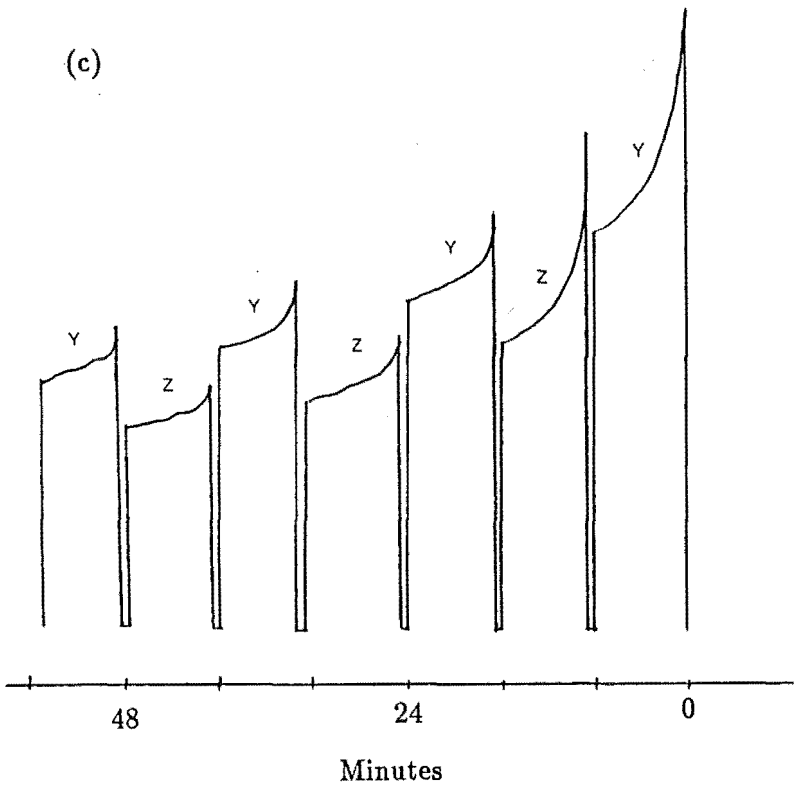

Figure 8.15 Bleaching of the $C_s(4)$ center satellites in the $Sr_{1-x}Ca_xF_2 : Pr^{3+}$ mixed crystal at 11K

(a) Before bleaching.
(b)(i) Bleaching the $C_s(4)A$ center produces two photproducts labelled P1 and P2 at $16658cm^{-1}$and $16686cm^{-1}$respectively. (ii) The excitation spectrum after bleaching both these photoproducts restores partially the bleached intensity of the $C_s(4)A$ center.
(c) The bleaching cycle of the $C_s(4)A$ center showing some partial recovery between cycles.

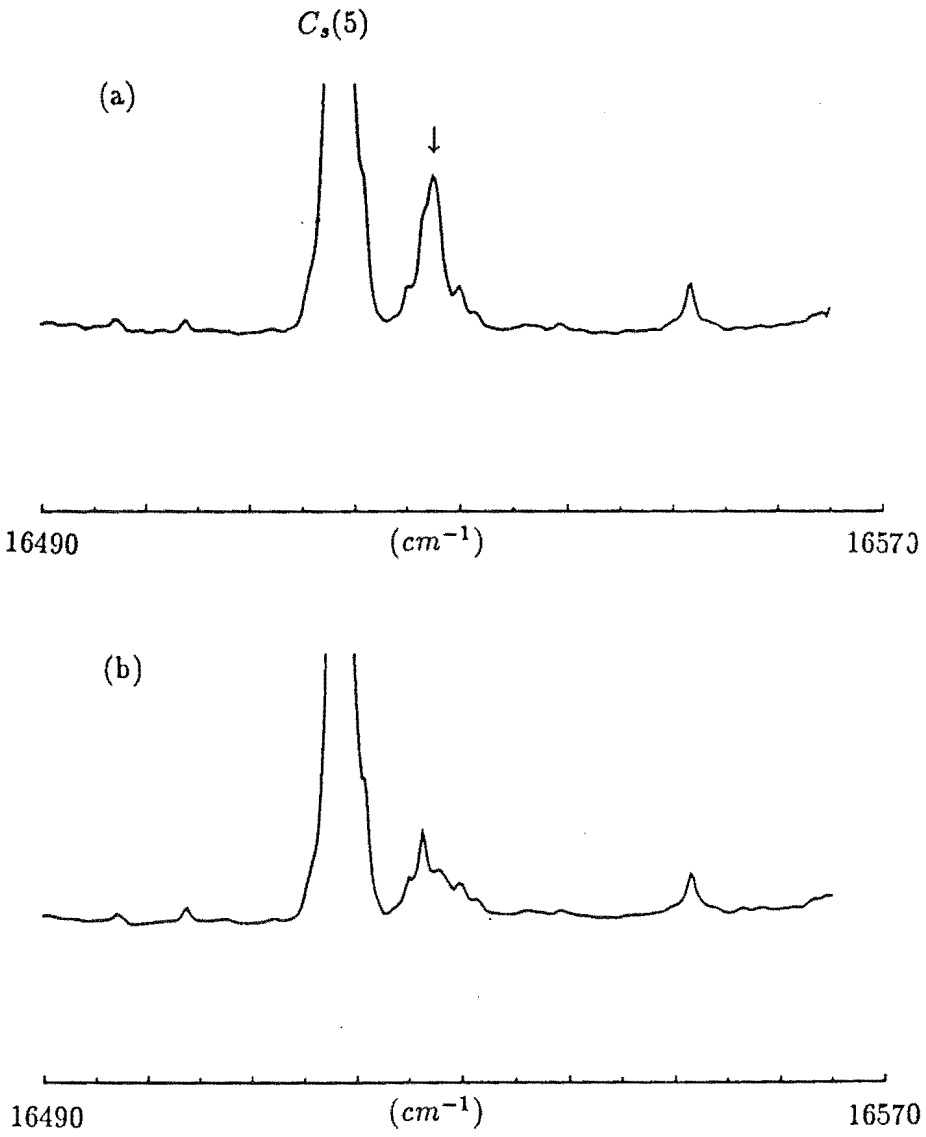

Figure 8.16 Bleaching of the $C_s(5)$ center satellites in the $Sr_{1-x}Ca_xF_2 : Pr^{3+}$ mixed crystal at 11K

(a) Before bleaching. At least four transitions contribute to the transition band marked with an arrow, which is only apparent after **(b)** exciting the peak of the band at $16529cm^{-1}$

Given that the polarisation measurements of the mixed centers studied in the Ca^{2+} doped SrF_2 crystal did not yield explicable models for the two $A3$ type mixed crystal centers previously studied, the opportunity of arriving at models for the mixed crystal bleaching centers will be remote with the spectral data available from this work, hence no attempts were made toward this goal.

In the case of the Sr^{2+} doped CaF_2 crystal, the possible substitutional positions of the alkaline earth dopant is fairly well established from previous work with the off-axis $A1$ and on-axis $A2$ mixed crystal centers as good starting configurations. Hence it is possible to deduce probable models for the satellite bleaching centers of this crystal system as presented below.

Models of mixed crystal bleaching centers in $Ca_{1-x}Sr_xF_2 : Pr^{3+}$

Bringing together the models for the mixed crystal centers shown in in figure 2.2 and the models of the multiple deuterium bleaching centers of figures 8.5, it was possible to arrive at probable models for some of the mixed crystal bleaching centers. Since definite models were proposed for the $C_s(1)$, $C_s(2)$ and $C_s(4)$ bleaching centers, the main part of the discussion in this sub-section will be concerned with how the alkaline earth dopants can be arranged to give some models for these mixed crystal satellite bleaching centers.

Models for the $C_s(1)$ satellite centers

Starting with the deuterium substitution model for the $C_s(1)$ center as shown in figure 8.5(a), and adopting the previously proposed NN cation positions that the dopant Sr^{2+} can occupy for the $A1$ center, there are only two inequivalent centers possible as shown in figures 8.17(a)(i) and (ii). For the on-axis Sr^{2+} substitution of the $A2$ center, only one possible bleaching center can be derived from the $C_s(1)$ parent center and this is shown in figure 8.17(b). Hence three bleaching sites are expected if only the $A1$ and $A2$ type cation substitutions are considered. However, four prominent $C_s(1)$ satellite centers were observed. The $A3$ center may hold the

key to the description of the fourth center and using the tentative $C_{2v}(a)$, two cation substitution model discussed in chapter 4.1.3, two further mixed crystal centers are possible.

Assigning particular transitions to a specific model is another matter and this will not be resolved with the set of spectroscopic data acquired in this work.

Models for the $C_s(2)$ satellite centers

Merging the model of the $C_s(2)$ center with the models for the $A1$ and $A2$ centers, four models of the $C_s(2)$ satellite centers emerge, shown in figure 8.18. There are only two prominent satellite lines observed in the excitation spectra of the $C_s(2)$ satellite centers (fig. 8.8(a)). It is thus concluded that not all of the proposed models for the $C_s(2)$ satellite center apply. There is insufficient information on the distortion of the lattice as a result of the deuterium substitutions to give further weight to particular models which may be more likely for the two prominent $C_s(2)$ satellite centers observed.

Models for the $C_s(4)$ satellite centers

The $C_s(4)$ center is interesting because with a $C_{2v}(a)$ symmetry configuration, it has higher symmetry than the other bleaching centers. Even with three deuterium substitutions in the local environment of the Pr^{3+} ion for the $C_s(4)$ center, there can arise only two inequivalent mixed crystal bleaching centers using the alkaline earth dopant arrangement of the $A1$ and $A2$ center models (figure 8.19). As observed, two definite $C_s(4)$ satellite centers were apparent (figure 8.10)

Models for the $C_s(3)$ and $C_s(5)$ centers

Since no models were assigned to the $C_s(3)$ and $C_s(5)$ centers, there is a lack of rational on how to present models for their satellite centers. The possibilities are not limitless when considering only two deuterium substitutions in the NN fluorine coordination shells with a single D^- interstitial in the usual C_{4v} position. These

are shown in figure 8.20. The model shown in figure 8.20(a) could probably be ruled out for the $C_s(3)$ center because it has a $C_s(a)$ symmetry configuration which is not in agreement with the polarisation ratios observed. The polarised emission spectra data suggest a lower symmetry. Attempts to propose models for the $C_s(3)$ and $C_s(5)$ satellite centers based on these would not be fruitful at this stage since it is uncertain which is the likely model for each of the parent bleaching centers.

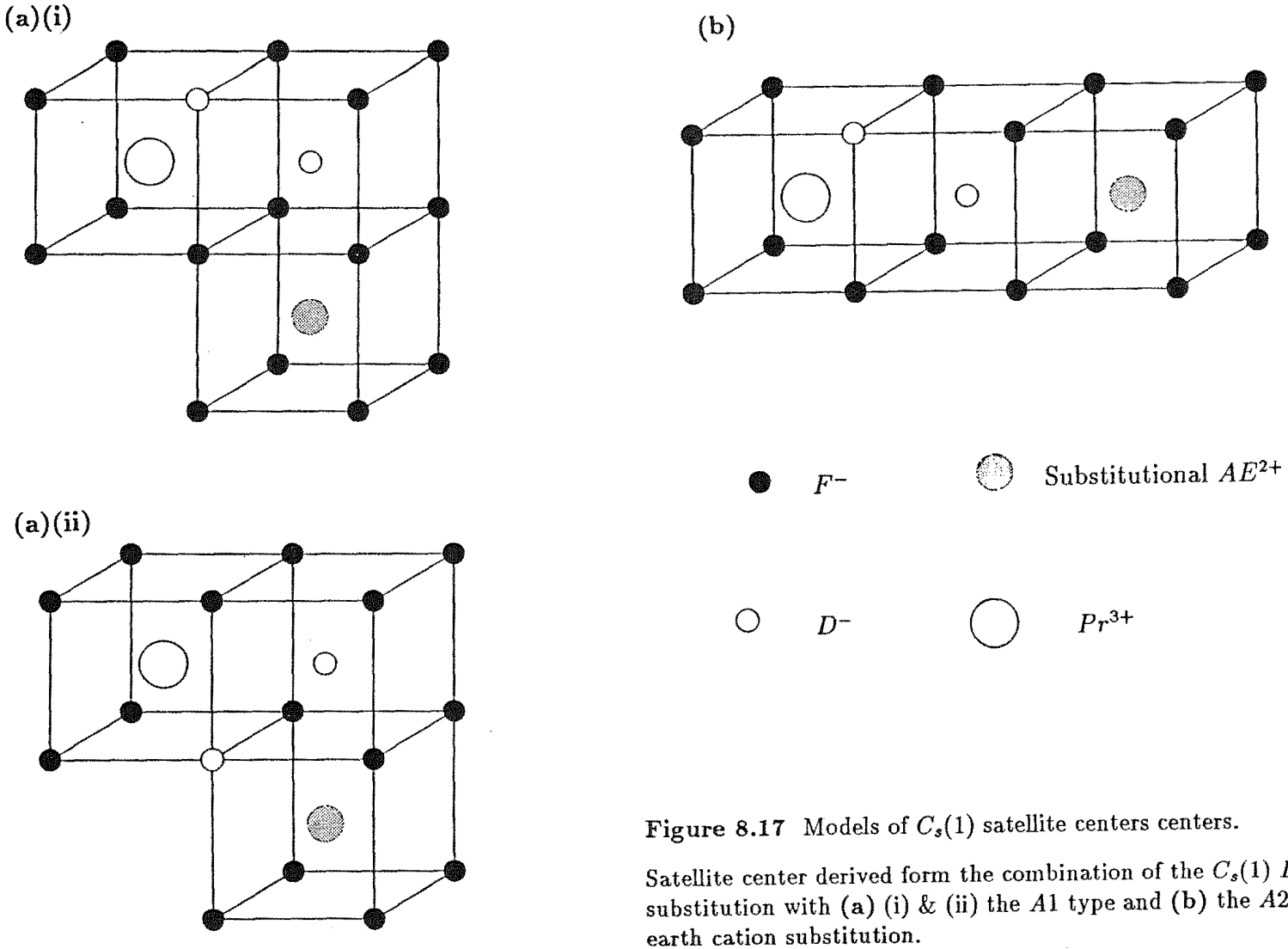

Figure 8.17 Models of $C_s(1)$ satellite centers centers.

Satellite center derived form the combination of the $C_s(1)$ D^- anion substitution with (a) (i) & (ii) the $A1$ type and (b) the $A2$ type alkaline earth cation substitution.

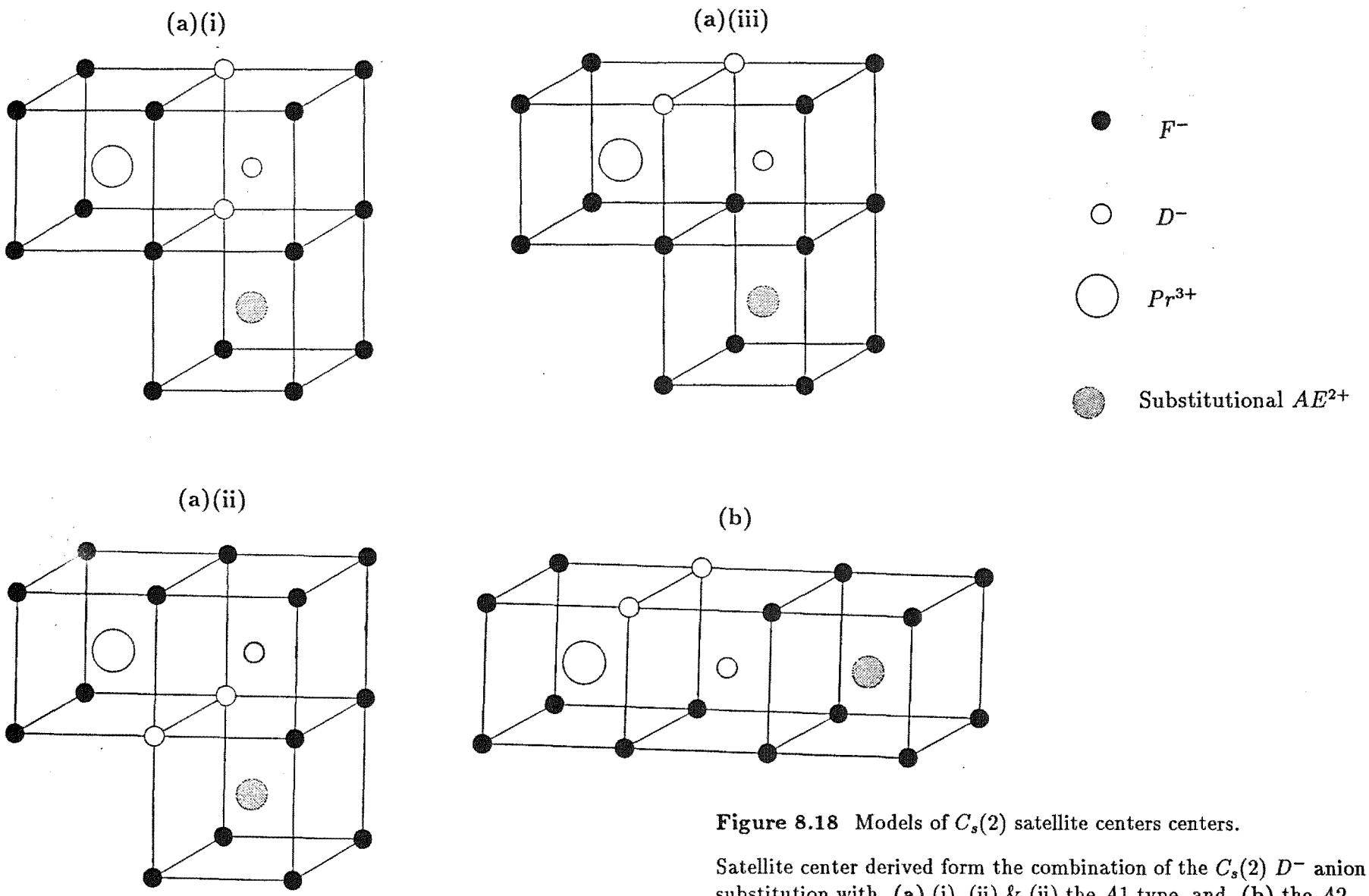

Figure 8.18 Models of $C_s(2)$ satellite centers centers.

Satellite center derived form the combination of the $C_s(2)$ D^- anion substitution with **(a)** (i), (ii) & (ii) the $A1$ type and **(b)** the $A2$ type alkaline earth cation substitution.

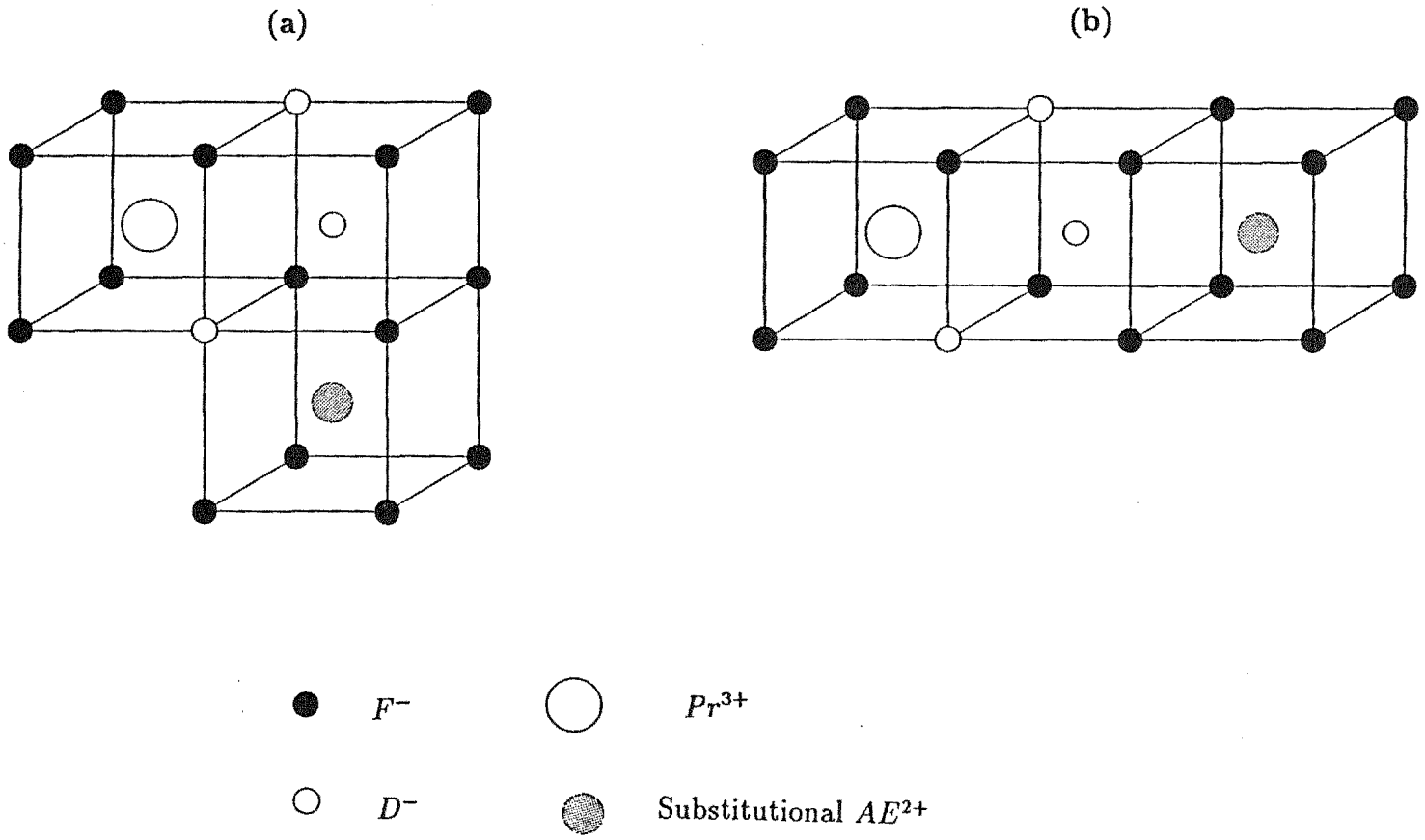

Figure 8.19 Models of $C_s(4)$ satellite centers centers.

Satellite center derived form the combination of the $C_s(4)$ D^- anion substitution with **(a)** the $A1$ type and **(b)** the $A2$ type alkaline earth cation substitution.

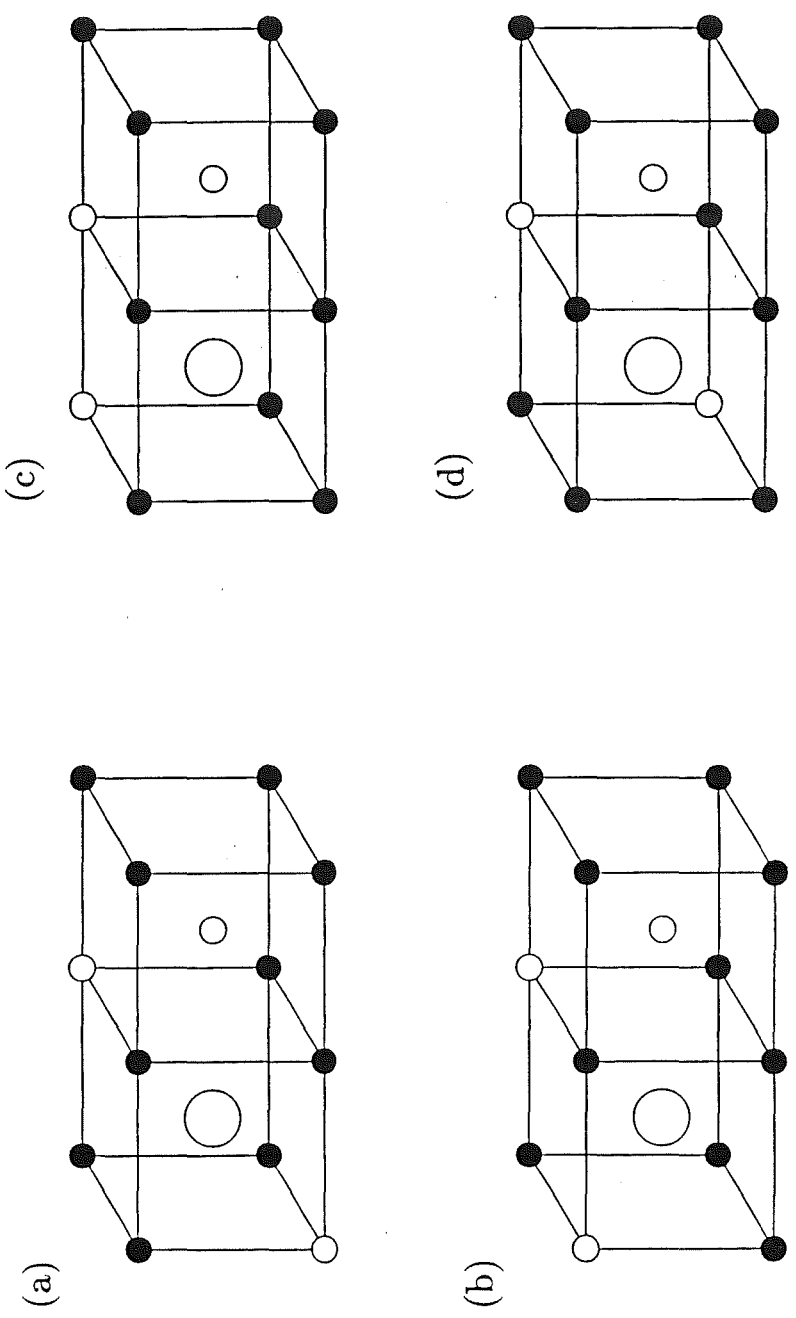

Figure 8.20 Some possible models for the $C_s(3)$ and $C_s(5)$ centers derived from the model for the $C_s(1)$ center which involves only three D^- anions in the neighbourhood of the Pr^{3+} ion.

Chapter 9

Summary and Conclusion

The principal aim of this work was to investigate the Pr^{3+} defect centers of doubly doped AE fluoride crystals using laser selective excitation. Choosing the two AE fluoride hosts CaF_2 and SrF_2 and three alkaline earth dopant cations Ca^{2+}, Sr^{2+} and Ba^{2+} , four mixed crystal systems were studied. The centers in these crystals studied were characterised on the basis of the polarised emission spectra observed and all the centers display one of four types of polarisation behaviour; these centers being arbitrarily labelled types $A1$, $A2$, $A3$ and $A4$.

Some models are proposed for the four types of center and these are derived from the parent C_{4v} center. The polarisation behaviour of the $A1$ centers fits the description of an *off-axis* substitution of a single dopant alkaline earth cation to give a C_s symmetry of the configuration shown in figure 2.2(a)(iii), while that of the $A2$ centers consists of an *on-axis*, i.e along the C_4 axis of the parent C_{4v} center, alkaline earth cation subsitution, thus retaining C_{4v} symmetry. It was not possible to arrive at an unambigous substitutional arrangement for the $A3$ type centers though their polarisation spectra appears to suggests a C_{2v} symmetry. This requires two AE dopants which is statistically less likely. The randomness of the polarisation ratios observed for the $A4$ centers suggests the lowest symmetry, C_1 for this center. A conclusive model has yet to emerge for this center.

For the $Ca_{1-x}Sr_xF_2 : Pr^{3+}$ crystal system, the two prominent mixed crystal centers are the $A1$ and $A2$ center with a weaker $A3$ center apparent. The $Ca_{1-x}Ba_xF_2 : Pr^{3+}$ is interesting in that there are many more mixed crystal centers than the Sr^{2+} doped crystal. However only three were successfully discriminated, two of these being $A1$ type centers and the third an $A2$ type center. Two $A3$ type centers were observed in the $Sr_{1-x}Ca_xF_2 : Pr^{3+}$ crystal system. It is believed that other mixed crystal centers are present but the difficulty with LSE studies of these is that the lines of these centers in the excitation range of the dye laser used appeared within a narrow frequency range and closely overlapped one another. It was possible to investigate one clear mixed crystal center in the $Sr_{1-x}Ba_xF_2 : Pr^{3+}$ system and this is the only center that exhibited the polarisation behaviour of an $A4$ type center.

LSE studies on the deuterated versions of the mixed crystals were also performed and all the mixed crystal centers studied displayed the same four types of polarisation behaviour. The substitution of an F^- ion with a D^- ion in a deuterated crystal should retain the charge compensation center symmetry though the crystal field will be altered. Additionally, vibronic features arising from the coupling of the local mode vibrational states of the lighter hydride ion with the electronic states are also observed.

Two D^- centers of the type $A1$ and $A2$ are studied in the $Ca_{1-x}Sr_xF_2 : Pr^{3+} : D^-$ crystal system and they would be the analogues of the equivalent F^- mixed crystal centers. The population of the $A3$ center is believe to be low in the undeuterated crystal and it is most likely that there will be less of the D^- variant of this center in a deuterated crystal, hence making detection difficult. The $A1$ and $A2$ type D^- centers are also observed in the $Ca_{1-x}Ba_xF_2 : Pr^{3+} : D^-$ crystal system while the $Sr_{1-x}Ca_xF_2 : Pr^{3+}$ crystal yielded two $A3$ type D^- centers like its undeuterated counterpart. The $Sr_{1-x}Ba_xF_2 : Pr^{3+} : D^-$ crystal gave an $A4$ type deuterium center and additionally, an $A2$ type center. The latter is not apparent in the undeuterated crystal. Though the $A2$ (F^-) center was not observed, it is most likely to be present but the levels in the $^1D_2$ mulitplet were not successfully discriminated and hence could not be studied.

The use of a relatively simple device in the form of a mechanical chopper proved most effective, at least within a certain range of decay rates, for discriminating transitions of centers by time resolution. This method clearly demonstrated the presence of further mixed alkaline earth centers in the SrF_2 host when the transitions of these centers were resolved under a scan performed with the chopper. An idea of the relative lifetimes of the centers was also possible by varying the speed of the chopper and comparing the relative emission intensities of the centers.

A more quantitative approach to the temporal studies of the centers in the mixed crystal using the pulsed dye laser revealed that the lifetime of the off-axis $A1$ center is not very different from that of the parent C_{4v} center. This suggests small alterations in the crystal field of the parent C_{4v} center to give rise to the $A1$ center. The lifetime of the $A2$ centers is roughly twice that of the parent C_{4v} center. Since both these centers are proposed to have the same symmetry, the smaller decay rate of the $A2$ center must correspond to smaller crystal field parameters for the $A2$ center compared to the parent center which suggests that the interstitial F^- is also further from the Pr^{3+} ion in the $A2$ center.

The excitation transfer of the C_{4v} center was proposed to be due to the long range intercluster dipole-dipole interaction. The decay rate for this form of interaction according to theory should be proportional to R^{-3}, where R is the mean distance between the C_{4v} centers. A fit of the decay rates from various concentration of Pr^{3+} in CaF_2 revealed a $R^{-2.7}$ relationship, close to the predicted value for a dipole-dipole interaction.

The crystal field fit of the various C_{4v} centers were attempted. Though the results of the fit are far from definitive, the problems and possible solutions are identified, namely the need for more levels in the $^1I_6$ and $^3P_2$ multiplets to be assigned and the probable need of the spin correlation crystal field to resolve the poor fit of the levels in the $^1D_2$ mulitplet.

The last part of this dissertation described the behaviour of the bleaching centers. The polarisation behaviour of the parent bleaching centers studied on the whole agreed with previously assigned models for the bleaching centers. From further con-

sideration of the dipole absorption and emission strengths along various axes of the centers based on the models assigned, excitation conditions which produced effects like the independent bleaching behaviour of transitions from the Z_1 and Z_2 levels were explained. An additional parent bleaching center, the $C_s(5)$ center was also studied though the polarisation results were not consistent with the models investigated in this work.

The most challenging part of this work experimentally is probably the study of the mixed crystal bleaching centers, firstly because there are so many of them and secondly because their emission strength is extremely weak requiring careful optimization of all the apparatus used. Nonetheless, the major satellite features around the transitions of the parent bleaching centers were studied and some probable models evolving around the parent bleaching centers are proposed for the mixed crystal bleaching centers.

In conclusion, the efficacy of the LSE technique for the study of the mixed crystal centers was demonstrated. It would be premature to declare that the Pr^{3+} doped mixed alkaline earth crystals have nothing left to teach us; experience has shown in the past a new twist could be just around the corner. This could come from the application of other techniques like EPR and ENDOR. It is almost certain that the application of high resolution lasers for holeburning or ODNMR studies would yield further results to answer some questions and perhaps raise a few more.

Appendix A

Calculation of the expected polarisation ratios for the C_s and C_{2v} centers

Calculations of the polarisation ratios for the C_s and C_{2v} centers are presented in sections A.1 and A.2 respectively. The degraded polarisation ratios of the C_{4v} center obtained as the laser polarisation E-vector departs from perfect alignment with the crystallographic axes are given in Section A.3 .

A.1 The C_s centers

Two different C_s configurations are derivable from the parent C_{4v} center for a single cation substitution in the NN cation sphere. These are labelled $C_s(a)$ and $C_s(b)$ and defined by the orientation of their C_s reflection plane relative to a (100) plane parallel to the C_4 axis of a C_{4v} center. Representative structures of these two possible configurations in a cubic lattice are shown in figure A.1.

The position of the dopant alkaline earth cation defines the x,y and z axes of the site and the C_s reflection plane of a particular C_s center. The oscillator strengths of the x, y and z components of a C_s center electric dipole are arbitrarily defined as **a**,**b** and **c** respectively. The global axes X,Y and Z are aligned with the crystallographic [100] axes. The polarisation of the laser parallel to the Y or Z axes was designated in chapter 2 as E_Y and E_Z.

The method by which the polarisation ratios are worked out is demonstrated by way of an example, using the $C_s(a)$ site configuration of figure A.1. Consider the case for the laser polarised E_Z, then under a γ_1(x or y) absorption, only the **x** component contributes with an absorption strength of $\frac{1}{\sqrt{2}}\mathbf{a}$ since the E_Z vector is 45° from the x-axis. If the emission in the Z-direction is also γ_1(x or y), then the **x** and **y** components emit with strengths of $\frac{1}{2}\mathbf{a}^2$ and $\frac{1}{\sqrt{2}}\mathbf{ab}$ respectively.

In the CaF_2 or SrF_2 host, there are six inequivalent orientations of the same center configuration and the determination of the net polarisation ratios involves evaluation of the absorption and emission strengths for all six orientations.

A.1.1 The $C_s(a)$ center

The six inequivalent positions for this center are shown in figure A.2 and tables A.1(a) and A.1(b) list the net polarisation ratios expected for the laser polarised E_Z and E_Y. I_X and I_Y refer to the emission intensities of light polarised in the X and Y directions. For the laser polarised E_Z, centers of this configuration are not expected to display any polarisation effects.

For the case of a γ_1(x or y) absorption with laser polarised E_Y and γ_1(x or y) emission, the predicted polarisation ratio is:

$$\frac{I_X}{I_Y} = \frac{\mathbf{a}^2 + \frac{4}{\sqrt{2}}\mathbf{ab}}{2(\mathbf{a}^2 + \mathbf{b}^2)} = k, \qquad \text{(A.1)}$$

where k is a real number, greater than or equal to 0. **a** and **b** must be real and

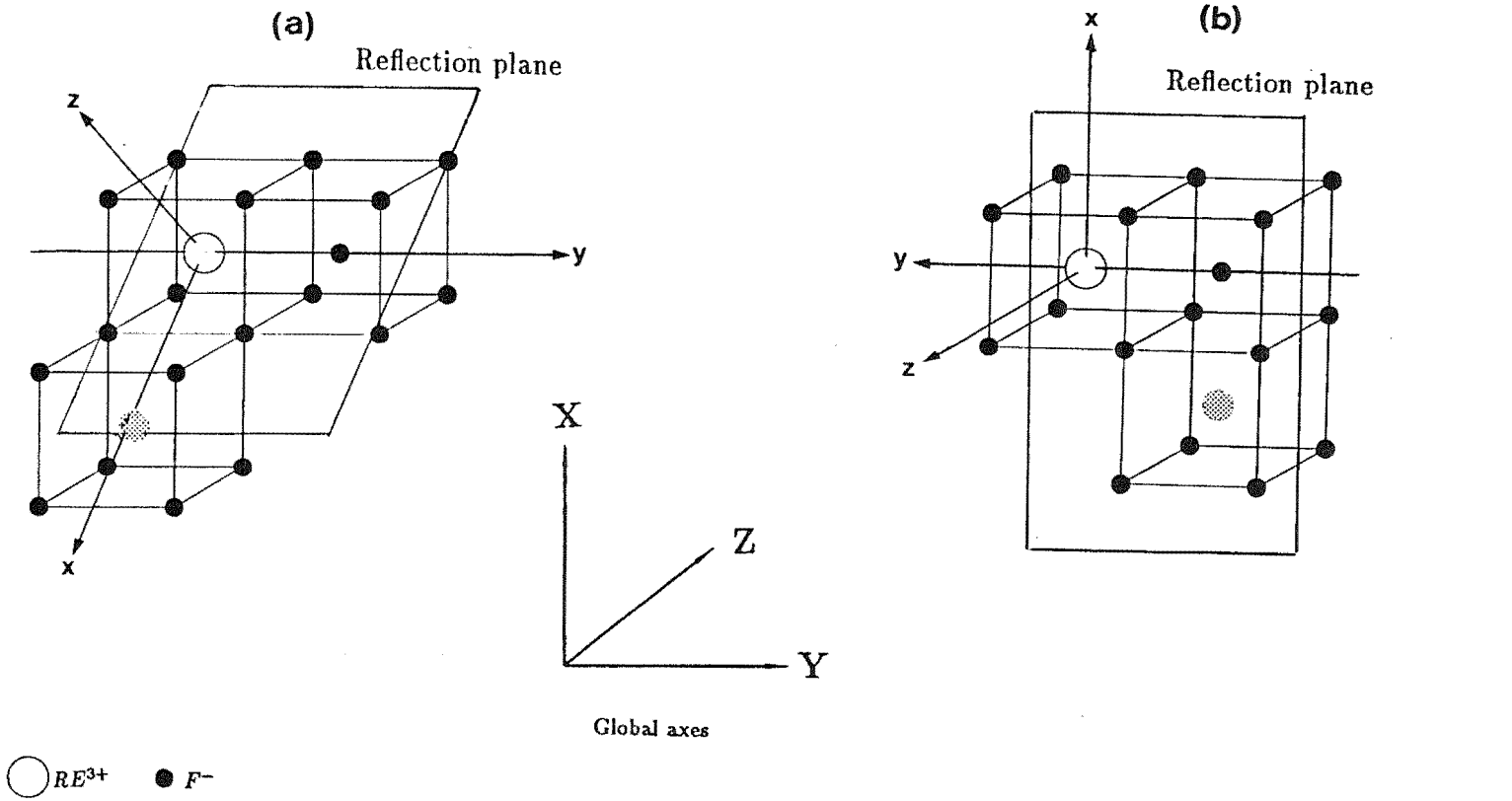

Figure A.1 Examples of the two C_s center configurations in a cubic lattice.

(a) and 1(b) are the $C_s(a)$ and $C_s(b)$ configurations respectively. The parent C_4 axis is aligned with the center y-axis. The x and y-axes are chosen by the group table of Nielson and Koster(1963) to lie in the reflection plane. The orientation of the C_s reflection plane which distinguishes the center configuration is determined by the foreign cation. Note also the global or crystallographic axes in relation to the center axes.

positive for these values to be physically meaningful. Rearranging,

$$2k\mathbf{b}^2 - \left(\frac{4}{\sqrt{2}}\mathbf{a}\right)\mathbf{b} + (2k-1)\mathbf{a}^2 = 0 \tag{A.2}$$

and therefore ,

$$\mathbf{b} = \frac{\mathbf{a}}{\sqrt{2}}\left[1/k \pm (-2 + 1/k + 1/k^2)^{1/2}\right]. \tag{A.3}$$

For real values of **a** and **b**, it is required that :

$$\begin{aligned} (-2 + 1/k + 1/k^2) &\geq 0 \\ 0 &\geq 2k^2 - k - 1 \\ -1/2 &\leq k \leq 1. \end{aligned} \tag{A.4}$$

Since k $\geq$ 0 , the polarisation ratio allowed must fall with the range:

$$0 \leq \frac{I_X}{I_Y} \leq 1 \tag{A.5}$$

When the absorption is under $\gamma_2(z)$ and emission is under γ_1(x or y), or absorption under γ_1 and emission under γ_2, the range of polarisation values allowed can be similarly found by letting the polarisation ratio be

$$\frac{I_X}{I_Y} = \frac{\mathbf{a} + \sqrt{2}\mathbf{b}}{2\mathbf{a}} = k, \tag{A.6}$$

giving :

$$\mathbf{b} = \frac{\mathbf{a}}{\sqrt{2}}(2k-1). \tag{A.7}$$

For positive values of **a** and **b**,

$$\begin{aligned} 2k - 1 &\geq 0, \\ k &\geq \frac{1}{2}, \end{aligned} \tag{A.8}$$

hence the allowed range of the polarisation ratios is:

$$\frac{I_X}{I_Y} \geq \frac{1}{2}. \tag{A.9}$$

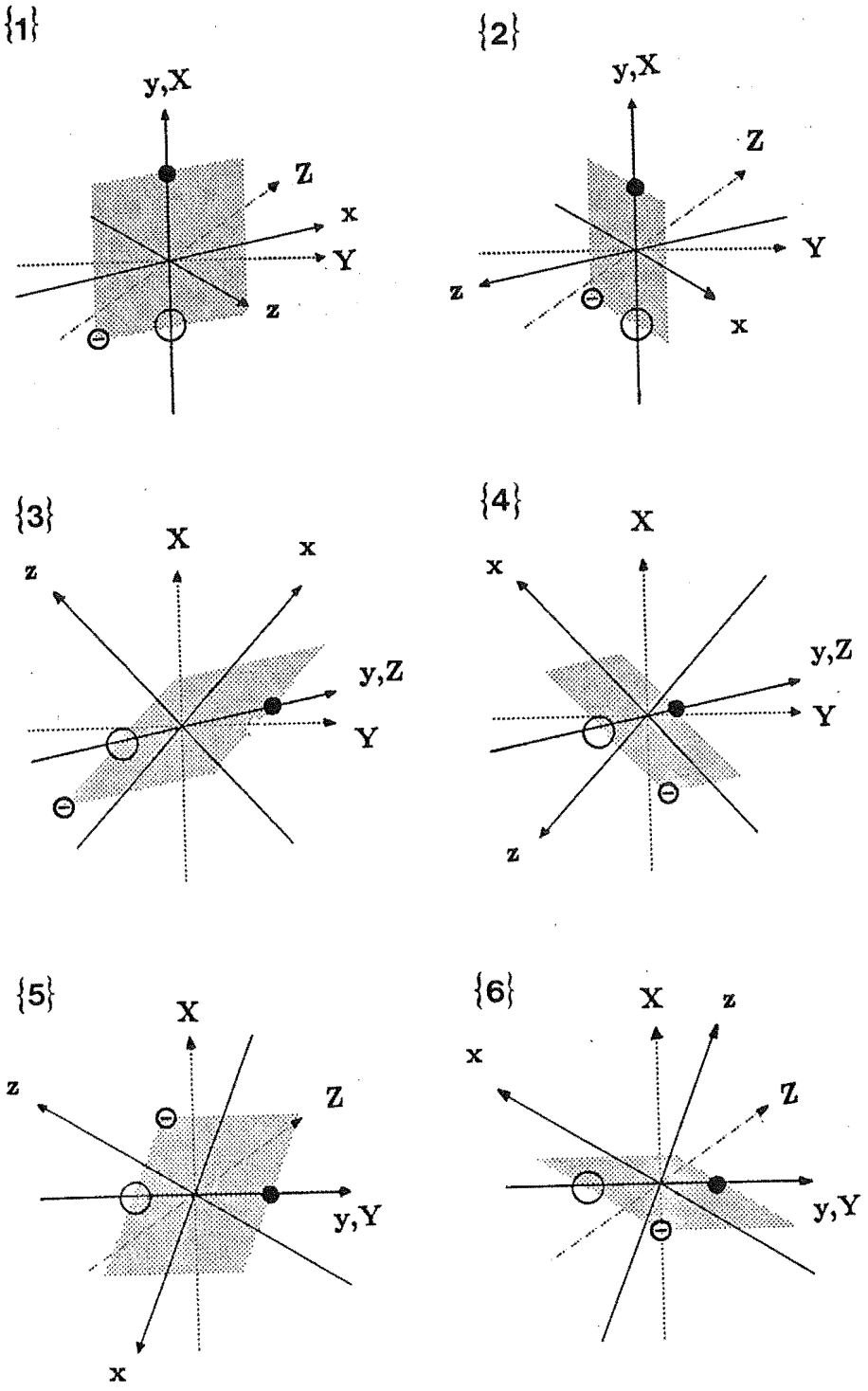

Figure A.2 The six inequivalent orientations of the $C_s(a)$ configuration.
The lower case labels denote the center axes and the upper case labels the global or (100) oriented crystal axes. The laser polarisation is aligned with a crystal axis in either the Z or Y direction. Each orientation is labelled with a number which is referred to by table A.1. The different circles represent ions that form the reflection planes.

Absorption		Emission			
γ_1(x or y)		γ_1(x or y)		γ_2(z)	
		I_X	I_Y	I_X	I_Y
1	$\frac{1}{\sqrt{2}}a$	$\frac{1}{\sqrt{2}}ab$	$\frac{1}{2}a^2$	-	$\frac{1}{2}ac$
2	$\frac{1}{\sqrt{2}}a$	$\frac{1}{\sqrt{2}}ab$	$\frac{1}{2}a^2$	-	$\frac{1}{2}ac$
3	$\frac{1}{\sqrt{2}}a$	$\frac{1}{2}a^2$	$\frac{1}{2}a^2$	$\frac{1}{2}ac$	$\frac{1}{2}ac$
4	$\frac{1}{\sqrt{2}}a$	$\frac{1}{2}a^2$	$\frac{1}{2}a^2$	$\frac{1}{2}ac$	$\frac{1}{2}ac$
5	b	$\frac{1}{\sqrt{2}}ab$	b^2	$\frac{1}{\sqrt{2}}bc$	-
6	b	$\frac{1}{\sqrt{2}}ab$	b^2	$\frac{1}{\sqrt{2}}bc$	-
Net Ratio		$a^2 + \frac{4}{\sqrt{2}}ab : 2(a^2 + b^2)$		a + $\sqrt{2}b : 2a$	

(a)

Absorption		Emission			
γ_2(z)		γ_1(x or y)		γ_2(z)	
		I_X	I_Y	I_X	I_Y
1	$\frac{1}{\sqrt{2}}c$	$\frac{1}{\sqrt{2}}bc$	$\frac{1}{2}ac$	-	$\frac{1}{2}c^2$
2	$\frac{1}{\sqrt{2}}c$	$\frac{1}{\sqrt{2}}bc$	$\frac{1}{2}ac$	-	$\frac{1}{2}c^2$
3	$\frac{1}{\sqrt{2}}c$	$\frac{1}{2}ac$	$\frac{1}{2}ac$	$\frac{1}{2}c^2$	$\frac{1}{2}c^2$
4	$\frac{1}{\sqrt{2}}c$	$\frac{1}{2}ac$	$\frac{1}{2}ac$	$\frac{1}{2}c^2$	$\frac{1}{2}c^2$
Net Ratio		$a + \sqrt{2}b : 2a$		1:2	

Table A.1 The absorption and emission strengths, and the net polarisation ratios for the $C_s(a)$ configuration.

The first column identifies a particular $C_s(a)$ orientation, the second column the aborption strength and the columns under I_X and I_Y are the emission strengths for the X and Y polarisation direction. The γ_i labels in the second row identify the particular electric dipole component which will be absorbing or emitting, while the last row gives the net polarisation ratios expected. The letters **a**, **b** and **c** refer to the oscillator stengths of the x,y and z components respectively of the electric dipole.

(a) and (b) list seperately the absorption and emission efficiencies for the laser polarised E_Y and E_Z

Absorption		Emission			
γ_1(x or y)		γ_1(x or y)		γ_2(z)	
		I_X	I_Y	I_X	I_Y
1	$\frac{1}{\sqrt{2}}a$	$\frac{1}{\sqrt{2}}ab$	$\frac{1}{2}a^2$	-	$\frac{1}{2}ac$
2	$\frac{1}{\sqrt{2}}a$	$\frac{1}{\sqrt{2}}ab$	$\frac{1}{2}a^2$	-	$\frac{1}{2}ac$
3	b	$\frac{1}{\sqrt{2}}ab$	$\frac{1}{\sqrt{2}}ab$	$\frac{1}{2}bc$	$\frac{1}{2}bc$
4	b	$\frac{1}{\sqrt{2}}ab$	$\frac{1}{\sqrt{2}}ab$	$\frac{1}{2}bc$	$\frac{1}{2}bc$
5	$\frac{1}{\sqrt{2}}a$	$\frac{1}{2}a^2$	$\frac{1}{\sqrt{2}}ab$	$\frac{1}{2}ac$	-
6	$\frac{1}{\sqrt{2}}a$	$\frac{1}{2}a^2$	$\frac{1}{\sqrt{2}}ab$	$\frac{1}{2}ac$	-
Net Ratio		1:1		1:1	

(b)

Absorption		Emission			
γ_2(z)		γ_1(x or y)		γ_2(z)	
		I_X	I_Y	I_X	I_Y
1	$\frac{1}{\sqrt{2}}c$	$\frac{1}{\sqrt{2}}bc$	$\frac{1}{2}ac$	-	$\frac{1}{2}c^2$
2	$\frac{1}{\sqrt{2}}c$	$\frac{1}{\sqrt{2}}bc$	$\frac{1}{2}ac$	-	$\frac{1}{2}c^2$
5	$\frac{1}{\sqrt{2}}c$	$\frac{1}{2}ac$	$\frac{1}{2}bc$	$\frac{1}{2}c^2$	-
6	$\frac{1}{\sqrt{2}}c$	$\frac{1}{2}ac$	$\frac{1}{2}bc$	$\frac{1}{2}c^2$	-
Net Ratio		1:1		1:1	

A.1.2 The $C_s(b)$ center

The six inequivalent configurations of the $C_s(b)$ type centers are shown in figure A.3 and the net polarisation ratios under different absorption and emission geometries are listed in table A.2(a) and (b) for the laser polarised E_Z or E_Y . Only under γ_1(x or y) absorption and γ_1(x or y) emission is there a range of polarisation ratios expected. The rest display well defined $I_X : I_Y$ ratios of 1:0 or 0:1 when absorbing E_Y laser radiation. For the laser polarised E_Z , under γ_2(z) absorption and γ_2(z) emission, no fluorescence will be observed in the Z direction.

To determine the range of polarisation ratios for the case of the γ_1 absorption and γ_1 emission in this configuration, let

$$\frac{I_X}{I_Y} = \frac{\mathbf{ab}}{\mathbf{a}^2 + \mathbf{b}^2} = k. \tag{A.10}$$

Rearranging,

$$k\mathbf{b}^2 - \mathbf{ab} + k\mathbf{a}^2 = 0, \tag{A.11}$$

and therefore

$$\mathbf{b} = \frac{\mathbf{a}}{2k}[1 \pm (1 - 4k^2)]. \tag{A.12}$$

For real solutions,

$$1 - 4k^2 \geq 0, \tag{A.13}$$

or

$$\frac{1}{2} \geq k, \tag{A.14}$$

hence the allowed range of polarisation ratios is

$$0 \leq \frac{I_X}{I_Y} \leq \frac{1}{2}. \tag{A.15}$$

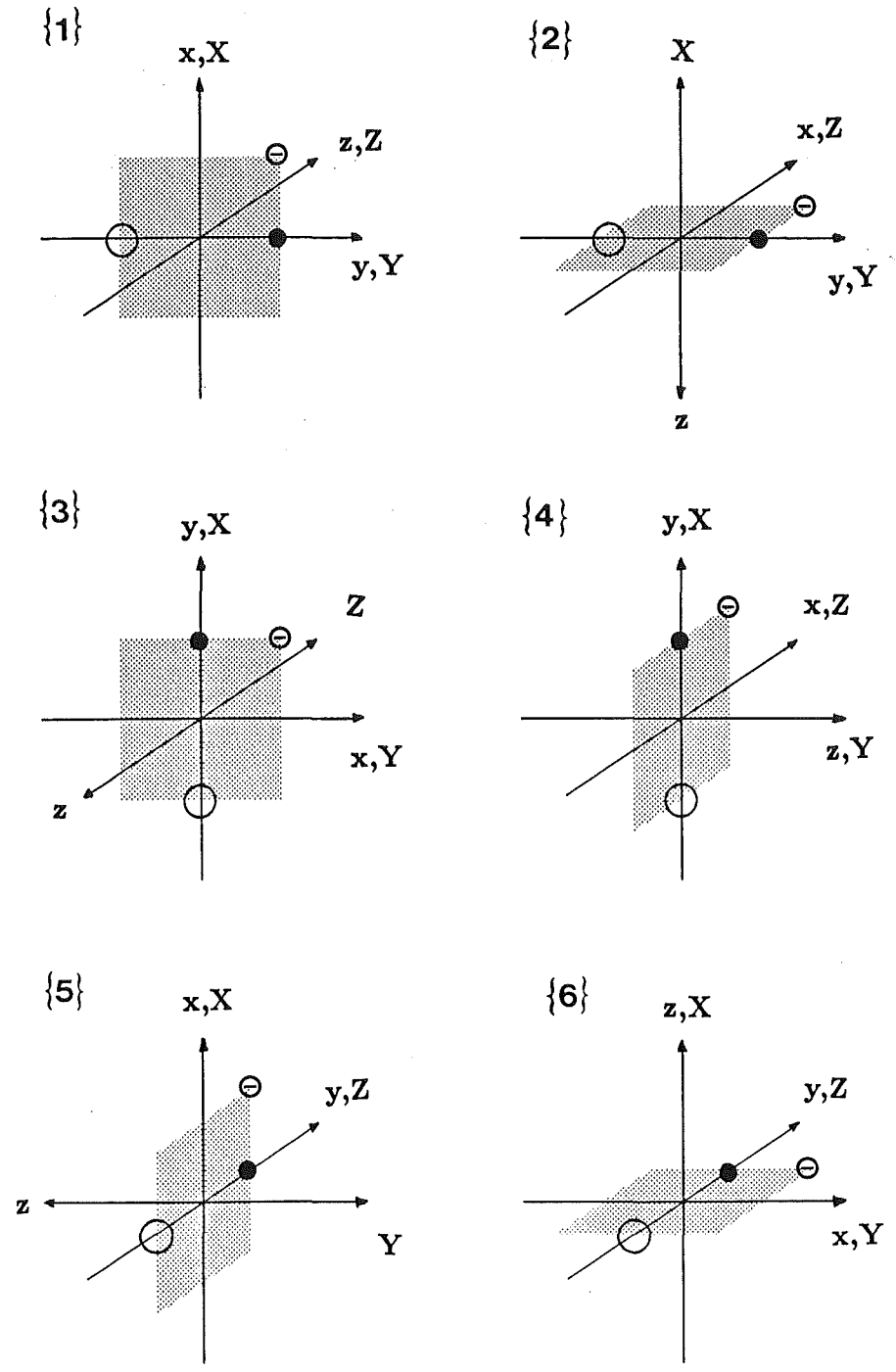

Figure A.3 The six equivalent orientations of the $C_s(b)$ configuration. The label definitions are the same as for figure A.2

Absorption		Emission			
γ_1(x or y)		γ_1(x or y)		γ_2(z)	
		I_X	I_Y	I_X	I_Y
1	b	ba	bb	-	-
2	b	-	bb	bc	-
3	a	ba	aa	-	-
6	a	-	aa	ac	-
Net Ratio		$ba : b^2 + a^2$		1:0	

(a)

Absorption		Emission			
γ_2(z)		γ_1(x or y)		γ_2(z)	
		I_X	I_Y	I_X	I_Y
4	c	bc	—	—	c^2
5	c	ac	—	—	c^2
Net Ratio		1:0		0:1	

Absorption		Emission			
γ_1(x or y)		γ_1(x or y)		γ_2(z)	
		I_X	I_Y	I_X	I_Y
2	a	—	ab	ac	-
4	a	ab	-	-	ac
5	b	ab	—	-	bc
6	b	-	ab	bc	-
Net Ratio		1:1		1:1	

(b)

Absorption		Emission			
γ_2(z)		γ_1(x or y)		γ_2(z)	
		I_X	I_Y	I_X	I_Y
1	c	ac	bc	—	—
3	c	bc	ac	—	—
Net Ratio		1:1		0:0	

Table A.2 The absorption and emission strengths, and the net polarisation ratios for the $C_s(b)$ configuration.

See table A.1 for definition of the symbols used.

A.2 The C_{2v} centers

The two C_{2v} configurations, $C_{2v}(a)$ and $C_{2v}(b)$ are distinguished by the orientation of their σ_v reflection planes(fig. A.4). Figures A.5 and A.6 give the six different orientations of each of the $C_{2v}(a)$ and $C_{2v}(b)$ configurations respectively. Going through the same procedure as for the C_s center configurations, the tables to work out the net polarisation ratios for these two C_{2v} configurations are constructed (tables A.3 and A.4). The polarisation ratios are more clear cut for both configurations of the C_{2v} center and do not have a range of values like the ratios found for the C_s centers.

A.3 Deviation from the expected polarisation ratios in the C_{4v} center.

The principal C_4 or z-axis of the C_{4v} center coincides with the crystallographic axis. The three inequivalent orientations of the z-axis of a C_{4v} center are labelled X, Y and Z (fig A.7). Under the present experimental conditions, it is difficult to achieve perfect alignment of the laser polarisation with a crystallographic axis. To calculate the degradation of the observed polarisation ratios, the laser polarisation is allowed to deviate from the direction of perfect alignment (fig. A.7), thus giving a component of the E-vector along all three inequivalent orientations of the z-axis. The net polarisation as a function of θ and ϕ is given in table A.5 and expressed graphically in figure 2.5

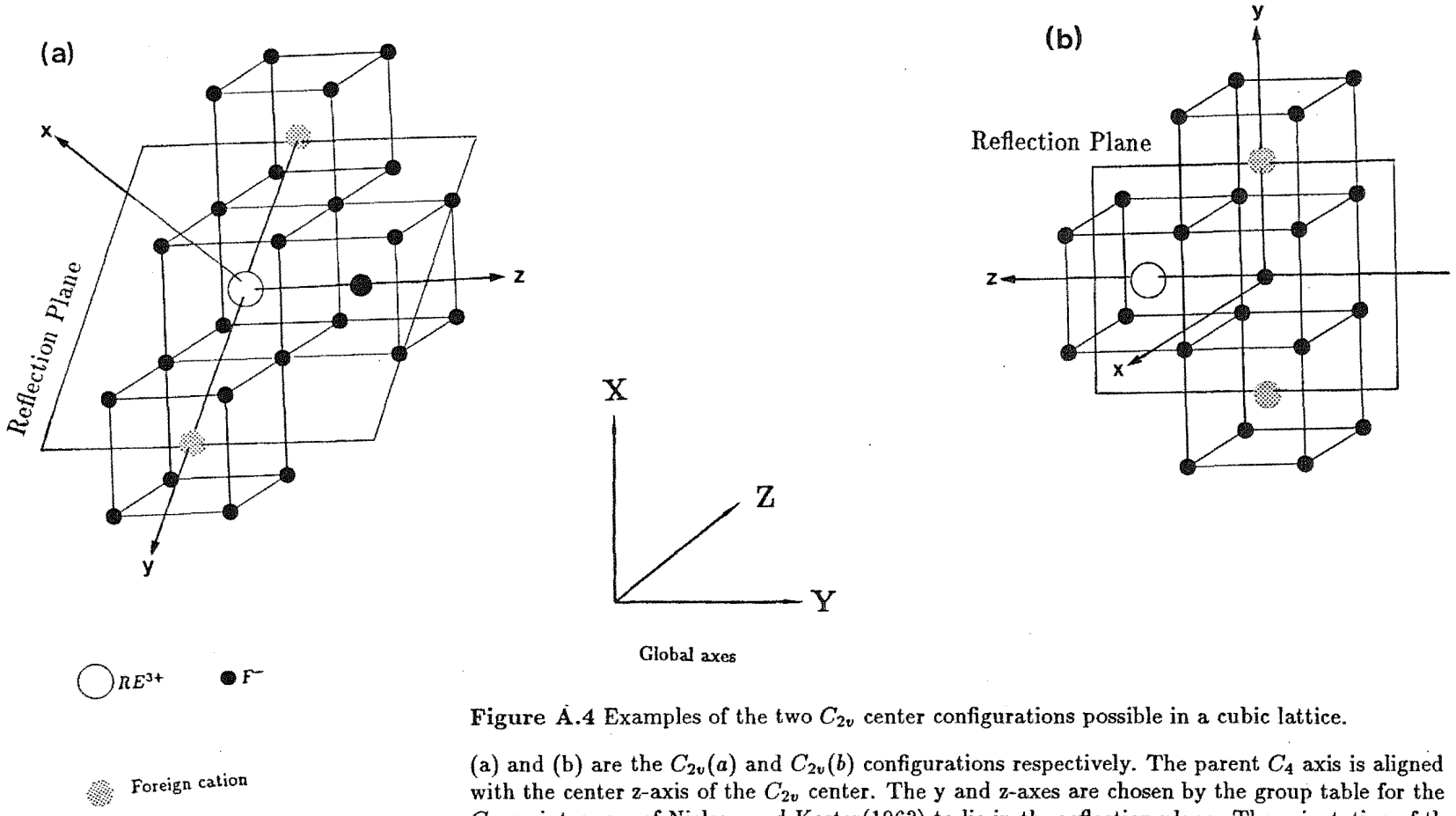

Figure A.4 Examples of the two C_{2v} center configurations possible in a cubic lattice.

(a) and (b) are the $C_{2v}(a)$ and $C_{2v}(b)$ configurations respectively. The parent C_4 axis is aligned with the center z-axis of the C_{2v} center. The y and z-axes are chosen by the group table for the C_{2v} point group of Nielson and Koster(1963) to lie in the reflection plane. The orientation of the the C_{2v} reflection plane which distinguishes the center configuration is determined by two foreign cations. Note also the global or crystallographic axes in relation to the center axes.

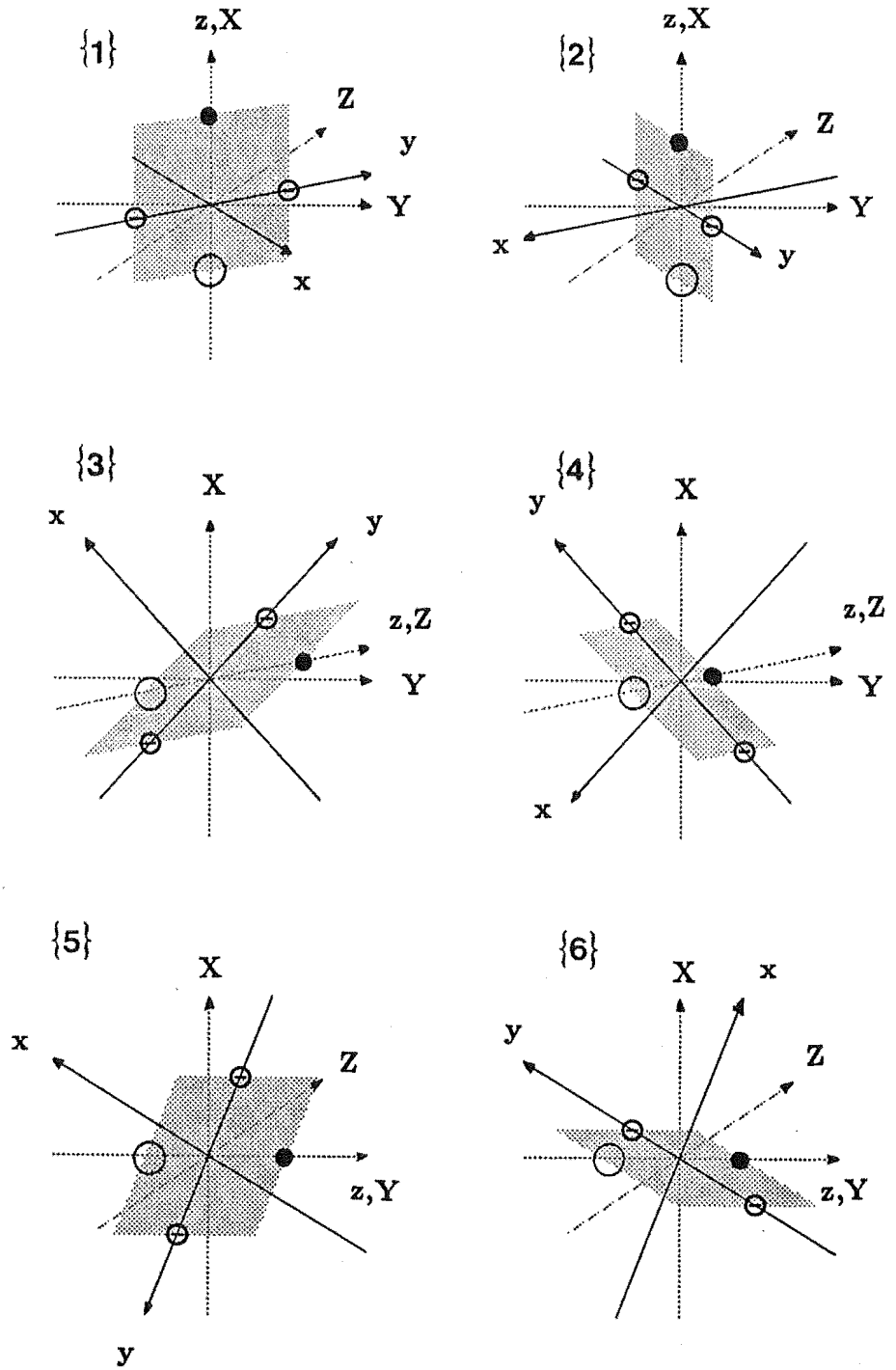

Figure A.5 The six equivalent orientations of the $C_{2v}(a)$ configuration.
The global axes are labelled in upper case and the center axes in lower case. The z-axis of the centre is now aligned with the parent C_4 axis while the x and y-axes are perpendicular and parallel respectively to the σ_v reflection plane of the C_{2v} center.

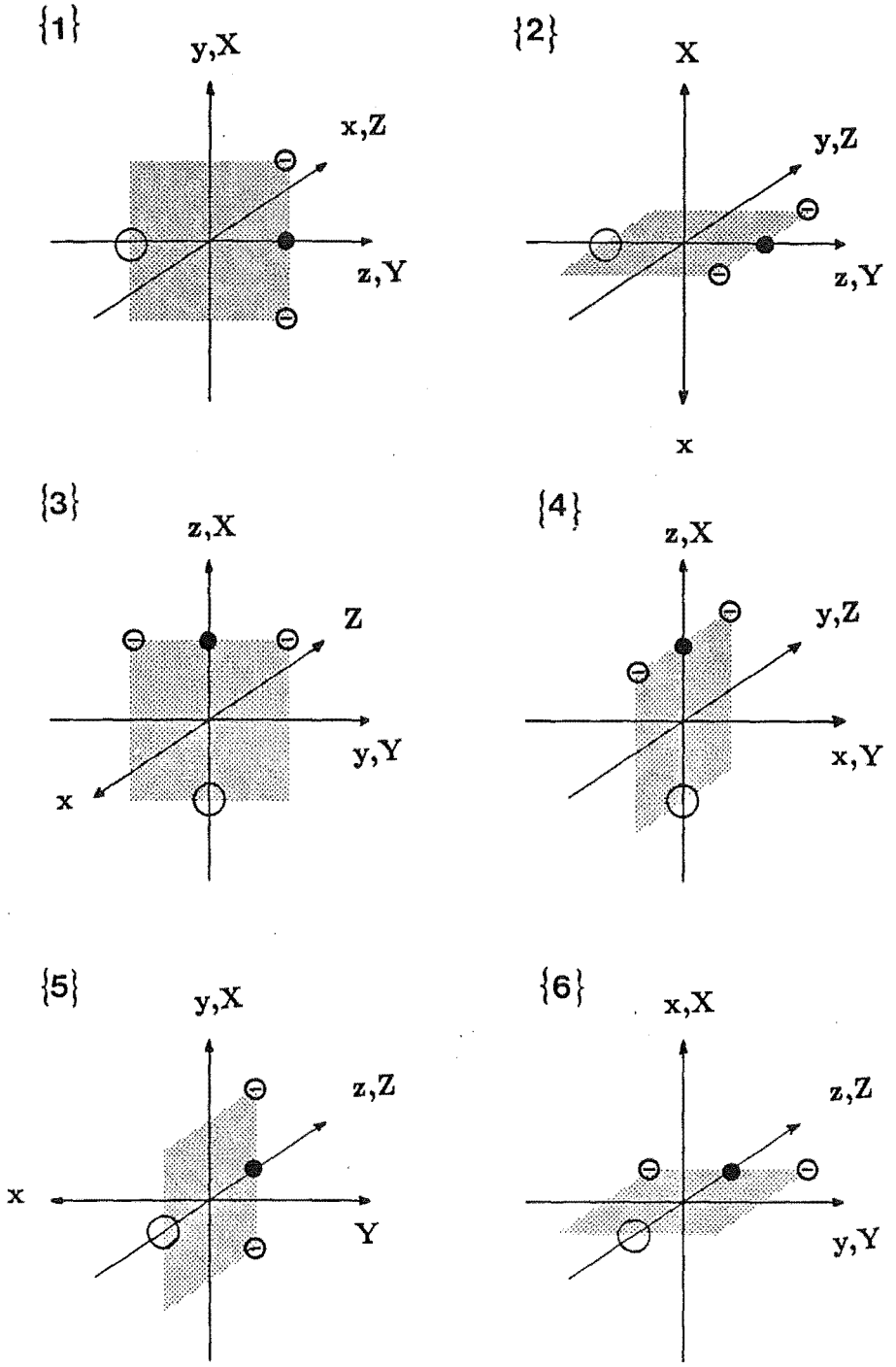

Figure A.6 The six equivalent orientations of the $C_{2v}(b)$ configuration. The axes labels are as defined for figure A.5.

(a)

Absorption		Emission					
σ_x		π_z		σ_x		σ_y	
		I_X	I_Y	I_X	I_Y	I_X	I_Y
1	$\frac{1}{\sqrt{2}}a$	$\frac{1}{\sqrt{2}}ac$	-	-	$\frac{1}{2}a^2$	-	$\frac{1}{\sqrt{2}}ab$
2	$\frac{1}{\sqrt{2}}a$	$\frac{1}{\sqrt{2}}ac$	-	-	$\frac{1}{2}a^2$	-	$\frac{1}{\sqrt{2}}ab$
3	$\frac{1}{\sqrt{2}}a$	-	-	$\frac{1}{2}a^2$	$\frac{1}{2}a^2$	$\frac{1}{2}ab$	$\frac{1}{\sqrt{2}}ab$
4	$\frac{1}{\sqrt{2}}a$	-	-	$\frac{1}{2}a^2$	$\frac{1}{2}a^2$	$\frac{1}{2}ab$	$\frac{1}{\sqrt{2}}ab$
Net Ratio		1:0		1:2		1:2	

Absorption		Emission					
σ_y		π_z		σ_x		σ_y	
		I_X	I_Y	I_X	I_Y	I_X	I_Y
1	$\frac{1}{\sqrt{2}}b$	$\frac{1}{\sqrt{2}}bc$	-	-	$\frac{1}{2}ab$	-	$\frac{1}{\sqrt{2}}b^2$
2	$\frac{1}{\sqrt{2}}b$	$\frac{1}{\sqrt{2}}bc$	-	-	$\frac{1}{2}ab$	-	$\frac{1}{\sqrt{2}}b^2$
3	$\frac{1}{\sqrt{2}}b$	-	-	$\frac{1}{2}ab$	$\frac{1}{2}ab$	$\frac{1}{2}b^2$	$\frac{1}{\sqrt{2}}b^2$
4	$\frac{1}{\sqrt{2}}b$	-	-	$\frac{1}{2}ab$	$\frac{1}{2}ab$	$\frac{1}{2}b^2$	$\frac{1}{\sqrt{2}}b^2$
Net Ratio		1:0		1:2		1:2	

Absorption		Emission					
π_z		π_z		σ_x		σ_y	
		I_X	I_Y	I_X	I_Y	I_X	I_Y
5	c	-	c^2	ac	-	bc	-
6	c	-	c^2	ac	-	bc	-
Net Ratio		0:1		1:0		1:0	

Table A.3 The absorption and emission strengths, and the net polarisation ratios for the $C_{2v}(a)$ configuration.

The absorption and emission corresponding to the electric dipole alignment along the z, x and y axes are represented in the second row by π_z, σ_x and σ_y . (a) and (b) list seperately the absorption and emission strengths for the laser polarised E_Y and E_Z respectively.

(b)

Absorption		Emission					
σ_y		π_z		σ_x		σ_y	
		I_X	I_Y	I_X	I_Y	I_X	I_Y
1	$\frac{1}{\sqrt{2}}b$	$\frac{1}{\sqrt{2}}bc$	-	-	$\frac{1}{2}ab$	-	$\frac{1}{\sqrt{2}}b^2$
2	$\frac{1}{\sqrt{2}}b$	$\frac{1}{\sqrt{2}}bc$	-	-	$\frac{1}{2}ab$	-	$\frac{1}{\sqrt{2}}b^2$
5	$\frac{1}{\sqrt{2}}b$	-	$\frac{1}{2}bc$	$\frac{1}{2}ab$	-	$\frac{1}{\sqrt{2}}b^2$	-
6	$\frac{1}{\sqrt{2}}b$	-	$\frac{1}{2}bc$	$\frac{1}{2}ab$	-	$\frac{1}{\sqrt{2}}b^2$	-
Net Ratio		1:1		1:1		1:1	

Absorption		Emission					
σ_x		π_z		σ_x		σ_y	
		I_X	I_Y	I_X	I_Y	I_X	I_Y
1	$\frac{1}{\sqrt{2}}a$	$\frac{1}{\sqrt{2}}ac$	-	-	$\frac{1}{2}a^2$	-	$\frac{1}{\sqrt{2}}ab$
2	$\frac{1}{\sqrt{2}}a$	$\frac{1}{\sqrt{2}}ac$	-	-	$\frac{1}{2}a^2$	-	$\frac{1}{\sqrt{2}}ab$
5	$\frac{1}{\sqrt{2}}a$	-	$\frac{1}{\sqrt{2}}ac$	$\frac{1}{2}a^2$	-	$\frac{1}{2}ab$	-
6	$\frac{1}{\sqrt{2}}a$	-	$\frac{1}{\sqrt{2}}ac$	$\frac{1}{2}a^2$	-	$\frac{1}{2}ab$	-
Net Ratio		1:1		1:1		1:1	

Absorption		Emission					
π_z		π_z		σ_x		σ_y	
		I_X	I_Y	I_X	I_Y	I_X	I_Y
3	c	-	-	$\frac{1}{\sqrt{2}}ac$	$\frac{1}{\sqrt{2}}ac$	$\frac{1}{\sqrt{2}}bc$	$\frac{1}{\sqrt{2}}bc$
4	c	-	-	$\frac{1}{\sqrt{2}}ac$	$\frac{1}{\sqrt{2}}ac$	$\frac{1}{\sqrt{2}}bc$	$\frac{1}{\sqrt{2}}bc$
Net Ratio		0:0		1:1		1:1	

(a)

Absorption		Emission					
σ_x		π_z		σ_x		σ_y	
		I_X	I_Y	I_X	I_Y	I_X	I_Y
4	a	ac	-	-	a^2	ab	-
5	a	-	-	-	a^2	-	-
Net Ratio		1:0		0:1		1:0	

Absorption		Emission					
σ_y		π_z		σ_x		σ_y	
		I_X	I_Y	I_X	I_Y	I_X	I_Y
3	b	bc	-	-	-	-	b^2
6	b	-	-	ab	-	-	b^2
Net Ratio		1:0		1:0		0:1	

Absorption		Emission					
π_z		π_z		σ_x		σ_y	
		I_X	I_Y	I_X	I_Y	I_X	I_Y
1	c	-	c^2	-	-	bc	-
2	c	-	c^2	ac	-	-	-
Net Ratio		0:1		1:0		1:0	

Table A.4 The absorption and emission strengths, and the net polarisation ratios for the $C_{2v}(a)$ configuration.

See Table A.3 for defintions of symbols.

(b)

Absorption		Emission					
σ_y		π_z		σ_x		σ_y	
		I_X	I_Y	I_X	I_Y	I_X	I_Y
2	b	-	bc	ab	-	-	-
4	b	bc	-	-	ac	-	-
Net Ratio		1:1		1:1		0:0	

Absorption		Emission					
σ_x		π_z		σ_x		σ_y	
		I_X	I_Y	I_X	I_Y	I_X	I_Y
1	a	-	ac	-	-	ab	-
3	a	ac	-	-	-	-	ab
Net Ratio		1:1		0:0		1:1	

Absorption		Emission					
π_z		π_z		σ_x		σ_y	
		I_X	I_Y	I_X	I_Y	I_X	I_Y
5	c	-	-	-	ac	bc	-
6	c	-	-	ac	-	-	bc
Net Ratio		0:0		1:1		1:1	

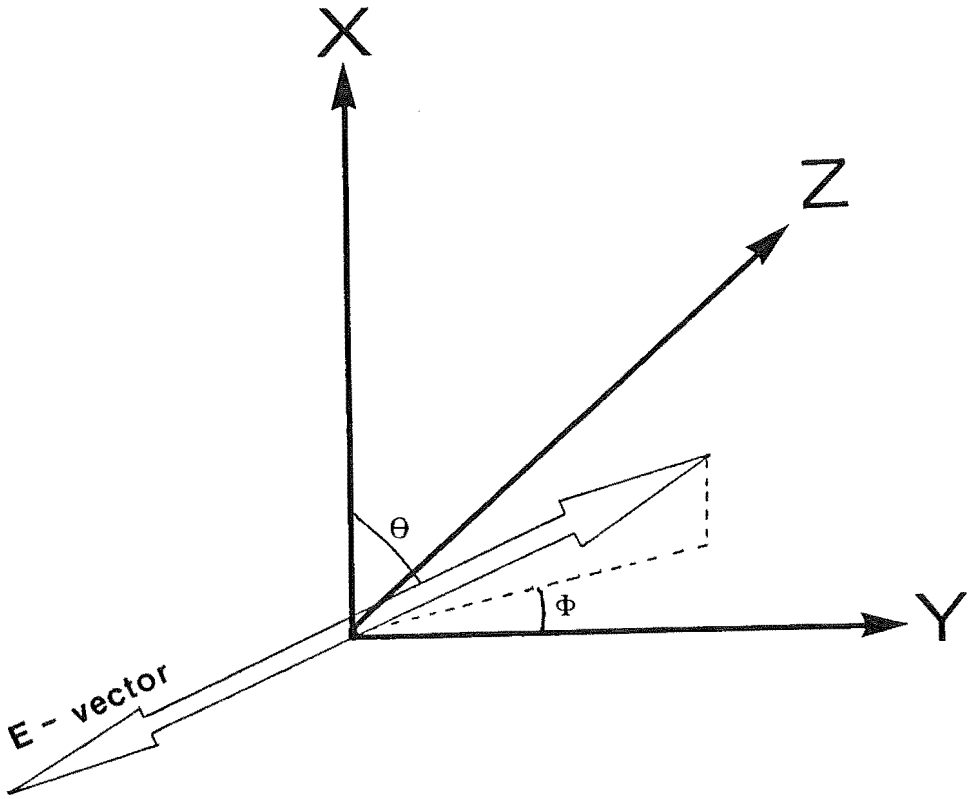

Figure A.7 The three orientations of the principal axis of the C_{4v} center aligned with the X, Y **and** Z**-axis** of the crystal and the E-vector deviation from the direction of perfect alignment with the Y-axis.

Absorption		Emission			
$\sigma_{x \text{ or } y}$		π_z		$\sigma_{x \text{ or } y}$	
		I_X	I_Y	I_X	I_Y
X	$E\cos\theta\sin\phi$ $+E\sin\theta\cos\phi$	$E\cos\theta\sin\phi$ $+E\sin\theta\cos\phi$	-	-	$E\cos\theta\sin\phi$ $+E\sin\theta\cos\phi$
Y	$E\cos\theta$ $+E\sin\theta\sin\phi$	-	$E\cos\theta$ $+E\sin\theta\sin\phi$	$E\cos\theta$ $+E\sin\theta\sin\phi$	-
Z	$E\cos\theta$ $+E\sin\theta\cos\phi$	-	-	$E\cos\theta$ $+E\sin\theta\cos\phi$	$E\cos\theta$ $+E\sin\theta\cos\phi$
Net Ratio		$\sin\theta(\sin\phi$ $+\cos\phi)$	: $\sin\theta\sin\phi+$ $\sin\theta\sin\phi$	$2(\cos\theta+$ $\sin\theta\cos\phi)$	: $2(\sin\theta+\cos\phi)+$ $\cos\theta+\sin\theta\sin\phi$

Absorption		Emission			
π_z		π_z		$\sigma_{x \text{ or } y}$	
		I_X	I_Y	I_X	I_Y
X	$E\cos\theta$	$E\cos\theta$	-	-	$E\cos\theta$
Y	$E\sin\theta\cos\phi$	-	$E\sin\theta\cos\phi$	$\sin\theta\cos\phi$	-
Z	$E\sin\theta\sin\phi$	-	-	$E\sin\theta\sin\phi$	$E\sin\theta\sin\phi$
Net Ratio		$1:\tan\theta\cos\phi$		$\sin\theta(\cos\phi+\sin\phi)$: $\cos\theta+\sin\theta\sin\phi$	

Table A.5 The degraded absorption and emission efficiencies , and net polarisation in the X and Y direction for the C_{4v} center as a function of θ and ϕ (see fig. A.7)

Bibliography

[Lezama et al, 1985] Arturo Lezama, Marcos Oria and Cid B. de Araujo Site selective spectroscopy via energy up-conversion in $CaF_2 : Pr^{3+}$ *Physics Review B* 33(7):4493

[Aizenberg et al., 1975] Aizenberg, I. B., S., O. M., and Stolov, A. L. (1975). Spectra of the Er^{3+} ion in mixed crystals. *Opt. Spectrosc.*, 38:660.

[Burum et al., 1982] Burum, D. P., Shelby, R. M., and Macfarlane, R. M. (1982). Hole burning and optically detected fluorine NMR in $Pr^{3+} : CaF_2$. *Physics Review B*, 25(5):3009.

[Butler, 1981] Butler, P. H. (1981). *Point Group Symmetry Applications.* Plenum Press, New York and London.

[Carnall et al., 1989] Carnall, W. T., Goodman, G. L., Rajnak, K., and Rana, R. S. (1989). A systematic analysis of ther spectra of the lanthanide doped into single crystal LaF_3. *The Journal of Chemical Physics*, 90(7):3443.

[Chang et al., 1966] Chang, R. K., Lacina, B., and Pershan, P. S. (1966). Raman scattering from mixed crystals $(Ca_xSr_{1-x})F_2$ and $(Sr_xBa_{1-x})F_2$. *Physics Review Letters*, 17(14):755.

[Cockroft et al., 1986] Cockroft, N. J., Thompson, D., Jones, G. D., and Syme, R. W. G. (1986). Site-selctive spectroscopy of hydrogenic sites in $CaF_2 : Er^{3+} crystals$. *The Journal of Chemical Physics*, 86(2):521.

[Corish et al., 1982] Corish, J., Catlow, C., Jacobs, P., and Ong, S. (1982). Defect aggregation in anion excess fluorites. dopants monomers and dimers. *Physics*

Review B, 25:6425.

[Dexter, 1953] Dexter D L (1953) A Theory of Sensitized Luminescence in Solids *The Journal of Chemical Physics* 21(5):836

[Dieke, 1968] Dieke, G. H. (1968). *Spectra and Energy Levels of Rare Earth Ions in Crystals.* Interscience Publishers, New York.London.Sydney.Toronto.

[Fricke, 1978] W. Fricke (1978) Satellite Lines in the Optical Absorption Spectra of Doped (La,Pr)Cl_3 - crystals *Physik B* 33:255

[Goldschmidt, 1978] Goldschmidt, Z. B. (1978). Atomic properties (free atom). In Gschneider Jr., K. A. and Eyring, L. R., editors, *Handbook on the Physics and Chemistry of Rare Earths.* North Holland Publishing Company, Amsterdam New York Oxford.

[Han, 1988] Han, T P J (1988) Laser Selective Excitation Studies of Neodymium PhD thesis, University of Canterbury

[Hargreaves, 1972] Hargreaves W A (1972). Energy levels of tetragonally sited Pr^{3+} ions in CaF_2 crystals *Phys. Rev. B* 6(9):3417

[Hüfner, 1978] Hüfner, S. (1978). *Optical Spectra of Transparent Rare Earth Compounds.* Academic Press, New York San Francisco London.

[Jayanaskar et al., 1987] Jayanaskar, C., Richardson, F., and Reid, M. (1987). Spin-correlated crsytal-field interactions in NdF_3, $Nd^{3+} : LaF_3$ and $Nd^{3+} : LiYF_4$. *Inorganica Chimica Acta*, 139:287.

[Judd, 1977] Judd, B. R. (1977). Correlation crystal field for lanthanide ions. *Physics Review Letters*, 39(4):242.

[Judd, 1985] Judd, B. R. (1985). Complex atomic spectra. *Reports of Progress in Physics*, 48:907.

[Judd, 1988] Judd, B. R. (1988). Atomic theory and optical spectroscopy. In Karl A. Gschneider, J. and Eyring, L. R., editors, *Handbook on the Physics and Chemistry of Rare Earths*, volume 11, chapter 74, page 81. North Holland, Amsterdam,Oxford,New York,Tokyo.

[Judd et al., 1968] Judd, B. R., Crosswhite, H. M., and Crosswhite, H. (1968). Intra-atomic magnetic interactions for f electrons. *Physics Review*, 169(1):130.

[Khong, 1985] Khong, Y. L. (1985). Optical absorption and laser selective excitation of the mixed crystals $Ca_{1-x}Sr_xF_2 : Er^{3+}$. *Honours III Project Report.*

[Kliava et al, 1978] Kliava J., Evesque P. and Duran J. (1978) Laser Selective Excitation and enrgy transfer in a multisite system:$CaF_2 : P^{3+}$ *J. Phys. C: Solid State Phys* 86:3357

[Laudise, 1970] Laudise, R. (1970). *The Growth of Single Crystals.* Prentice Hall, New Jersey.

[Li and Reid, 1990] Li, C. L. and Reid, M. F. (1990). Correlation crystal field analysis of the $^2H(2)_{11/2}$ multiplet of Nd^{3+}. *Physics Review B*, 42(4).

[Macfarlane and Shelby, 1987] Macfarlane, R. and Shelby, R. (1987). Coherent transient and holeburning spectroscopy of rare earth ions in solids. In Kaplyanskii, A. and Macfarlane, R., editors, *Modern Problem in Condensed Matter Sciences. Volume 21 -Spectroscopy of Solids Containing Rare Earth Ions.* North-Holland.

[Margolis, 1961] Margolis, J. S. (1961). Energy levels of $PrCl_3$. *The Journal of Chemical Physics*, 35(4):1367.

[Morrison and Leavitt, 1982] Morrison, C. A. and Leavitt, R. P. (1982). Spectroscopic properties of triply ionized lanthanides in transparent hosts crystals. In Gschneider Jr., K. A. and Eyring, L. R., editors, *Handbook on the Physics and Chemistry of Rare Earths.* North Holland Publishing Company, Amsterdam New York Oxford.

[Newman, 1973] Newman, R. C. (1973). *Infra-red Studies of Crystal Defects.* Taylor & Francis Ltd, London.

[Nielson and Koster, 1963] Nielson, C. W. and Koster, G. F. (1963). *Spectroscopic Coefficients for p^n, d^n and f^n Configurations.* M.I.T. Press, Cambrideg, Massachussets.

[Pollack and Satten, 1962] Pollack, S. A. and Satten, R. A. (1962). Electron - phonon interaction for paramagmentic ions in crystalline fields. *The Journal of Chemical Physics*, 36(3):804.

[Rajnak and Wybourne, 1963] Rajnak, K. and Wybourne, B. G. (1963). Configuration interaction effects in l^n configurations. *Physics Review*, 132(1):280.

[Reeves, 1987] Reeves, R. J. (1987). *Laser Selective Excitation of Praseodymium Ions in Hydrogenated Fluorite Crystals.* PhD thesis, University of Canterbury.

[Reeves et al., 1991] Reeves, R. J., Jones, G. D., and Syme, R. W. G. (1991). Laser site selective spectrsocopy of Pr^{3+} C_{4v} symmetry centres in hydrogenated $CaF_2 : Pr^{3+}$ and $SrF_2 : Pr^{3+}$. To be Published.

[Reid, 1987] Reid, M. F. (1987). Correlation crystal field analysis with orthogonal operators. *The Journal of Chemical Physics*, 87(5):2875.

[Mike Reid, 1990] Reid, M. F. (1990). Private Communications

[Prinz and Cohen, 1968] Prinz G A and Cohen E (1968) New Satellite structure of Nd^{3+} ions in RE trichlorides. *Phy. Rev.* 165(2):335

[Rotenberg et al., 1959] Rotenberg, M., R., B., N., M., and Wooten, J. K. (1959). *The 3-j and 6-j Symbols.* Technology Press, Cambridge Massachussets.

[Tallant et al,1974] Tallant D R and Wright J C (1974) Selective Laser Excitation of charge compensated sites in $CaF_2 : Er^{3+}$ *The Journal of Chemical Physics* 63:2074

[Wood et al] Wood D L and Kaiser W (1962) Absorption and Fluorescence of Sm^{2+} in CaF_2, SrF_2 and BaF_2 *Phys. Rev.* 126(4):2079

[Wybourne, 1965] Wybourne, B. G. (1965). *Spectroscopic Properties of Rare Earths.* John Wiley & Sons , Inc, New York.London.Sydney.

[Yeung and Newman, 1987] Yeung, Y. Y. and Newman, D. J. (1987). Orbitally correlated crystal field parametrization for lanthanide ions. *The Journal of Chemical Physics*, 82(12):6717.